Investigation into the Effect of Fibre Geometry on the Performance of Macro Synthetic Fibre Reinforced Concrete

by
Jean Oliver Lerch

Thesis presented in fulfilment of the requirements for the degree of Master of Engineering (Research) in the Faculty of Engineering at Stellenbosch University

Supervisor: Prof William Peter Boshoff
Co-supervisor: Mr Algurnon Steve van Rooyen

March 2016

Declaration

By submitting this thesis/dissertation electronically, I declare that the entirety of the work contained therein is my own, original work, that I am the sole author thereof (save to the extent explicitly otherwise stated), that reproduction and publication thereof by Stellenbosch University will not infringe any third party rights and that I have not previously in its entirety or in part submitted it for obtaining any qualification.

Date: March 2016

Abstract

Unreinforced concrete has the inherent shortcomings of low tensile strength and low strain capacity at fracture (ACI Committee 544, 2002). In order to overcome these shortcomings, fibres can be added to the fresh concrete with the aim to introduce ductility to the brittle concrete matrix. Synthetic fibre reinforced concrete (FRC) gained popularity over the past years (Bolat et al., 2014), finding its primary application in ground supported slabs.

The purpose of this research is to improve the general understanding of macro synthetic FRC on the single-fibre and the macro-mechanical level. Special attention is given to fibres with various geometric properties such as fibre length, profile and fibre shape.

Single-fibre pull-out (SFPO) experiments have been conducted on macro synthetic fibres with various embedment lengths. Fibres were premixed prior to embedment into the fresh concrete paste matrix to investigate in-service conditions. The effect of premixing was especially noted for flat fibres, indicating an increase in interfacial bond exceeding 100 % in contrast to virgin unmixed fibres, depending on the embedment length. Embossed fibre profiling proved to be the most efficient fibre geometry, providing the highest interfacial bond with the surrounding paste matrix. It is generally accepted that a high interfacial bond is a good indication for the overall performance required in typical macro synthetic FRC applications.

Additionally, time dependent pull-out (TDPO) experiments have been conducted on single embedded fibres. It was found that premixing has a significant influence on the TDPO performance, withstanding sustained loads considerably longer than unmixed fibres. Embossed fibre geometries revealed substantial resistance against sustained loads, undergoing very little displacement, being representative for small time dependent crack openings in contrast to non-embossed fibre geometries. Non-embossed fibre geometries typically exhibited considerable pull-out displacement, demonstrative for large crack openings. Small time dependent crack opening is a property desired when structural soundness is required.

Macro-mechanical tests were performed in order to establish parameters required in the structural design aspect of synthetic FRC, as these type of tests represent the in-service conditions of macro synthetic FRC. It was found that the embossed fibre profile indicated the highest performance followed by that of the flat fibre type. Robust macro-mechanical

performance is required for the development of economic macro synthetic FRC elements and a reduced eco-footprint.

In addition, macro-mechanical experiments have been conducted on macro synthetic FRC subjected to prolonged mixing times. It has been established that prolonged mixing typically decreases the post-cracking performance of macro synthetic FRC. Therefore, mixing time has a significant influence on the structural performance of macro synthetic FRC.

It has been recognised that the best overall structural performance is achieved by embossed fibre geometries. In addition, the mixing stage was found to have a significant influence on the fibre performance in the hardened state, especially for flat fibres. Depending on the type of macro synthetic FRC application, longer fibre lengths are required for higher levels of deformation, while shorter fibre lengths revealed adequate performance for lower levels of deformation. Furthermore, TDPO experiments revealed concerning behaviour of non-embossed polypropylene macro synthetic fibres.

Opsomming

Ongewapende beton het die inherente tekortkominge van lae treksterkte en lae vervormingsvermoë met breking (ACI Committee 544, 2002). Om hierdie tekortkominge te oorbrug, kan vesels by die vars beton gevoeg word met die doel om die bros betonmengsel meer rekbaar te maak. Die gewildheid van sintetiese vesel-versterkte beton (VVB) het oor die afgelope jare toegeneem (Bolat et al., 2014), met die vernaamste toepassing in grondondersteunde blaaie.

Die doel van hierdie navorsing was om algemene begrip van makrosintetiese VVB op die enkelvesel- en die makromeganiese vlak te verbeter. Spesiale aandag is geskenk aan vesels met verskillende geometriese eienskappe, soos vesellengte, profiel en veselvorm.

Enkelvesel-uittrek-eksperimente is uitgevoer op makrosintetiese vesels met verskillende vasleggingslengtes. Vesels is gemeng voor vaslegging in die vars betonbrymatriks om indiens-toestande te ondersoek. Die uitwerking van voorafvermenging is veral gemerk by plat vesels, wat ’n toename in tweevlak-binding van meer as 100 % getoon het in vergelyking met suiwer onvermengde vesels, na gelang van die vasleggingslengte. Gebosseleerde veselprofilering het geblyk die doeltreffendste veselgeometrie te wees, en het die hoogste tussenvlak-binding met die omliggende brymatriks getoon. Daar word algemeen aanvaar dat ’n hoë tussenvlak-binding ’n goeie aanduiding is van die algehele verrigting wat vereis word in tipiese makrosintetiese VVB-toepassings.

Hierbenewens is tydafhanklike uittrek-eksperimente op enkelvasgelegde vesels uitgevoer. Daar is bevind dat voorafvermenging ’n aanmerklike invloed op die tydafhanklike uittrek-verrigting het, en dat volgehoue ladings aansienlik langer as onvermengde vesels weerstaan is. Gebosseleerdevesel-geometrieë het aanmerklike weerstand teen volgehoue ladings getoon, en het min verplasing ondergaan, wat verteenwoordigend is van klein tydafhanklike kraakopeninge in teenstelling met niegebosseleerdevesel-geometrieë. Niegebosseleerdevesel-geometrieë het tipies aanmerklike uittrek-verplasing getoon, met groot kraakopeninge. ’n Klein tydafhanklike kraakopening is ’n wenslike eienskap wanneer strukturele treksterkte vereis word.

Makromeganiese toetse is uitgevoer om parameters te bepaal wat vereis word vir die strukturele ontwerpaspek van sintetiese VVB, aangesien hierdie soort toetse die indiens-toestande van makrosintetiese VVB verteenwoordig. Daar is gevind dat die

gebosseleerdevesel-profiel die hoogste verrigting toon, gevolg deur dié van die platvesel-tipe. Robuuste makromeganiese verrigting is nodig vir die ontwikkeling van ekonomiese makrosintetiese VVB-elemente en ’n verminderde eko-voetspoor.

Makromeganiese eksperimente is ook uitgevoer op makrosintetiese VVB wat aan verlengde mengtye blootgestel is. Daar is bevind dat verlengde vermenging tipies die nákrakingsverrigting van makrosintetiese VVB verlaag. Die mengtyd het dus ’n aanmerklike invloed op die strukturele verrigting van makrosintetiese VVB.

Daar is gevind dat die beste algehele strukturele verrigting deur gebosseleerdevesel-geometrieë verkry is. Hierbenewens is gevind dat die mengfase ’n aanmerklike invloed op die veselverrrigting in die verharde toestand het, veral vir plat vesels. Na gelang van die soort makrosintetiese VVB-toepassing, is langer vesellengtes nodig vir hoër vlakke vervorming, terwyl korter vesellengtes genoegsame verrigting vir laer vlakke vervorming getoon het. Voorts het tydafhanklike uittrek-eksperimente kommerwekkende gedrag van niegebosseleerde polipropileen- makrosintetiese vesels getoon.

Acknowledgements

I would like to thank the following people for their assistance and support throughout this study:

- My supervisors, Prof. Billy Boshoff and Tata van Rooyen, for their guidance and support during this study, while allowing me space to develop my own ideas.
- The laboratory and workshop staff at the Department of Civil Engineering of the University of Stellenbosch, for their assistance during many hours of mixing and experimental work.
- The Division of Structural Engineering and Engineering Informatics at the University of Stellenbosch.
- My parents for providing me with the opportunity to attend university
- Anthea Herrle, for her love and unconditional support during this research.
- The fibre suppliers Geotex and Elasto Plastic Concrete for providing macro synthetic fibres for this research.
- Alex, Nuraan, Vital, Deon, Bernard and Vianney for their friendship and providing a fun atmosphere in the office.

Table of Contents

List of Figures

List of Tables

List of Symbols

A	Area
a_O	Height of crimping profile
b	Beam width
c	Crack width
d	Measured average diameter
d_0	Nominal diameter
d_{eq}	Equivalent fibre diameter
d_f	Fibre diameter
d_l	Large equivalent diameter
d_s	Small equivalent diameter
E	Modulus of elasticity
E_E	Energy
F	Force/load
F_{avg}	Average load
$F_{avg,3}$	Average post-peak beam load up to 3mm central beam displacement
f_{ck}	Characteristic compressive strength (cylinder)
f_{cu}	Concrete compression strength (cube)
$f_{fct,L}$	Limit of proportionality
F_i	Load response at specific instance i
F_j	Post peak load corresponding to specific CMOD
F_L	Load at limit of proportionality
F_{max}	Maximum single-fibre pull-out load
F_{peak}	Peak maximum beam load from load-displacement
$f_{R,j}$	RFTS at specific CMOD for EFNARC square panel test
f_{R1}, f_{R2}, f_{R3}, f_{R4}	Residual flexural tensile strength at 0.5, 1.5, 2.5, 3.5 mm CMOD

g	Gravity on earth (9.81 m/s^2)
h	Beam height
h_{sp}	Beam height excluding notch
h_{ux}	Depth of section to neutral axis
i	Specific instance i
l	Beam span
l_c	Critical fibre length
l_d	Developed fibre length
l_e	Fibre embedment length
l_f	Fibre length
L_{free}	Free fibre length
l_i	Fibre embedment length at instance i
l_r	Fibre pull-out length prior to rupture
m	mass
M_u	Ultimate moment capacity
N	Compressive force resultant
N_s	Sample size
P	Corrected load
P'	Measured load
P_1	Load at first crack
P_A, P_B, P_C, P_D	Beam load at 0.5, 0.75, 1.00 and 1.25 mm central deflection
P^D_{150}	Residual four point bending test load at deflection of span/150
P^D_{600}	Residual four point bending test load at deflection of span/600
P_p	Peak load corresponding to four point bending test
r	Round determinate panel radius
R^2	Coefficient of determination of a linear regression
$R^D_{T,150}$	Equivalent flexural strength for four point bending experiments

$R_{e,3}$	Equivalent flexural tensile strength
r_f	Fibre radius
t	Specimen thickness
T	Tensile force resultant
t_0	Nominal thickness
T^D_{150}	Beam toughness up to a deflection of span/150
u	Instantaneous fibre elongation
V_f	Fibre volume fraction
W	Corrected energy absorption
W'	Measured energy absorption
β	Round determinate panel energy correction constant (2.0 – (δ-05.)/80)
β_y	y-intercept for CMOD conversion
γ_m	Partial safety factor for materials
δ	Displacement/deflection
δ_B	Central round determinate panel displacement
ε_f	Strain in fibre
θ	Contact angle
θ_C	Crack rotation angle
θ_s	Snubbing angle
λ	Amplitude of crimped fibre
λ_f	Fibre aspect ratio
ρ	Density
σ_c	Tensile stress applied to concrete
σ_f	Tensile stress in fibre
σ_{fu}	Fibre fracture stress
σ_{r1}, σ_{r2}	Mean axial tensile strength at 0.5 and 3.5 mm CMOD respectively
τ	Shear stress

τ_{avg}	Average interfacial bond stress
τ_i	Interfacial bond at specific instance i

List of Abbreviations

ACI	American Concrete Institute
ARS	Average residual strength
ASTM	American Society for Testing and Materials
C&CI	Cement & Concrete Institute
CMOD	Crack mouth opening displacement
CoV	Coefficient of variation
CPO	Complete pull-out
EN	European Standard
FRC	Fibre reinforced concrete
HCP	Hardened cement paste
JSCE	Japan Society of Civil Engineering
LOP	Limit of proportionality
LVDT	Linear variable displacement transducer
MOR	Modulus of rupture
NA	Neutral axis
RDP	Round determinate panel
RFTS	Residual flexural tensile strength
RILEM	Reunion Internationale des Laboratoires et Experts des Materiaux
SANS	South African National Standard
SEM	Scanning electron microscopy
SFPO	Single-fibre pull-out
TDPO	Time dependent pull-out
TPB	Three-point bending
TR	Technical Report

CHAPTER 1
Introduction

Cementitious materials are strong in compression while having poor tensile characteristics, impact resistance and toughness (Domone & Illston, 2010). Concrete used in everyday structural and non-structural application is such a cementitious material consisting primarily of hydraulic cement, sand, stone and water.

The primary shortcoming of concrete as a construction material is its susceptibility to cracking. This is due to its brittle nature, meaning it has small tensile strain capacity. In contrast to brittle behaviour is ductile behaviour. A ductile material can undergo significant plastic deformation before failure occurs.

In order to overcome the inherent brittle nature of concrete, fibres can be added in its fresh state. The introduction of fibres add ductility as well as toughness to the concrete in its hardened state. Ductile fibres are surrounded by a brittle concrete matrix resulting in an overall ductile and tough fibre reinforced concrete (FRC) composite as opposed to plain concrete.

Synthetic fibre reinforced concrete is used in a wide variety of applications, with its primary use in cast in place concrete such as slabs-on-grade, pavements and tunnel linings (ACI Committee 544, 2002). Factory manufactured products include pre-cast concrete elements, cladding panels and sidings.

The performance of macro synthetic FRC is however greatly influenced by certain fibre properties, which are required for structurally sound FRC. These properties are primarily dependent on the geometry of the fibre such as the profile, shape, aspect ratio and the fibre length as well as the fibre parent material (Kim et al., 2011). In addition, the anchorage/bond mechanism of macro synthetic fibres is a function of such fibre properties.

It is therefore essential to understand the mechanisms responsible for the mechanical behaviour of macro synthetic FRC on the single-fibre (mesoscopic) and macroscopic level.

1.1 Research Objectives

The aim of this research is to improve the general understanding of cracked macro synthetic FRC. This includes the performance based assessment on the single-fibre as well as macro-mechanical level.

The primary objective of this research is to investigate the effect of geometry in terms of deformation, profile and length of macro synthetic fibres. Moreover, the phenomenon of fibre roughening caused by mixing of fresh macro synthetic FRC on its performance in the hardened state is of high interest. This research focuses specifically on the mechanical properties of macro synthetic fibres, on the macro-mechanical and single-fibre level, and whether a link between the two levels of investigation exists.

1.2 Scope and Methodology

The scope of this study is to quantify the performance of macro synthetic FRC on the single as well as macro-mechanical level. This is achieved by an experimental framework directed towards the two levels of investigation. In addition, logical conclusions are drawn from the obtained results.

In order to achieve the outcomes of the stated objectives within the limitation of the scope, a research plan is adopted as set forth below:

- Investigation into the effect of fibre geometry on the single-fibre level using fibre pull-out experiments. In addition, macro synthetic fibres are premixed in order to investigate the in-service condition. Single-fibre pull-out performance is quantified using basic energy dissipation and constant bond stress principles.
- Quantification of the time dependent pull-out behaviour of single fibres subjected to a sustained load, partially responsible for time dependent crack widening of macro synthetic FRC.
- Determination of macro-mechanical properties of macro synthetic FRC. Flexural beam and round determinate panel test methods are adopted to quantify the behaviour with focus on the post-cracking response of FRC. International accepted test standards are used for the interpretation of the performance measurements.

1.3 Outline of the Thesis

This thesis consists of six chapters with the following chapter layout:

- CHAPTER 2 provides a theoretical background on FRC as well as internationally recognised test methods to measure the performance of FRC. Furthermore notable research with parallels to that presented in this report is provided.
- CHAPTER 3 provides the methodology adopted for the investigation on the single-fibre level regarding single-fibre pull-out and time dependent pull-out experiments, including specimen preparation and adopted test setups.
- CHAPTER 4 gives an overview of the methodology used for the investigation on the macro-mechanical level regarding three-point bending and round determinate panel tests, including specimen preparation and the related equipment used.
- CHAPTER 5 presents the results obtained for the investigation on the single-fibre as well as a discussion of the result.
- CHAPTER 6 displays the results obtained for the macro-mechanical investigation followed by a result discussion.
- CHAPTER 7 concludes the research documented in this thesis and provides future prospects and recommendations.

CHAPTER 2
Fibre Reinforced Concrete Background

This chapter provides a general background on fibres used in reinforcing cementitious materials as well as fibre reinforced concrete and its applications. In addition, a description of internationally acknowledged testing methods used to investigate the performance of fibre reinforced concrete (FRC) on a single-fibre and macro-mechanical level is given.

2.1 General Overview

2.1.1 Historical aspects

Since ancient times, fibres have been used to reinforce brittle materials such as concrete. Sun-baked bricks were reinforced using straw, while horsehair was used to reinforce mortar utilised for masonry units as well as plaster. It is believed that the oldest house constructed of straw reinforced sun-baked brick units was built around 1540 AD (ACI Committee 544, 2002).

In more recent times, asbestos fibres were commercially used to reinforce cement paste matrices, which has been the most common used fibre reinforced cement. Asbestos is a natural fibrous silicate that was used as reinforcement. Its use was widespread in roofing, cladding and fireproofing. Asbestos cement was discontinued after health concerns about its use have been raised (Domone & Illston, 2010).

The popularity of introducing various types of manmade fibres into concrete has grown as to replace asbestos cement with other fibre reinforced cementitious products (Concrete Society, 2007).

2.1.2 Usage of fibre reinforced concrete

Concrete is the most widely man-made construction material in the world (Aitcin, 2000). The main disadvantage of concrete however is its inherent poor tensile property. Once the induced tensile stresses exceed the tensile capacity of the concrete, cracks form as a result thereof. In order to overcome this problem, different alternatives to increase the tensile resistance of concrete are available. One such alternative is the use of steel reinforcement in the form of

bars. Typically concrete cracks before any significant tensile load is transferred to the steel reinforcement as a result of the lower tensile failure strain of concrete which is usually around 0.03 % (Domone & Illston, 2010).

Another reason for the introduction of reinforcement into concrete is to provide control for cracking. Where concrete elements are continuously in contact with a substrate such as for slabs-on-grade or tunnel linings and therefore forming a restraint, such reinforcement may be necessary. Reinforcement provided for such application is typically in the form of a welded wire steel mesh which more recently is commonly replaced by the addition of fibres into concrete (Ding & Kusterle, 1999). Typical types of fibres commercially available include synthetic, glass, natural and steel fibres.

In order for fibres to be effective in hardened concrete, certain distinct fibre properties are required. Generally the fibre should be significantly stiffer than the surrounding concrete matrix with a high aspect ratio. As fibres typically affect the tensile capacity of the concrete matrix, fibres are tensioned upon cracking. Due to Poisson's effect, causing lateral contraction of the fibre as a result of longitudinal elongation upon cracking, the bond between the concrete matrix and the fibre is reduced. Thus, some form of deformation of the fibre is introduced, in order to provide sufficient anchorage away from the cracked concrete section and therefore supporting the contact loss between the concrete matrix and the fibre surface (Hannant, 1978). However, the amount of fibre added to concrete is also important as to prevent fibre balling, which is the entanglement of individual fibres forming balls and causing weak spots within the concrete. Moreover, the workability of concrete is affected by the amount of fibres added. Hence, an adequate volume of fibre content is essential.

2.1.3 Types of Fibres

Fibres for use in concrete are classified into steel and polymer fibres by EN 14889-1 (2006) and EN 14889-2 (2006) respectively. Steel fibres consist primarily of carbon steel but galvanised and stainless steel fibres are also permitted (Wimpenny et al., n.d.). Steel fibres have been used in concrete since the early 1900's in the form of round and smooth chopped wire pieces. Modern steel fibres typically have rough surfaces, hooked ends or a crimped profile. The aspect ratio of steel fibres ranges between 20 to 200 (The Concrete Institute, 2013). Various shapes of steel fibres are shown in Figure 2.1.

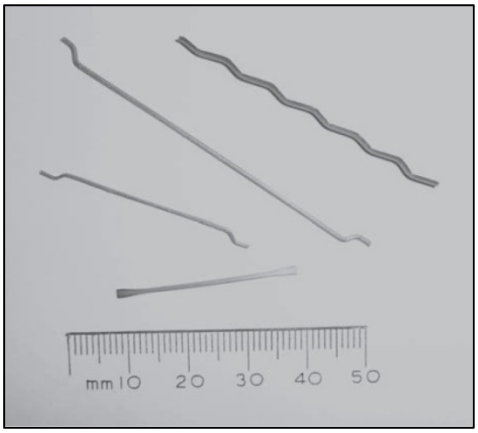

Figure 2.1: Various shapes of steel fibres (Domone & Illston 2010)

According to The Concrete Institute (2013) steel fibres have a high tensile strength (0.5 to 2 GPa) and a modulus of elasticity of 200 GPa. Steel fibres have a ductile stress strain behaviour providing post-crack load carrying capacity to the brittle concrete matrix (Concrete Society, 2007). It was found that steel fibres do not undergo significant creep under sustained loading.

The length of steel fibres ranges from 10 to 60 mm with diameters between 0.4 to 1.4 mm. Typical steel fibre dosages for use in concrete are 20 to 80 kg/m^3 (0.25-1.0 % by volume). According to Concrete Society (2007) the dosage for steel fibres is limited due to both economic and practical considerations.

The advantages of introducing steel fibres into concrete include:

- improved impact resistance, and
- greater ductility of failure in compression, flexure and torsion

The disadvantage of steel fibre reinforced concrete is the lack of corrosion resistance of steel (Hasan et al., 2011) in aggressive environments where spalling and surface staining are likely to occur.

Steel fibres are grouped according to EN 14889-1 (2006) as shown in Table 2.1.

Table 2.1: Steel fibre groups according to EN 14889-1 (2006)

Group	Type
I	Cold drawn steel
II	Cut Steel
III	Melt extract
IV	Shaved cold drawn wire
V	Milled from blocks

EN 14889-2 (2006) classifies polymer or synthetic fibres as straight or deformed pieces of extruded, orientated and cut material which are suitable to be homogeneously mixed into fresh concrete. A polymer is a material such as polyolefin, which can be regarded as polypropylene, polyethylene, nylon, pva, polyester, polyacrylic, aramids or a blend of these materials.

Polymer fibres are classified according to their physical form into micro and macro fibres. The difference according to EN 14889-1 (2006) is shown in Table 2.2.

Table 2.2: Polymer fibre classification according to EN 14889-2 (2006)

Classification	Type of Fibre	Length
Ia	Micro	<0.30 mm diameter; Mono-Filament
Ib	Micro	<0.30 mm diameter; Fibrillated
II	Macro	>0.30 mm diameter

Examples of synthetic mono-filament micro and macro fibres are shown in Figure 2.2

Figure 2.2: Synthetic micro fibres (left) and macro fibres (right)

Polypropylene micro fibres have been in use since the mid 1980's (Concrete Society, 2007) as a potential means to modify the properties of fresh concrete. Micro fibres are used in small dosages (typically 0.9 kg/m^3) typically as a controlling aid for plastic shrinkage cracking. Micro fibres may further affect the bleeding rate of plastic concrete leading to an improved near-surface property of hardened concrete. Additionally micro fibres have been found to reduce spalling of concrete exposed to fire.

Macro synthetic fibres have been commercially available since the 2000's and are sometimes referred to as "structural synthetic fibres" (Concrete Society, 2007). This term might lead to confusion as at the volume fractions currently used in practice (up to 12 kg/m^3), macro synthetic fibres are not an appropriate alternative to steel bar reinforcement designed to carry

tensile forces in free standing structural elements. Furthermore the post-cracking strength of macro synthetic fibre reinforced concrete does not exceed the cracking strength of the unreinforced concrete matrix.

Properties of selected macro synthetic fibre types are shown in Table 2.3.

Table 2.3: Selected synthetic fibre types and properties (ACI 544.1R-96 1996)

Fibre Type	Equivalent diameter, µm	Relative density	Tensile strength, MPa	Elastic modulus, GPa	Ultimate Elongation, %	Ignition temperature, °C	Melt, Oxidation or decomposition temperature, °C	Water absorption per ASTM D 570, % by mass
Acrylic	13-104	1.16-1.18	270-1000	14-19	7.5-50.0	-	220-235	1.0-2.5
Aramid I	12	1.44	2900	60	4.4	high	480	4.3
Aramid II[1]	10	1.44	2350	115	2.5	high	480	1.2
Carbon, PAN HM[2]	8	1.6-1.7	2500-3000	380	0.5-0.7	high	400	nil
Carbon, PAN HT[3]	9	1.6-1.7	3450-4000	230	1.0-1.5	high	400	nil
Carbon, pitch GP[4]	10-13	1.6-1.7	480-790	27-35	2.0-2.4	high	400	3-7
Carbon, pitch HP[5]	9-18	1.8-2.15	1500-3100	150-480	0.5-1.1	high	500	nil
Nylon[6]	23	1.14	970	5	20	-	200-220	2.8-5.0
Polyester	20	1.34-1.39	230-1100	17	12-150	600	260	0.4
Polyethylene[6]	25-1000	0.92-0.96	75-590	5	3-80	-	130	nil
Polypropylene[6]	-	0.90-0.91	140-700	3.5-4.8	15	600	165	nil
Notes								
*	Not all fibre types are currently used for commercial production of fibre reinforced concrete.							
1	High modulus.							
2	Polyacrylonitrile based, high modulus.							
3	Polyacrylonitrile based, high tensile strength.							
4	Isotropic pitch based, general purpose.							
5	Mesophase pitch based, high performance.							
6	Data listed is only for fibres commercially available for fibre reinforced concrete.							

The oldest form of reinforcement for cementitious materials is the incorporation of natural fibres. Natural fibres are of vegetable origin and are prone to the alkalinity of the concrete matrix often resulting in degradation of the natural fibres (Wei & Meyer, 2014). The main reason for making use of natural fibres is the desire to use a cost friendly, locally available and sustainable resources (Toledo Filho et al., 2009; Domone & Illston, 2010). Their use is widespread in less economically developed countries. Natural fibres are categorised into processed and unprocessed fibres.

Unprocessed fibres are made from natural fibres that have not undergone a process to extract the cellulose-rich fibre from the organic matrices. Fibres belonging to this family include coconut coir, sisal, sugarcane bagasse, bamboo, jute wood and other vegetable fibres. Long-term durability issues have been reported with fibre reinforced concrete containing natural unprocessed fibres (Tolêdo Filho et al., 2000; Perrie, 2009). Unprocessed fibres are typically

added as a minimum of 3 % by volume of concrete to show some improvement in mechanical properties of fibre reinforced concrete (The Concrete Institute 2013). These properties depend on a number of factors including the length and content of the fibres.

Processed natural fibres derived from plant stems, leaves or woody parts are processed to extract the cellulose-rich fibres from the organic matrices (Domone & Illston 2010). The degree of processing applied to extract processed fibres, determines the quality of the fibre. Sisal, jute and flax fibres are obtained by a process called "retting" whereas wood cellulose is obtained by the "Kraft" process. Retting is the employment of micro-organisms and moisture to dissolve cellular tissue, thus separating fibres from the plant stem. The Kraft process facilitates a mixture of sodium hydroxide and sodium sulphide, breaking the bond that links the lignin to the cellulose, thus converting wood into cellulose fibres. Wood-cellulose fibres have good mechanical properties comparable to macro synthetic fibres (The Concrete Institute, 2013) as shown in Table 2.4 and enhance the mechanical performance of wood-cellulose fibre reinforced cement based composites (Hakamy et al., 2015).

Table 2.4: Typical properties of natural fibres (ACI 544.1R-96, 1996)

Fibre Type	Coconut	Sisal	Sugar cane bagasse	Bamboo	Jute	Flax	Elephant grass	Water reed	Plantain	Musamba	Wood fibre (Kraft pulp)
Fibre length, mm	50-100	N/A	N/A	N/A	175-300	500	N/A	N/A	N/A	N/A	2.5-5.0
Fibre diameter, mm	0.1-0.4	N/A	0.2-0.4	0.05-0.4	0.1-0.2	N/A	N/A	N/A	N/A	N/A	0.025-0.075
Relative density	1.12-1.15	N/A	1.2-1.3	1.5	1.02-1.04	N/A	N/A	N/A	N/A	N/A	1.5
Modulus of elasticity, GPa	19-26	13-26	15-19	33-40	26-32	100	5	5	1.5	1.0	N/A
Ultimate tensile strength, MPa	120-200	275-570	180-290	350-500	250-350	1000	180	70	90	80	700
Elongation at break, %	10-25	3-5	N/A	N/A	1.5-1.9	1.8-2.2	3.6	1.2	5.9	9.7	N/A
Water absorption, %	130-180	60-70	70-75	40-45	N/A	N/A	N/A	N/A	N/A	N/A	50-75
Notes											
N/A	Properties not readily available or not applicable										

Another form of fibres that can be used in concrete is glass fibres. Glass fibres however were found to be alkali reactive and products in which they were used, deteriorated rapidly (Chira et al., 2016). During the 1960's and 1970's alkali resistant glass was introduced containing zirconia. Alkali resistant glass is used in the manufacturing process of glass-fibre-reinforced cement products, having a wide range of application (The Concrete Institute, 2013).

Glass fibres are available in continuous filaments or chopped length ranging up to 35 mm for spray applications (The Concrete Institute, 2013). The tensile strength of glass fibres has been reported to be between 2-4 GPa with a modulus of elasticity of 70-80 GPa. The stress-strain characteristic of glass fibres however was found to be of a brittle nature (Banthia & Boyd, 2000) without being susceptible to creep.

Glass fibre reinforced concrete exposed to damp environment has been reported to show loss in strength and ductility (Purnell & Beddows, 2005). According to the The Concrete Institute (2013) the reason for this is not clear and speculations are directed towards alkali attack or fibre embrittlement.

Glass fibre reinforced concrete is suitable for use in spray as well as premix application. It has been claimed that fibre contents of up to 5 % by volume of concrete have been used successfully in sand-cement mortar applications without showing signs of balling behaviour (The Concrete Institute, 2013). Glass fibre reinforced products find extensive application in the agricultural sector, architectural cladding as well as smaller containers.

2.1.4 Concrete matrix

The majority of matrices for fibre reinforced concrete are based on Portland cement as binder material (Domone & Illston, 2010). Various matrices can be used in accordance with fibre reinforced concrete. Fibres can either be added to conventional concrete to improve the mechanical properties or cementitious matrices may be specially developed with a specific fibre in order to optimise the fibre-matrix interaction.

For fibre reinforced concrete with a fibre content (polypropylene) of more than 3.5 % by volume, the basic physical requirements according to Domone & Illston (2010) of the matrix are:

- small aggregate particle size and sufficient binder content to ensure reinforcement elements such as strands and rovings are encapsulated.
- satisfactory filler and aggregate content to prevent shrinkage
- adequate water content to ensure complete compaction is achieved, fibres are surrounded by cement paste and to ensure quality surface finish
- low water:cement ratio to ensure adequate matrix strength

It is furthermore common to introduce admixtures to modify the plastic concrete mix.

For fibre reinforced concrete utilised in tunnel linings or slabs on grade, concrete mixes may differ slightly or not at all, although the introduction of fibres into the plastic concrete matrix has an adverse effect on the workability of fresh concrete (Domone & Illston, 2010).

An increase in coarse aggregate size will furthermore affect the fibre distribution within the concrete matrix. Smaller particle sizes will have the effect of better fibre distribution in contrast to larger particle sizes causing a poor fibre distribution as shown in Figure 2.3.

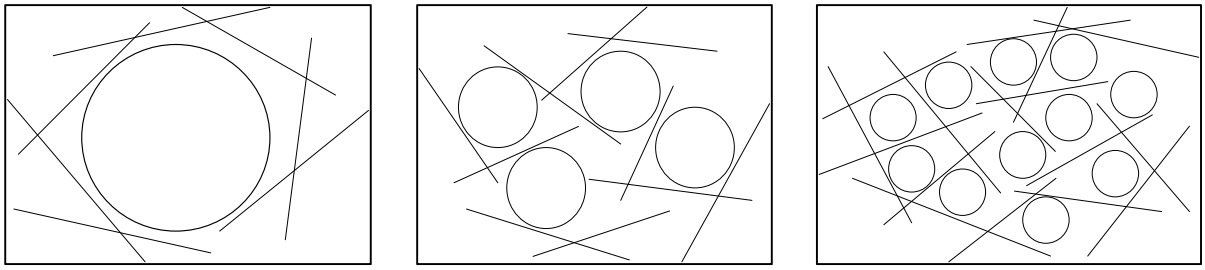

Figure 2.3: The effect of coarse aggregate particle size on fibre distribution (Hannant, 1978)

2.2 Single-Fibre Mechanisms and Behaviour

FRC subjected to a tensile load greater than its matrix's resistance to withstand the load will cause the concrete to crack. As an effect of crack formation, the load will be transferred to fibres bridging the crack, which are anchored in the concrete matrix by the mechanisms described in this section.

2.2.1 Bond mechanisms

The matrix-fibre interface in fibre reinforced concrete (monofilament fibres) has a complex interaction behaviour. This is mainly due to the bond strength, the type of bonding present and the interface morphology/chemistry which may change with time as the surrounding concrete hydrates (Won et al., 2006; Richardson, 2006; Domone & Illston, 2010). In monofilament or macro fibre reinforced concrete, the interfacial transition zone between the fibre and the concrete matrix is affected. This zone is within 10 μm of the fibre which has an increased content of silicate hydrate crystals, which are formed as the hydration process continues. These crystals have a high porosity and thus the interfacial transition zone can be regarded as a weakness within fibre reinforced concrete (Won et al., 2006).

There are three types of bonds that occur at the fibre-matrix interface resisting fibre pull-out:

- Elastic bond
- Frictional bond
- Mechanical bond

Additionally, a chemical bond can be established for fibres that undergo a process called surface treatment in order to improve its bond characteristic with the concrete matrix.

2.2.1.1 Elastic bond

The elastic or physicochemical bond can be seen as a chemical bond in so far as fibres adhere to the matrix. Physicochemical bond properties are predominantly determined by the cementitious matrix packing density and fibre surface properties (Wille & Naaman, 2012). In Figure 2.4 a typical fibre pull-out load-displacement plot is shown. The initial part of the curve indicates fibre stretching within and outside the cementitious matrix, causing gradual de-bonding of the elastic bond. Following the initial linear portion of the plots, the turning points are a symptom of the completion of the elastic bond (Li et al., 1990).

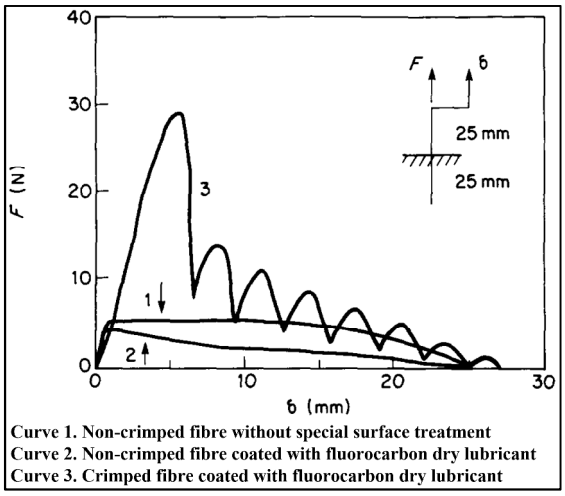

Figure 2.4: Pull-out load-displacement curves for surface treated synthetic fibres (Li et al., 1990)

Common macro synthetic fibres used to reinforce the brittle concrete matrix consist of polypropylene. This synthetic hydrocarbon polymer can be regarded as a hydrophobic material with the disadvantage of poor bond characteristics with the concrete matrix due to its hydrophobicity. A surface is regarded hydrophobic if it does not absorb water. This implies that cohesive forces associated with bulk water are greater than the forces associated with the interaction of water with the surface (Arkles, 2006) and hence no strong bond interaction between the concrete matrix and the fibre surface can be established. Whereas hydrophobic surfaces do not absorb any water, hydrophilic surfaces tend to absorb water contributing towards a stronger bond interaction between the concrete matrix and the fibre. The concept of hydrophobicity and hydrophilicity is shown in Figure 2.5.

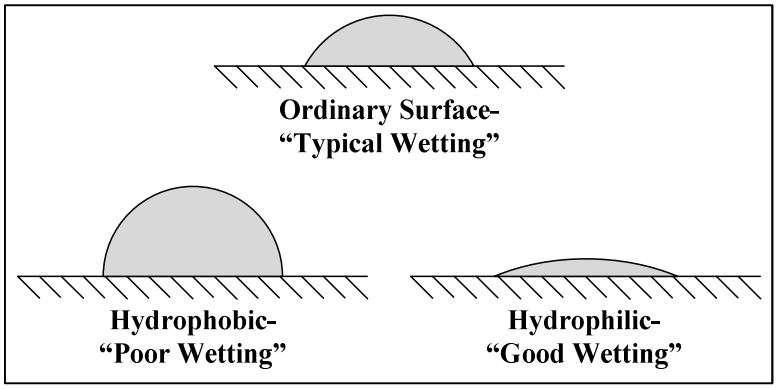

Figure 2.5: Surface wetting types (Arkles, 2006)

Chemical surface treatment consists of the use of a solution to improve the bond between polymeric fibres and the cementitious matrix (Payrow et al., 2011). The process of chemical etching involves the modification of the fibre surface by abstraction of hydrogen atoms from the polymer backbone and replacement with polar groups (Tissington et al., 1991). The introduction of polar groups containing oxygen improves the wettability of the surface and the possible available sites for chemical reactions with the cementitious matrix resulting in additional hydrogen bonding at the oxidised polymer surface (Silverstein & Breuer, 1993).

A study on surface treating macro synthetic fibres was completed by Li et al. (1990). Macro synthetic fibres were treated with fluorocarbon dry lubricant, used as a mould release compound. For fibres not treated, the pull-out load did not drop over a wide range of displacements due to the increased sliding resistance as a result of fibre abrasion caused by pull-out as shown by curve 1 in Figure 2.4. The pull-out load for surface treated fibres decreased almost linearly, proposing a constant frictional bond with the matrix during pull-out (curve 2 in Figure 2.4). Mechanically deformed fibres without surface treatment experienced fracture during pull-out, in contrast to surface treated fibres pulling out of the matrix (curve 3 in Figure 2.4).

Payrow et al., (2011) conducted a study on the effect of surface treatment on post-peak residual strength of macro synthetic FRC. Five beam tests containing surface as well as non-treated macro synthetic fibres showed that surface treatment did not significantly increase the peak or post-cracking performance of FRC. The standard deviation of the results for beams reinforced with surface treated and non-surface treated fibres showed overlap. Hence, the result scatter was approximately equal. It was however found that fibres treated with chromic acid using potassium dichromate solution yielded the most promising results in improving the mechanical properties of FRC.

2.2.1.2 Mechanical bond

A mechanical bond is provided by deforming fibres for a better interlock between the concrete matrix and the fibre itself, thus supporting the reduction in contact resulting from the Poisson's ratio (Hannant, 1978). Therefore, the mechanical bond properties are highly dependent on the geometric fibre deformation and the transversal tensile stress resistance of the concrete matrix (Wille & Naaman, 2012). Common anchorages provided for an enhanced mechanical bond are shown in Figure 2.6.

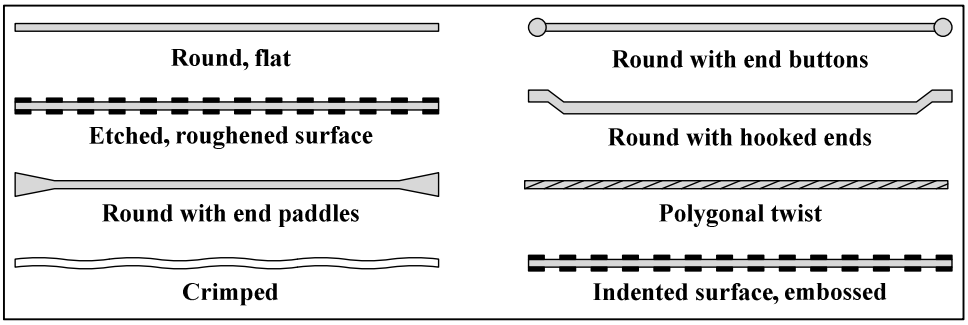

Figure 2.6: Mechanical deformation provided for enhanced interlock

2.2.1.3 Frictional bond

The frictional bond provides additional resistance against pull-out due to the friction present at the fibre-matrix interface. Frictional resistance is thus encountered, as the fibre slips through the concrete matrix.

2.2.2 Fibre-Matrix behaviour

The frictional bonding between fibres and the concrete matrix is of high interest, as this type of bonding dominates in the post-cracking region (after de-bonding of fibres) of fibre reinforced concrete (Marotzke & Qiao, 1997; Domone & Illston, 2010). This region is an important part in the stress-strain behaviour of reinforced concrete as it enhances the toughness of concrete. Toughness can be defined as the area under the stress strain curve of a particular material. As fibres only act after cracking of the concrete occurred, it is evident that fibres are added to alter the post-cracking behaviour of fibre reinforced concrete (Buratti et al., 2011; Prisco et al., 2009; Perrie, 2009). As shown in Figure 2.7, the toughness of fibre reinforced concrete is greatly increased. Therefore fibres substantially increase the ability of concrete to sustain loads at deflections and strains past those at which cracking of the matrix first appeared.

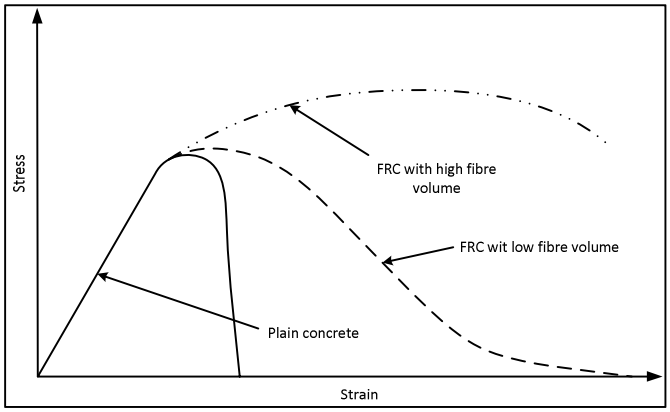

Figure 2.7: Typical stress-strain behaviour of fibre reinforced concrete (Proctor, 1979)

If fibres are incorporated in concrete, the load is transferred from the concrete matrix to the fibre as the concrete starts to crack. Figure 2.8 shows how a relatively stiff fibre influences the deformation of the concrete matrix and therefore sets up shear stresses at the interface and in the matrix. The tensile stresses carried by the fibres therefore rise rapidly with increasing distance from the end of the fibre.

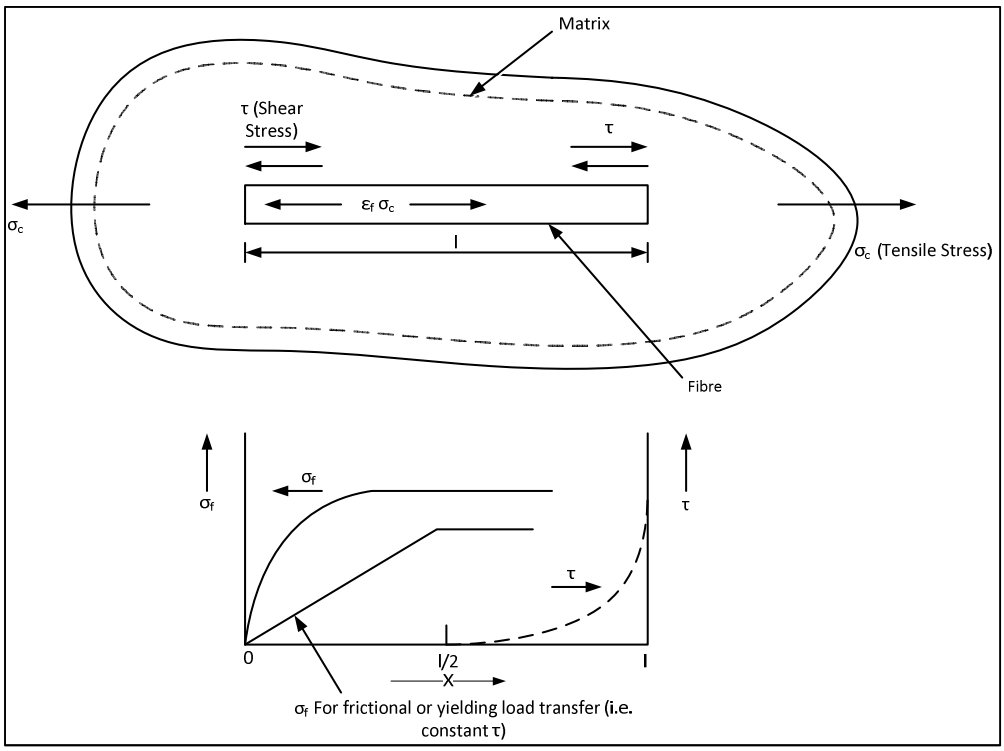

Figure 2.8: Load transfer mechanism between fibre and matrix (Proctor, 1979)

The interfacial bond stress is assumed to follow a constant shear stress distribution along the fibre length. Together, with the assumption of a circular cross-section, the following equation can be derived:

$$\pi {r_f}^2 \sigma_f = 2\pi r_f \tau l_f \quad (2.1)$$

with

r_f = fibre radius

σ_f = tensile stress in fibre at distance x from fibre end

τ = interfacial bond stress along fibre

l_f = fibre length

It is worth noting that a good matrix-fibre bond, adequate fibre length and high perimeter to cross-sectional area of a fibre is required for effective fibre reinforcing (Kim et al., 2011; Perrie, 2009).

2.2.3 Single-fibre behaviour

As concrete cracks and the load is transferred to the fibres bridging the crack opening, the following assumptions for single-fibre behaviour need to be incorporated:

- Fibres and stress direction are in line
- Fibres are distributed uniformly throughout the matrix
- The embedded fibre surface is continuously in contact with the surrounding matrix

In order for equilibrium to be satisfied, the applied force causing fibre pull-out needs to be counteracted by a gripping force exerted by the matrix onto the embedded fibre surface in the form of a bond stress at the fibre-matrix interface. A visualisation of the established equilibrium condition at pull-out is shown in Figure 2.9.

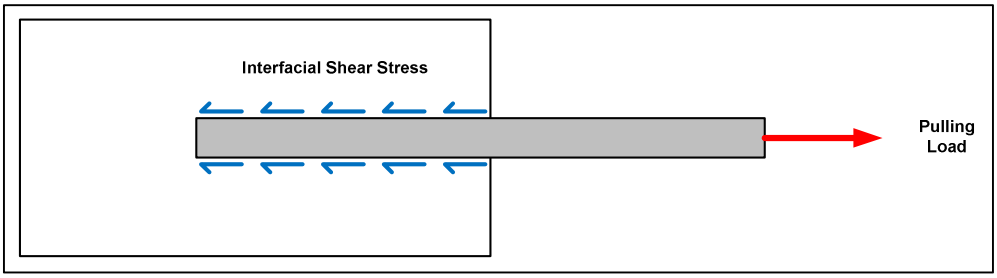

Figure 2.9: Fibre pulling-load transfer mechanism

The interfacial shear stress (τ) at fibre pull-out can be determined by rearranging Equation (2.1):

$$\tau = \frac{F_{max}}{\pi d_f l_e} \tag{2.2}$$

with

F_{max} = peak pull-out load

d_f = fibre diameter

l_e = fibre embedment length

For fibres having irregular cross-sections, EN 14889-2 (2006) proposes to calculate an equivalent diameter (d_{eq}):

$$d_{eq} = \sqrt{\frac{4 \times m \times 10^6}{\pi \times l_d \times \rho}} \tag{2.3}$$

with

m = mass of a single-fibre

l_d = developed fibre length

ρ = fibre material density

2.2.4 Critical fibre length

One of the aims of introducing fibres into concrete, is to avoid brittle failure (Wimpenny et al., n.d.) associated with unreinforced concrete and rather force a more ductile failure. Noting that Equation (2.1) is dependent on the embedded length of the fibre, it is safe to argue that the pull-out force will increase as the fibre length is increased. Fibre rupture will be caused if the pull-out force exceeds the maximum force that can be sustained by the fibre itself. Therefore, the critical length of a fibre can be regarded as the minimum length of a fibre required such that on failure of the matrix, the full strength of the fibre is utilised. At the critical length:

$$l_c = \frac{d_{eq}\sigma_{fu}}{4\tau} \tag{2.4}$$

with l_c and σ_{fu} the critical length and material fracture stress of the fibre respectively.

The concept of the critical fibre length is shown in Figure 2.10.

Therefore, the critical bond length is the maximum length of a fibre that can be embedded on either side of a potential crack, at which the residual strength or post-crack performance reaches higher levels of ductility (MacDonald et al., 2009).

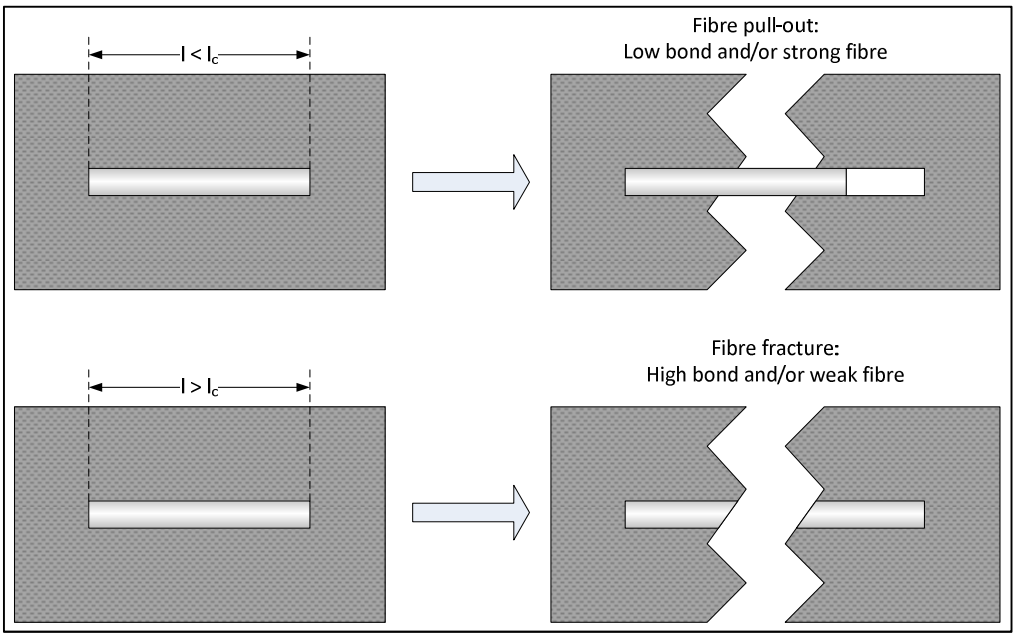

Figure 2.10: Critical fibre length (Purnell, 1998)

2.2.5 Fibre snubbing angle

Due to the random orientation nature of fibres in the concrete matrix, these will not necessarily be aligned perpendicular to the crack, and might therefore bridge the crack by an angle. This event is called fibre snubbing and was studied by Li et al. (1990). The snubbing-angle is defined as shown in Figure 2.11.

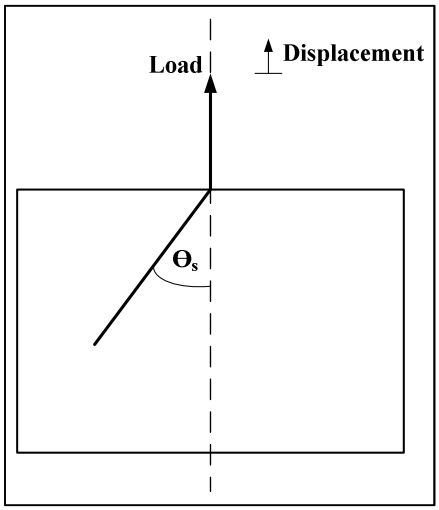

Figure 2.11: Schematic of fibre snubbing (Li et al., 1990)

Pull-out tests were performed by Li et al. (1990) on nylon and polypropylene macro fibres embedded in normal and high strength hardened cement paste (HCP) at inclining angels of 0,

15, 30, 45, 60 and 75°. Insignificant difference in pull-out resistance was found for the two grades of HCP for an angle of 0°. Larger inclining angles however showed an increase in pull-out resistance of the fibres. This was attributed to a normal force exerted by the wedge on the fibre. For higher angles, these wedges experienced spalling as a result of too high normal forces, exceeding the bearing capacity of the HCP for the normal strength HCP. Additionally a higher pull-out resistance was observed for the specimens embedded in the high strength HCP matrix.

Similar results were obtained by Odendaal (2015) for flat fibres whose orientation could be controlled. Significant increase in pull-out resistance was recorded for inclining angles of 30° and 60° in contrast to a zero inclining angle. However, non-flat fibres whose orientation could not be controlled did not display consistent snubbing. Such fibres rather experienced rupture, indicating that the snubbing effect does not exist for non-flat fibres.

2.2.6 Fibre bundling

The tendency of fibres to form bundles within the matrix, is a phenomenon often observed in synthetic FRC (Li et al., 1990). Bundling is regarded as undesirable, as the fibre reinforcing capacity is not fully utilised and weak spots may be introduced by the bundles. It is important to note that fibre bundling should not be confused with fibre balling. A unit triangular element in a hexagonally packed bundle is shown in Figure 2.12.

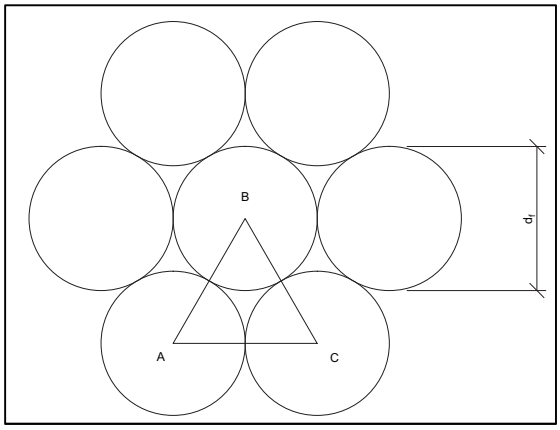

Figure 2.12: Unit triangular element in a hexagonally packed bundle (Li et al., 1990)

Although fibre bundling is occasionally regarded as advantageous for the performance of macro synthetic FRC, as an increase in energy absorption can be observed by allowing some fibre pull-out, which might not have been possible if fibres were separated. A direct modification of the fibre-matrix interaction however is more effective according to Li et al. (1990).

Li et al. (1990) investigated the effect of fibre bundling on the pull-out behaviour of macro synthetic fibres. It was concluded that bundle pull-out tests are difficult to characterise quantitatively, as bundle size distribution, compaction density of the bundles and the degree of paste penetration into the fibre bundles are unknown quantities. For a closely packed macro synthetic fibre bundle embedded in a cement matrix, the exposed surface that is in contact with the surrounding matrix is less than the total surface area of the fibre bundle. This can cause the outside bundle layer to develop a full bond with the cement matrix, resulting in fibre rupture of the fibres in this layer. Fibres inside the bundle would pull-out and higher energy absorption as a result thereof can be achieved. This effect is referred to as a telescopic mode of pull-out. Typical load-displacement curves for bundle pull-out tests are shown in Figure 2.13.

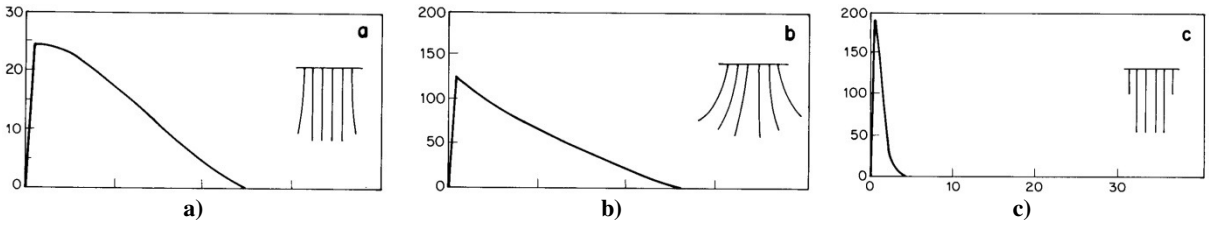

Figure 2.13: Typical load-displacement curves according to Li et al. (1990) for fibre bundle pull-out tests for relatively straight embedment (a) non-straight embedment (b) very straight embedment (c)

2.2.7 Fibre pull-out experiments

Fibre pull-out tests are used to estimate the bond between the concrete matrix and the fibre under consideration. According to Domone & Illston (2010) typical values for the interfacial shear stress of smooth cylindrical monofilament fibres are around 0.1, 0.5 and 1.0 MPa for polyethylene, polypropylene and steel fibres respectively. These values can be effectively increased by a factor of four if a mechanical bond in terms of fibre crimping is used (Bentur & Mindess, 2006).

The bond performance of macro synthetic fibres depends on the stiffness, strength, geometry and elastic modulus of the fibre. To overcome the low bond strength of macro synthetic fibres, mechanical anchorage is provided in the form of deformed geometry. Moreover, as cracks form, macro synthetic fibres deform mechanically enhancing their bond strength with the concrete matrix. Won et al. (2006) performed single-fibre pull-out experiments (see Figure 2.14a) on macro synthetic fibres shown in Figure 2.15, to investigate fibre performance and establish an optimum geometry.

Won et al. (2006) determined that the optimum fibre geometry for macro synthetic FRC is a crimped fibre profile with a height (a_0) of 1.8 mm and amplitude (λ) of 6.0 mm as shown in

Figure 2.15b. The fibres were pulled-out of a normal strength matrix (25 MPa) as well as a high strength matrix (40 MPa).

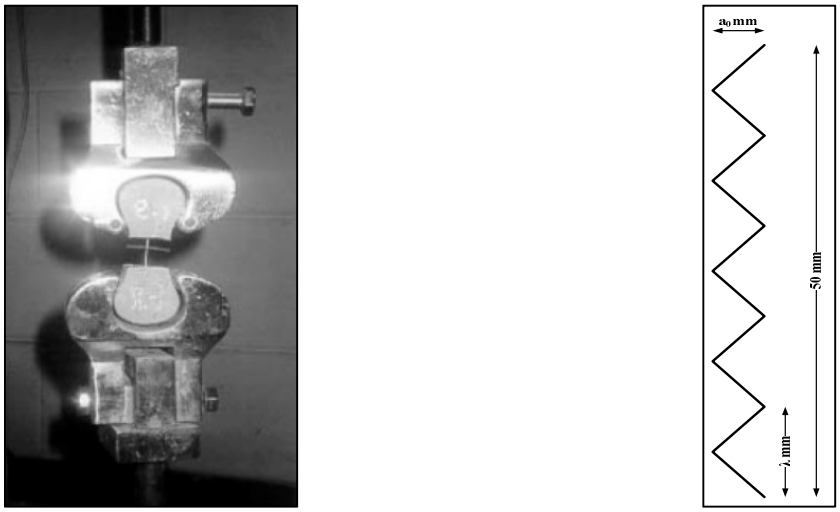

Figure 2.14: Fibre pull-out test setup and optimum macro synthetic fibre geometry by (Won et al., 2006)

From the macro synthetic fibre geometries shown in Figure 2.15, the crimped fibre performed the best. Only Fibre F3 and Fibre F6 were found to undergo fibre fracture for both, normal strength and high strength concrete. All other fibres were pulled out of the normal strength concrete matrix, however, the pull-out strength and interface toughness of the crimped fibre showed the best performance. However, 40 % of the crimped fibres fractured being pulled out of the high strength matrix.

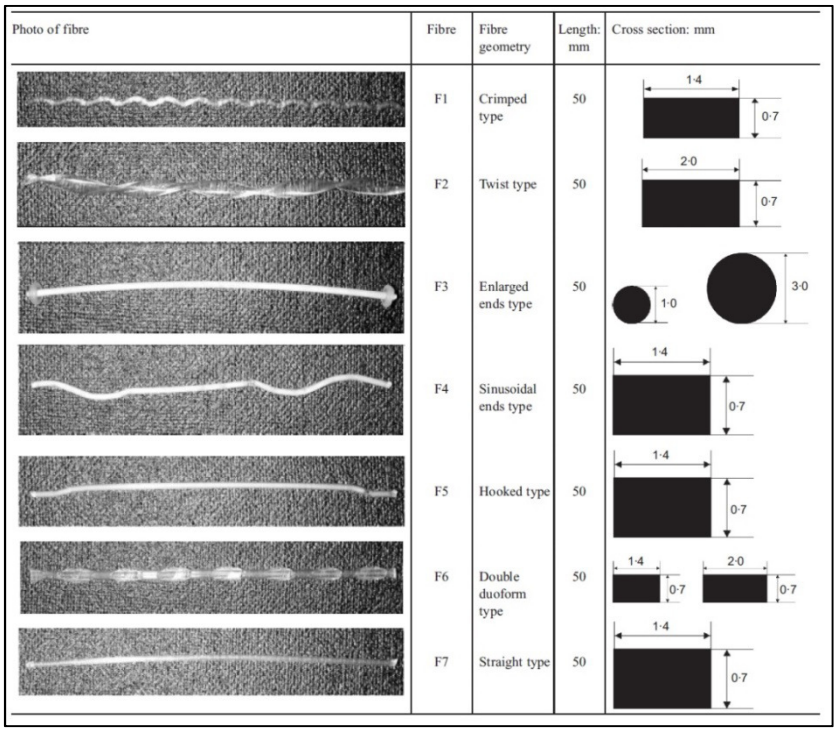

Figure 2.15: Geometry of macro synthetic fibres investigated by Won et al. (2006)

Beglarigale & Yazici (2015) investigated the effect of parameters such as the end condition of steel fibres, embedment length and water/binder ratio amongst other parameters, conducting single-fibre pull-out tests as shown in Figure 2.16. It was determined that fibre-matrix bond characteristics improved as the embedment length increased, which was much more pronounced for smooth steel fibres without hooked-end conditions. Additionally, low water/binder ratios enhanced the bond strength of embedded steel fibres and reduced the importance of embedment length for hooked-end steel fibres. It was also concluded that the load drop directly after reaching the peak pull-out load was higher for hooked-end steel fibres compared to smooth profiles. As a result of this behaviour, the de-bonding toughness of some smooth steel fibres was found to be higher than that of hooked-end conditions. However, peak pull-out loads of hooked-end steel fibres were up to three times higher than the peak load of smooth steel fibres, and the overall toughness of hooked-end steel fibres was found to be higher for all pull-out experiments. This difference between the two steel fibres with unalike end conditions however decreased with an increase in water/binder ratio.

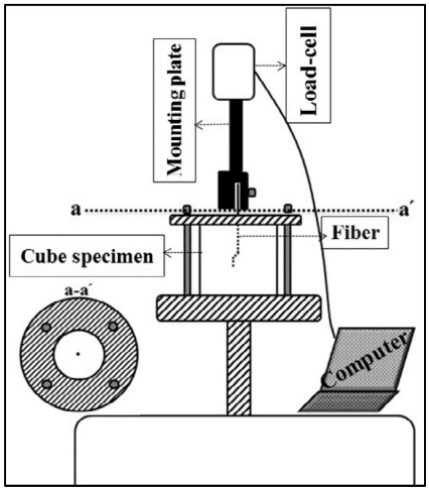

Figure 2.16: Fibre pull-out test setup by Beglarigale & Yazici (2015)

Odendaal (2015) conducted single-fibre pull-out tests as shown in Figure 2.17 on macro polypropylene fibres, investigating the effect of water to binder ratio and cross-sectional shape of the fibre on the average bond stress. It was found that the water to binder ratio has an insignificant influence on the bond behaviour of non-flat fibre types and untreated flat fibres. Furthermore, the fibre geometry was found to have a large influence on the single-fibre performance of macro synthetic fibres. A crimped fibre profile with an X-shaped cross-section developed the highest interfacial bond stress (1.94 MPa) followed by a round-shaped cross-sectional crimped fibre profile (1.69 MPa). Untreated flat fibres exhibited the lowest bond stresses (0.62 MPa) while significantly higher bond stresses (1.66 MPa) were observed

for surface treated flat fibres with similar cross-sectional properties. The uniform bond model as described in Section 2.2.2 was found to be inadequate for non-flat fibres, as high bond stresses at the fibre end near the surface were recorded.

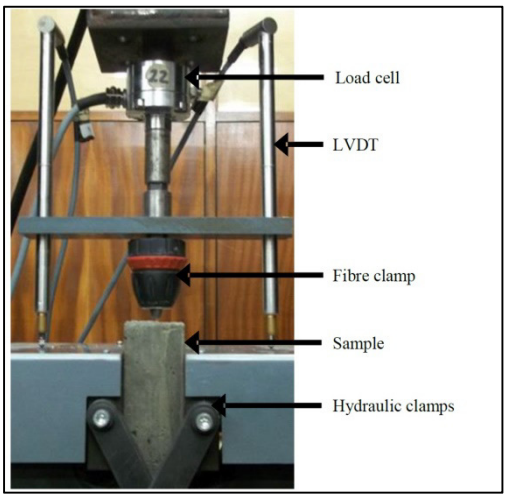

Figure 2.17: Fibre pull-out test setup by Odendaal (2015)

2.2.8 Typical single-fibre pull-out response

The typical single-fibre pull-out response obtained by the single-fibre pull-out experiments is depicted in Figure 2.18. It is evident that the presence of pull-out displacement prior to the peak load is a consequence of fibre elongation as the elastic or physicochemical bond exceeds the stress required for de-bonding the fibre. Upon de-bonding the corresponding stress to the peak load exceeds the interfacial bond stress offered by the concrete matrix causing the pull-out of the fibre. Different trends are observed in the post-peak region. The oscillating load during the pull-out response portrayed by the crimped fibre profile is attributed to its sinusoidal shape. In contrast, flat fibres experience smoother pull-out responses as a result of the absence of any significant fibre deformation.

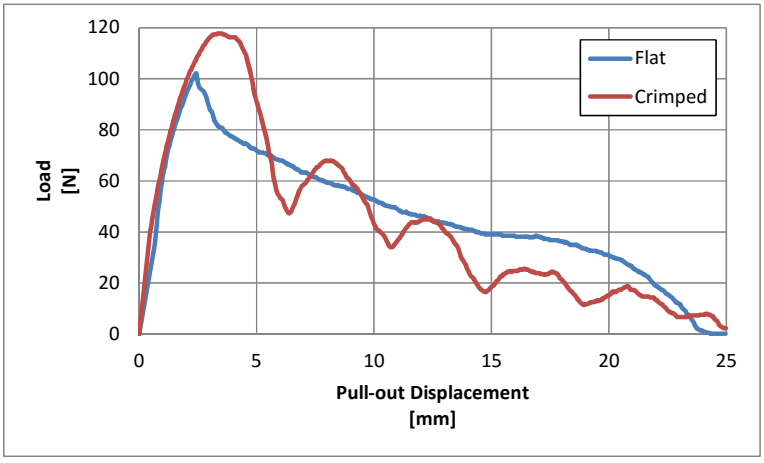

Figure 2.18: Typical single-fibre pull-out response

It is important to note, that the single-fibre pull-out responses illustrated in Figure 2.18, all exhibit complete fibre pull-out without undergoing rupture. It is therefore evident, that the critical fibre length is not exceeded. However, once the critical fibre length is utilised, the instance of the peak load in the fibre pull-out response is governed by the fracture stress of the fibre parent material. As a consequence thereof, the fibre experiences rupture. Fibre rupture typically occurs before de-bonding of a fibre as shown in Figure 2.19a. It is however noteworthy, that some fibres may experience rupture during pull-out as depicted in Figure 2.19b. The most logical explanation for this phenomenon is that substantial fibre damage is caused to the fibre during de-bonding or pull-out, thus creating localised weak spots producing a susceptibility to rupture.

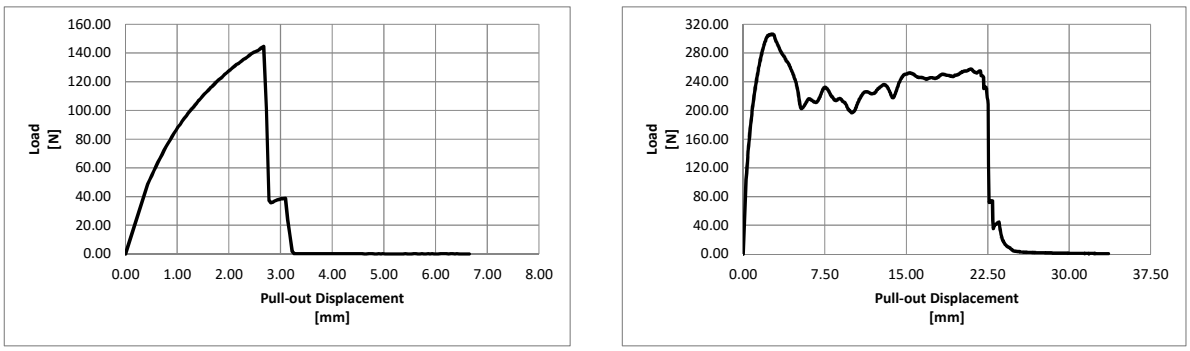

Figure 2.19: Fibre rupture during single-fibre pull-out experiment

2.3 Macro-Mechanical Test Methods for the Performance Assessment of FRC

Fibre reinforced concrete is becoming widely used in the civil engineering practice due to its favourable mechanical properties (Walraven, 2009). Fibres significantly contribute to the residual tensile strength in the post-cracking regime and enhanced capacity to absorb strain energy (Caggiano et al., 2012). This is mainly due to the bridging mechanism of the fibres across the crack surface. Furthermore, fibres tend to contribute to the toughness, ductility, durability and other mechanical properties when distributed in a homogeneous way and used in an appropriate quantity (Bolat et al., 2014).

By incorporating fibres into concrete, the post cracking regime of FRC can be affected in a strain hardening or strain softening way. The phenomenon of strain hardened and strain softened FRC is presented in Figure 2.7.

The methods typically used to assess the performance of macro synthetic fibres for FRC are described in this section. These include the three-point bending, four point bending, round

determinate panel and square panel test. In addition, links that have been established between various macro-mechanical tests are discussed.

2.3.1 Three-point bending test

The three-point bending (TPB) test is a beam bending test standardised by EN 14651 (2005), specifically for testing FRC. Concrete Society (2013) endorses the final recommendation as described in RILEM TC 162-TDF (2003), which is a reproduction of EN 14651 (2005).

2.3.1.1 Test setup

The test method consists of a 150 x 150 x 550 mm beam that is simply supported and subjected to a centrally (at mid-span) applied load. A notch of 25 mm (δ) on the tension face at the position of the applied load is required in order to control the positioning of the crack to propagate at mid-span. A schematic setup of the test is illustrated in Figure 2.20.

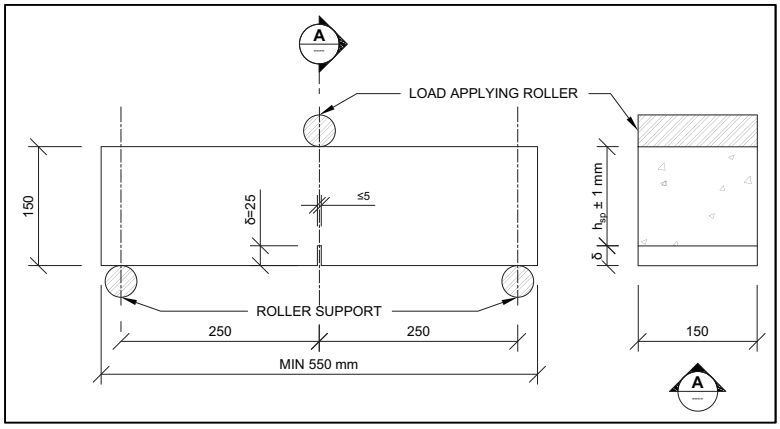

Figure 2.20: Schematisation of a TPB setup showing positions of supports and loading device

2.3.1.2 Typical three-point bending test output

The typical load-displacement response exhibited by six beam specimens tested in TPB is shown in Figure 2.21a. However, the corresponding load-CMOD response is often of interest as depicted in Figure 2.21b. Crack mouth opening displacement (CMOD) is the displacement of a formed crack, measured at the surface where the crack is formed. It is important to note that the result scatter in the post-cracking region of the load-deflection curves is attributed to the relatively small crack plane measuring 125 x 150 mm (18,650 mm^2). This is caused by the varying nature in the number of fibres bridging the crack over the crack plane.

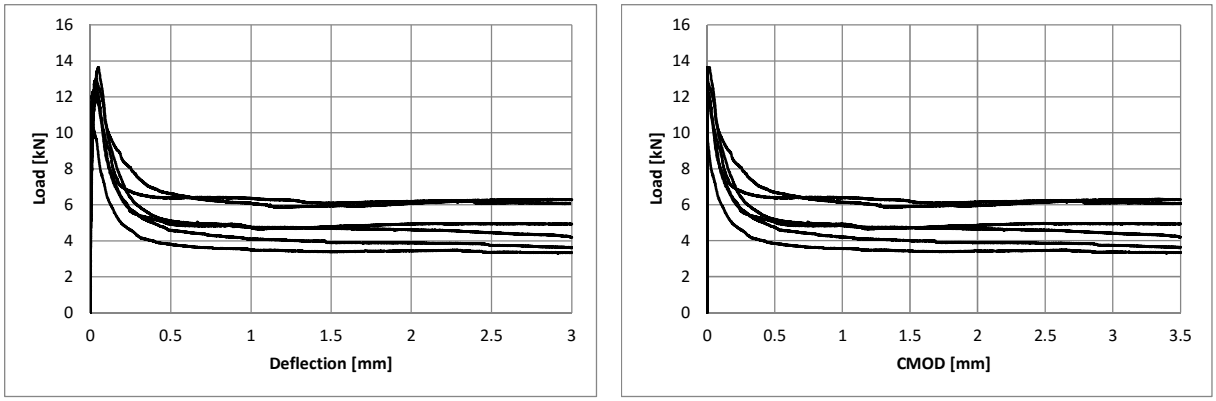

a) b)

Figure 2.21: Load-deflection (a) and Load-CMOD (b) response obtained by TPB beam bending tests

It is customary to illustrate the elastic portion of the load-displacement and load-CMOD response, which is depicted in Figure 2.22a and Figure 2.22b respectively, for further analysis. It is important to note, that a crack mouth only forms once the FRC beam specimens experience cracking, hence no linear load-CMOD response is discernible before the load at first crack of the tested FRC beam specimens is reached.

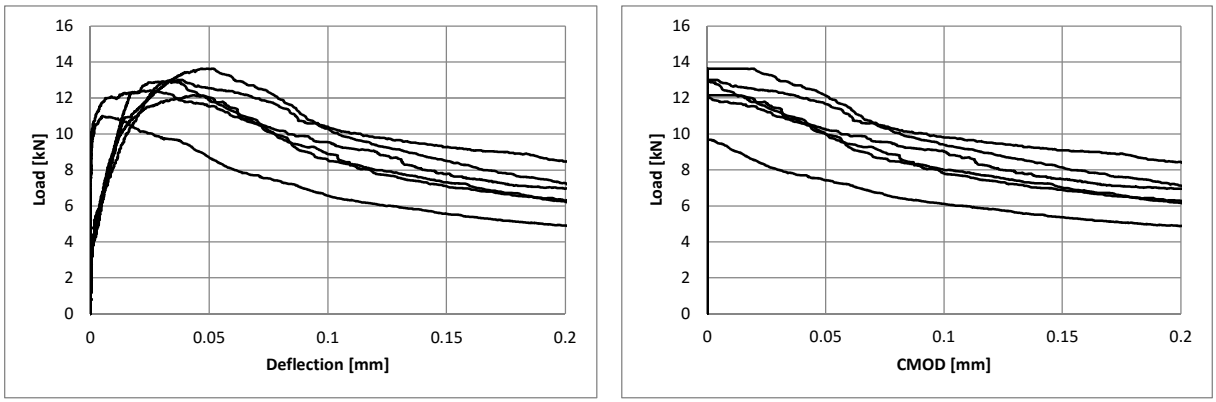

a) b)

Figure 2.22: Discernible elastic portion of the TPB FRC beam response for load-deflection (a) and load-CMOD (b)

Three distinct trends can be observed from the load-CMOD response and are commonly of interest, namely:

- peak load
- minimum post-cracking load
- maximum post-cracking load

These are demonstrated in Figure 2.23.

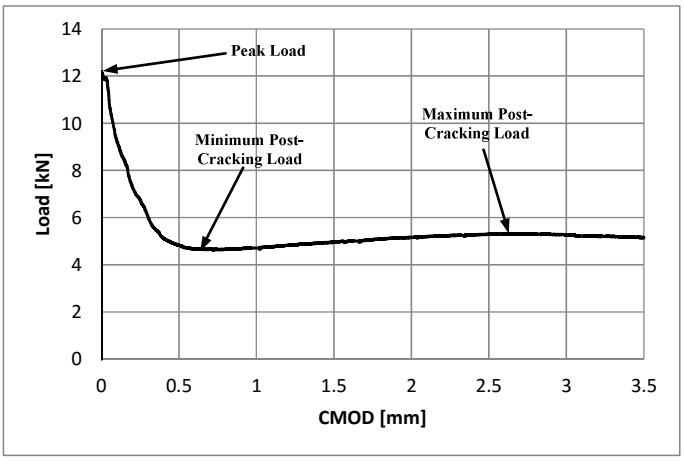

Figure 2.23: Load-CMOD response indicating important trends

2.3.1.3 Limit of proportionality

The load at the limit of proportionality (LOP), F_L, is equal to the highest load value within the interval of 0 mm - 0.05 mm of central deflection or crack mouth opening displacement (CMOD). A load-CMOD plot typical for the TPB test is shown in Figure 2.24

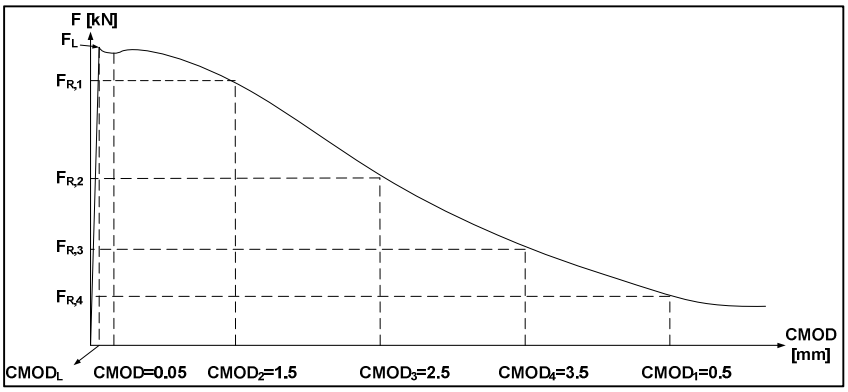

Figure 2.24: Load-CMOD diagram (RILEM TC 162-TDF 2003)

The LOP ($f_{fct,L}$) can be calculated using:

$$f_{fct,L} = \frac{3F_L l}{2bh_{sp}{}^2} \tag{2.5}$$

with

F_L = peak flexural load

l = beam span

b = beam width

h_{sp} = notched beam height

It is important to note, that the LOP differs from the modulus of rupture (MOR), as the MOR is calculated by the load at which first cracking occurs, while the LOP is calculated according

to the peak load within a CMOD of 0 mm - 0.05 mm. For strain softening FRC the MOR equals the LOP, however for the case of strain hardening FRC this is not necessarily true.

2.3.1.4 Equivalent flexural strength

The equivalent flexural strength ratio ($R_{e,3}$) for TPB is a measure of ductility and is defined as the average load carrying capacity after cracking of the beam. $R_{e,3}$ is measured up to a vertical deflection of 3 mm at mid-span as a fraction of the load at first crack (load at MOR), F_{peak}. In Figure 2.25 a schematic representation of the parameters used for calculating the $R_{e,3}$ value is shown.

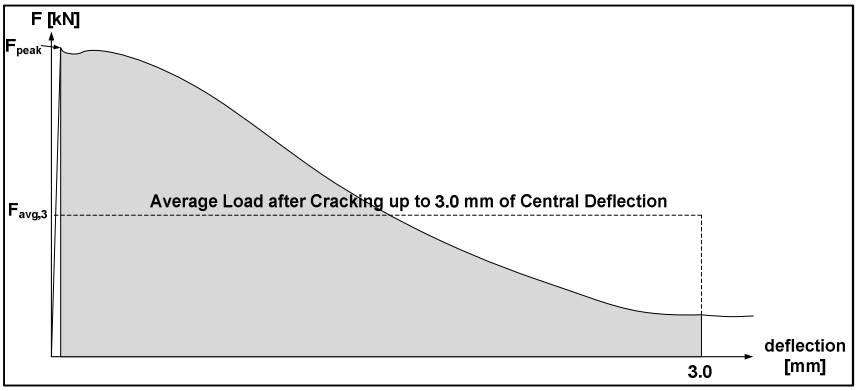

Figure 2.25: Parameter calculations for $R_{e,3}$ value

The $R_{e,3}$ value, which is often expressed as a percentage, is calculated as:

$$R_{e,3} = \frac{F_{avg,3}}{F_{Peak}} \tag{2.6}$$

with $F_{avg,3}$ and F_{peak} the average resisted load up to 3 mm central deflection and the peak flexural load resisted by the FRC beam respectively.

As the $R_{e,3}$ value is a measure of ductility, it is used in the calculations of the design moment capacities for ground supported floors. For design purposes, this provides a residual positive bending moment capacity. The limiting criterion however, is the onset of cracking on the top surface. Hence, residual negative bending moment capacity is not included in the design. Additionally, it is required that sufficient fibres must be provided, in order to accomplish a minimum $R_{e,3}$ value of 0.3 (Concrete Society, 2003). However, due to the $R_{e,3}$ value being dependent on the peak flexural concrete strength, this parameter seems to be misleading (Odendaal, 2015). Consequently an increasing trend of the $R_{e,3}$ value with decreasing water to binder ratio value was observed.

2.3.1.5 Mean axial tensile strength

In the most recent version of the Technical Report no 34 (Concrete Society, 2013) the use of the $R_{e,3}$ value is superseded by the mean axial tensile strength for a CMOD of 0.5 mm and 3.5 mm. These are σ_{r1} and σ_{r4} being calculated according to:

$$\sigma_{r1} = 0.45 f_{R1} \tag{2.7}$$

$$\sigma_{r4} = 0.37 f_{R4} \tag{2.8}$$

with f_{R1} and f_{R4} the residual flexural tensile strength at CMODs of 0.5 and 3.5 mm respectively, which correspond to a crack depth of 0.66 and 0.90 of the beams depth.

The mean axial tensile strength for a CMOD of 0.5 mm and 3.5 mm are used to calculate the positive ultimate moment capacity (M_u) for the design of ground supported floors, given by:

$$M_u = \frac{h^2}{\gamma_m}(0.29\sigma_{r4} + 0.16\sigma_{r1}) \tag{2.9}$$

with h and γ_m the section depth and partial material factor respectively (Concrete Society, 2013).

The ultimate moment capacity given by Equation (2.9) is based on a conservative approach by making the following simplified assumptions:

- At the ultimate moment of the section, the concrete reaches its compressive strain simultaneously with the limiting tensile strain developed in the FRC. As a result, strain compatibility will be achieved in contrast to force equilibrium due to the compressive force always exceeding the tensile force in the FRC.
- Thus the depth of neutral axis will be a constant multiple of the section depth.

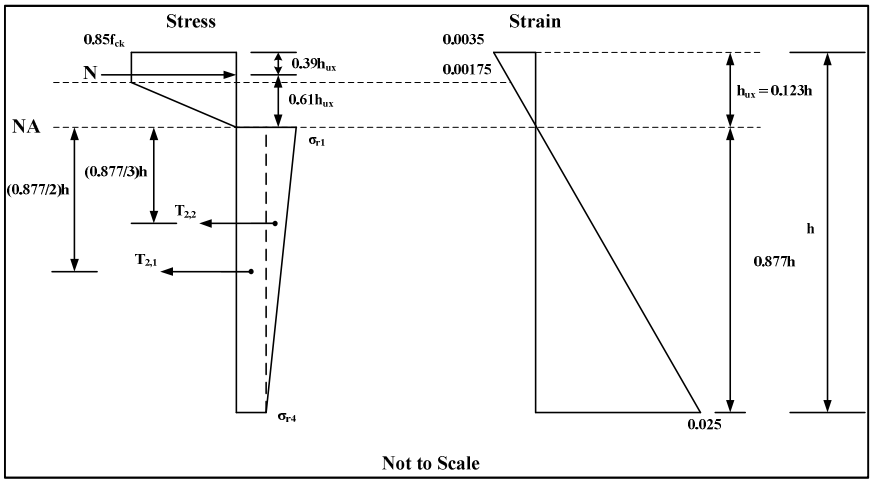

Figure 2.26: FRC stress block (Concrete Society, 2013)

The ultimate moment capacity given by Equation (2.9) can be derived by taking moment about the centroid of the compression zone denoted N in Figure 2.26. It is important to note that the thickness design approach according to the yield line theory, as given by the ultimate moment capacity of slabs, is purely dependent on the combination of the mean axial tensile strengths ($0.29\sigma_{R4} + 0.16\sigma_{R1}$).

2.3.1.6 Result scatter

The main disadvantage of the beam test is the relatively small crack area of a maximum of 150 x 125 mm, causing significant scatter in the post cracking region as a consequence of the small number of fibres bridging the crack surface (Buratti et al., 2011). It was found that the scatter of experimental results in the post cracking region for macro synthetic fibres is much smaller than for steel fibres. This is attributed to the fact that stiff fibres are less likely to spread themselves homogeneously during the casting of concrete specimens, which depends on fibre dosage, fibre geometry and the size of the specimen. This is verified by Alberti et al. (2014), as higher dispersions of the results were found for higher fibre dosages. In contrast to Buratti et al. (2011), fracture surface analysis of steel FRC beams determined that many steel fibres showed an anchorage/pull-out failure. For the case of synthetic fibres, most fibres experience rupture explaining the dispersion of macro synthetic FRC.

Alani & Aboutalebi (2013) reported that a higher consistency is achieved by macro synthetic fibre reinforcement in contrast to steel fibre using the same dosages. This is attributed to a uniform presence of macro synthetic fibres within the crack opening, mainly due to the high fibre count.

Traditionally, six beams were specified for the test, however Concrete Society (2013) and EN 14889-2 (2006) increased the number of beams to twelve in order to account for the high variability of the test method. According to Buratti et al. (2011) round determinate panel (RDP) tests should rather be used to determine the residual strength of the fibre reinforced concrete. This is confirmed by Odendaal (2015), as it was established that the RDP test results variation is significantly less (typically 0.1) than for TPB tests (typically 0.2).

2.3.1.7 Significant research

The mechanical properties and fracture behaviour of polyolefin fibre reinforced self-compacting concrete was researched by Alberti et al. (2014). Medium and high synthetic fibre contents were compared with the reference self-compacting concrete used as well as

self-compacting concrete reinforced with steel fibres. The dosages used in the study are shown in Table 2.5.

Table 2.5: Fibre dosage used by Alberti et al. (2014)

Dosage Classification	Change in Mix Design	Dosage (kg/m^3)	Fibre Type	Mix Definition
Medium	No change	3	Polyolefin	P3
Medium	No change	4.5	Polyolefin	P4.5
Medium	No change	6	Polyolefin	P6
High	No change	10	Polyolefin	P10a
High	Increased sand content	10	Polyolefin	P10b
High	P10b with a bond improver	10	Polyolefin	P10m
Control	No change	26	Steel	SC26
Control	No change	0	NA	CC

TPB tests were performed on non-standardised beams with dimensions of 100 x 100 x 430 mm. The specimens reinforced with steel fibres all behaved similarly with little scattering, whereby load-deflection curves indicated a staggered behaviour. This is attributed to either failure of the fibre anchorage or to the failure of the fibre itself (Alberti et al., 2014). Smoother load-deflection curves were obtained for synthetic fibre reinforcement.

Even the smallest quantity of synthetic fibre reinforcement showed an increase in the load bearing capacity in the post-cracking region as well as the ability to absorb the energy released in the fracture process, implying increased ductility when compared to the reference concrete.

Higher synthetic fibre contents (10 kg/m^3) were introduced with the aim of improved mean values close to those found by the addition of steel fibres. The peak load values recorded were higher than those of the reference concrete, but lower than those registered with steel fibre reinforced specimens and specimens containing medium content of synthetic fibres. Comparison of the fracture energy up to 5 mm deflection showed a better performance of the synthetic fibres than that of the steel fibres. In addition, the maximum post-cracking load at a central deflection of 4.5 mm for high synthetic fibre content with the addition of adhesion improver was found to be higher than that of the steel fibre. The minimum post-cracking load of all synthetic fibre reinforced specimens was however found to be significantly lower than that of the steel fibre reinforced concrete due to the better mechanical property and to the anchorage of the hooked end of the steel fibre (Alberti et al., 2014). The mean values for the minimum and maximum post-cracking load capacity is shown in Figure 2.27.

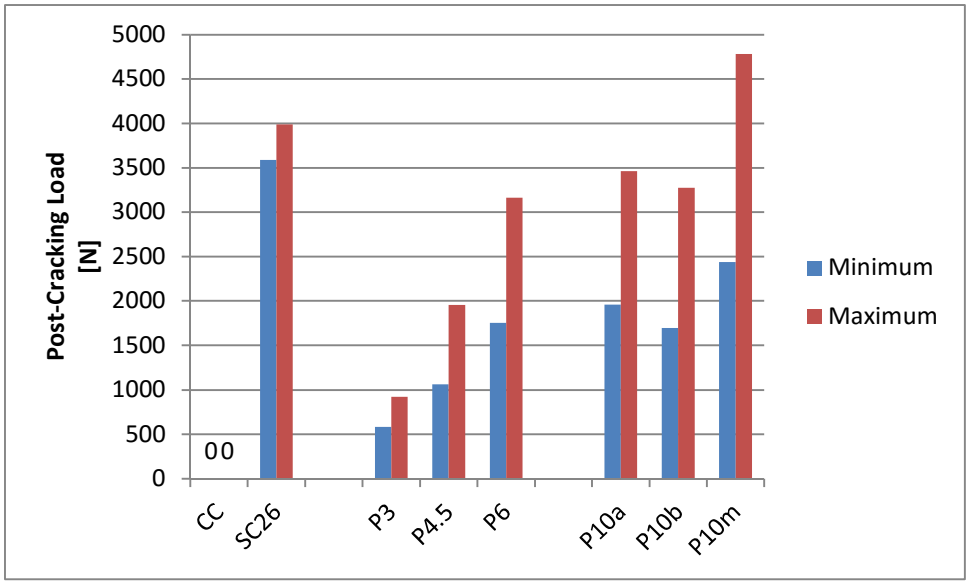

Figure 2.27: Minimum and Maximum post-cracking load (Alberti et al. 2014)

Alani & Aboutalebi (2013) performed a comparative experimental study on the performance of steel and synthetic fibre reinforced concrete. Flexural tests were conducted on standardised beams specimens with a steel and synthetic fibre content of 7 kg/m^3.

The flexural strength at 7 days of the steel fibre reinforced beam specimens was found to be slightly higher than that of the synthetic fibre reinforced beam specimens. The post-cracking residual flexural strength at a concrete age of 7 days was found to be better for steel fibres for smaller crack openings in contrast to synthetic fibre reinforcement. Synthetic macro FRC beams however gained a relative constant residual flexural strength at larger crack openings, exceeding that of steel fibre reinforced specimens.

No significant difference was recorded for the tested flexural strength at 28 day concrete strength.

Macro synthetic FRC beams showed a gradual but continuous decrease in 28 day residual flexural strength values. Steel FRC beams displayed more constant residual flexural strength values and proved to be more efficient in post-crack development control and ductility (Alani & Aboutalebi, 2013).

Buratti et al. (2011) reported on the post-cracking capacity of macro synthetic fibres compared to steel fibres. Synthetic fibres and steel fibres at a dosage of 2 kg/m^3 and 20 kg/m^3 were added to concrete respectively. The authors showed that steel fibres showed generally a better performance than macro synthetic fibres. This was determined by TPB tests according

to EN 14651 (2005) with 150 x 150 x 550 mm prismatic beam specimens. The performance comparison of macro synthetic and steel fibres is shown in Figure 2.28.

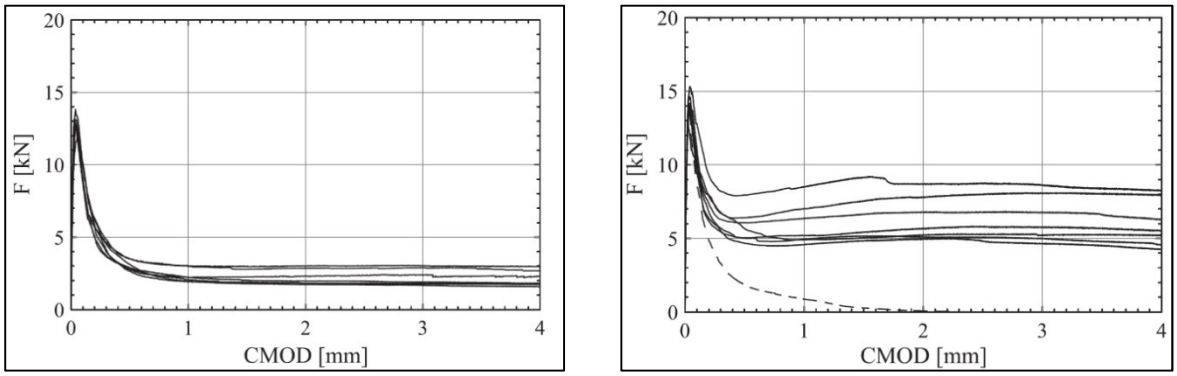

Figure 2.28: Performance of macro synthetic (a) and steel fibre (b) reinforced concrete (Buratti et al., 2011)

2.3.2 Four point bending test

The four point bending test for FRC is documented by the American Society for Testing and Materials (ASTM) (2012) as well as JSCE SF-4 (1985).

2.3.2.1 Test setup

The setup consists of a simply supported beam with third-point loading arrangements. The preferred sizes are either 100 x 100 x 350 mm or 150 x 150 x 500 mm as specified by ASTM C1609 (2012), however, different specimen sizes are also permissible. The schematic test setup is demonstrated in Figure 2.29.

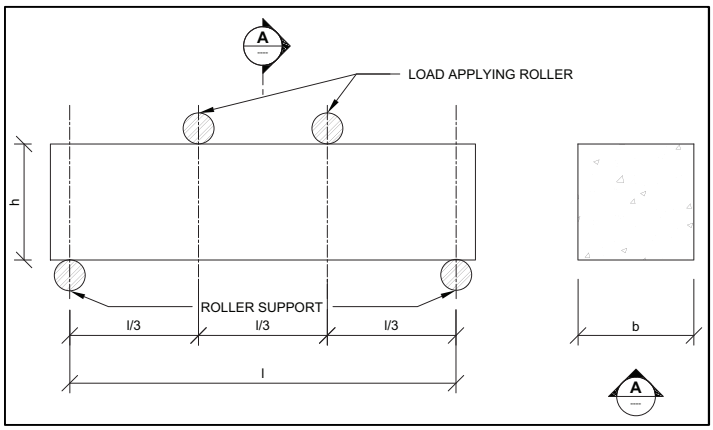

Figure 2.29: Schematisation of a four point bending setup showing positions of supports and loading device

2.3.2.2 Residual strength

ASTM C1609 (2012) requires to calculate the residual strength of FRC beams used in four point bending configuration at deflections of 1/600 and 1/150 of the span length. These stresses are not calculated in accordance with plastic section properties, but are rather computed using bending theory based on linear elastic material behaviour and un-cracked

section properties. The residual stresses f^D_{600} and f^D_{150} are calculated using the modulus of rupture (MOR) according to:

$$MOR = \frac{P_1 l}{bh^2} \tag{2.10}$$

with P_1 the load at first crack being replaced with corresponding residual loads P^D_{600} and P^D_{150} for deflections of span/600 and span/150 respectively, as shown in Figure 2.30.

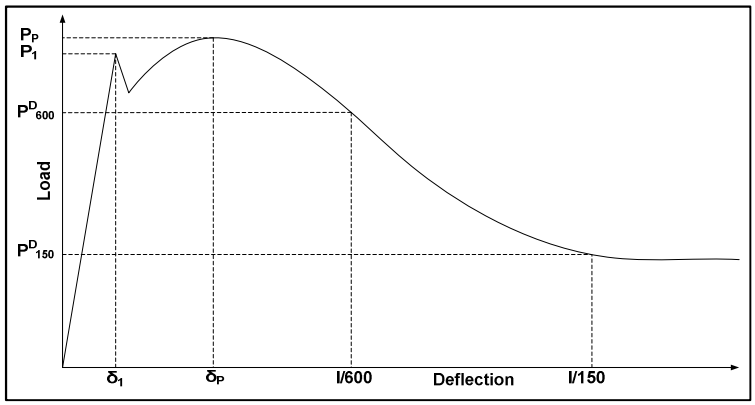

Figure 2.30: Parameter calculation for residual strength

2.3.2.3 Equivalent flexural strength ratio

The equivalent flexural strength ratio is a measure of toughness as a fraction of the first-peak strength or MOR as described by the American Society for Testing and Materials (2012). The toughness, T^D_{150} is defined as the area below the load-deflection diagram up to a deflection of span/150 in Joule. The equivalent flexural strength ratio ($R^D_{T,150}$) for four point bending is expressed as a percentage according to:

$$R^D{}_{T,150} = \frac{150T^D{}_{150}}{MOR \times bh^2} \times 100\% \tag{2.11}$$

2.3.2.4 Average residual-strength

The average residual-strength (ARS) is determined according to ASTM C1399 (2010). The method provides a quantitative measure and comparative analysis among FRC beams. 100 x 100 x 350 mm beams are to be tested in a third-point loading configuration spanning 300 mm and placed onto a 12 x 100 x 350 mm steel plate and loaded up to a central deflection of 0.2 mm which, when reached, the specimen must have cracked (blue curve Figure 2.31). Cracked beams are reloaded without the aid of the steel plate at the tension surface producing a reloading curve (red curve Figure 2.31). The ARS is then calculated using the loads determined at reloading curve deflections of 0.50, 0.75, 1.00 and 1.25 mm according to:

$$ARS = \frac{(P_A+P_B+P_C+P_D)}{4} \times \frac{l}{bh^2} \quad (2.12)$$

with P_A, P_B, P_C and P_D the beam loads at central deflections of 0.5, 0.75, 1.00 and 1.25 mm respectively.

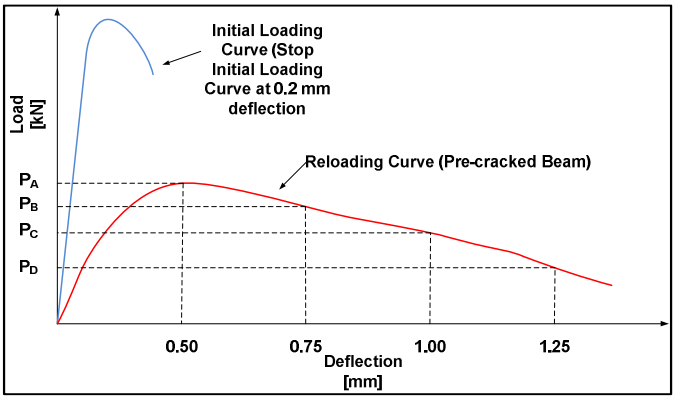

Figure 2.31: Load-deflection curve (ASTM C1399, 2010)

2.3.2.5 Significant research

Soutsos et al. (2012) performed research on the flexural performance of fibre reinforced concrete made with steel and macro polyolefin fibres. The flexural strength, post-cracking ductility and toughness performance of the fibres were investigated at different fibre contents. The type of fibres used and dosages are shown in Table 2.6. Additionally, steel fibres having different profile shapes were used as depicted in Figure 2.32a.

Table 2.6: Description of fibres used by Soutsos et al. (2012)

Name	Type	Dosage [kg/m^3]
HE 60	Steel	30/40/50
WP 60	Steel	30/40/50
WP 50	Steel	30/40/50
FE 50	Steel	30/40/50
S	Synthetic	4.6/5.3

It was found that the incorporation of fibres (steel and synthetic) did not significantly increase the flexural strength of the fibre reinforced concrete specimens tested in four point bending (Soutsos et al., 2012). It was rather determined that one benefit of introducing fibres into concrete is the improved ductility in the post-cracking region. Synthetic fibres at a dosage of 4.6 kg/m^3 and 5.3 kg/m^3 had comparable flexural toughness values to certain steel fibres (WP50 and FE50) at a dosage of 30 kg/m^3 and 50 kg/m^3 respectively, as shown in Figure 2.32b. In addition, macro synthetic fibres could be a better solution for light weight concrete structures, provide higher corrosion resistance as opposed to steel fibres, as well as high impact and abrasion performance (Hasan et al., 2011).

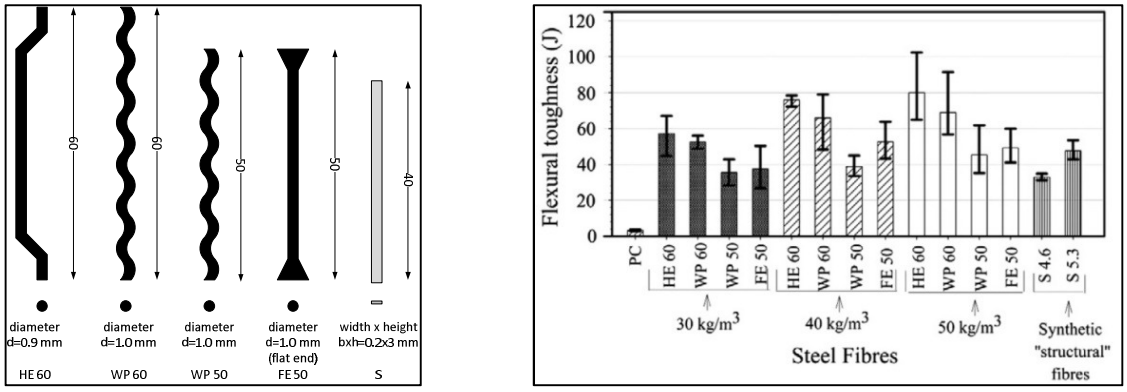

Figure 2.32: Steel and synthetic fibres used with corresponding flexural toughness (Soutsos et al., 2012)

2.3.3 Round determinate panel test

Round determinate panel (RDP) tests are performed according to ASTM C1550-12 (2012). The test method provides a good representation of the post-crack behaviour of beam/slab-like, structural FRC members.

2.3.3.1 Test setup

The setup consists of FRC specimens with an overall diameter of 800 mm and a thickness of 75 mm, supported on three symmetrically arranged pivots about the circumference. The panels are subjected to a centrally applied load up to a deflection of 40 mm in the centre. In response to the applied point load, such panels experience bi-axial bending and therefore exhibit a mode of failure similar to that of in situ conditions (ASTM C1550-12, 2012).

A successfully tested panel will develop at least three radial cracks as a result of the centrally applied point load as shown in Figure 2.33a. Specimens failing in a beam-like mode with a single crack are discarded and characterised by low energy absorption.

A schematic configuration of the RDP test is illustrated in Figure 2.33b.

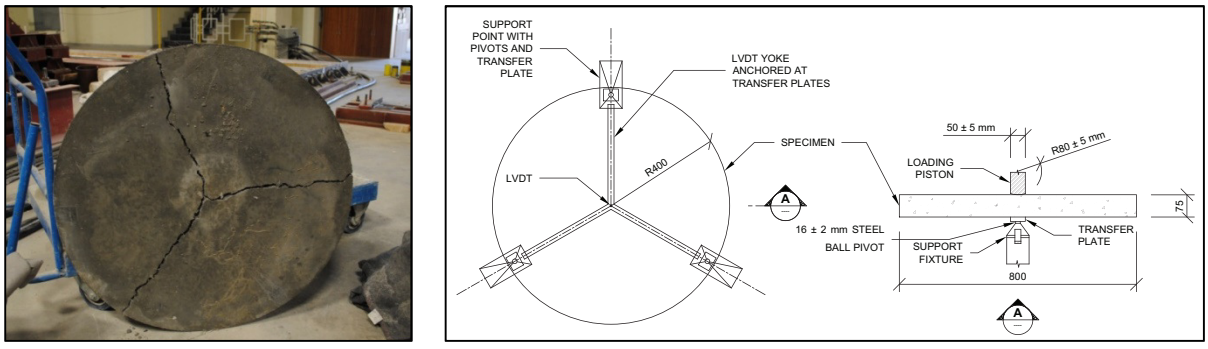

Figure 2.33: Valid crack pattern of RDP test with radial cracks (a) schematisation of RDP test setup (b)

2.3.3.2 Typical round determinate panel test output

The typical load-deflection response exhibited by three FRC RDP test specimens is shown in Figure 2.34a. The performance of the RDP test is quantified as the area under the load-deflection response, representative for the toughness or energy dissipated by panels up to a central deflection of 40 mm. The failure mode experienced by RDP specimens is that of three radial cracks developing at the tension face, originating at the position of load application. Therefore, the crack plane area is relatively large in contrast to that exhibited by a TPB beam specimen, being 3 x radius x thickness (90,000 mm^2). Thus, significantly more fibres bridge the crack plane resulting in less result scatter as depicted in Figure 2.34a. Additionally, the elastic portion of the load-deflection response is highlighted in Figure 2.34b.

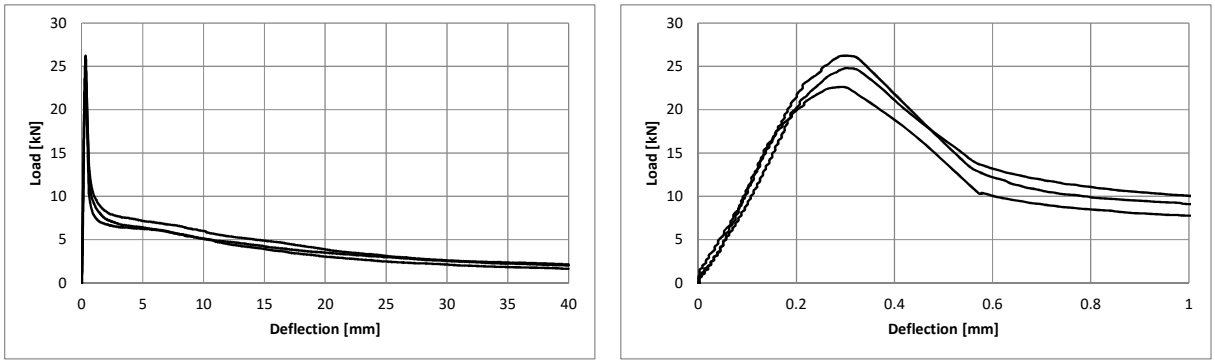

a) b)

Figure 2.34: Typical output obtained by RDP experiments (a) and discernible elastic portion of the load-deflection response (b)

2.3.3.3 Energy dissipation

The energy dissipation (in Joule) of the fibres bridging the crack plane can be determined by integrating the load-deflection curve in the post peak region up to a central deflection of 40 mm. Two energy absorption regions can be identified as the energy absorbed by concrete (blue region Figure 2.35) and the energy absorbed by the fibres (red region Figure 2.35).

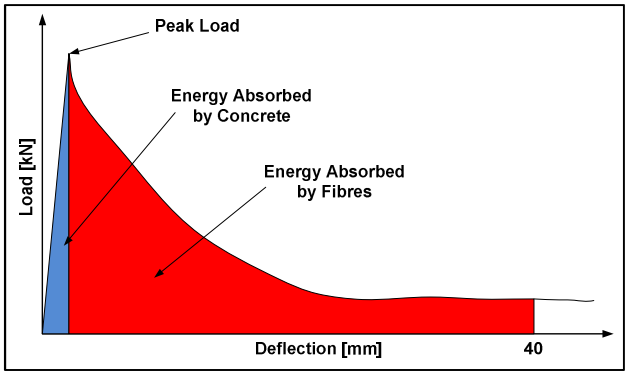

Figure 2.35: Energy dissipation regions of FRC for RDP test

For averaged thickness and diameter RDP measurements, differing from 75 and 800 mm respectively, ASTM C1550-12 (2012) recommends the following adjustments to the peak flexural load and energy dissipation:

$$P = P' \left(\frac{t_0}{t}\right)^2 \left(\frac{d_0}{d}\right) \tag{2.13}$$

$$W = W' \left(\frac{t_0}{t}\right)^{\beta} \left(\frac{d_0}{d}\right) \tag{2.14}$$

with

P = corrected load

P' = measured load

t = measured average panel thickness

t_0 = nominal panel thickness (75 mm)

d = measured average panel diameter

d_0 = nominal panel diameter (800 mm)

W = corrected energy absorption

W' = measured energy

δ = central deflection at which energy dissipation is measured

β = 2.0 – (δ-05.)/80

2.3.3.4 Test invalidity

A valid RDP test set consists of three panels of which at least two successful tests are required. Test specimens exhibiting different failure modes to that of at least three radial cracks as demonstrated in Figure 2.33a are discarded. The failure mode of a single crack across the specimen is regarded as a beam-like failure mode and is characterised by low energy absorption. A beam-like failed specimen is shown in Figure 2.36a.

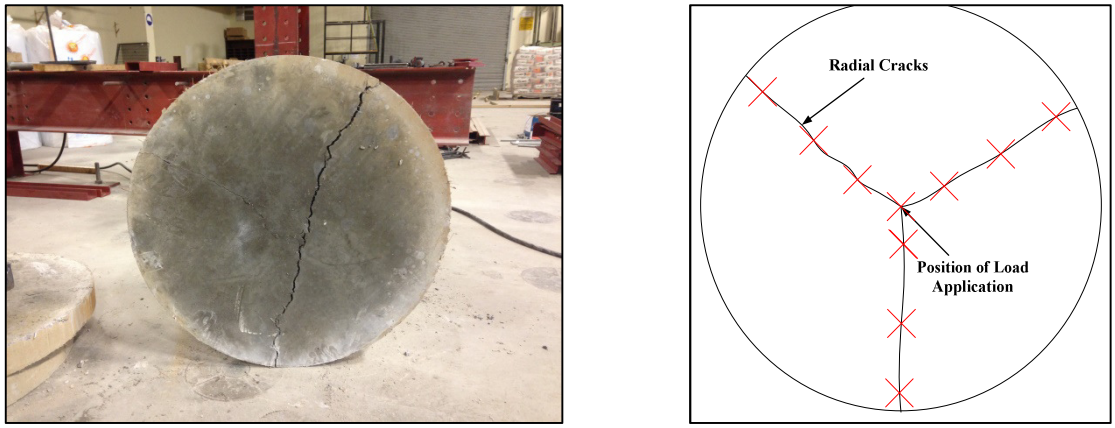

Figure 2.36: Beam-like failure mode of RDP specimen (a) positions of specimen thickness measurement (b)

In addition, ASTM C1550-12 (2012) stipulates that the average of ten individual thickness measurements along the radial cracks formed during testing, as indicated by the red "Xs" in Figure 2.36b, must fall within the limit of 75 -5/+15 mm. Moreover, the standard deviation of the ten thickness measurements is limited to 3 mm. Specimens not conforming to these limits must be excluded from the test set.

2.3.3.5 Significant research

Martin et al. (2011) performed research on the use of fibre reinforced shotcrete in weak rock mines with the objective of reducing fatalities and injuries resulting from rock fall accidents. The fibres used in the study included steel fibres with a length of 40 mm at a dosage of 44.5 kg/m^3 as well as synthetic fibres with a length of 50 mm at a dosage of 4.15 kg/m^3.

Round determinate panel (RDP) tests were performed in order to determine peak and residual loads as well as the corresponding toughness and energy absorption. Martin et al. (2011) found that the type of fibre did not appear to significantly affect the peak load value. As the shotcrete cured for 28 days, the toughness increased considerably compared to earlier curing times. This may indicate that fibres interlock better in the matrix as the shotcrete ages, as shown in Figure 2.37.

Furthermore, the RDP tests for the steel fibre reinforced shotcrete produce more uniform results compared to synthetic fibre reinforced shotcrete. While the peak flexural load generally increased with curing time, the residual load for a given deflection varied depending on the curing age. As for synthetic fibre reinforced shotcrete, the failure appears more brittle with increased curing time. Therefore the post-cracking load that the synthetic fibre reinforced shotcrete was able to support decreased with increasing curing time (Martin

et al., 2011). The authors however acknowledge that the two sets of data curves shown in Figure 2.37a and Figure 2.37b demonstrate the quality control issues associated with different types of shotcrete mixes.

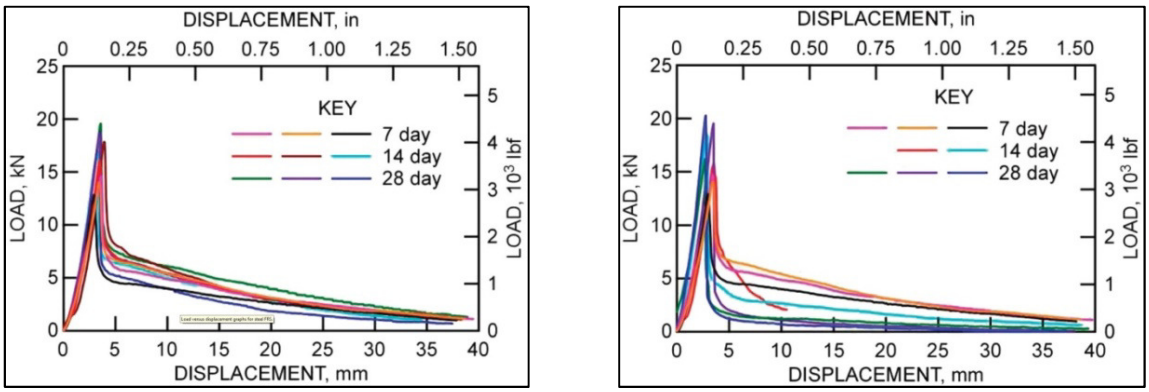

Figure 2.37: Load displacement response of steel (a) and synthetic (b) FRC (Martin et al., 2011)

2.3.4 Square panel test

The three-point bending test on a square panel for testing sprayed concrete is recommended by EFNARC (2011). This test method provides the performance of fibre reinforced shotcrete in terms of residual strengths at specific crack mouth opening displacements.

2.3.4.1 Test setup

The setup for the square panel test consists of a square panel measuring 600 x 600 x 100 mm, simply supported by two parallel rollers 500 mm apart. A load at a rate of 0.2 mm/min is applied along the centre of the panel through a roller up to a CMOD of not less than 5 mm. The test specimen is furthermore notched on the tension surface below the load applying roller in order to control the position of crack propagation. The schematic test setup is shown in Figure 2.38.

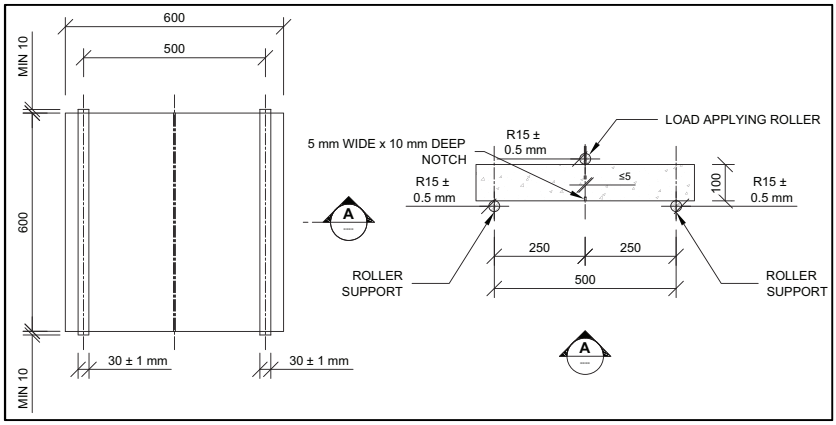

Figure 2.38: Schematisation of a square panel test setup

2.3.4.2 Residual flexural tensile strength

The performance of fibre reinforced shotcrete panels, according to the panel test recommended by EFNARC (2011), is determined in terms of residual flexural tensile strength (RFTS) corresponding to a CMOD of 0.63, 1.89, 3.16 and 4.42 mm respectively (see Figure 2.39). The RFTS ($f_{R,j}$) is given by:

$$f_{R,j} = \frac{3F_j l}{2bh_{sp}^2} \tag{2.15}$$

with F_j the load corresponding to a specific CMOD as shown in Figure 2.39 and h_{sp} the panel height excluding the notch.

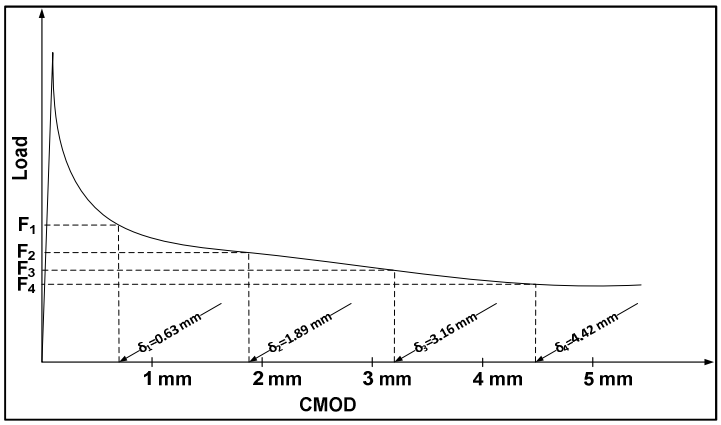

Figure 2.39: Load-CMOD diagram for EFNARC square panel test

2.3.5 Correlation between test methods

As numerous test methods to evaluate the performance of FRC exist, research has been conducted in order to assess the correlation between these methods.

2.3.5.1 Correlation between panel tests

Bernard (2002) performed research on the correlation between the RDP test and square panel test proposed by EFNARC (1996). It was concluded that the results of the two test methods are largely inter-changeable in the post-cracking region, as a linear relationship with an R^2 value of 0.9 was observed (see Figure 2.40). The strong correlation suggests that both panel tests would be a suitable choice in determining the post-crack performance under severe deformations.

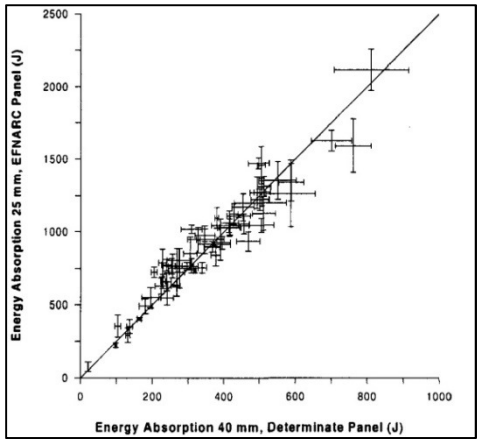

Figure 2.40: Correlation between panel tests (Bernard, 2002)

2.3.5.2 Correlation between beam and panel tests

The research done by Bernard (2002) concluded that a good correlation exists between beam and panel performance parameters at similar crack widths as shown in Figure 2.41a.

Parmentier et al. (2008) conducted research on the correlation between the RDP test and the three-point bending test proposed by RILEM (2003) for different fibre types (steel and synthetic fibres). The obtained test data for only steel fibres appears to be very promising with an R^2 value of 0.99 for the same level of deflection/cracking as shown in Figure 2.41b. However, the question whether the correlation can be attributed to the fibre type or the fibre dosage is left unanswered. The authors furthermore state that by the inclusion of the synthetic fibre data, the correlation appears less promising.

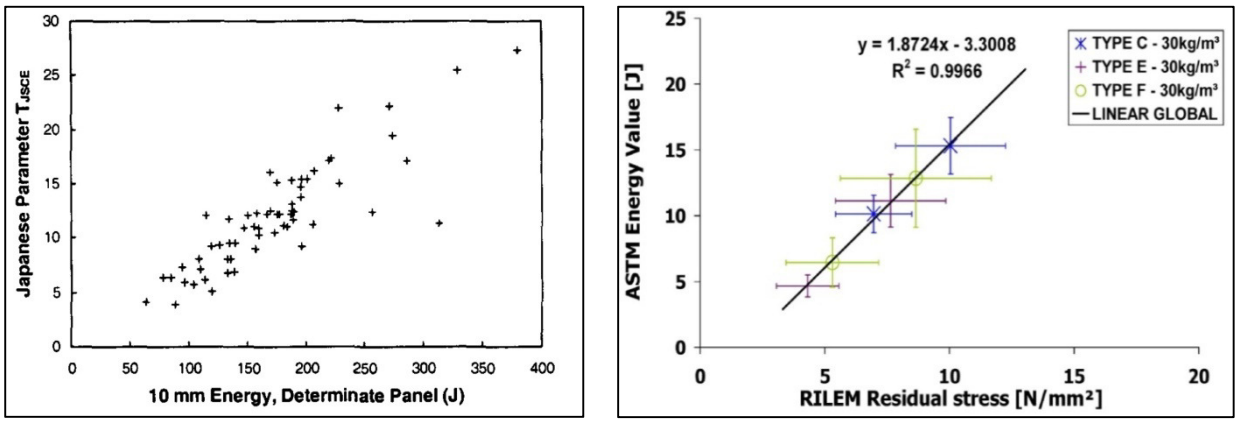

a) b)

Figure 2.41: Correlation between beam and panel parameters at 10 mm central panel deflection (Bernard, 2002) (a) and beam and panel test (Parmentier et al., 2008) (b)

2.4 Time dependent behaviour

The deformation of concrete with time is a consequence of environmental effects such as moisture gain/loss and applied stresses. Kovler (1995) acknowledged that creep and shrinkage are vital factors when durability, serviceability and long-term reliability aspects of

concrete are discussed. While creep is a function of sustained stress, shrinkage is independent of stress and rather a time dependent volume change primarily caused by the movement of water in both fresh and hardened concrete states (Neville, 1996).

Creep is the time dependent deformation of concrete under a sustained load. The bulk concrete response to a sustained stress is depicted in Figure 2.42. When concrete is exposed to a constant load, it undergoes an instantaneous deformation within the elastic range of the material, followed by primary creep. The rate, at which the creep deformation is experienced, decreases in due course. Upon unloading an immediate elastic strain recovery is experienced, often less than the initial strain on loading as the modulus of elasticity of concrete increases with time (Babafemi, 2015; Domone & Illston, 2010). This is followed by a time dependent creep recovery, which is less than the creep strain experienced on loading. A permanent residual deformation will remain as a result. Creep strains can be of higher magnitude than the elastic strain on loading, and can therefore have a highly significant influence on the structural behaviour of concrete.

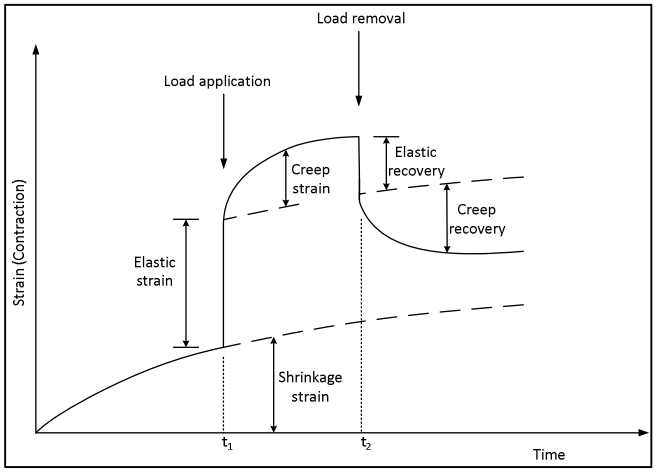

Figure 2.42: Response of concrete to a compressive stress applied (Domone & Illston, 2010)

In contrast to creep of concrete, much remains unknown about creep of FRC, especially with the focus on macro synthetic fibre reinforcement. While the effect of fibres is only triggered upon crack formation, attention should be devoted towards creep of the cracked FRC state. According to Richardson et al. (2010) the structural use of synthetic fibres is governed by the low value elastic modulus of polypropylene producing a tendency for the material to creep under a tensile load, which is a quality not desired when structural performance is required. To date, there seems to be no design code addressing the potential issue that is related to creep of cracked FRC (Babafemi, 2015).

2.4.1 Uni-axial tensile creep

Babafemi & Boshoff (2014) investigated the time dependent behaviour of fibre reinforced concrete under sustained loading. Investigations were performed on the time dependent behaviour of pre-cracked macro synthetic fibre reinforced concrete specimens subjected to uni-axial tensile sustained loading.

The fibres used in the study were polypropylene macro fibres with an "X" shaped cross-section and slightly crimped profile of 40 mm length and 0.8 mm equivalent diameter. The uni-axial tensile creep test was performed on specimens measuring 100 x 100 x 500 mm loaded in creep frames. The load was applied at different stress levels based on 30, 40, 50, 60 and 70 percent of the average residual tensile strength determined from uni-axial tensile tests. All specimens were pre-cracked to an average residual crack width of 0.5 mm to simulate the in-service fibre behaviour. It was observed that as soon as the specimens cracked on reaching their peak ultimate load, the stress dropped leading to extensive crack opening that could be attributed to the low stiffness of the fibres compared to the concrete matrix (Babafemi & Boshoff, 2014).

As specimens were unsealed, drying shrinkage was measured separately on two load-free specimens and subtracted from the total creep deformation. Material creep of the concrete matrix was neglected as it is insignificant (Babafemi & Boshoff, 2014).

Babafemi & Boshoff (2014) identified significant crack widening over time under sustained loading. This was even the case for low levels of applied stresses, based on the residual post-cracking tensile strength. Furthermore, variability in the results was observed for the crack mouth opening displacement of each specimen. The average visible fibre count on both surfaces adjacent to the crack was determined. It was established that the more fibres on the cracked plane, the lesser the time dependent crack widening.

Furthermore, it was determined that the mechanisms causing the continuous crack-widening of the macro synthetic fibre reinforced specimens subjected to uni-axial tensile sustained loads, can be attributed to fibre pull-out as well as fibre creep (Babafemi & Boshoff, 2014). Crack widening was still observed after 8 months of sustained loading at the lowest applied load as shown in Figure 2.43.

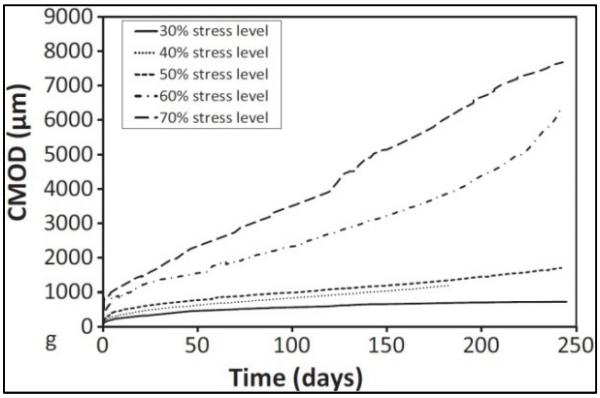

Figure 2.43: Time dependent response of cracked uni-axial tensile loaded specimens (Babafemi & Boshoff, 2014)

2.4.2 Flexural creep

Gossla & Rieder (2009) performed research on long-term load tests on pre-cracked macro synthetic fibre reinforced concrete beams measured to the load level above which creep failure occurred. The objective of the study was to experimentally determine the time dependent deformation behaviour on material and component level quantitatively. Concrete beams of dimensions 150 x 150 x 450 mm with a fibre content of 4.5 kg/m^3 were tested in four-point bending. Creep of fibre reinforced concrete beams is influenced by different creep characteristics, being:

- Creep of the concrete matrix in the tensile and compression zone.
- Creep of the fibre filament bridging the crack as well as the pull-out creep between the fibre and the concrete interface.

The pre-cracked beams were loaded at different fractions of the service load level to determine the time until creep failure occurs. The beam specimens were pre-cracked to a crack width of 4.5 mm. Sustained flexural loads at load levels of 58 % did not cause flexural creep failure at the time of research publishing, but are expected to cause failure after about 2 years, as shown in Figure 2.44. Specimens loaded to around 60 % typically failed within 3 months to 2 years. Only beam specimens loaded to 70 % of the in-service load in the cracked condition failed within a few hours or days (Gossla & Rieder, 2009).

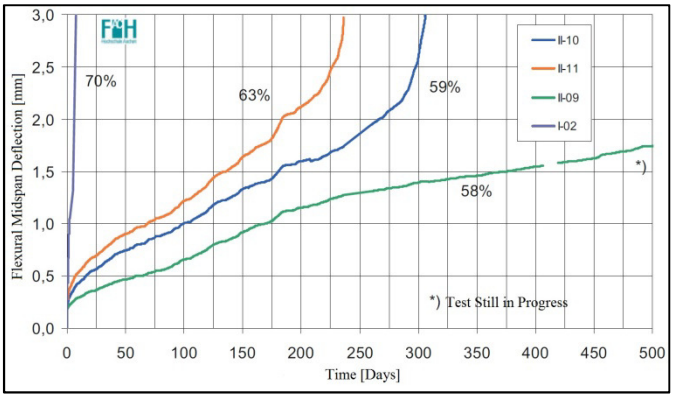

Figure 2.44: Results of the long term flexural load tests of cracked FRC (Gossla & Rieder, 2009)

2.4.3 Single-fibre creep

Creep of single macro synthetic fibres is believed to be one of the mechanisms causing time dependent crack widening (Babafemi & Boshoff, 2014). A single macro synthetic fibre was subjected to a sustained tensile load of 30 % of the fibres capacity. It was observed that the fibre elongated with up to 40 % after 4 days. It is thus clear that fibre creep contributes to the time dependent crack opening of the uni-axial tensile creep test.

2.4.4 Time dependent single-fibre pull-out

Time dependent single-fibre pull-out experiments are used to understand the mechanisms causing time dependent crack widening on the mesoscopic scale. In concrete embedded single fibres are subjected to a sustained load, and thus undergoing pull-out. However, according to (Mouton & Boshoff, 2012), the test is not a true reflection of the actual creep, as fibres are orientated randomly at different angles within the cracked plane.

2.4.4.1 Typical time dependent response of single fibres subjected to sustained loads

The typical test output obtained for the TDPO test is shown in Figure 2.45. Figure 2.45a includes elastic fibre elongation which occurs directly upon loading and can therefore be regarded as instantaneous fibre elongation, not contributing to the time dependent pull-out. The instantaneous fibre elongation is governed by two mechanisms, namely the instantaneous fibre elongation as a result of free length and instantaneous fibre elongation within the embedded length. Ideally, the instantaneous fibre elongation caused by the free length should be equal to zero which is achieved by gripping the fibre at the exact position of exposure from the hardened paste matrix surface.

In order to investigate the time dependent crack widening, the instantaneous fibre elongation is subtracted from the displacement readings as shown in Figure 2.45b. However, due to the

occurrence of time dependent fibre pull-out, free length becomes available. Therefore, time dependent crack widening is also a function of non-instantaneous elastic fibre elongation.

The instantaneous fibre elongation (u), of the free length can be calculated according to Hooke's law:

$$u = \frac{F \times L_{free}}{A \times E} \tag{2.16}$$

with

F = applied load

L_{free} = available free length

A = cross-sectional fibre area

E = modulus of elasticity of the fibre material

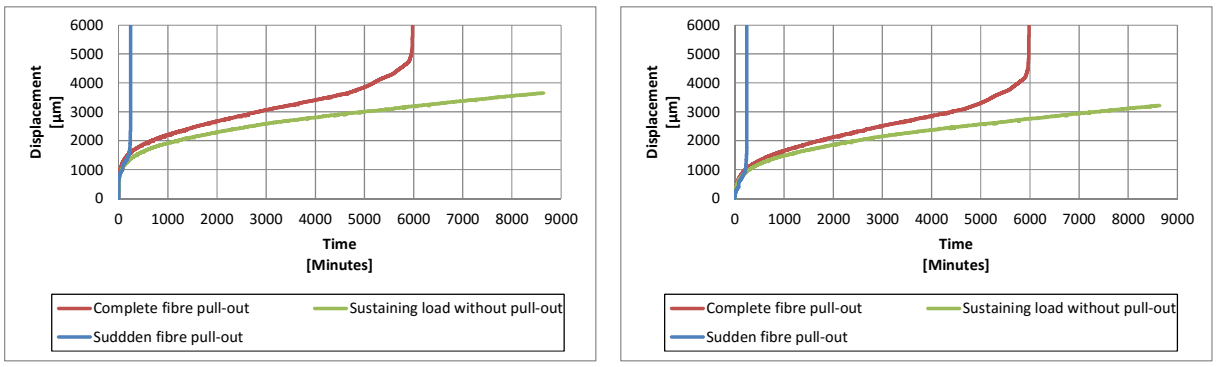

a) **b)**

Figure 2.45: Time dependent single-fibre pull-out response including (a) and excluding (b) instantaneous fibre elongation

Time dependent fibre pull-out tests on macro synthetic fibres were conducted by Babafemi & Boshoff (2014) in order to understand the mechanism causing creep in pre-cracked uni-axial loaded specimens. Free hanging loads were applied to individual fibres embedded 25 mm in the concrete matrix. The chosen sustained loads were between 50 and 80 % of the average interfacial shear stress, determined from the force reading from single-fibre pull-out tests. The time dependent pull-out was observed optically with the aid of a microscope. All fibres experienced complete pull-out within less than a week as shown in Figure 2.46.

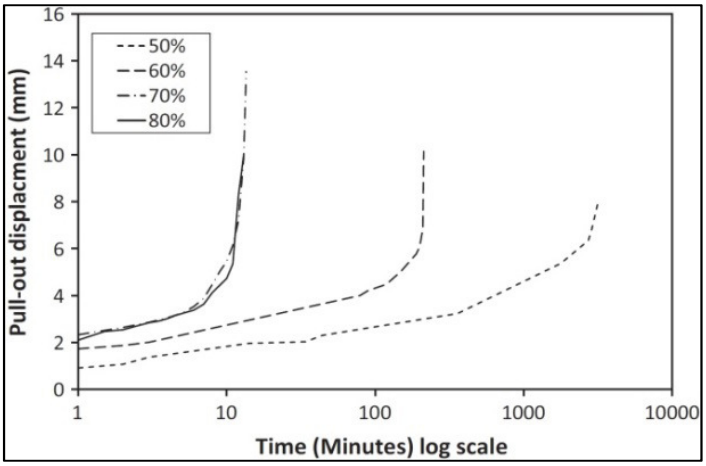

Figure 2.46: Tensile loaded single fibres for various levels of loading (Babafemi & Boshoff, 2014)

It was reported by Babafemi & Boshoff (2014) that the crack width increase determined by the uni-axial tensile creep test can be partially attributed to the fibre pull-out from the concrete matrix. Additionally, it was determined that the fibre pull-out rate increases with higher sustained loads.

2.5 Inherent Shortcomings of Fibre Reinforced Concrete

Random fibre orientation in the three-dimensional concrete matrix space is regarded as waste of material, since a small percentage of the introduced fibres align with the tensile stresses induced during cracking. Thus, only fibres aligned perpendicular to the crack, and therefore parallel to the induced tensile stresses are optimal efficient (Hannant, 1978). Furthermore, the fibre location across a propagated crack highly influences the fibre efficiency. The highest efficiency is attained as the crack passes through the centre of a fibre aligned perpendicular to the crack, while low efficiency is achieved as the crack passes near the fibre end.

Additionally, fibre pull-out is the anticipated mode of failure when post-cracking toughness is of interest. Thus, the post-cracking toughness of FRC is governed by the bond mechanism of the fibre during pull-out, rather than the parent material of the fibre. Therefore, the full potential of the fibre material is not exploited, as would be the case during fibre rupture (Hannant, 1978).

Furthermore, Babafemi (2015) and Gossla & Rieder (2009) reported on concerning time dependant behaviour of cracked FRC, without any design guidelines addressing the issue of creep, as highlighted in Section 2.4.

2.6 Concluding Summary

The use of fibre reinforcement is said to date back to 1540 (ACI Committee 544, 2002). While several works have been published on the use of fibre reinforcement, still much remains unknown about the mechanisms and behaviour of macro synthetic fibre reinforced concrete (FRC). Furthermore, numerous test methods are available to quantify its performance. Especially the three-point bending test enjoys popularity due to its useful design parameter. In addition, the round determinate panel test provides a good indication on the flexural toughness of FRC for larger crack openings.

Little is known about the time dependent behaviour of macro synthetic FRC. To date no design standard addresses the issue of creep for FRC. Researchers have determined concerning time dependent behaviour of macro synthetic FRC under uni-axial sustained loading conditions.

Nevertheless, the popularity of macro synthetic fibres for use in concrete increases, and is said to presumably replace conventional steel reinforcement in the form of welded steel mesh. Therefore an increasing demand for use of macro synthetic FRC in the industry exists with a potential to simplify construction site operations and lower construction- and overall building costs.

CHAPTER 3
Investigation on the Single-Fibre Level

The performance of macro synthetic fibre reinforced concrete (FRC) is greatly influenced by the geometry of the fibres (Kim et al., 2011; Domone & Illston, 2010). It is therefore necessary to investigate the effect of fibre geometry with regard to the length and profile on the single-fibre level.

Single-fibre pull-out (SFPO) experiments provide information on geometrical properties responsible for good fibre performance. Parameters of interest measurable from the SFPO response are the interfacial bond resisting fibre pull-out as well as the energy dissipated by individual fibres.

Another important performance criteria which is dependent on the geometrical properties of macro synthetic fibres, is the time dependent behaviour. Single fibres subjected to sustained uni-axial loads provide an indication for the time dependent crack widening that may be exhibited by macro synthetic FRC under in-service conditions.

This chapter provides information on the materials, as well as macro synthetic fibres used for this research. Additionally, the experimental framework adopted for the investigation on the single-fibre level is described in detail. Special attention is focused on specimen preparation and test approach used for SFPO and TDPO experiments.

3.1 FRC Materials

This section provides information on the materials used during the course of this research. The materials described are the main constituent materials used in FRC concrete, namely cement, fine/coarse aggregate, water as well as macro synthetic fibres.

3.1.1 Macro synthetic fibres

The macro synthetic fibres used in this study were either propylene or modified olefin material based monofilament fibres. Regardless of their parent material, the specific gravity of all the fibres was taken as 0.91, which is in agreement with the specified range provided by suppliers.

Equivalent fibre diameters or number of fibres per kilogram (rounded to the nearest 100) were typically supplied. However, supplied values proved not to be very accurate, and equivalent diameters were rather determined using Equation (2.3). Based on the parameters required for the calculation of the equivalent fibre diameter, 30 fibres in accordance with EN 14889-2 (2006) were weighed using a scale with a resolution of 1/10,000 gram.

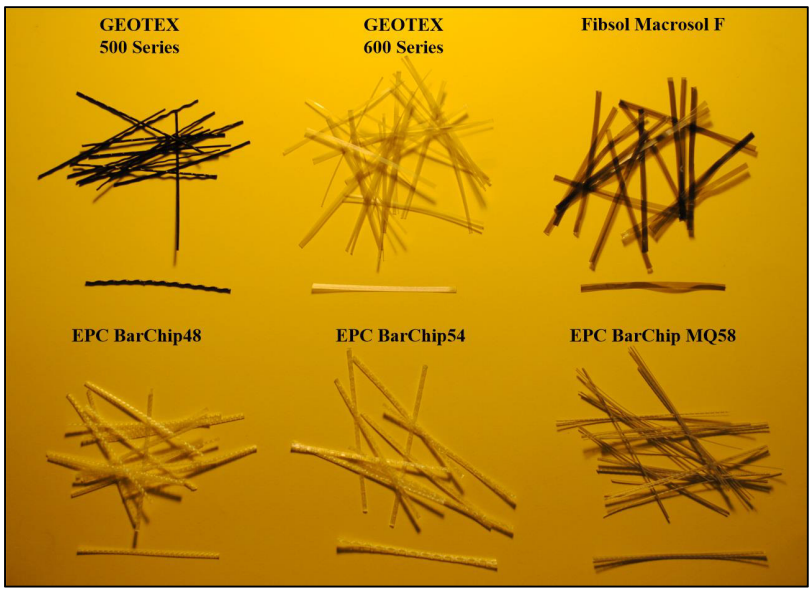

Figure 3.1: Macro synthetic fibres considered for single-fibre pull-out test

Table 3.1 provides an overview of the fibre characteristics, including labels used for designating the various macro synthetic fibres. Additionally, the fibre aspect ratio (λ_f) has been included, which is defined as:

$$\lambda_f = \frac{l_f}{d_{eq}} \tag{3.1}$$

with l_f and d_{eq} the fibre length and equivalent diameter respectively.

Table 3.1: Characteristics of fibres used for single-fibre pull-out tests

Fibre	Label	Length [mm]	Fibre Material	Specific Gravity	Tensile Strength [MPa]	Modulus of Elasticity [GPa]	d_{eq} calculated [mm]	λ_f calculated	Type	Deformation
GEOTEX 500 Series[1]	C1	50	Polypropylene	0.88-0.92	405	1.62-2.7	0.74	67.6	Round	Crimped
GEOTEX 600 Series[1]	F1	50	Polypropylene	0.88-0.92	450	1.8-3.0	0.64	78.1	Flat	Corrugated (both sides)
Fibsol Macrosol F[1]	F2	50	Polypropylene	0.91	400	1.6-2.67	0.60	83.3	Flat	Corrugated (one side only)
EPC BarChip48	E1	48	Modified Olefin	0.90-0.92	640	10.0	0.71	67.6	Irregular	Embossed
EPC BarChip54	E2	54	Modified Olefin	0.90-0.92	640	10.0	0.85	63.5	Irregular	Embossed
EPC BarChip MQ58	EB1	58	Modified Olefin	0.90-0.92	620	> 7.0	0.68	85.3	Irregular	Embossed/bundled

[1] Modulus of elasticity based on the tensile strength and elongation at yield between 15 and 25% as specified by suppliers

3.1.2 Concrete constituents

Portland composite cement CEM II/A-L 52.5 N, with an addition of 6-20 % limestone extender and a specific gravity of 3.14, supplied by Pretoria Portland Cement, was used for the investigation. The cement complied with SANS 50197-1 (2000).

Fine natural siliceous pit sand with a good particle shape and continuous grading was used as filler. The sand commonly known as fine Malmesbury sand with a specific gravity of 2.64, determined in accordance with SANS 5844 (2006), was used throughout the course of this research. Four different batches of sand were used due to storage limitations. The grading curves, determined in accordance with SANS 1083 (2006), are shown in Figure 3.2. Based on the grading similarity, results were expected not to be influenced by the different batches of sand used.

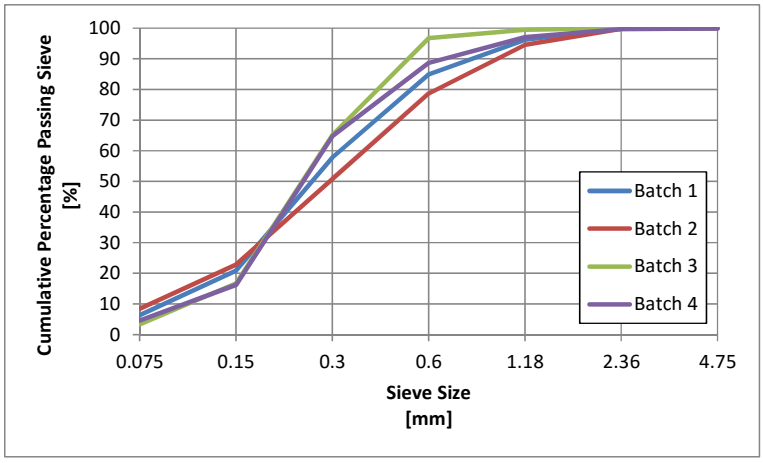

Figure 3.2: Sand grading according to SANS 1083 (2006)

The fineness modulus of the different batches is shown in Table 3.2

Table 3.2: Fineness moduli of different sand batches

Batch no.	Fineness moduli
1	1.40
2	1.54
3	1.22
4	1.34

It is important to note that only sand from batch three was used for the investigation on the single-fibre level.

The coarse aggregate which was used throughout the duration of this research is commonly known as Malmesbury shale or Greywacke stone, and is characterised by its grey colour and angular shape. The nominal size of the used aggregate was 13.2 mm with the properties shown in Table 3.3.

Table 3.3: Coarse aggregate properties

Property	Value	Conformity
Loose bulk density	1470 kg/m^3	SANS 5845 (2006)
Compacted bulk density	1560 kg/m^3	SANS 5845 (2006)
Specific gravity	2.77	SANS 5844 (2006)
Aggregate crushing value	13.2 %	SANS 5841 (2006)

Potable mixing water supplied by the local municipality was used.

No chemical admixtures were used in order to eliminate additional sources of variability.

3.2 Concrete Mix Proportion and Consistency

A concrete mix was designed using the materials described in Section 3.1 according to the C&CI method (Addis & Goodman, 2009) derived from ACI 211.1-91 (1999). A water-binder ratio of 0.64 yielding a 28 day target compressive strength of approximately 38.2 MPa (30 MPa characteristic strength) was chosen. Fibres were added at 4 kg/m^3 to the concrete mix corresponding to a volume fraction (V_f) of 0.44 % of macro synthetic fibres. It is important to note that the fine and coarse aggregate proportions were slightly adjusted in order to achieve the desired workability .The adjusted concrete mix proportions are depicted in Table 3.4.

Table 3.4: Concrete mix design proportioning

Constituent	Mass [kg/m^3]	Specific gravity	Volume [m^3]
Cement	318.6	3.14	101.5
Water	204.1	1.0	204.1
Stone	995.6	2.77	359.4
Sand	872.9	2.64	330.6
Fibre	4	0.91	4.4
Total	**2395.1**		**1000**

In order to ease the use and handling of the macro synthetic FRC in its fresh state, sufficient workability was required. A slump in accordance with SANS 5862-1 (2006) of 120 mm without the addition of fibres was aimed for, while a slump of ± 75 mm including macro synthetic fibres was targeted.

Standard 100 x 100 x 100 mm cube moulds conforming to SANS 5860 (2006) were prepared according to SANS 5861-3 (2006) for testing the compressive strength of different concrete batches as a measure of consistency in the hardened state.

According to SANS 5861-3 (2006), all control cubes were cured for 28 days in water tanks with a water temperature of 25°C.

Compressive control tests were performed in accordance with SANS 5863 (2006) using a Contest material testing machine with a capacity of 2000 kN. Individual compression test results for SFPO experiments are documented in Appendix A. The average compressive strength for the concrete mix was 36.6 MPa with a standard deviation of 2.2 MPa (CoV 0.06), while the average compressive strength of the paste only was 37.9 MPa with a standard deviation of 2.9 MPa (CoV 0.08).

3.3 Single-Fibre Pull-Out Experiments

This section provides a comprehensive overview of the adopted methodology used for SFPO experiments.

3.3.1 Specimen preparation, mixing procedure, moulds and curing

Single fibres were embedded either in a virgin or premixed fibre state. Virgin fibre state refers to the original fibre appearance as received by the suppliers, while premixed fibre state refers to the fibre appearance achieved as a result of the mixing process, causing roughening of the fibre surface. It was found that fibres looked somewhat different from their virgin state when added to the concrete and mixed for several minutes. The difference is illustrated in Figure 3.3 for the EPC BC MQ58 macro synthetic fibre as an example.

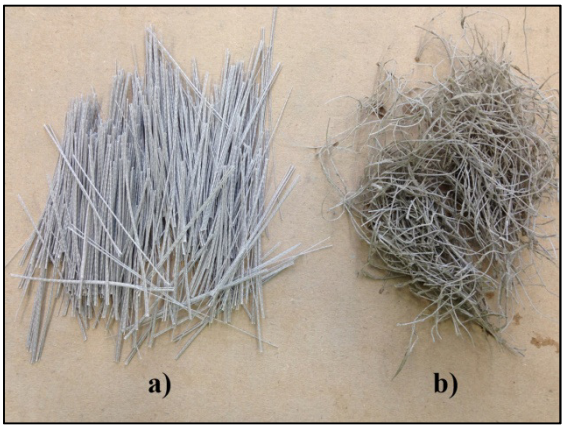

Figure 3.3: Virgin (a) and premixed (b) macro synthetic fibres

Eight specimens containing virgin fibres and twelve specimens containing premixed fibres were prepared in order to account for potential variability in test results caused by the additional surface roughening as a consequence from premixing.

Typical 100 x 100 x 100 mm concrete cube moulds were used and divided using a wooden cross-like separator into four equal compartments measuring 39 x 39 x 100 mm, as shown in Figure 3.4. The wooden separator was coated using PLASCON ROOFSEAL waterproofing

paint in order to eliminate water absorption of the wood. Additionally, the moulds along with the separator were oiled using mould release oil.

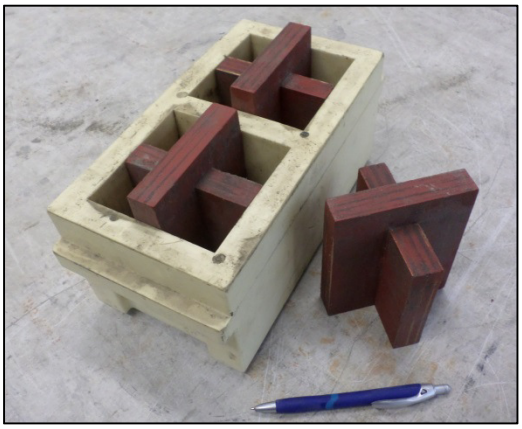

Figure 3.4: Wooden separator

The FRC materials described in Section 3.1 were batched by weight and added to a 50 litre concrete pan mixer in the order of sand, cement, stones. Prior to mixing, the mixer was rinsed with water and dried using industrial tissue paper in order to ensure the same conditions for each mixing batch and eliminate additional water absorption of the pan. The dry materials were mixed for one minute before the mixing water was added, followed by an additional mixing time of five minutes.

Premixed fibres were prepared using a 10 litre concrete pan mixer. The aforementioned mixing procedure was adopted with the addition of fibres after the five minutes of wet mixing. This was followed by an additional five minutes of mixing in order to cause the anticipated fibre roughening as a result of the mixing process. Afterwards, the premixed fibres for the SFPO experiments were rinsed using water with the aim to only retain the roughened (premixed) fibres.

After mixing, a slump test according to SANS 5862-1 (2006) was performed as a measure of consistency as well as to ensure sufficient workability for different concrete batches.

Specimens cast for SFPO tests did not contain any fibres as only the behaviour of a single-fibre was of interest. Single fibres were embedded with great care into the concrete at specific pre-marked embedment lengths. The embedment lengths were taken as 12.5, 25.0 and 37.5 mm as well as half the fibre length for fibres not being 50 mm in length. Fibres were embedded as straight as possible by hand with the aid of visual assessment for straightness from all directions.

The main obstacle was however the insertion of flat and bundled fibres as a result of the low axial stiffness. Non-stiff fibres tend to bend within the paste matrix, resulting in skew embedment. In order to simplify the insertion process, the concrete was sieved using a 2.36 mm sieve to eliminate the stone content. This furthermore had the effect of the fibres being in continuous contact with surrounding paste without stones causing weak spots creating additional possible variability in the test results. The individual fibres were inserted by hand up to a pre-marked embedment length. Depending on the fibre colour, either correction fluid or black ink was used to pre-mark the desired embedment length. In order to embed the fibre exactly in the middle of the 39 x 39 x 100 mm specimen, a piece of flat roof sheeting was slightly stencilled across opposite corners into the fresh paste leaving behind a mark on the paste surface. Moulds were gently vibrated after fibre insertion, in order to ensure a good paste compaction around the fibre. Subsequently, fibres were visually assessed from all sides to ensure orthogonality with the exposed fresh paste surface. The SFPO test specimen as well as a schematisation of the specimen preparation is shown in Figure 3.5. The freshly cast SFPO specimens were left to set for 24 hours before de-moulding.

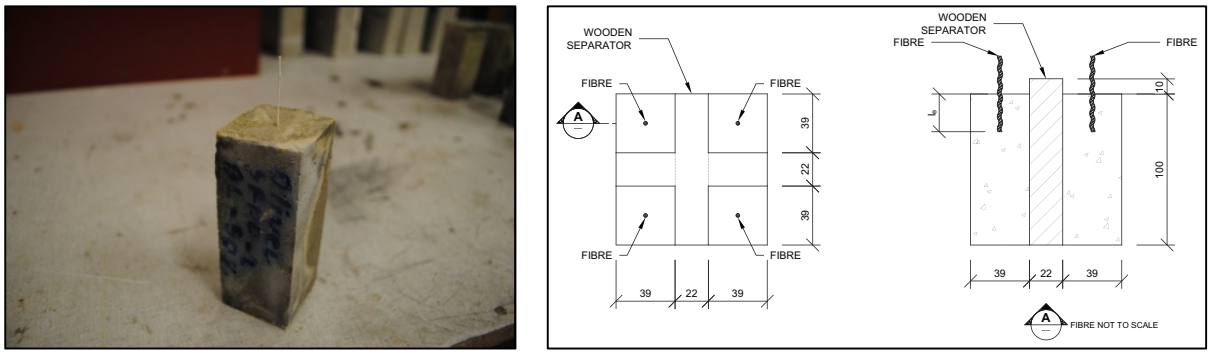

a) b)

Figure 3.5: SFPO specimen (a) and specimen casting scheme (b)

After SFPO specimens were de-moulded, these were transferred to temperature controlled curing tanks with a water temperature of 25°C. All specimens were cured by complete immersion in water and were left to cure for additional 27 days before the preparation for testing. SFPO specimens were prepared for testing shortly after their removal from the curing tanks.

3.3.2 Test setup

The SFPO test was performed using a ZWICK/ROELL Z250 universal materials testing machine with a capacity of 250 kN. The SFPO specimen as well as the gripping system was held in position by means of hydraulic clamps. The fibre-portion protruding from the hardened paste was gripped with the aid of a fibre clamp, consisting of two 40 x 8 mm flat

mild steel bars as shown in Figure 3.6a. The fibre was gripped as close as possible to the hardened paste surface in order to ensure consistency as well as to simulate the in-service behaviour of the fibre i.e. the formation of a crack. Two linear variable displacement transducers (LVDTs) were used on either side of the fibre to measure the pull-out displacement. The average LVDT reading linearly interpolates the true pull-out displacement of the fibre. These had a differential range of 50 mm, allowing sufficient measurement for the maximum embedment length of 37.5 mm. In addition, a load-cell with a capacity of 500 kg was used to record the pull-out force. The SFPO test method was displacement controlled using a crosshead displacement rate of 0.2 mm/s. The SFPO test setup is shown in Figure 3.6b.

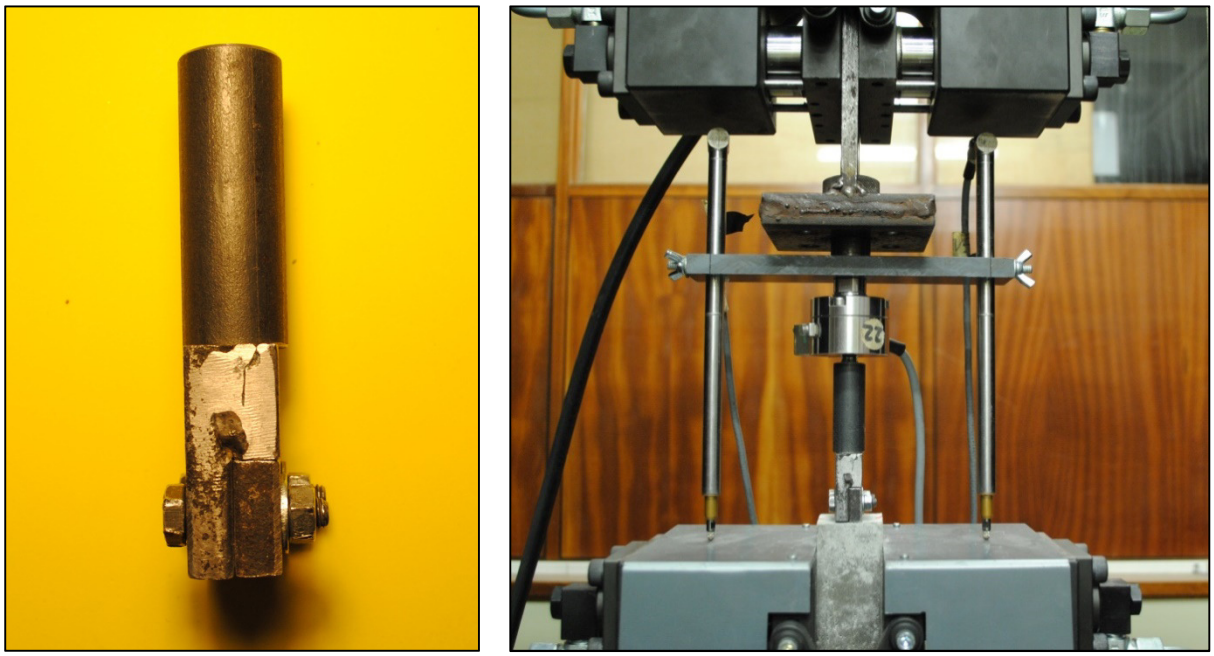

a) b)

Figure 3.6: SFPO experiment fibre grip (a) and setup (b)

The edges of the fibre grip used were rounded in order to avoid sharp edges which potentially could cause premature fibre rupture. Furthermore, it was important to ensure that no fibre slip is permitted by sufficient tightening of the two 6 mm bolts, clamping the two steel bars.

3.4 Time Dependent Pull-Out Experiments

The approach adopted for the TDPO test is discussed in this section, providing information on the specimens and the test setup used.

3.4.1 Specimen preparation

The mixing procedure adopted for TDPO specimen preparation is described in Section 3.3.1. Again, in order to achieve continuous contact between the fibre surface and the surrounding

matrix, stones were eliminated by sieving the concrete using a 2.36 mm sieve to only retain the paste.

The moulds used for the TDPO specimens were standard 100 x 100 x 100 mm cube moulds complying with SANS 5860 (2006). The moulds were filled immediately after mixing and a flat piece of flat roof sheeting was used to identify the middle of the cube. This was done by imprinting the roof sheeting slightly into the paste, leaving behind a visual indent, marking the insertion position of the macro synthetic fibre.

The fibres were pre-marked with either black ink or correction fluid, depending on their colour. The fibres were inserted directly after marking the paste surface in order to eliminate any significant bleed water accumulation and therefore intrusion, causing a potential weak layer around the fibre with a higher water to binder ratio. The investigated embedment length of interest was chosen as half the fibre length, being the maximum fibre length that can be facilitated each side of a formed crack.

The cast specimens were de-moulded after 24 hours and cured in temperature controlled tanks for an additional 26 days at a water temperature of 25°C, followed by one additional day of drip-drying.

Three days prior to testing, the specimens were removed from the curing tanks, and a 10 mm hole was drilled 30 mm deep into the middle of the opposite side of the embedded fibre. The specimen was placed onto a steel channel section with a hole and restraints, in order to prevent fibre damage during the drilling process. The function of the hole was to facilitate a 10 mm threaded bar used to attach the cube to the frame shown in Figure 3.8a. After completion, the specimens were placed into the water tanks for the remaining two days of curing. The 10 mm threaded bars were inserted and glued into the hole using Sikadur®-AP, supplied by Sika, one day prior to testing in order to allow for sufficient setting time of the epoxy. Specimens were placed on wooden blocks with a hole to prevent fibre damage during the insertion process. A steel section angle was used to ensure straight insertion of the threaded bar from all directions as shown in Figure 3.7a. A schematisation of the specimen is shown in Figure 3.7b.

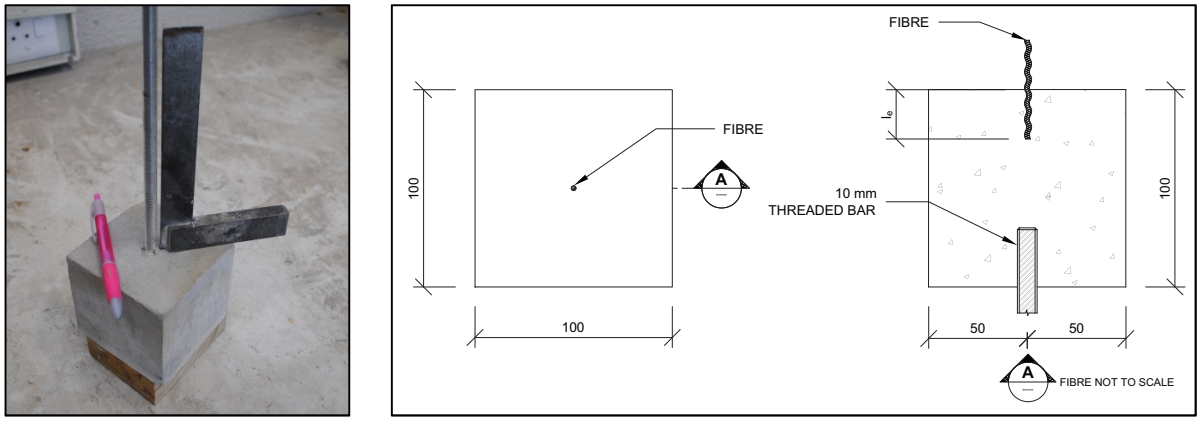

a) b)

Figure 3.7: Threaded bar glued into specimen (a) and specimen schematisation (b)

3.4.2 Test setup

A TDPO experimental test method was developed, automatically measuring the pull-out displacement with the aid of LVDTs. Two HBM Spider8 data acquisition systems were used to log the LVDT displacements. The LVDTs were attached to the 100 x 100 x 100 mm TDPO cube specimen using an aluminium frame as shown in Figure 3.8b. Two LVDTs were used per loaded fibre positioned at opposite sides. A horizontal extension made from Perspex was attached to the bottom of the fibre grip and used as a rest for the tip of the two LVDTs. As the Perspex plate was only attached to the fibre, gradual pull-out allowed the extension of the LVDTs, recording the pull-out displacement.

Due to limitations of sufficient LVDTs with an adequate range for half the embedment length measuring 29 mm at maximum, only 10 mm LVDTs were available. However, 10 mm pull-out, being equivalent to a crack opening of 20 mm, can be regarded as failure of FRC elements.

Due to the low torsional resistance of the macro synthetic fibres, possible fibre twist could have resulted in LVDT sliding with the consequence of the LVDTs slipping off the Perspex rest plate. In order to prevent any torsional rotations, smooth long 6 mm rods were extended from the LVDT support frame through a hole in the Perspex LVDT rest plate, allowing only vertical displacement while preventing any torsional movement of the macro synthetic fibres.

Fabric bags filled with sand bags were attached to steel hooks screwed into the bottom of the fibre grip. The weight of the sand bags (m) was based on 50 % of the average fibre specific peak load determined under SFPO, calculated according to:

$$m = \frac{F_{max}}{g} \tag{3.2}$$

with F_{max} and g the peak pull-out load under SFPO and gravitational acceleration (9.81 m/s^2) on earth respectively.

In addition, the adopted TDPO setup allowed the fibre to be gripped as close to the hardened paste interface as possible, simulating in-service conditions during crack formation. Specimens subjected to TDPO conditions are shown in Figure 3.8a.

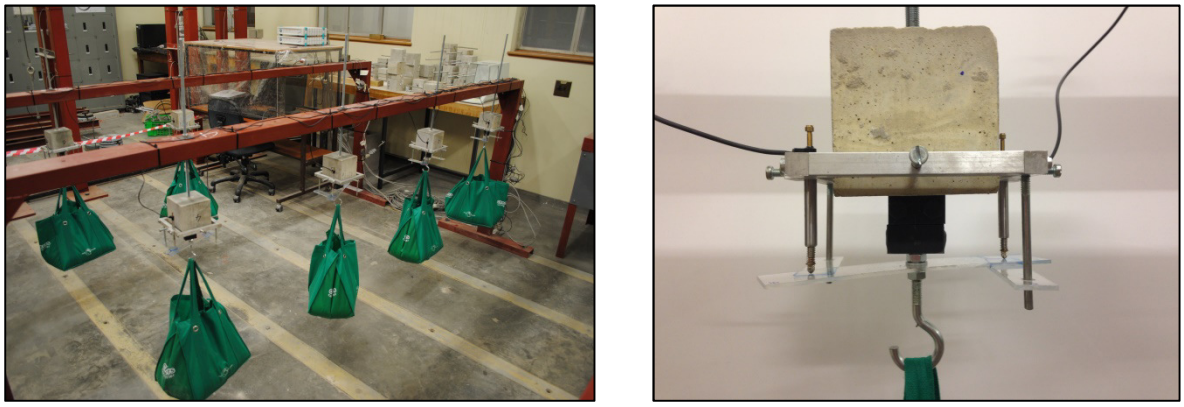

a) b)

Figure 3.8: Specimens subjected to sustained loads (a) and LVDT attachment (b)

3.5 Scanning Electron Microscopy

Scanning electron microscopy (SEM) uses the focus of an electron beam to produce images of scanned samples. Scanning electron images were generated of individual fibres in their virgin state, premixed fibres as well as fibres pulled out of the hardened paste matrix by means of SFPO experiments.

The imaging of the fibres was accomplished using a Leo® 1430VP SEM. Prior to imaging, the fibre samples were mounted onto stubs using double sided carbon tape. In order to make the fibre surface electrically conductive, these were coated with a thin layer of gold. The images produced by the SEM show the surface structure of the fibre material. Electron beam conditions during the surface analysis were set to 10 kV and approximately 1.5 nA with a spot size of 150.

The acquired images allow to visually assess the damage of individual fibres resulting from pull-out as the fibres gradually slip through the hardened paste matrix, being partially responsible for the bond characteristics. A pulled out fibre showing extensive surface damage is representative of a higher bond than fibres showing less surface damage.

Additionally, comparing images of fibres in their virgin state with premixed fibres, conclusions can be drawn whether the bond characteristics of different macro synthetic fibres can be attributed to the profile used for enhancing the mechanical interlock or the fibre damage caused by the premixing process.

3.6 Concluding Summary

This chapter presents the methodology as well as experimental framework adopted for the investigation on the single-fibre level. In addition, concrete constituents as well as macro synthetic fibres used are presented with the primary characteristics of interest.

Furthermore, specimen preparation, fibre reinforced concrete mixing procedures, mould preparation as well as the adopted test procedures are described in detail. The experimental framework on the single-fibre level is split into single-fibre pull-out and time dependent pull-out, both providing information on geometric properties enhancing fibre pull-out behaviour.

Additionally, scanning electron microscopy imaging used for the visual assessment of macro synthetic fibre performance is described in detail. Furthermore, the procedure of analysis adopted to interpret scanning electron microscopy images is stated.

CHAPTER 4
Investigation on the Macro-Mechanical Level

Macro synthetic fibre reinforced concrete (FRC) finds its primary application in ground supported slabs and tunnel linings (ACI Committee 544, 2002). The exhibited behaviour in this type of application is often that of beam/slab-like elements. Common existing test methods used as a performance criterion for FRC on a macro-mechanical level are the three-point bending (TPB) and round determinate panel (RDP) test.

The TPB test provides important parameters used in the design approach for ground supported slab, as given by TR 34 (2013). Flexural beam tests indicate the performance of FRC for low levels of deformation i.e. small crack openings.

The RDP test provides information on the toughness of FRC. Panel tests are typically used to simulate the behaviour of FRC subjected to high levels of deformation, resulting in larger crack openings.

This chapter reports on the three-point bending and round determinate panel tests used to establish performance criteria for each macro synthetic fibre type and FRC mix design. Additional focus is directed towards specimen preparation for the investigation on the macro-mechanical level.

4.1 Materials

The concrete constituents as well as macro synthetic fibres used for the investigation on the macro-mechanical level are provided in Section 3.1. Due to the large number of specimens and therefore high volume of required concrete, not all concrete batches were mixed using the same batch of sand. The grading of the different sand batches is shown in Figure 3.2. Appendix B and Appendix C provide information regarding the sand batch used for each specific TPB and RDP specimen set respectively.

In addition to the macro synthetic fibres listed in Table 3.1, fibres supplied by Geotex were received in additional lengths of 25 and 75 mm.

4.2 Concrete Mix Proportion

The mix proportions as depicted in Table 3.4 were used for all macro-mechanical specimens. For the investigation on the macro-mechanical level, macro synthetic fibres were used at a quantity of 4 kg/m^3 in FRC.

The consistency of each fresh FRC batch was measured using the slump test according to SANS 5862-1 (2006). Additionally, four standard cubes measuring 100 x 100 x 100 mm were cast from each batch in order to determine the compressive strength of the FRC mix designs at an age of 28 days. The compressive strength and slump measurements are provided in Appendix B and Appendix C for TPB and RDP specimens respectively. The average slump values and compressive strength results are presented in Table 4.1.

Table 4.1: Slump measurements and compressive strength results

	Average	Standard Deviation	CoV
Slump [mm]:			
Excluding fibres	125.8	15.7	0.12
Including fibres[1]	78.0	13.7	0.18
Including fibres[2]	79.4	9.8	0.12
Including fibres[3]	28.8	9.5	0.33
Compressive strength [MPa]	37.1	2.0	0.05

[1] Normal mixing time (5 minutes FRC mixing)
[2] Extended mixing time (20 minutes FRC mixing)
[3] Extended mixing time (40 minutes FRC mixing)

4.3 Three-Point Bending Test

Bending tests under three-point loading conditions were performed according to EN 14651 (2005). Beam tests are essential for FRC, as the received output is required for the yield line design approach as documented by TR 34 (2013).

4.3.1 Specimen preparation

Beam specimens measuring 150 x 150 x 700 mm were prepared using the FRC mix design shown in Table 3.4. Although TR 34 (2013) and EN 14889-2 (2006) specify 12 beam specimens for establishing design parameters, it was decided that 6 beam specimens per fibre type are sufficient for the purpose of this research. The materials for the concrete mix design were batched by weight and added to a 120 litre concrete pan mixer in the order of sand, cement, stone. Prior to mixing, the mixer was rinsed with water and dried using industrial tissue paper in order to ensure the same conditions for each mixing batch and eliminate additional water absorption of the pan. The concrete constituent materials were dry-mixed for one minute before the introduction of mixing water. After the addition of the mixing water, the materials were mixed for an additional five minutes to ensure all materials were mixed to

a homogenous concrete mixture. Subsequently, fibres were sprinkled carefully into the mixer to prevent the formation of fibre balls. The FRC mixture was additionally mixed for another five minutes to ensure fibres were thoroughly distributed within the fresh FRC.

In order to examine the consistency of the fresh FRC batches, two slump tests were performed. The first slump test was conducted before the addition of any fibres while another slump test was performed after the addition of the fibres.

Wooden beam moulds with aforementioned dimensions were constructed using plywood. To prevent water absorption of the wooden moulds, PLASCON ROOFSEAL waterproofing paint was used to coat the moulds as shown in Figure 4.1a. Moulds were assembled prior to filling and oiled using mould release oil. The moulds were filled according to the recommended filling sequence given by EN 14651 (2005) as shown in Figure 4.1b. In order to ensure adequate compaction and prevent the presence of major air voids, the fresh FRC was vibrated inside the moulds using a typical poker vibrator. Afterwards, the FRC casting face was trowelled using a hand-trowel for a neat and levelled finish.

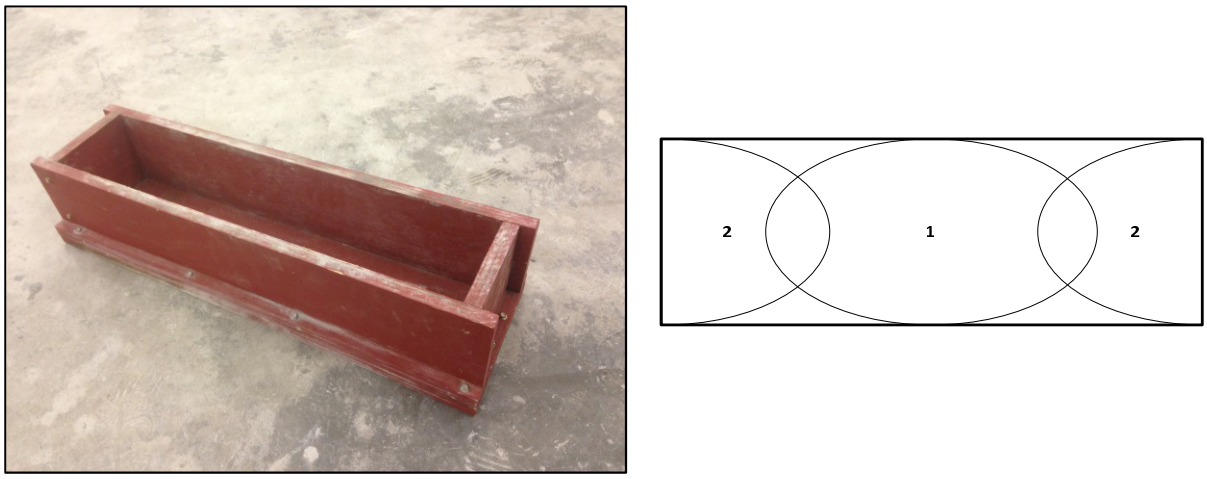

a) b)

Figure 4.1: Plywood beam moulds (a) and specimen filling sequence (b)

Four control cubes for compression tests were cast for each concrete batch. The compressive strength results of the individual FRC batches used for beam specimens are provided in Appendix B.

All specimens were de-moulded after 24 hours and immediately immersed in temperature controlled curing tanks. The temperature of water was controlled at 25°C. The beams were completely submerged in an upright position as shown in Figure 4.2

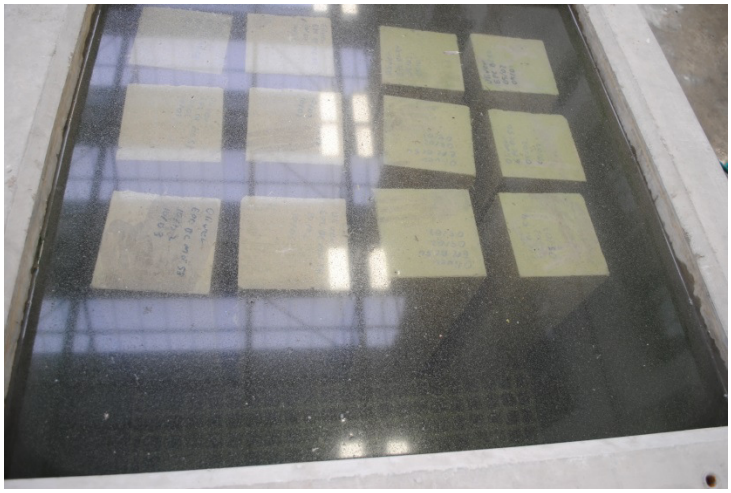

Figure 4.2: Curing of beam specimens

Beam specimens were left to cure for 26 days before removal from the curing tanks, followed by a day of test preparations. The mid-span position of a non-casting face adjacent to the casting face was marked using a permanent marker for notching. The beam specimens were wet-notched using a saw with a 3.5 mm diamond-tipped concrete blade along the pre-marked position. The notching depth was set to 25 mm. The function of the notch is to reduce the section depth and force the crack formation at mid-span, being the position of maximum moment during flexural testing as visually demonstrated in Figure 4.3.

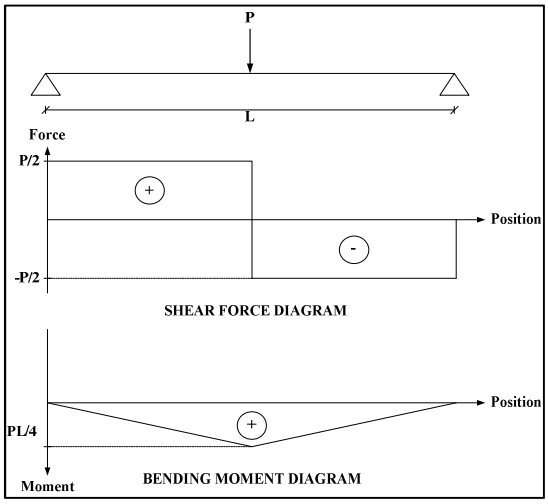

Figure 4.3: Shear force and bending moment diagram for three-point bending tests

Steel wings made from flat roof sheeting were glued onto the sides of the beam, positioned directly above the notch. The wings were attached onto the specimen using PRATLEY Quickset Clear Glue®. The function of the metal wings was to restrict LVDT extension. During testing, the load applying crosshead would cause downward displacement of the FRC beam specimen, along with the metal wing, resulting in compressing the LVDTs. The downward compression of the LVDTs is representative for the central downward

displacement of the FRC beam at mid-span. The function of the metal wings is illustrated in Figure 4.4.

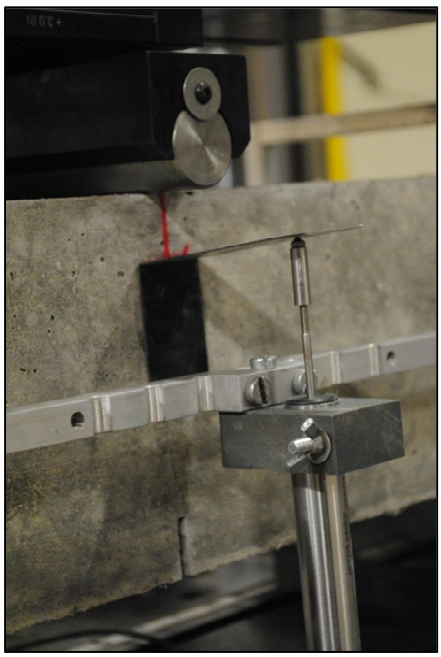

Figure 4.4: Metal wing restricting LVDT extension

4.3.2 Test setup

An aluminium frame was attached by means of sharpened screws to the beam specimens prior to testing. The frame was positioned onto the height of the neutral axis at 75 mm, anchored directly above the roller supports. The frame had the function to facilitate the LVDTs positioned at mid-span.

The experiment was conducted using an Instron 2000KPX universal materials testing machine with a capacity of 2 MN. However, a smaller load cell with a capacity of 250 kN was used to record the load. The beam specimens were positioned onto two roller supports, spaced 500 mm apart. A load applying roller located at mid-span applied the load at a constant displacement rate of 0.2 mm/min. Data was continuously recorded at a frequency of 10 Hz. Two LVDTs with a differential range of 30 mm were used on either side of the beam to measure the central deflection as shown in Figure 4.4. The adopted setup used for the TPB beam test is shown in Figure 4.5.

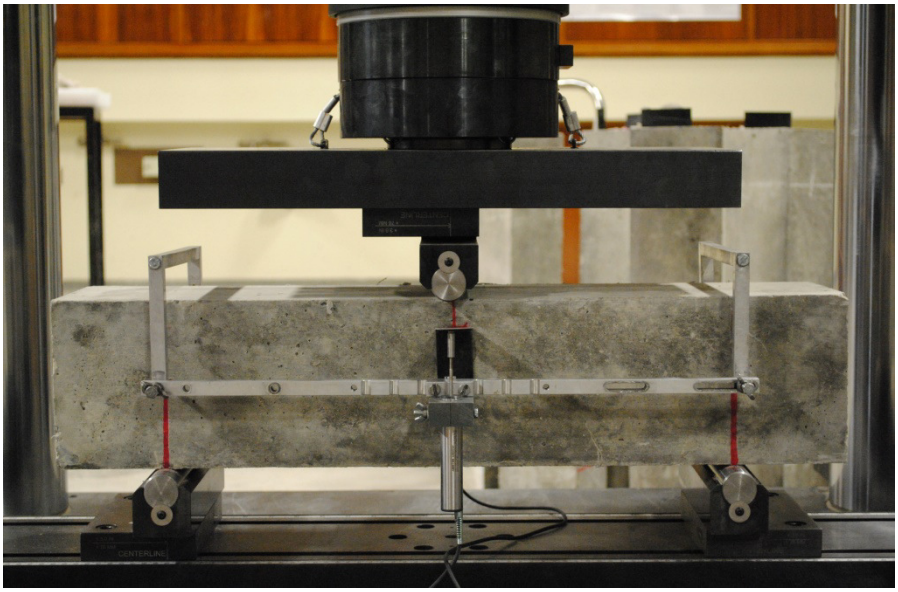

Figure 4.5: Beam specimen tested in three-point bending

Due to the nature of the adopted setup, the flexural beam response is received in the form of load-deflection. However, the desired output required for the design approach is the measure of residual flexural tensile strength determined at a CMOD of 0.5 and 3.5 mm. RILEM TC 162-TDF (2003) provides a relationship between CMOD and central deflection, given by:

$$CMOD = 1.18 \times \delta + \beta_y \tag{4.1}$$

with δ the central beam deflection and β_y equal to -0.0416 mm respectively.

RILEM TC 162-TDF (2003) stresses that the relationship provided by Equation (4.1) is only applicable in the post-cracking region of the load-deflection response. The load-CMOD response corresponding to the load-deflection behaviour (see Figure 2.21a) is shown in Figure 2.21b.

4.4 Round Determinate Panel Test

The RDP test as documented by ASTM C1550-12 (2012) provides a good indication for the flexural toughness of FRC at higher levels of deformation. In addition, the RDP test enjoys popularity due to the advantage of generating reproducible results, representative of little result scatter.

4.4.1 Specimen preparation

Round panels measuring 800 x 75 mm (diameter x height) were cast using the mixing procedure adopted for three-point flexural beam specimens as described in Section 4.3.1. Due to limited storage capacity, different batches of sand were used during the investigation. Each

RDP concrete batch was intended for three panel specimens, hence three RDP specimens were cast per fibre type and length.

Round steel moulds with a rigid base were used as shown in Figure 4.6. The moulds were oiled prior to filling using mould release oil in order to simplify the de-moulding process. As the moulds measured 80 mm in height, filling was done to approximately 5 mm below the rim. In order to ensure adequate compaction and removal of air voids, the FRC was exposed to vibration inside the moulds using a poker vibrator. 50 mm long ski ropes with steel washers held by knots on the ends were inserted on opposite sides into the fresh concrete in order to function as handles for transportation purposes in the hardened state.

Figure 4.6: Simple steel form with rigid base and handles for transport and handling

The RDP specimens were de-moulded after 24 hours. Due to the specimen size, RDP samples could not be cured in the conventional temperature controlled tanks. Therefore, specimens were relocated to larger tanks, suitable to accommodate the samples. The alternative curing tanks shown in Figure 4.7 were however not temperature controlled. The estimated water temperature was ± 18°C. The specimens were removed from the curing tanks at an age of 28 days and tested under moist conditions.

Figure 4.7: In water submerged RDP specimens for curing purposes

4.4.2 Test setup

The adopted test setup facilitated for the RDP experiments is schematically shown in Figure 2.38. RDP specimens were lifted onto three symmetrically arranged pivot supports consisting of a steel plate situated on a steel ball bearing. The steel balls were lubricated using conventional bearing grease in order to utilise full bearing action, hence minimising undesirable presence of friction. The bearing support is shown in Figure 4.8a.

After positioning the panel specimen onto the supports, an LVDT with a differential range of 100 mm was supported by an LVDT yoke below the centre of the panel. In order to establish continuous contact with the panel bottom, the LVDT was pushed/compressed against the bottom of the panel and rigidly fixed to the yoke, as depicted in Figure 4.8b. A small flat roof sheeting plate was placed between the LVDT tip and the panel surface. The function of the plate was to prevent the LVDT tip to slip into the crack opening upon failure, as shown in Figure 4.9a.

a) b)

Figure 4.8: Support bearing used for RDP setup (a) and LVDT attachment (b)

A centrally located piston with a 50 mm diameter and hemispherical tip having a radius of ± 80 mm was used to apply the load at the centre of the panel. The load was logged using a load-cell with a capacity of 50 kN while the corresponding vertical deflection was logged using the LVDT attached to the tension face of the RDP specimen. The test was performed using a hydraulic Instron actuator, using a displacement rate equal to 4 mm/min. The test was

automatically stopped once the crosshead displaced 50 mm. The RDP test setup used is shown in Figure 4.9b.

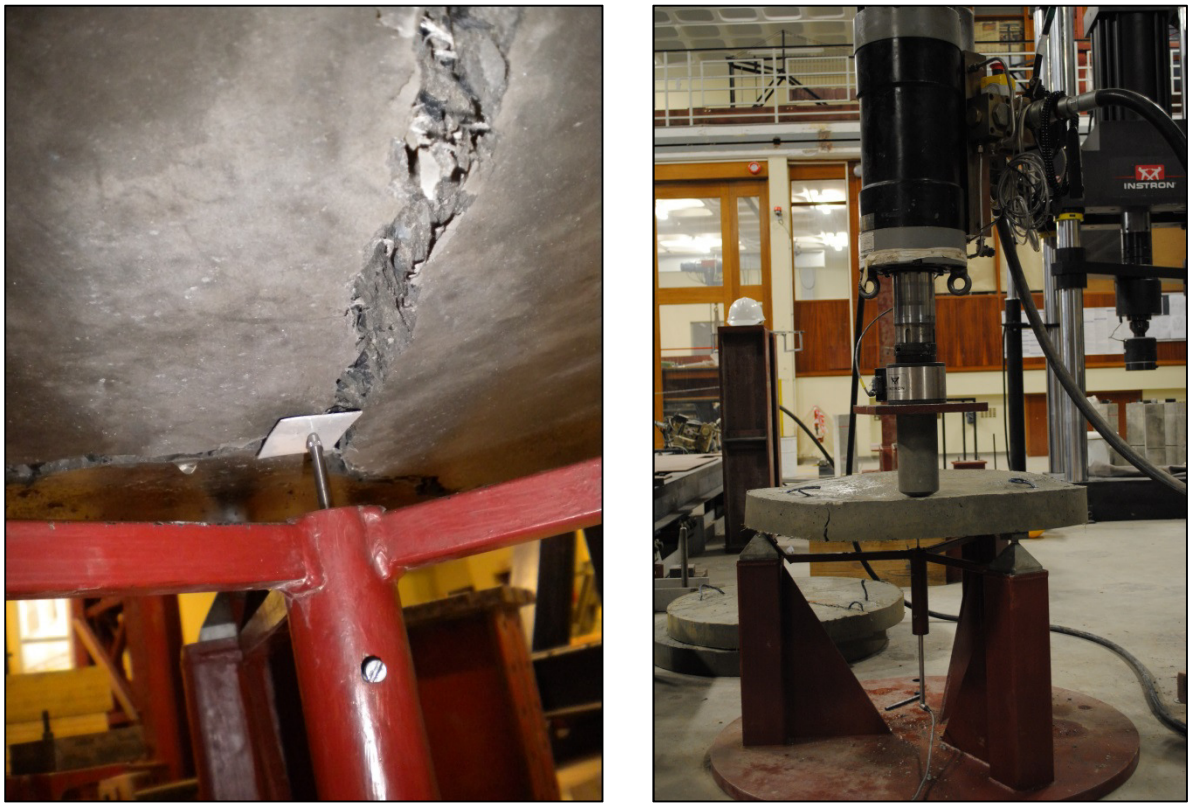

a) b)

Figure 4.9: Steel plate restricting LVDT slip (a) and RDP test setup (b)

The thickness of each tested panel specimen was measured using a Vernier calliper. The thickness was recorded to the nearest millimetre. The average thicknesses and corresponding standard deviations for each panel specimen are presented in Appendix C.

4.5 Concluding Summary

This chapter reports on the methodology adopted for the investigation on the macro-mechanical level. The three-point bending beam test, required in the design procedure for ground supported slabs, and round determinate panel test, providing good fibre reinforced concrete (FRC) toughness indications, are utilised. Furthermore, specimen preparation, FRC mixing procedures, mould preparation as well as the adopted test procedures are explained in detail.

CHAPTER 5
Single-Fibre Results

This chapter reports on the results obtained for the investigation on the single-fibre level. The results include findings of single-fibre pull-out (SFPO) as well as time dependent pull-out (TDPO) experiments.

The SFPO results are discussed with regard to the interfacial bond stress and energy dissipation of single fibres with various geometrical properties. Fibres were embedded either in a virgin state as received by suppliers, or in a premixed fibre state, undergoing the mixing procedure and thus causing fibre surface roughening, prior to embedment. Accordingly, results obtained for virgin and premixed fibres are compared in order to establish the effect of fibre mixing on the performance of FRC.

A similar approach is adopted for the investigation on TDPO of single macro synthetic fibres. The performance of virgin fibres subjected to a sustained load is compared to that of premixed fibres, in order to investigate the effects of premixing on the time dependent behaviour of single fibres.

Macro synthetic fibres subjected to various in-service SFPO conditions are furthermore analysed with the aid of scanning electron microscopy (SEM) images. SEM images provide information on the effectiveness of fibre geometries by the degree of surface damage identified.

5.1 Single-Fibre Pull-Out

SFPO experiments were conducted on macro synthetic fibres with corresponding fibre designations/labels as listed in Table 3.1. The considered embedment lengths are 12.5 (L12.5), 25.0 (L25) and 37.5 mm (L37.5) corresponding to one quarter, one half and three quarters of the length of fibres measuring 50 mm in length. Fibres with lengths other than 50 mm were also embedded one half of the fibre length (LH).

5.1.1 Crimped C1 SFPO

The load corresponding to the elastic or physicochemical bond exhibited during SFPO can be identified as the peak load from the SFPO response. Figure 5.1 depicts the peak load for the Geotex 500 range (C1) fibre for three embedment lengths in the virgin and premixed fibre state. It is important to note, that as a consequence of increasing embedment lengths, typically an increase in peak load is observed. The decrease in peak load at embedment L37.5 can be attributed to the predominant failure mode being fibre rupture as reported in Table 5.1. It is thus evident, that the critical length is well exceeded at L37.5 for the premixed C1 fibre. Therefore, the peak load for C1 at an embedment L37.5 is rather governed by the fracture stress of the fibre material (polypropylene) in contrast to the load required for de-bonding.

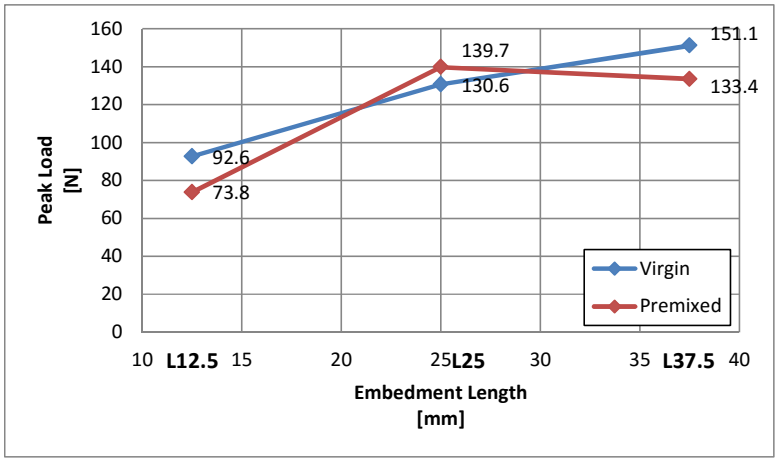

Figure 5.1: Peak load for various embedment lengths of C1

It is important to note that the maximum pull-out load encountered by a fibre, regardless of the fibre state, is limited to the fracture stress of the parent material. However, significant variability exists in fibre length, pronunciation of the crimping profile as well as the fibre diameter of C1, as depicted in Figure 5.2. The decrease in load of C1 at L37.5 can therefore be attributed to an inconsistency in cross sectional-area of the crimped fibres. This is additionally emphasised by the relatively high coefficient of variation (0.14) of C1 under SFPO at L37.5, as all fibres tested experienced fracture.

Additionally, it could be argued, that the concrete grade influenced the decrease in load at L37.5. However, control cubes revealed that no significant difference exists between the concrete grade used for virgin (concrete = 37.1 MPa; paste = 37.0 MPa) and premixed (concrete =39.5 MPa; paste = 42.3 MPa) C1 fibres.

Table 5.1 depicts the percentage of fibres encountering rupture as well as the number of results used for data analysis of SFPO experiments. Due to variable nature of SFPO

experiments, data not representing the typical fibre trend was excluded. To satisfactorily eliminate unrepresentative data in an unbiased manner, Chauvenet's criterion, as also used by Bedi et al. (n.d.) and Kaur et al. (2012), conducting research on similar topics, was adopted. Chauvenet's criterion classifies data as non-representative, not falling within the confidence interval of a standard normal distribution with a probability of $1\text{-}1/(2N_s)$, with N_s representing the number of samples (Coleman & Steele, 2009). The outlier criterion was based on the peak load of the SFPO response. According to Tayler (2009), Chauvenet's criterion is unsuitable for data elimination of a sample space equal to four or less. Data subjected to outlier elimination however always exceeded the minimum suggested sample space. It is important to note, that Chauvenet's criterion was used to identify and exclude outliers. Hereafter, the remaining data was used to calculate the CoV presented in Table 5.1.

Table 5.1: C1 SFPO information

Fibre state	Embedment length [mm]	Fibre rupture [%]	Usable results	CoV
Virgin	12.5	0	8	0.24
	25.0	25	8	0.10
	37.5	75	7	0.05
Premixed	12.5	8	12	0.22
	25.0	67	11	0.10
	37.5	100	12	0.14

Figure 5.2: Variation in diameter, crimping profile and length of C1

It is well known that the pull-out resistance of a fibre is highly dependent on the surface area in contact with the hardened paste matrix. Result comparison can only be achieved by converting pull-out loads to interfacial bond stresses using Equation (2.2). Figure 5.3 demonstrates the bond stresses for the utilised embedment length of virgin and premixed C1. It is evident that a decreasing trend in interfacial bond is observed for an increase in embedment length.

The interfacial bond is expressed in terms of the elastic/physicochemical bond determined from the peak load during SFPO response. It is therefore evident that the elastic bond only represents the single-fibre behaviour at one particular instance during the pull-out response.

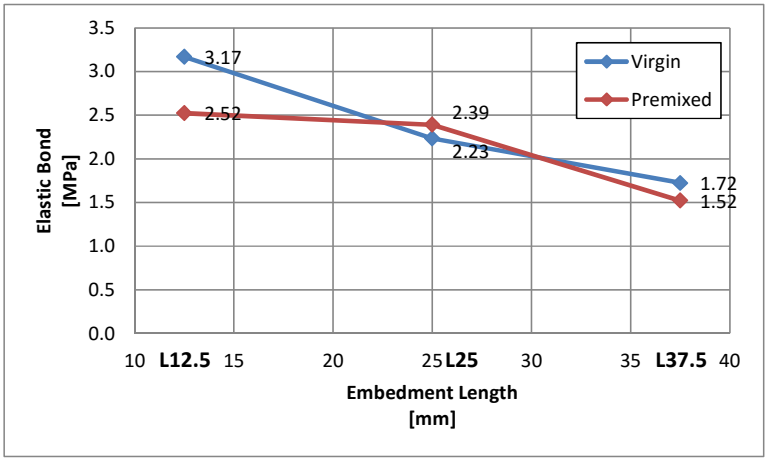

Figure 5.3: Elastic bond for various embedment lengths of C1

In order to investigate the entire pull-out response (elastic, mechanical and frictional influence), the single-fibre performance is quantified in terms of dissipated energy. The dissipated energy is defined as the area under the load-displacement response. It is important to note that an energy analysis is only useful for the comparison of fibres with equal cross-sectional areas, being the primary variable influencing pull-out loads at equal embedment depths. Figure 5.4 depicts the energy dissipated for different percentages of fibre pull-out. The display of energy dissipated for different percentages of fibre pull-out provides a useful indication for the fibre performance at various crack openings.

Longer embedded fibres tend to dissipate more energy as a result of a larger embedded surface area as well as the higher associated loads in contrast to shorter embedment lengths. It is therefore evident that upon fibre rupture no further energy can be dissipated, due to the pull-out load decreasing to zero. However, as energy dissipation is of a cumulative nature during pull-out, a constant trend in energy dissipation for increasing percentages of pull-out displacement can be attributed to two mutually exclusive scenarios:

- Fibre rupture
- Complete isolation of a fibre after de-bonding characterised by insufficient bond between the fibre and surrounding matrix, represented by zero resistance against pull-out

Figure 5.4a illustrates the dissipated energy for different levels of embedment of virgin C1. It is stressed, that the dissipated energy of L37.5 is lower than that of L25. This is attributed to the high number of fracture occurrences (75 %), as shown in Table 5.1, of virgin C1 at an embedment of L37.5, preventing further energy dissipation after fibre rupture.

Figure 5.4b depicts the energy dissipated by premixed C1. It is evident that at an embedment L37.5, constant energy dissipation exists throughout for increasing percentages of pull-out. It can therefore be deduced that fibre rupture occurred prior to de-bonding of the fibre. This is further highlighted by 100 % of rupture occurrences for C1 at an embedment of L37.5, as depicted in Table 5.1.

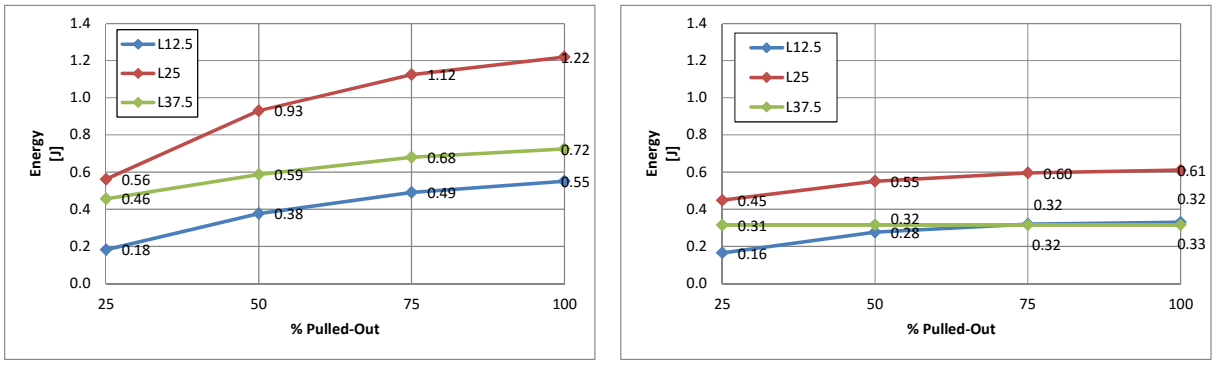

a) b)

Figure 5.4: Energy dissipation of virgin (a) and premixed (b) C1

5.1.2 Flat F1 SFPO

The peak load response of the Geotex 600 range (F1) for various embedment lengths is shown in Figure 5.5. It is important to note that the peak load responsible for fibre de-bonding under SFPO is considerably higher for premixed fibres in contrast to virgin fibres.

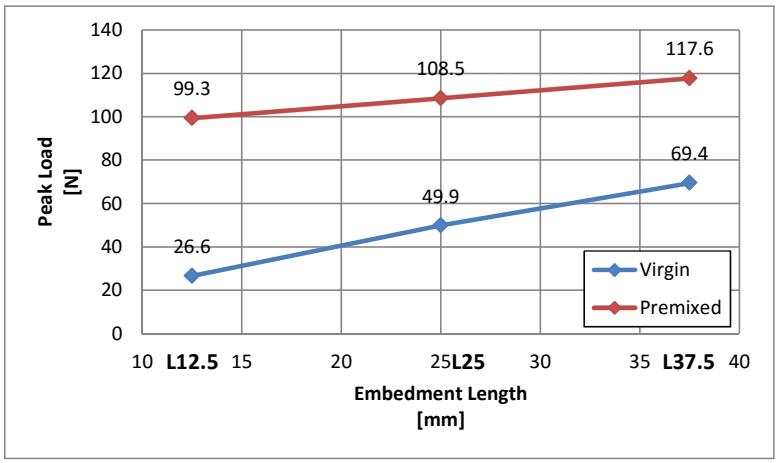

Figure 5.5: Peak load for various embedment lengths of F1

It is evident from Table 5.2 that fibre premixing has a significant effect on the SFPO behaviour, as fibre fractures can be observed for embedment lengths as low as 12.5 mm as

opposed to virgin fibres experiencing pure pull-out for all embedment lengths. The fibre length of 50 mm seems to approach the critical fibre length, as 58 % of premixed fibres at an embedment of L25 experience rupture. It is furthermore important to note that the CoV for premixed fibres is typically higher than that of virgin fibres. This can be attributed to the uncontrollable surface roughening caused by premixing.

Table 5.2: F1 SFPO information

Fibre state	Embedment length [mm]	Fibre rupture [%]	Usable results	CoV
Virgin	12.5	0	7	0.10
	25.0	0	8	0.09
	37.5	0	7	0.06
Premixed	12.5	25	12	0.20
	25.0	58	10	0.10
	37.5	92	11	0.11

Figure 5.6 depicts the interfacial bond stress for the considered embedment lengths. It is stressed that the fibre-matrix bond is significantly higher for premixed compared to virgin fibres. A nearly constant (slightly decreasing) trend in interfacial bond stress can be recognised for virgin fibres, while a decrease in interfacial bond with increasing embedment lengths is observed for premixed fibres. Thus it seems apparent that the primary mechanism responsible for the good fibre-matrix interlock is governed by the mixing process.

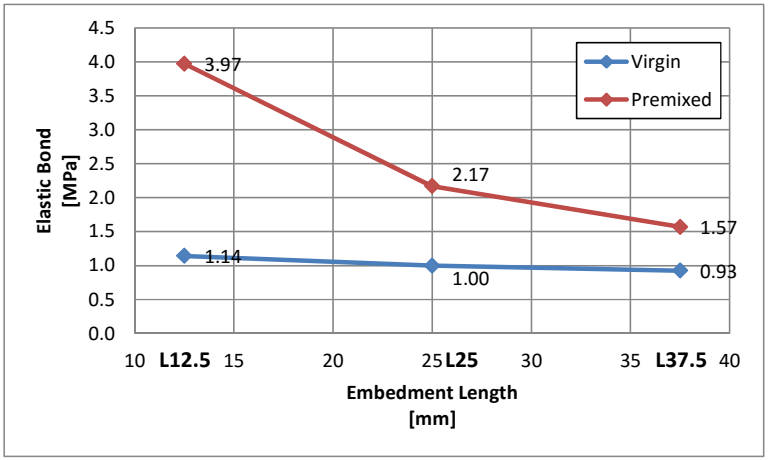

Figure 5.6: Elastic bond for various embedment lengths of F1

Figure 5.7 depicts the energy dissipation of virgin and premixed F1 for various embedment lengths, expressed as a percentage of the original embedment length. Similar results are obtained for an embedment of L25 and L37.5 for premixed fibres. This can be attributed to the high percentage of fibre ruptures at an embedment length L37.5 as highlighted in Table 5.2.

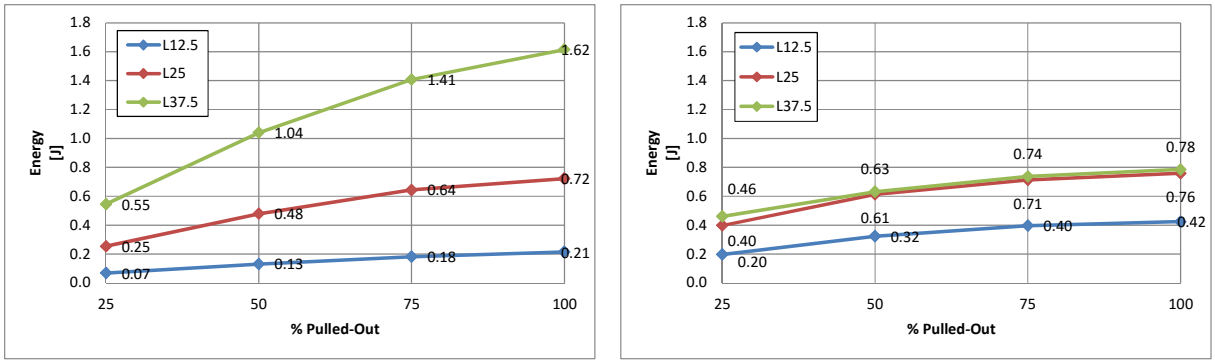

a) b)

Figure 5.7: Energy dissipation of virgin (a) and premixed (b) F1

5.1.3 Flat F2 SFPO

Figure 5.8 depicts the SFPO peak-load response for various embedment lengths of the flat fibre supplied by Fibsol, known as Fibsol Macrosol F (F2). The surface roughening caused by the premixing process has, similar to that of F1, a significant effect on the peak load of F2. The elastic pull-out load for premixed fibres, with embedment lengths L25 and L37.5, is primarily governed by the fracture stress of the fibre material. This is indicated by the high percentage of rupture occurrences of F2 in contrast to fibre pull-out, as highlighted in Table 5.3.

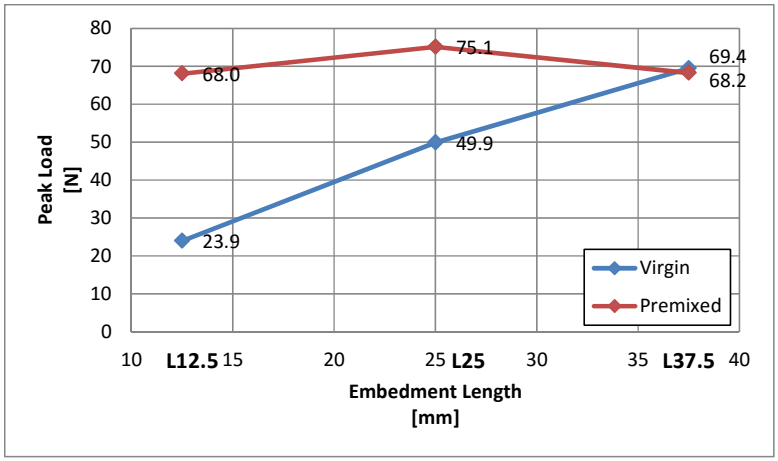

Figure 5.8: Peak load for various embedment lengths of F2

Table 5.3 provides an overview of the percentage of fibre rupture, usable results including eliminated data as well as the CoV for the various embedment lengths of virgin and premixed F2. Due to 83 % of premixed fibres experiencing rupture at an embedment length L25, it is evident that the fibre length of 50 mm exceeds the critical length.

Table 5.3: F2 SFPO information

Fibre state	Embedment length [mm]	Fibre rupture [%]	Usable results	CoV
Virgin	12.5	0	8	0.18
	25.0	13	8	0.17
	37.5	13	8	0.24
Premixed	12.5	25	12	0.36
	25.0	83	11	0.14
	37.5	100	10	0.14

The elastic bond achieved by the fibre profile of F2 for various embedment lengths is depicted in Figure 5.9. It is highlighted that the bond stress of virgin fibres is typically less than the bond of premixed fibres, similar to F1 as shown in Figure 5.6. A nearly constant bond stress is observed for virgin fibres with increasing embedment length. Similar behaviour was observed for virgin F1.

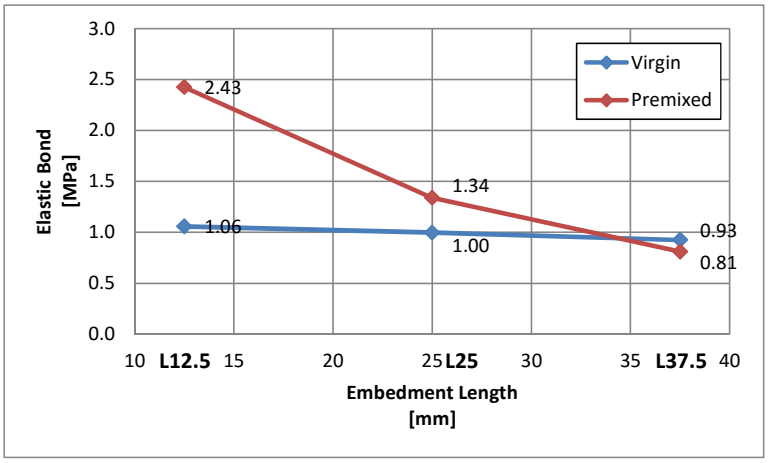

Figure 5.9: Elastic bond for various embedment lengths of F2

The energy dissipation of virgin and premixed F2 for various embedment lengths under SFPO is shown in Figure 5.10. The constant energy throughout for premixed F2 at an embedment of L37.5, as shown in Figure 5.10b, is an indication of fibre rupture prior to de-bonding.

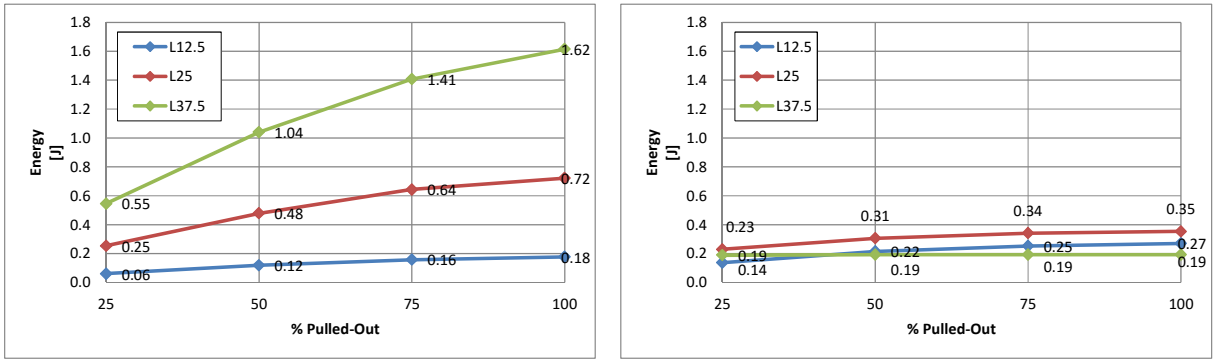

a) b)

Figure 5.10: Energy dissipation of virgin (a) and premixed (b) F2

5.1.4 Embossed E1 SFPO

Figure 5.11 depicts the load response under SFPO for various embedment lengths of EPC BC48 (E1) embossed fibre type. In contrast to the flat fibres F1 and F2, the peak load of E1 is not as affected by the surface roughening caused by premixing. Nevertheless, a slight increase in performance can be identified for the premixed E1 as depicted in Figure 5.11.

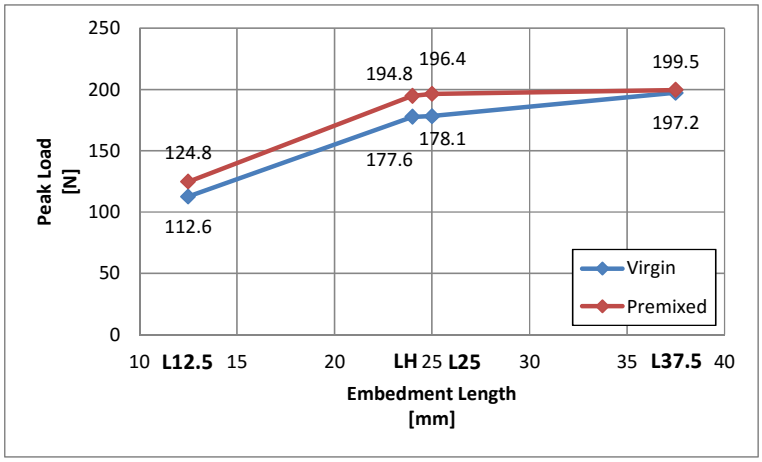

Figure 5.11: Peak load for various embedment lengths of E1

Table 5.4 provides an overview of the percentage of fractures occurrences as well as usable results of E1 under SFPO. Based on the high number of fibre ruptures in the virgin as well as premixed fibre state at an embedment of L37.5, it is evident that the peak load depicted in Figure 5.11 is primarily governed by the fracture stress of the fibre material. In addition, the fibre length of 48 mm appears to approach the critical length in both states, as approximately half the number of fibres tested at an embedment of LH experience rupture.

Table 5.4: E1 SFPO information

Fibre state	Embedment length [mm]	Fibre rupture [%]	Usable results	CoV
Virgin	12.5	0	8	0.17
	24.0	50	7	0.08
	25.0	50	6	0.04
	37.5	100	8	0.11
Premixed	12.5	0	12	0.14
	24.0	42	12	0.05
	25.0	42	12	0.08
	37.5	92	10	0.08

The interfacial bond stress achieved by the embossed fibre geometry of E1 for various embedment lengths is depicted in Figure 5.15. Similar to previous results obtained for C1 and the premixed flat fibres, a decreasing trend in interfacial bond can be observed.

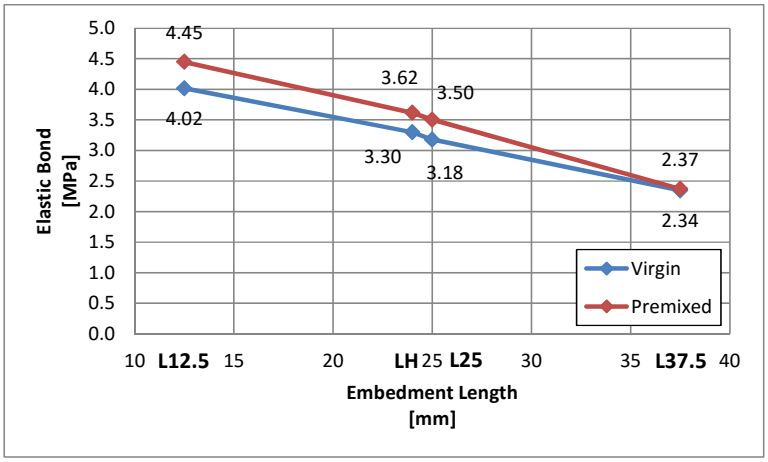

Figure 5.12: Elastic bond for various embedment lengths of E1

Figure 5.13 demonstrates the ability of E1 to dissipate energy in the virgin and premixed state. Due to the high percentage (100 %) in fibre rupture encountered by the virgin E1 for an embedment L37.5, no further energy prior to rupture was possible, resulting in overall constant energy dissipation. In contrast to the premixed fibre state for an embedment L37.5, less rupture occurrences resulted in some energy dissipation.

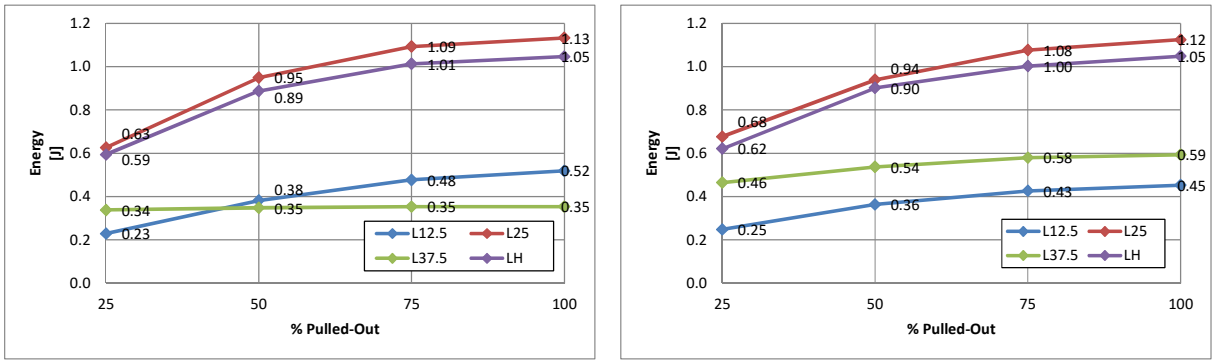

a) b)

Figure 5.13: Energy dissipation of virgin (a) and premixed (b) E1

5.1.5 Embossed E2 SFPO

The peak load response for various embedment lengths of the EPC BC54 (E2) fibre type is displayed in Figure 5.14.

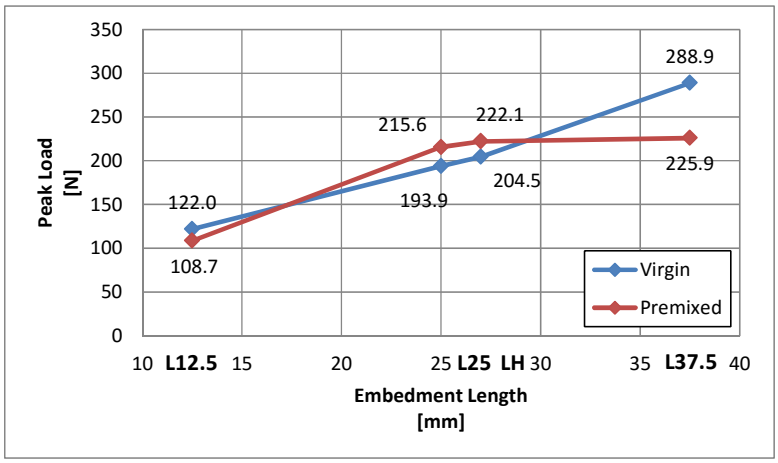

Figure 5.14: Peak load for various embedment lengths of E2

The significant difference in peak load at L37.5 for virgin and premixed fibres can be attributed to a significant loss in interlock caused by premixing. This is further highlighted by the higher percentage in pull-out experienced by premixed in contrast to virgin E2 specimens at an embedment L37.5 as shown in Table 5.5. Additionally, the low percentage in fibre rupture experienced by E1 in both states at an embedment of 27 mm suggests that the critical length exceeds the fibre length of 54 mm.

Table 5.5: E2 SFPO information

Fibre state	Embedment length [mm]	Fibre rupture [%]	Usable results	CoV
Virgin	12.5	0	8	0.12
	25.0	0	8	0.14
	27.0	0	7	0.10
	37.5	63	8	0.07
Premixed	12.5	0	12	0.19
	25.0	0	11	0.12
	27.0	17	12	0.14
	37.5	25	12	0.19

Figure 5.15 depicts the interfacial bond stress for various embedment lengths of E2. An increase in embedment lengths typically results in a decrease in bond stress.

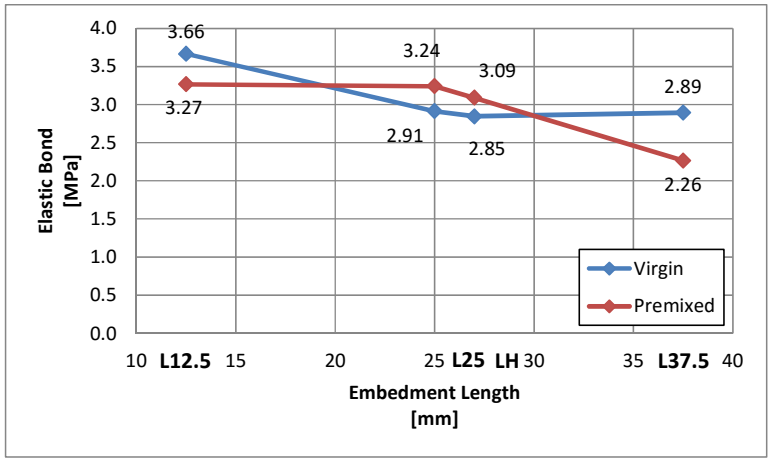

Figure 5.15: Elastic bond for various embedment lengths of E2

Figure 5.16a and Figure 5.16b depict the energy dissipated during the pull-out process of E2 in the virgin and premixed fibre state respectively.

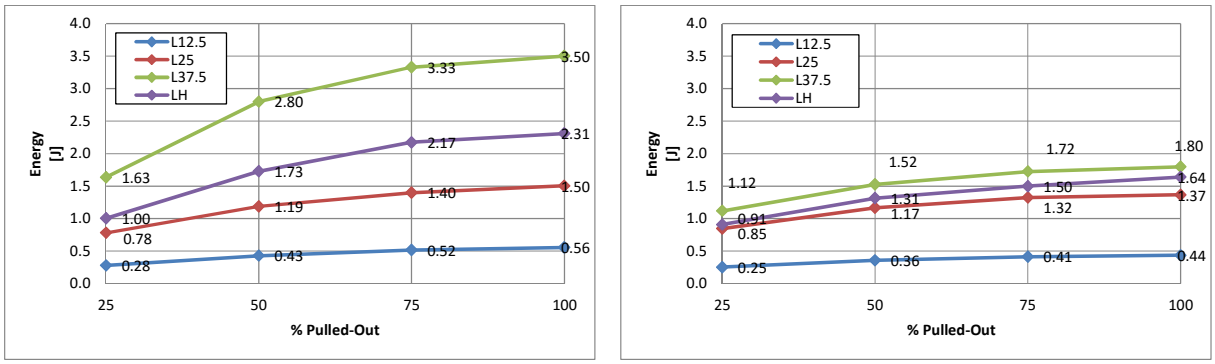

a) b)

Figure 5.16: Energy dissipation of virgin (a) and premixed (b) E2

5.1.6 Embossed built-up EB1 SFPO

It is important to note, that three load responses are provided in Figure 5.19 for the virgin EB1 state. This is attributed to the built-up nature of the fibre, consisting of a larger diameter fibre adjoined by two fibres having a smaller cross-sectional area as illustrated in Figure 5.17. As a result of the premixing process, the built-up fibres tend to split into the individual components. In addition, larger and smaller premixed fibre components could not be visually distinguished after premixing. The equivalent diameter (d_{eq}) for the premixed EB1 was thus determined as a weighted average of the fibres forming the fibre bundle according to:

$$d_{eq} = \frac{2 \times d_s + d_l}{3} \tag{5.1}$$

with d_s and d_l the equivalent diameter of the smaller and larger fibres forming the built-up fibre respectively.

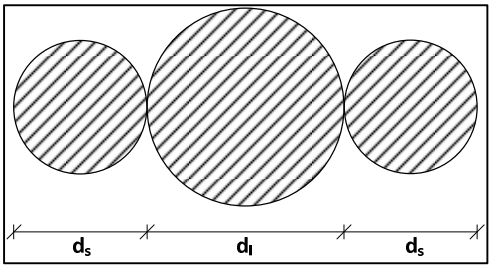

Figure 5.17: Cross-section of EB1 bundle

The contrast between the individual fibre components as well as built-up fibre in the virgin state and the premixed EB1 is depicted in Figure 5.18.

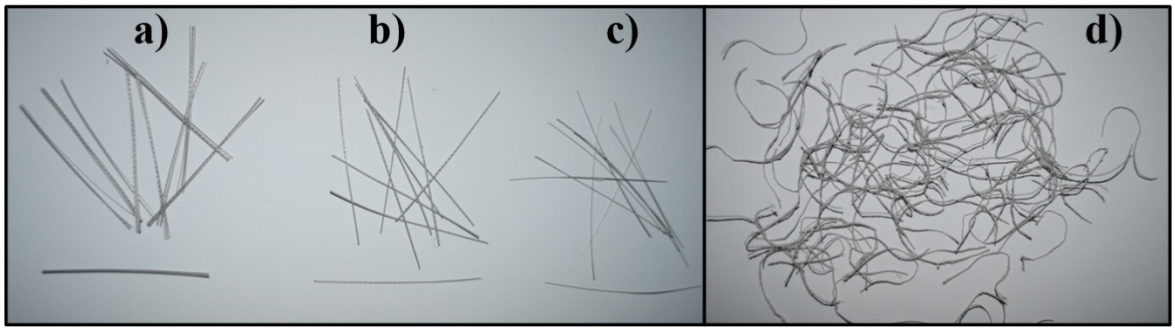

Figure 5.18: Virgin built-up fibre (a), virgin larger fibre (b), virgin smaller fibre (c), premixed fibre (d) of EB1

Figure 5.19 depicts the load response under SFPO for various lengths of the embossed built-up fibre supplied by EPC, namely the BC MQ58 (EB1), under SFPO.

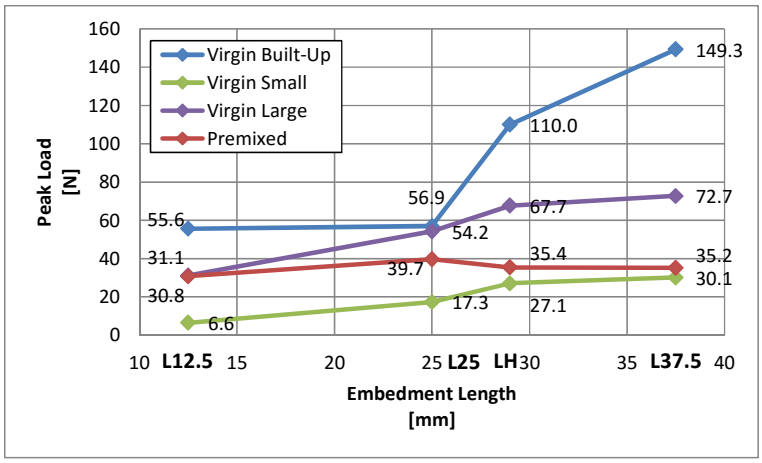

Figure 5.19: Peak load for various embedment lengths of EB1

The experimental information of EB1 under SFPO is provided in Table 5.6. It is important to note that the majority of premixed EB1 are characterised by fibre rupture. This phenomenon further affects 50 % of EB1 at the shortest embedment length L12.5. Based on the percentage of rupture occurrences in the premixed state, it is evident that the fibre length exceeds the critical length.

Table 5.6: EB1 SFPO information

Fibre state	Embedment length [mm]	Fibre rupture [%]	Usable results	CoV
Virgin built-up	12.5	0	7	0.11
	25.0	0	8	0.30
	29.0	0	8	0.07
	37.5	13	7	0.11
Virgin d_{small}	12.5	0	6	0.24
	25.0	0	8	0.26
	29.0	0	7	0.06
	37.5	38	8	0.16
Virgin d_{large}	12.5	0	8	0.39
	25.0	0	7	0.07
	29.0	13	7	0.04
	37.5	50	7	0.06
Premixed	12.5	50	12	0.18
	25.0	92	12	0.20
	29.0	92	12	0.13
	37.5	100	12	0.14

Figure 5.20 depicts the interfacial bond for various embedment lengths for virgin and premixed EB1. It is evident that the virgin built-up fibre does not follow the typical trend anticipated for the bond stress as the lowest bond is observed at an embedment of L25. This can be attributed to a telescopic mode of pull-out, demonstrated by pull-out of some fibre components, while components not exhibiting pull-out either undergo rupture or are characterised by an insufficient bond with the surrounding paste. Nevertheless, premixed EB1 exhibits the typical decreasing trend in bond with an increase in embedment length.

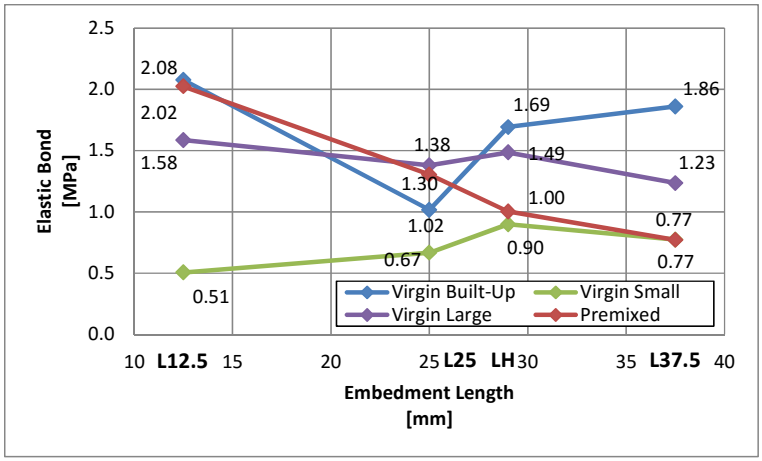

Figure 5.20: Elastic bond for various embedment lengths of EB1

The energy dissipation of the EB1 as a virgin built-up, individual component fibre as well as premixed fibre, is depicted in Figure 5.21. It is evident, that virgin EB1 dissipates energy inefficiently at an embedment L25 as shown in Figure 5.21a. This can be ascribed to the telescopic mode of pull-out, responsible for poor bond characteristics. The individual fibre

components of the built-up fibre follow the anticipated trend, as an increase in embedment length results in increased energy dissipation, as depicted in Figure 5.21b and Figure 5.21c.

The premixed EB1 state however appears to possess a poor ability to dissipate energy, as highlighted in Figure 5.21d. This can be attributed to the high fracture occurrences for an embedment length as little as L12.5 (see Table 5.6). This is characterised by zero energy dissipation after fibre rupture occurred.

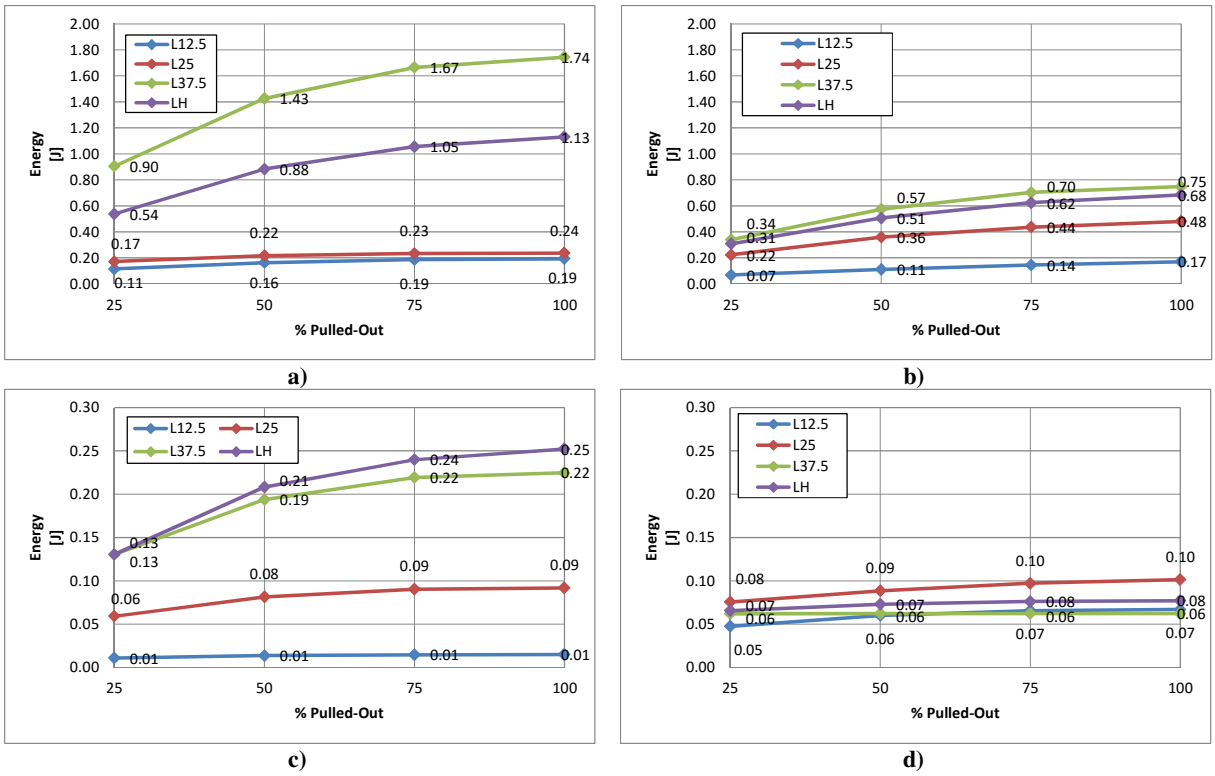

Figure 5.21: Energy dissipation of virgin built-up (a), d_{large} (b), d_{small} (c) and premixed (d) EB1

5.2 Time Dependent Pull-Out of Single Fibres

Time dependent pull-out (TDPO) experiments were conducted on virgin as well as premixed single fibres with the characteristics described in Table 3.1. The embedment length considered for the TDPO experimental framework was one half of the fibre lengths, being the maximum possible length present on each side of a formed crack.

Sustained loads, causing time dependent fibre pull-out, were based on the results obtained by SFPO experiments, utilised as 50 % of the exhibited peak load. Due to the virgin and premixed nature of embedded fibres, sustained loads were fibre state specific. The time dependent behaviour was investigated using three of each of the investigated fibres in the virgin and premixed conditions.

The time dependent single-fibre response is provided as the pull-out for the duration of the experiment, being six days at maximum. The maximum pull-out recording was limited to 10 mm, as a result of the 10 mm range of the LVDTs used. However, sudden pull-out was observed for all specimens exhibiting complete pull-out (CPO) prior to the full extension of the LVDTs.

Upon loading, specimens experienced oscillating effects, due to manual load application. Thus, an impulse was transferred to the fibres, causing difficulties to establish the instantaneous fibre elongation directly after loading. Therefore, the averaged LVDT displacement reading after ten second was used as the instantaneous elongation.

5.2.1 Crimped C1 TDPO

Figure 5.22 depicts the TDPO response of C1. It is important to note that the TDPO response excludes the instantaneous deformation. In addition, the TDPO displacement is only displayed to a maximum of 6 mm, corresponding to a significant crack widening of 12 mm which is often regarded as unaesthetic or unacceptable in practice.

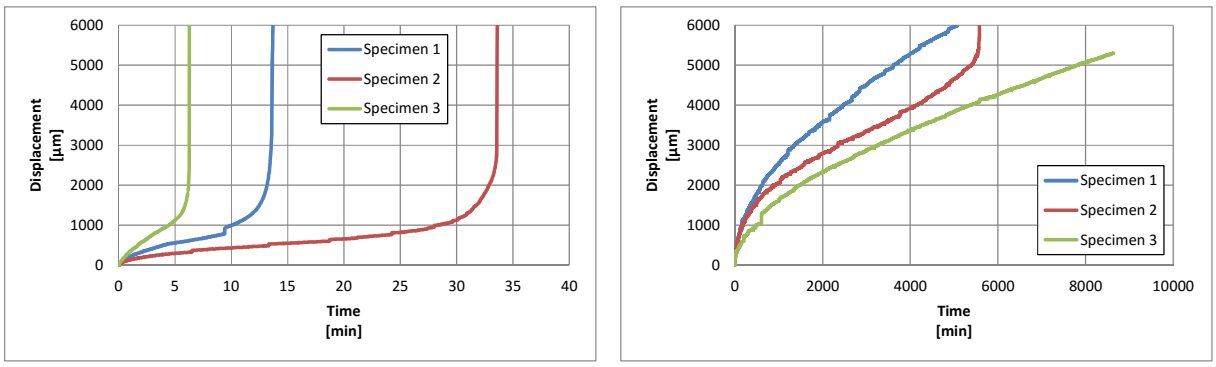

Figure 5.22: TDPO response of virgin (a) and premixed (b) C1

It is evident that all virgin C1 fibres experience CPO within 35 minutes. In contrast, premixed C1 fibres sustained the applied load considerably longer. The increased duration required for CPO is thus attributed to surface roughening caused by mixing. Figure 5.23 quantifies the time dependent fibre mechanism in the presence of a sustained load.

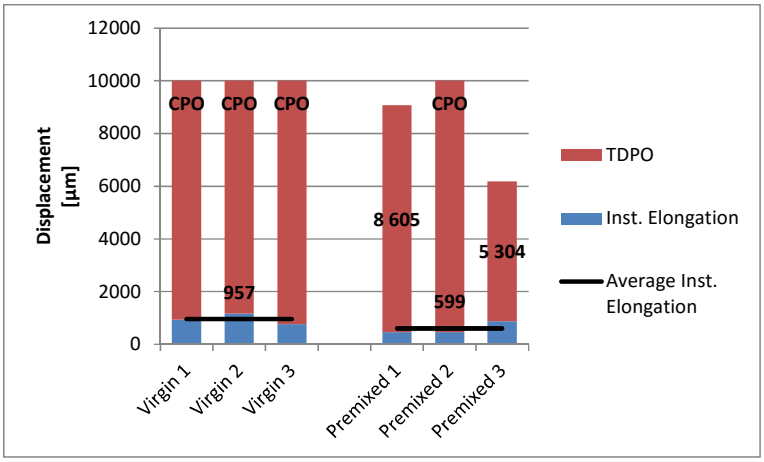

Figure 5.23: TDPO characteristics of C1

Table 5.7 provides the time C1 sustained the applied load.

Table 5.7: Time required for CPO of C1

Fibre State	Specimen	Time required for CPO [min]
Virgin	1	13.8
	2	33.6
	3	6.6
Premix	1	N.A.
	2	5226.6
	3	N.A.

5.2.2 Flat F1 TDPO

Figure 5.24 depicts the TDPO response of F1. It is evident that premixing significantly enhances the fibre-matrix interaction, as sustained loads are supported considerably longer. It must be noted that Specimen 3 of the virgin F1 fibre exhibited sudden pull-out (within 10.8 seconds) upon loading. The data is excluded, as no information on instantaneous fibre elongation and the TDPO behaviour was retainable.

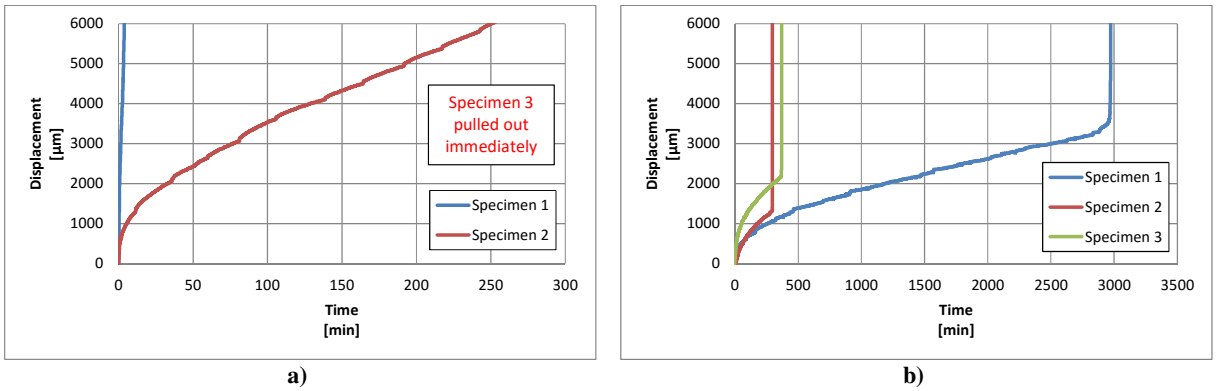

Figure 5.24: TDPO response of virgin (a) and premixed (b) F1

Figure 5.25 portrays the TDPO mechanisms. Virgin F1 fibres appear to undergo significantly more instantaneous elongation in contrast to premixed fibres. It must however be stressed,

that as a result of insignificant matrix-fibre bond, some pull-out displacement may be included in the instantaneous elongation, as the instantaneous elongation was only determined ten seconds after load application.

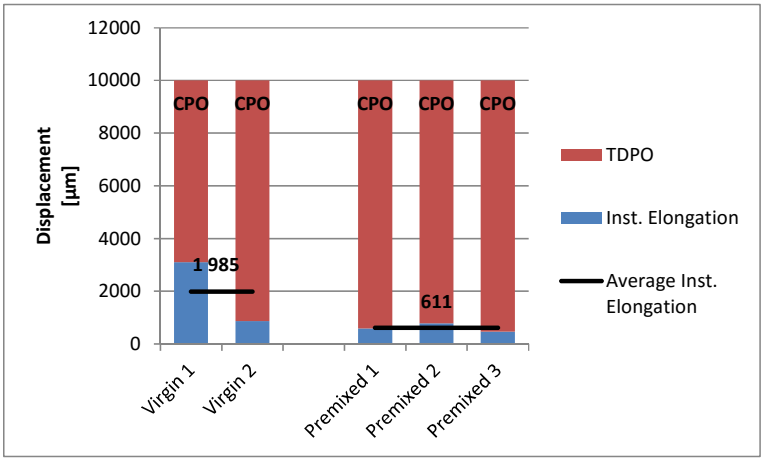

Figure 5.25: TDPO characteristics of F1

Table 5.8 provides an overview of the time required for CPO of F1 loaded to 50 % of its peak load capacity.

Table 5.8: Time required for CPO of F1

Fibre State	Specimen	Time required for CPO [min]
Virgin	1	3.6
	2	356.4
Premix	1	2975.4
	2	297.0
	3	369.0

5.2.3 Flat F2 TDPO

The TDPO response of the flat fibre F2 is provided in Figure 5.26. Parallels exist to the behaviour of the flat F1 fibre, as the pull-out duration required for CPO of virgin fibres is significantly less than that of the premixed fibres. In addition, the TDPO response exhibited by F2 does not correspond to the typical trend observed in previous results. A possible reasoning could be attributed to the poor bond characteristics of the fibre in its virgin state.

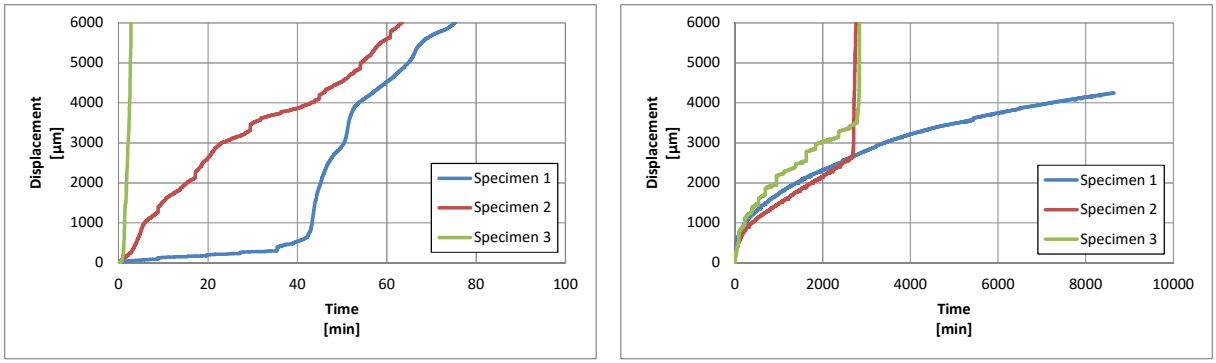

Figure 5.26: TDPO response of virgin (a) and premixed (b) F2

The TDPO mechanisms are quantified in Figure 5.27. Similar results are obtained for the instantaneous elongation upon loading.

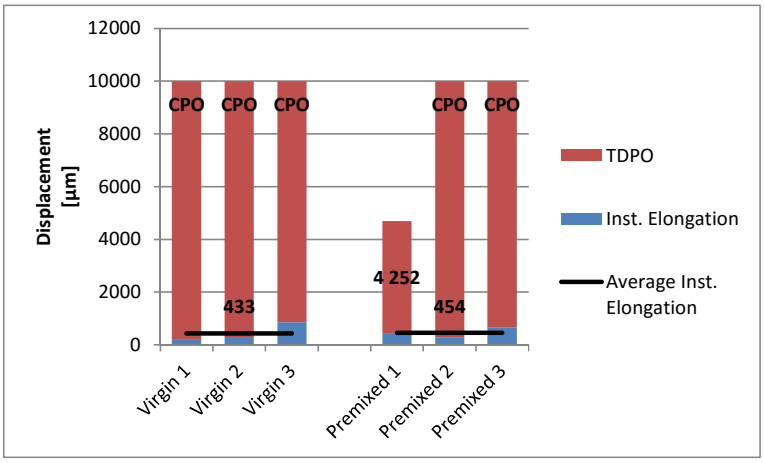

Figure 5.27: TDPO characteristics of F2

Table 5.9 provides the duration of load sustainment achieved by F2. It is apparent, that premixed fibres were able to sustain the load considerably longer compared to virgin fibres.

Table 5.9: Time required for CPO of F2

Fibre State	Specimen	Time required for CPO [min]
Virgin	1	96.6
	2	167.4
	3	3.0
Premix	1	N.A.
	2	2832.6
	3	2844

5.2.4 Embossed E1 TDPO

The TDPO response exhibited by E1 is shown in Figure 5.28. It is evident that E1 does not experience CPO for the duration of the test. This can be attributed to the good fibre-matrix interaction of the fibre geometry.

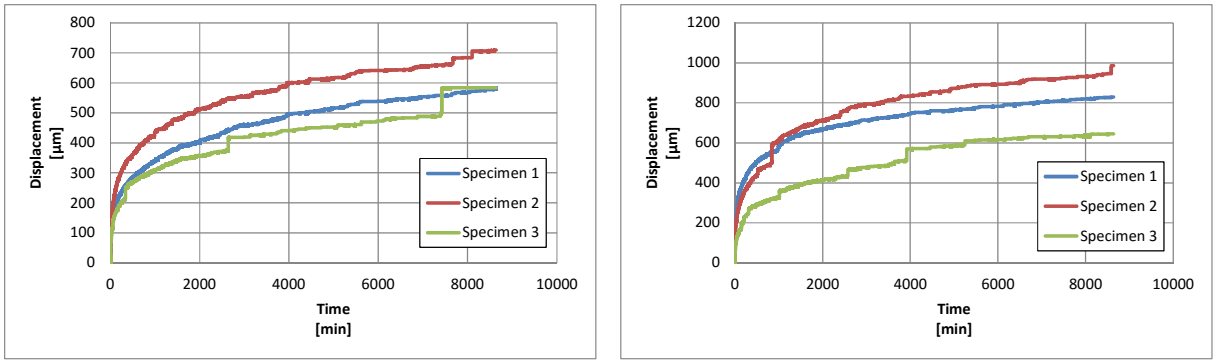

Figure 5.28: TDPO response of virgin (a) and premixed (b) E1

The mechanisms acting during TDPO are quantified in Figure 5.29. It is evident, that in addition to the effective fibre geometry of E1, the high modulus of elasticity of the fibre material contributes to the small pull-out displacements, especially the instantaneous fibre elongation upon loading. It is however evident that the performance of the E1 slightly decreased for fibres subjected to premixing.

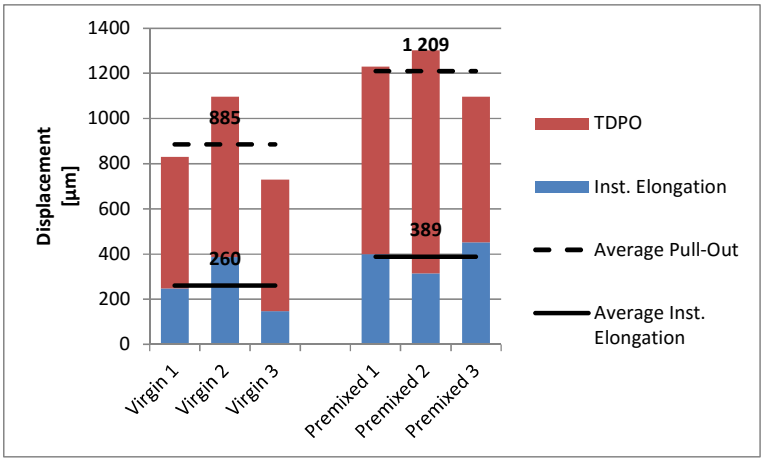

Figure 5.29: TDPO characteristics of E1

5.2.5 Embossed E2 TDPO

The behaviour of the embossed fibre type E2 under TDPO conditions is displayed in Figure 5.11.

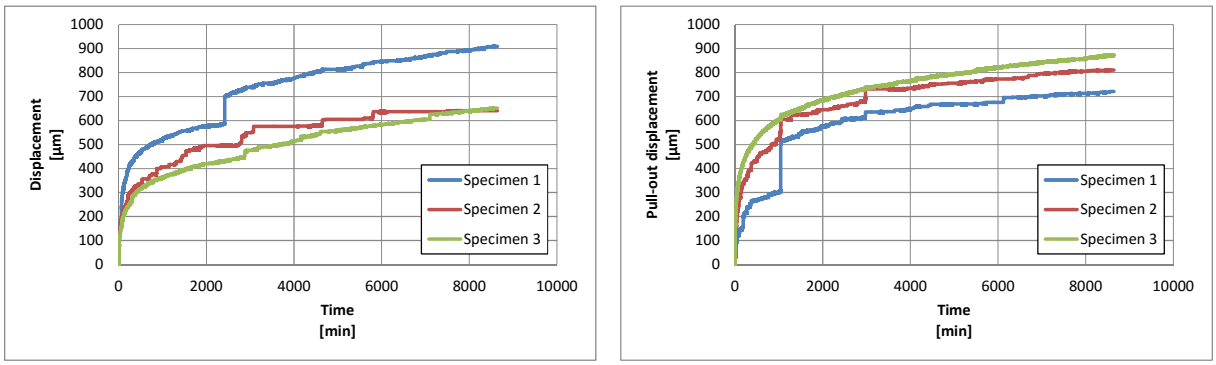

b) a)

Figure 5.30: TDPO response of virgin (a) and premixed (b) E2

The averaged TDPO displacement and instantaneous elongation of E2 subjected to sustained loading conditions is depicted in Figure 5.31. Parallels exist to the results obtained for E1, as a slight decrease in performance is exhibited by premixed fibres in contrast to the virgin fibre state.

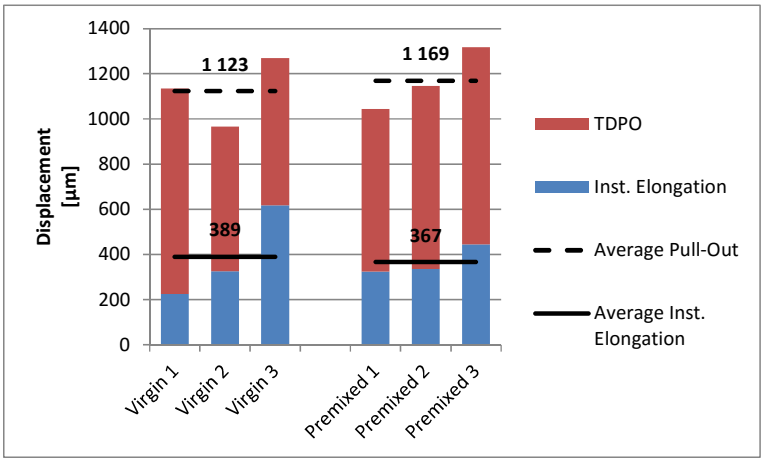

Figure 5.31: TDPO characteristics of E2

As anticipated, after six days upon test completion, no E2 specimens experienced CPO as a result of the favourable bond conditions achieved by the embossed fibre geometry.

5.2.6 Embossed built-up EB1 TDPO

Due to the built-up nature of EB1, comprising of individual fibre components, the following fibre conditions were considered for the TDPO investigation:

- Virgin built-up fibre
- Virgin larger cross-sectional fibre
- Virgin smaller cross-sectional fibre
- Premixed fibre state

The pull-out response exhibited by the aforementioned fibre conditions is presented in Figure 5.32.

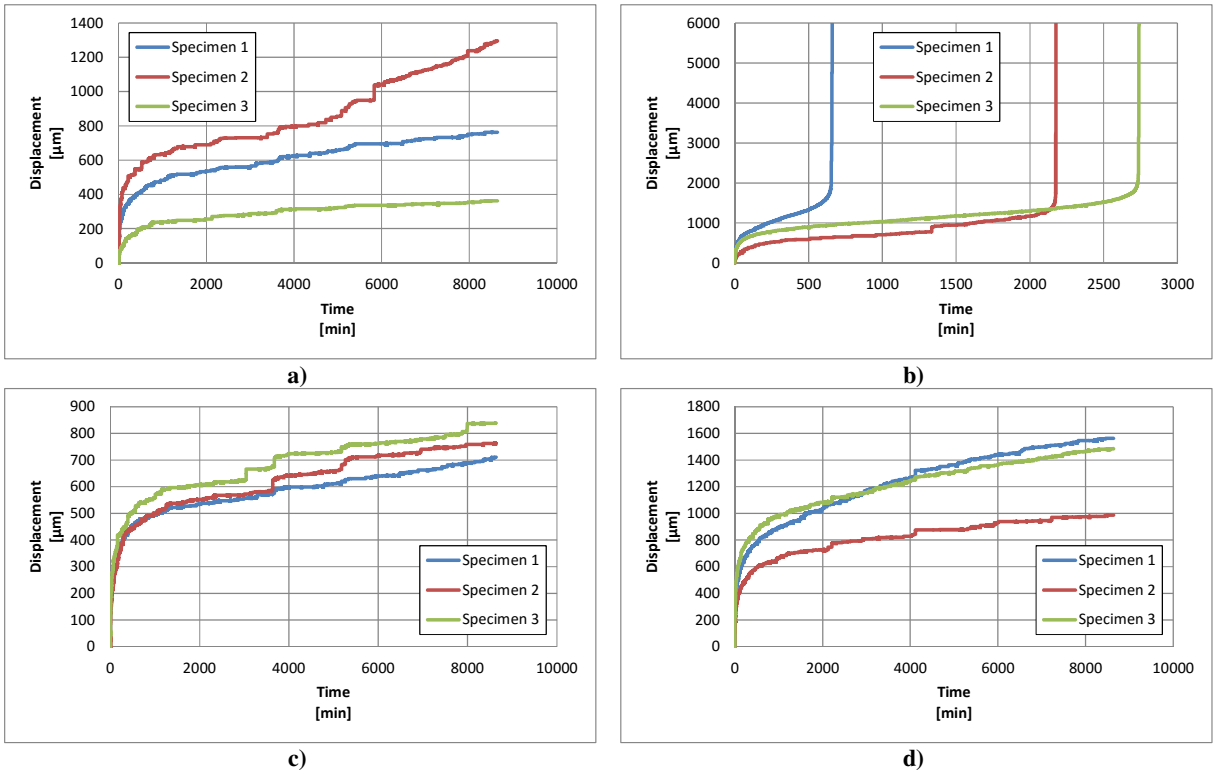

Figure 5.32: TDPO response of virgin built-up (a), d_{small} (b), d_{large} (c) and premixed (d) C1

The mechanisms exhibited by the different forms of EB1 during TDPO are depicted in Figure 5.33. It must be noted that the response exhibited by the small virgin fibre is presented using a different scale in contrast to the remaining forms of EB1, with reference to the secondary displacement axis. It is evident that the small cross-sectional fibre does not follow the typical trend exhibited by the embossed fibre type, as CPO is experienced.

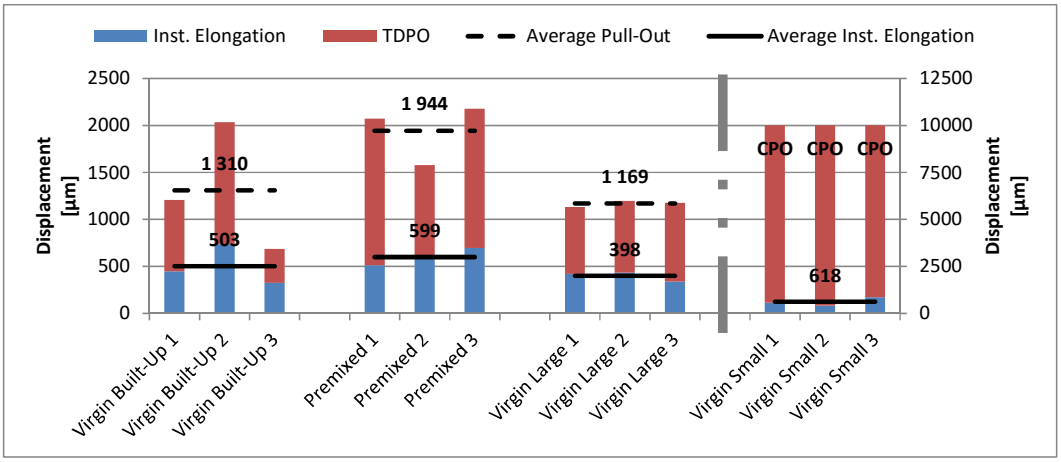

Figure 5.33: TDPO characteristics of EB1

Table 5.10 provides the time required for the small cross-sectional EB1 in the virgin state to exhibit CPO.

Table 5.10: Time required for CPO of EB1

Fibre state	Specimen	Time required for CPO [min]
Virgin small	1	664.2
	2	2177.4
	3	2743.2

5.3 Scanning Electron Microscopy

Scanning electron microscopy (SEM) was used for the surface analysis of macro synthetic fibres subjected to SFPO conditions. Such images provide valuable information regarding fibre geometries (profile and shape) responsible for an enhanced fibre-matrix interaction. It is anticipated that severe surface damage is identifiable on fibres exhibiting a sound interfacial bond with the surrounding matrix, while little surface damage is characterised by poor interfacial bond.

SEM images were taken of individual macro synthetic fibres in the following conditions:

- Virgin fibre state
- Premixed fibre state
- Virgin fibres subjected to SFPO experiencing pull-out
- Premixed fibres subjected to SFPO experiencing pull-out
- Fibres experiencing rupture under SFPO

A label was added to individual SEM images in order to simplify the identification process, with centre and edge designating the position of image acquisition on macro synthetic fibres.

5.3.1 Virgin fibres

Figure 5.34 depicts the surface of virgin macro synthetic fibres in the absence of any surface roughening caused by premixing or pull-out.

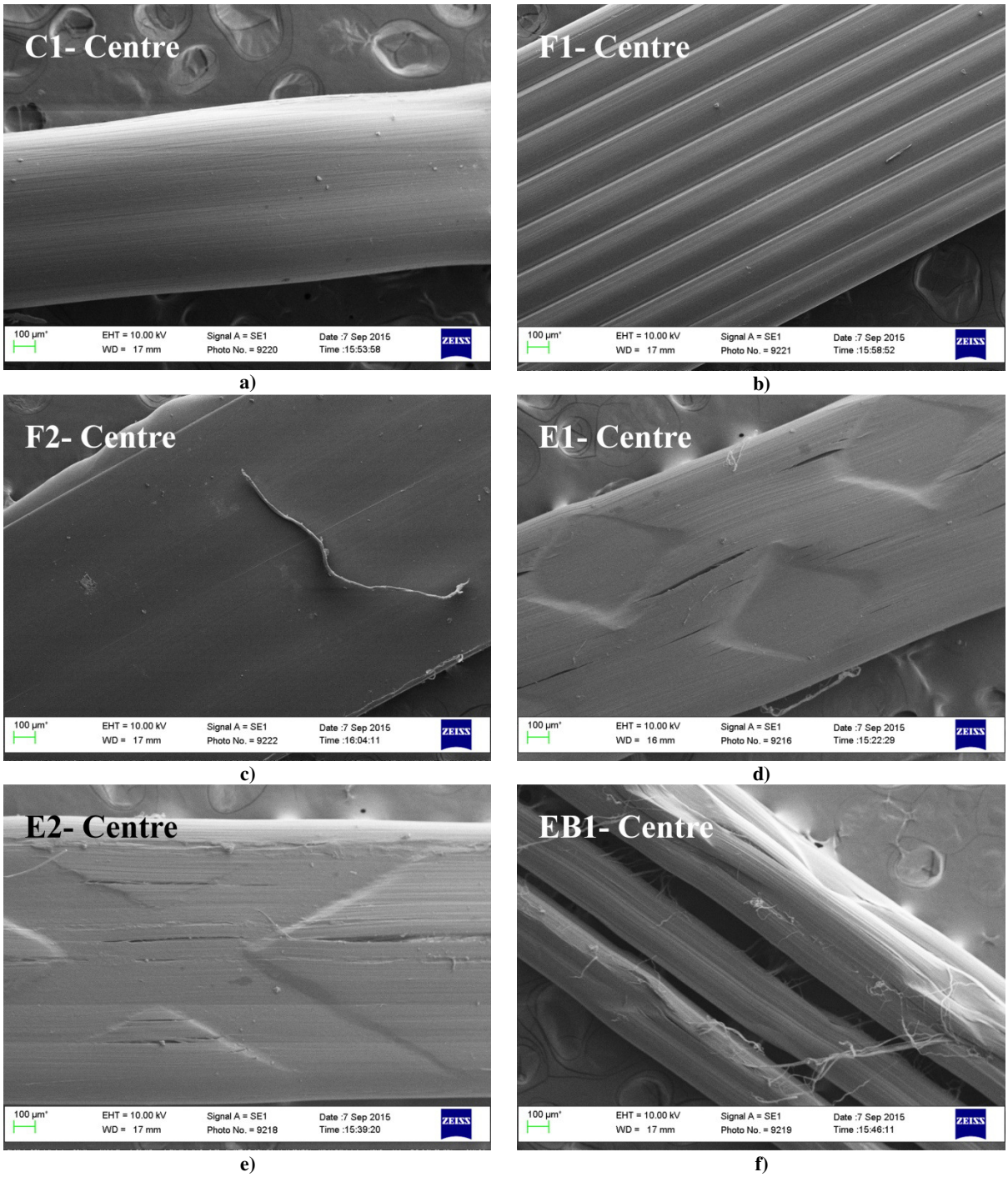

Figure 5.34: SEM image of virgin fibre surfaces

5.3.2 Premixed fibres

The fibre surfaces of various macro synthetic fibres subjected to premixing are shown in Figure 5.35. It is evident that a significant difference exists to virgin fibre surfaces. This can be attributed to the effect of aggregate crushing, causing fibre surface roughening during the mixing process.

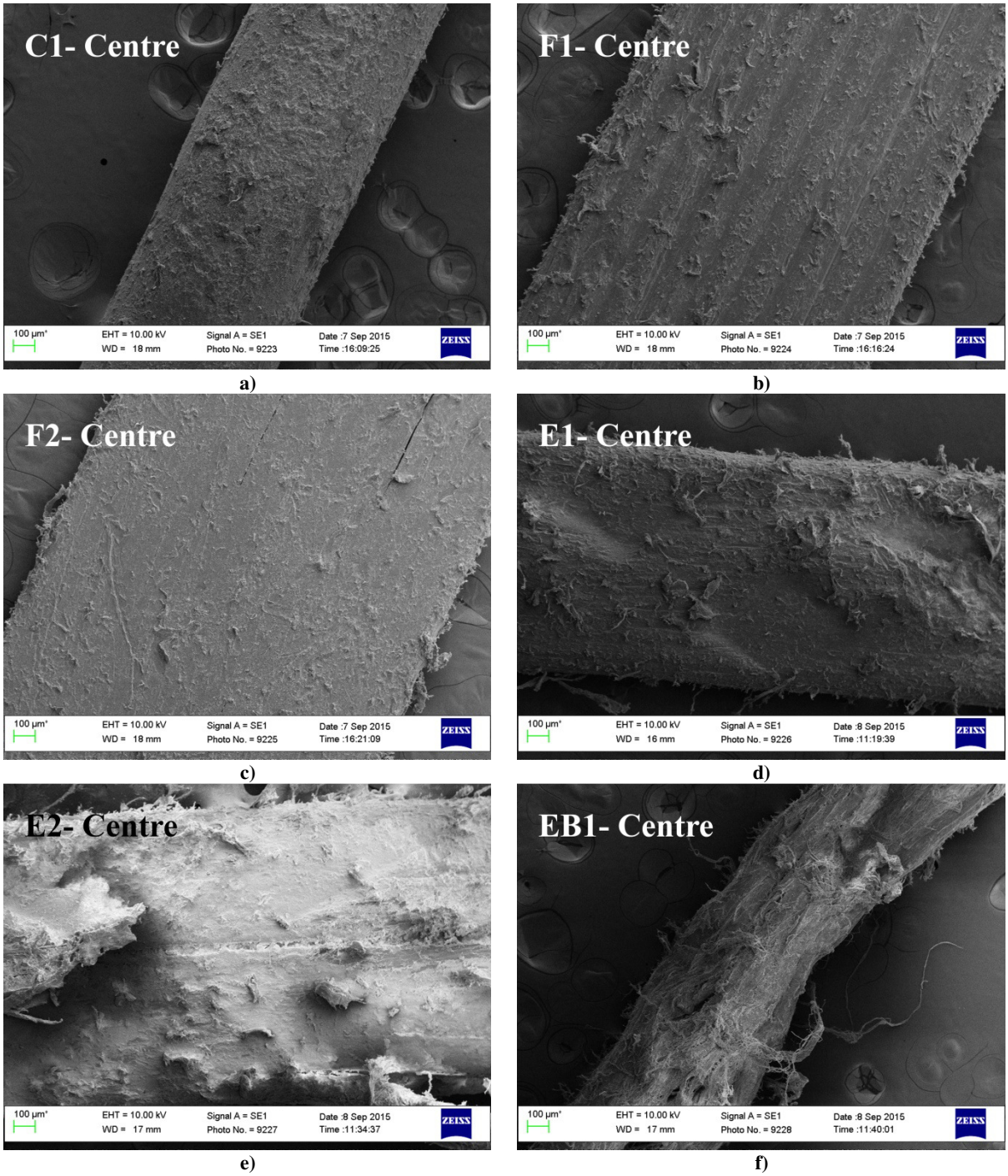

Figure 5.35: SEM image of premixed fibre surfaces

5.3.3 Virgin fibres subjected to SFPO

Figure 5.36 depicts the fibre damage caused by SFPO experiments conducted on virgin fibres. It is evident that certain fibres exhibit significantly more severe damage than others, as a result of a better fibre-matrix interaction in the virgin fibre state. Images were typically acquired in the centre as well as at the edge of the fibre in order to provide a good in indication of the fibre damage caused along the whole pull-out surface.

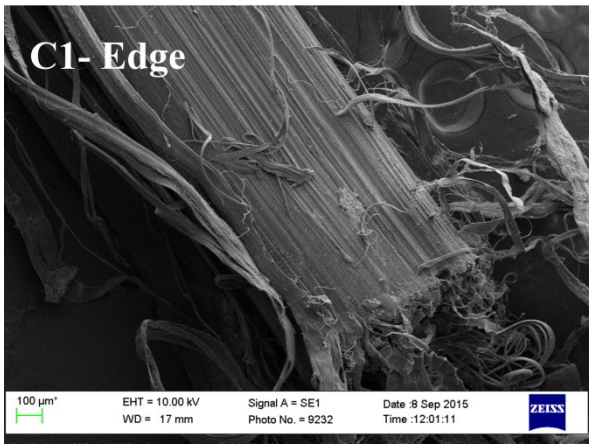

a)

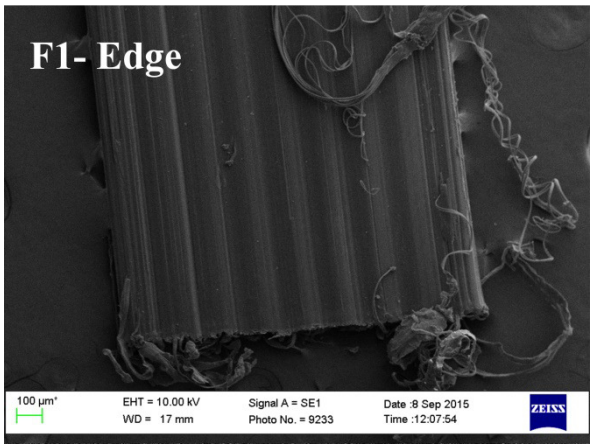

b)

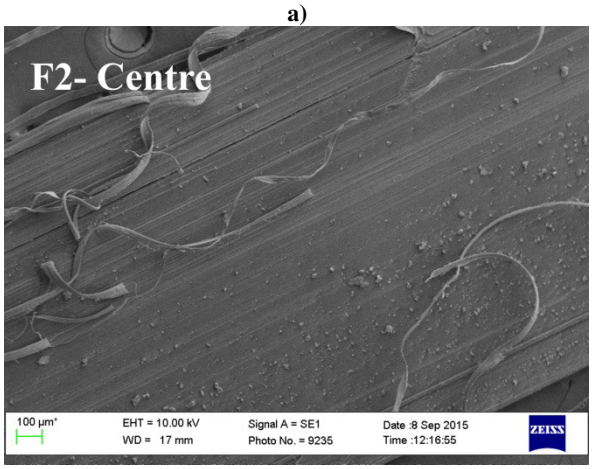

c)

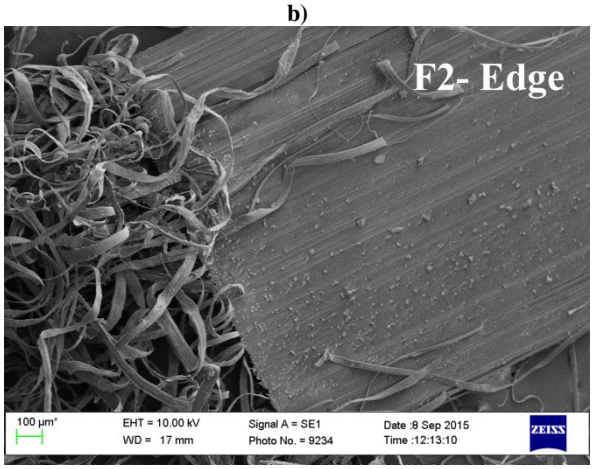

d)

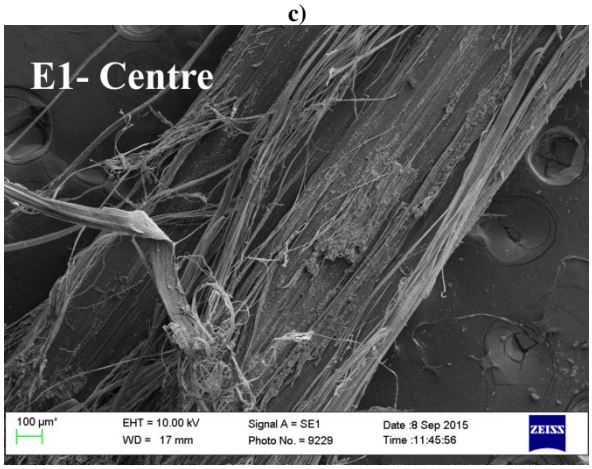

e)

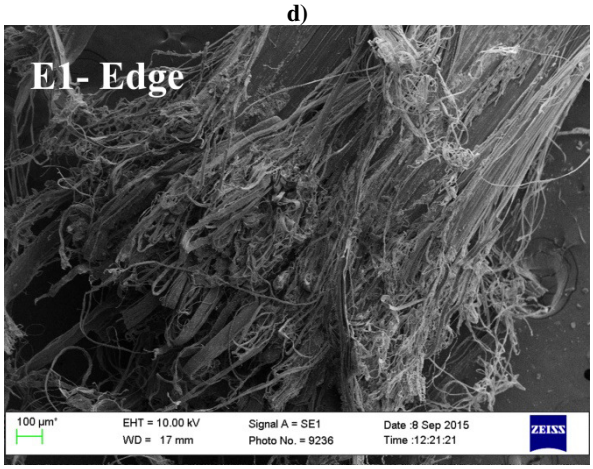

f)

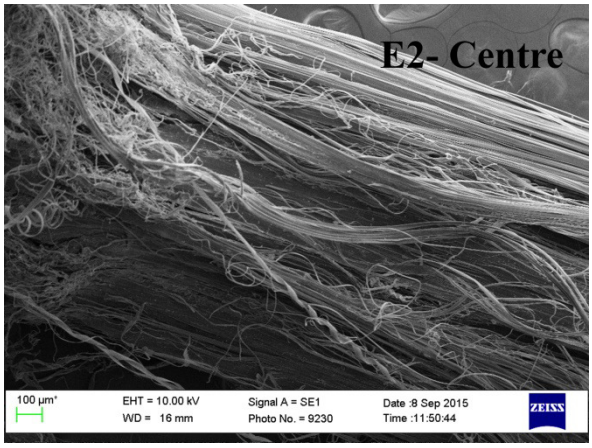

g)

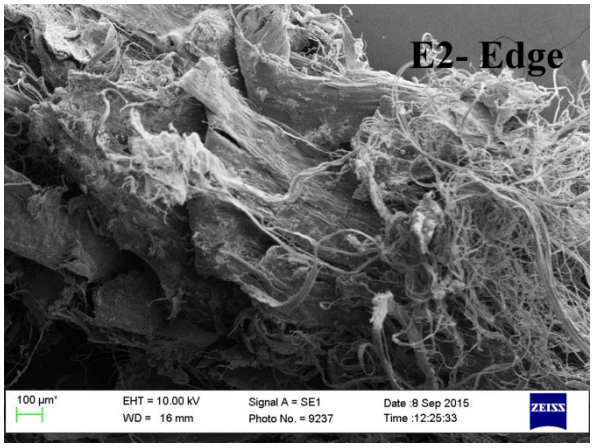

h)

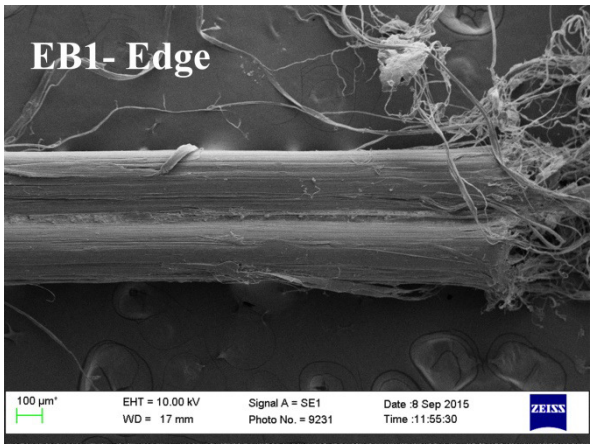

i)

Figure 5.36: SEM images of virgin fibres subjected to SFPO

5.3.4 Premixed fibres subjected to SFPO

The surface damage caused under SFPO to premixed fibres is shown in Figure 5.37. Edge and central images of premixed fibre surfaces subjected to SFPO are shown to provide a good indication of the damage caused at the respective positions. In contrast to Figure 5.36, flat fibres exhibit significantly more severe surface damage, caused by a better fibre-matrix interlock as a result of premixing.

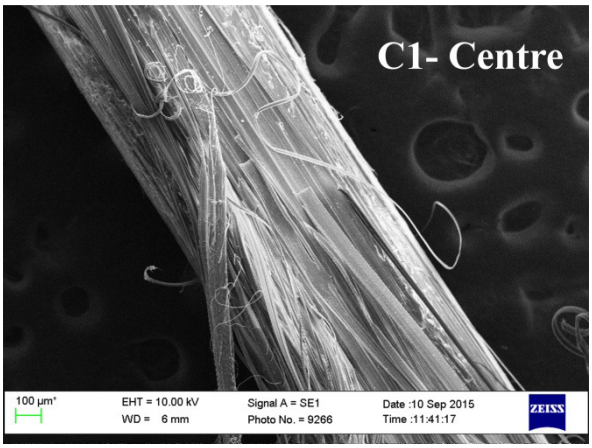

a)

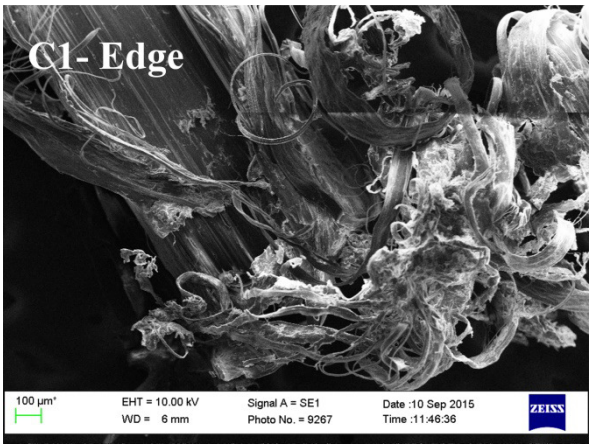

b)

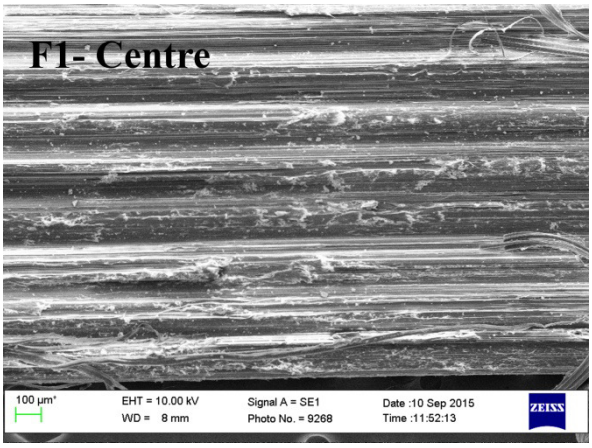

c)

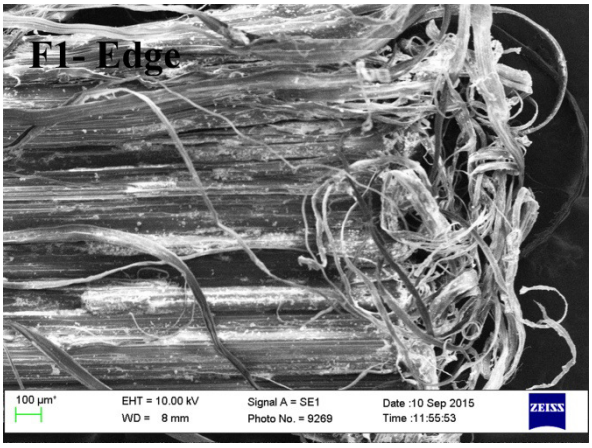

d)

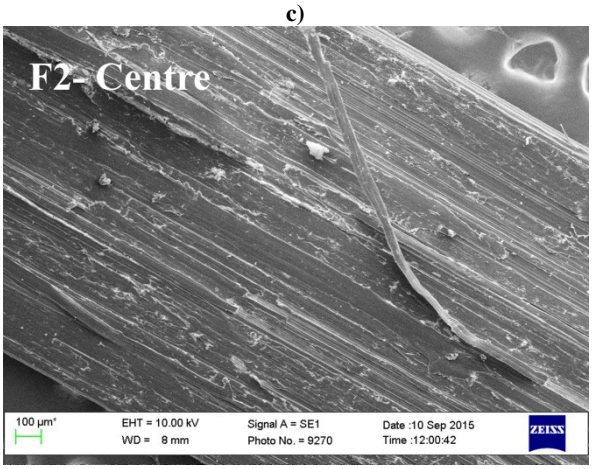

e)

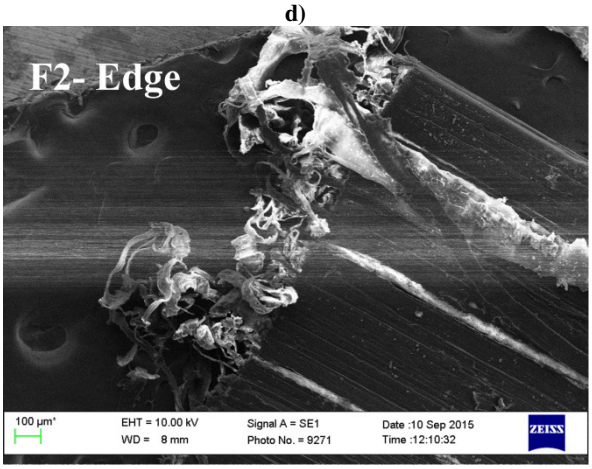

f)

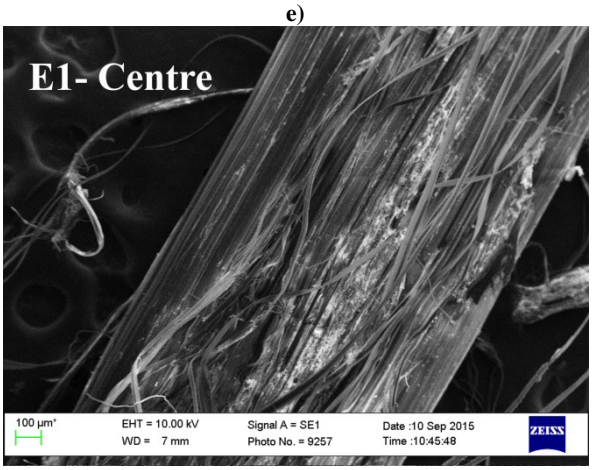

g)

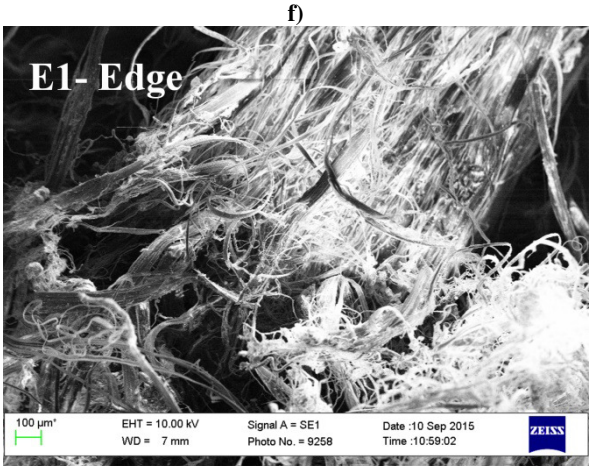

h)

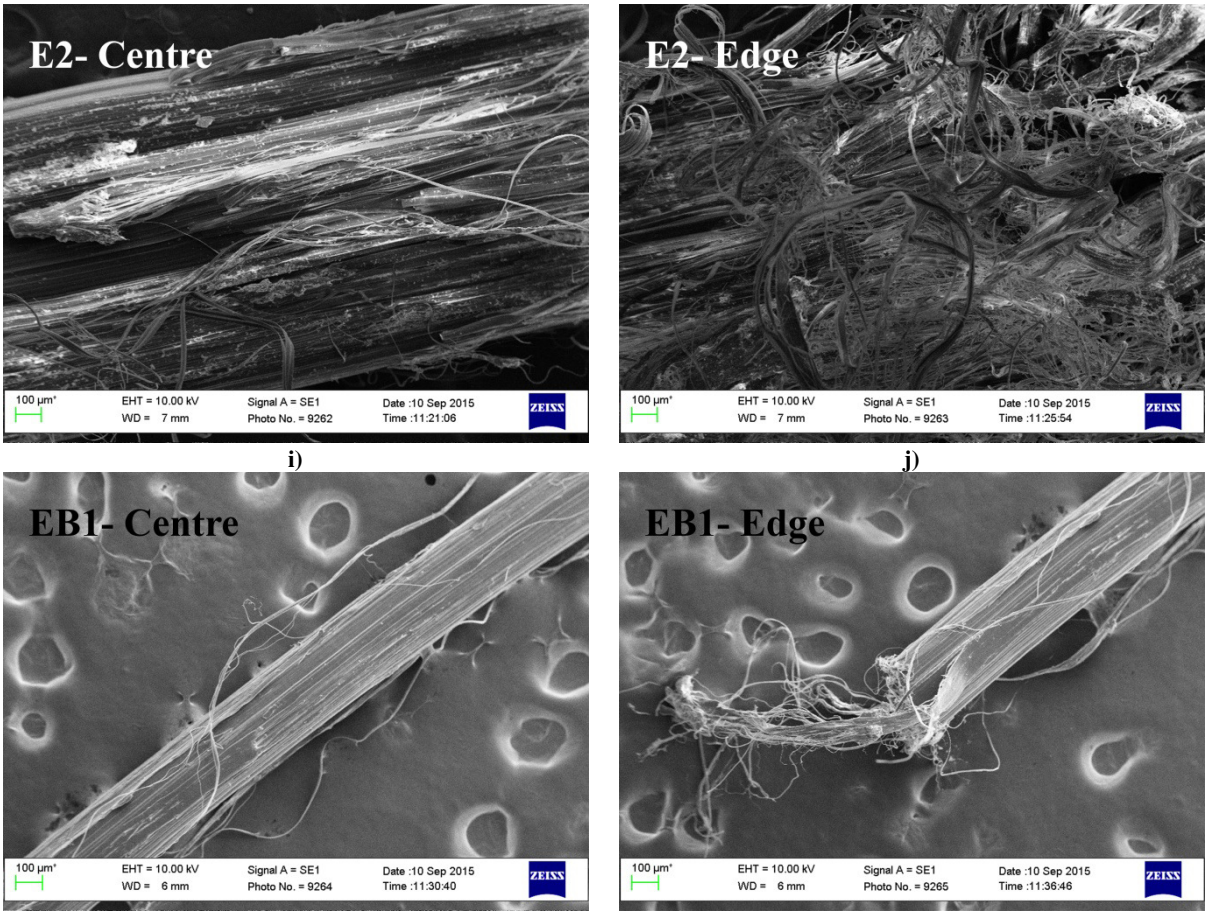

Figure 5.37: SEM images of premixed fibres subjected to SFPO

5.3.5 Fibre rupture under SFPO

As a result of a high interfacial bond development between the fibre-matrix interfaces, fibres encounter rupture once the interfacial bond stress exceeds the fracture stress of the fibre. The fracture modes typically exhibited by this scenario are depicted in Figure 5.38.

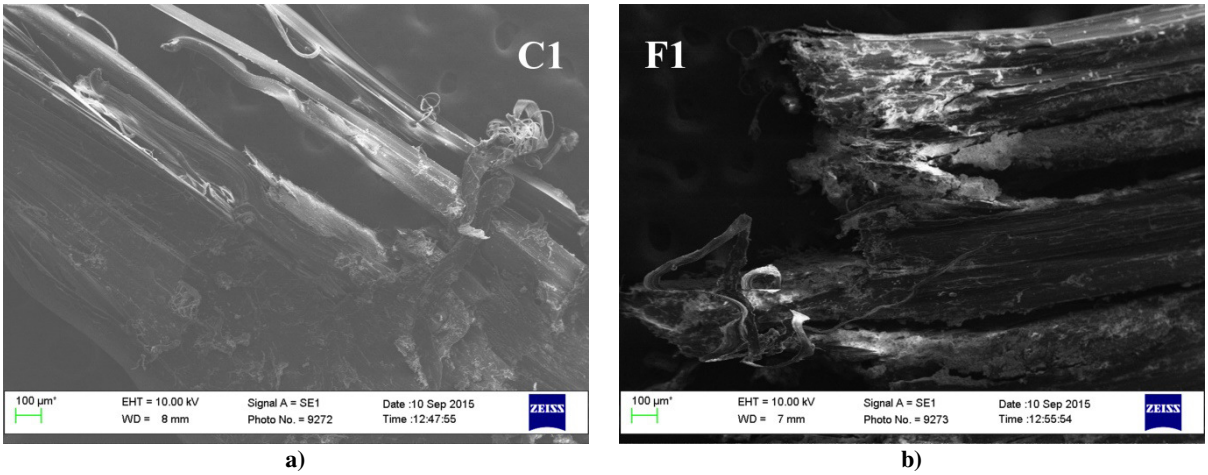

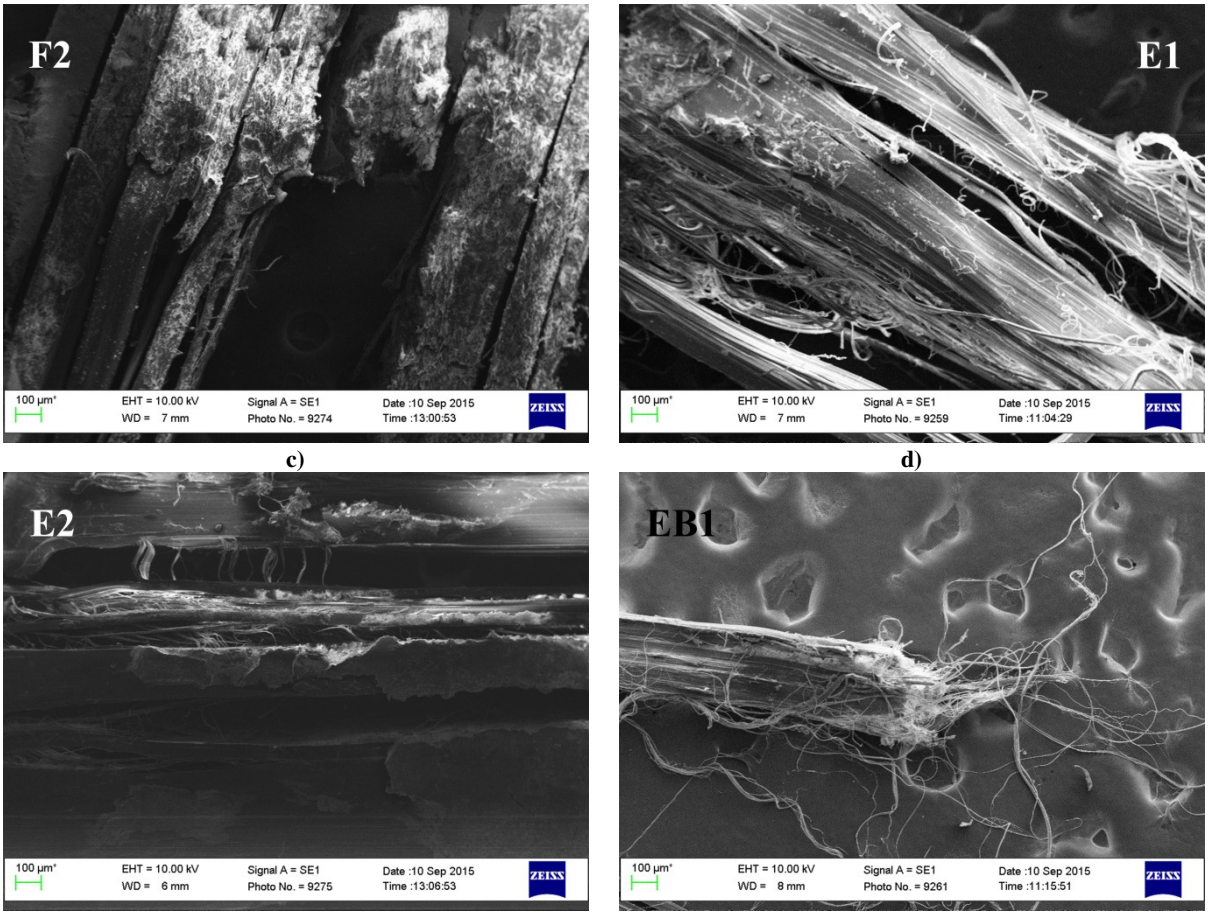

Figure 5.38: SEM images of ruptured fibres

5.4 Discussion

5.4.1 Peak load

The peak load corresponding to the peak pull-out load during the SFPO response was determined for different macro synthetic fibres embedded at various depths into the concrete paste matrix. The peak load was established using the results of eight virgin fibre specimens in contrast to twelve premixed fibres as a result of the possible higher variability generated by the uncontrollable surface roughening caused by the premixing process.

Due to the relationship of direct proportionality between embedment length and peak load, higher pull-out loads are expected for longer embedment lengths, as indicated by the initial portion of the pull-out response depicted in Figure 5.39a. Once the critical fibre length is attained, the peak load is governed by the fracture stress of the fibre as a consequence of material failure. It is however difficult to quantify the critical length in terms of fibre rupture, as no distinct length was found resulting in pure fibre rupture once exceeded. Fibre rupture rather occurs over certain range of embedment lengths. Therefore, a decrease in slope of the

peak load response under SFPO is typically observed for an increase in embedment length, approaching the critical length. The decrease in slope of the pull-out response is primarily attributed to some fibres exhibiting rupture, while at the same time other fibres undergo pull-out at an equal embedment length, characterised by a lower peak load. Therefore, the overall average peak load at the same embedment within the critical length region is often governed by both, pull-out load and the load limited to the fibre material, as illustrated in Figure 5.39b.

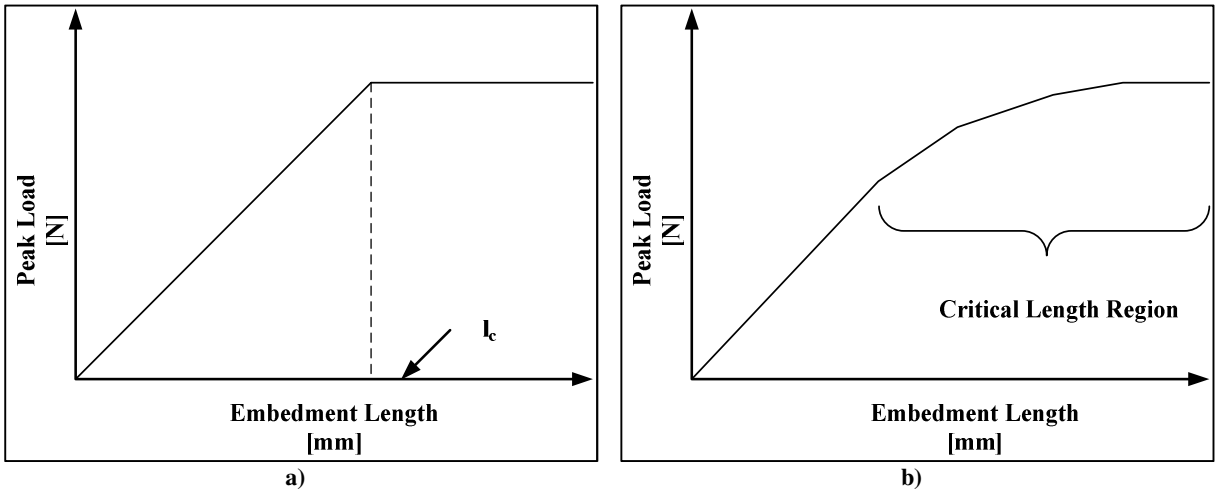

Figure 5.39: Ideal (a) and true (b) fibre pull out response

It is however stressed, that the peak load or pull-out resistance of a fibre is not suitable for comparing different fibres, as the embedded surface area significantly influences the elastic pull-out load. This is highlighted in Figure 5.40, depicting an increasing trend of peak load for larger equivalent diameters. It is important to note that peak loads are presented for an embedment length L25. Therefore, it is evident that the interfacial bond is a better representation for the comparison of macro synthetic fibre performance on a single-fibre level.

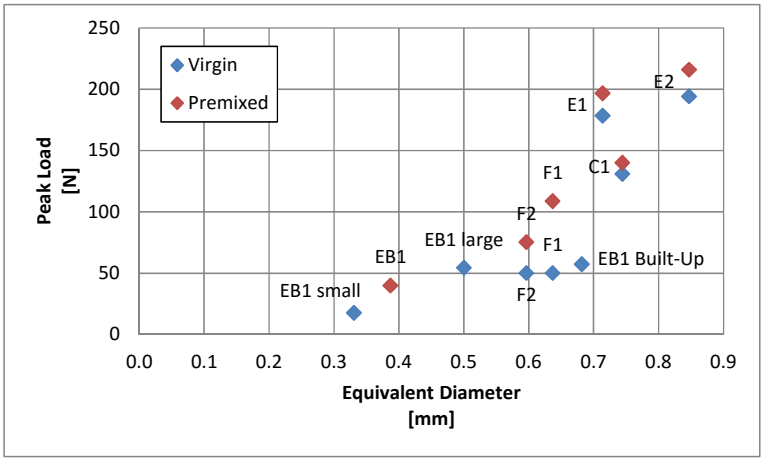

Figure 5.40: Effect of equivalent diameter on the peak load for 25 mm embedment

5.4.2 Interfacial bond stress

In order to successfully compare macro synthetic fibre performance on a single-fibre level, the uniform bond model as given by Equation (2.2) was adopted. The model provides the peak load distributed over the embedded surface area, synonymous for interfacial bond. However, based on the results provided in Section 5.1, the typical behaviour exhibited is that of a non-uniform bond with a downward trend for longer embedment lengths, with the exception of virgin flat fibres. The interfacial bond at different levels of embedment for the investigated macro synthetic fibres is provided in Figure 5.41. It is evident that E1 and E2 exhibit the highest bond performance under SFPO.

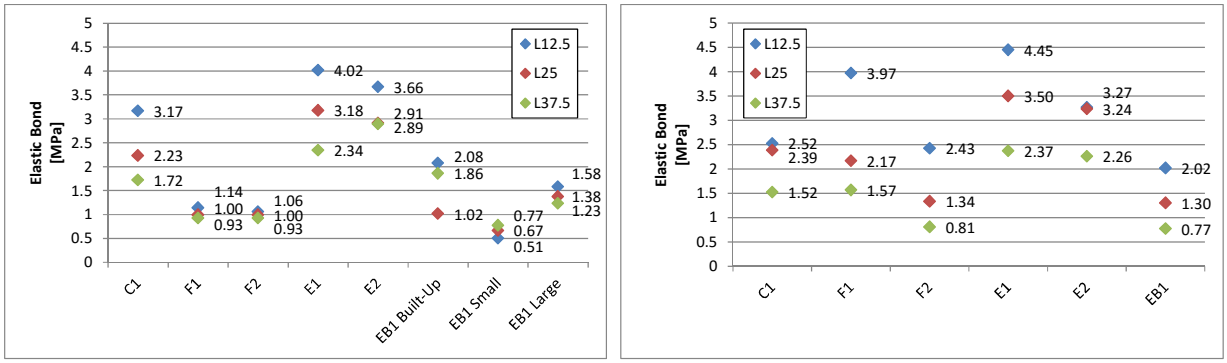

Figure 5.41: Elastic bond of virgin (a) and premixed (b) fibres

Figure 5.41 highlights the aforementioned non-constant bond observations for different levels of embedment of various macro synthetic fibres, typically indicating the highest bond for an embedment of L12.5. Virgin flat fibres verify to be an exception to the decreasing trend and rather correspond to the behaviour anticipated by the uniform bond stress model. In addition, it is essential to note that a significant difference in interfacial bond exists for virgin and premixed flat fibres. This is attributed to aggregate crushing during the mixing process, causing roughening of the flat fibre surface responsible for an enhanced interfacial bond. It is therefore apparent that the flat fibre geometry does not provide the primary mechanism for an enhanced bond. The strong bond characteristics are rather attributed to the surface roughening caused by premixing. The effect of mixing tends to have no significant effect on non-flat fibre geometries.

The strong elastic bond stress characteristics for shorter embedment lengths indicate a high initial mechanical interlock between the fibre-matrix interface, not following the anticipated behaviour of the uniform bond model depicted in Figure 5.42a. This is confirmed by Figure 5.42b and Figure 5.42c for an embedment of L12.5 and LH of E2 as an example, portraying

the interfacial bond stress calculated at individual instances along the fibre profile during the pull-out response. This is achieved by adjusting Equation (2.2) as follows:

$$\tau_i = \frac{F_i}{\pi d_{eq}(l_e - l_i)} \tag{5.2}$$

with

i = considered instance

τ_i = interfacial bond at specific instance

F_i = load response at specific instance

d_{eq} = equivalent fibre diameter

l_e = initial embedment length

l_i = pulled-out fibre length at specific instance during SFPO response

It is evident that a decrease in bond can be observed directly upon de-bonding. Such behaviour was typically observed for the majority of macro synthetic fibres. The true bond developed of a fibre is thus overestimated by the uniform bond model. A relatively uniform bond can be identified over the post-peak region of the SFPO response. It is evident that a good indication of the bond present in the post-peak region can be quantified by the average interfacial bond. It is proposed that in place of determining the interfacial bond by means of the peak elastic pull-out load, the average pull-out load (τ_{avg}) is used instead, given by:

$$\tau_{avg} = \frac{F_{avg}}{\pi d_{eq} l_e} \tag{5.3}$$

with F_{avg} the average load.

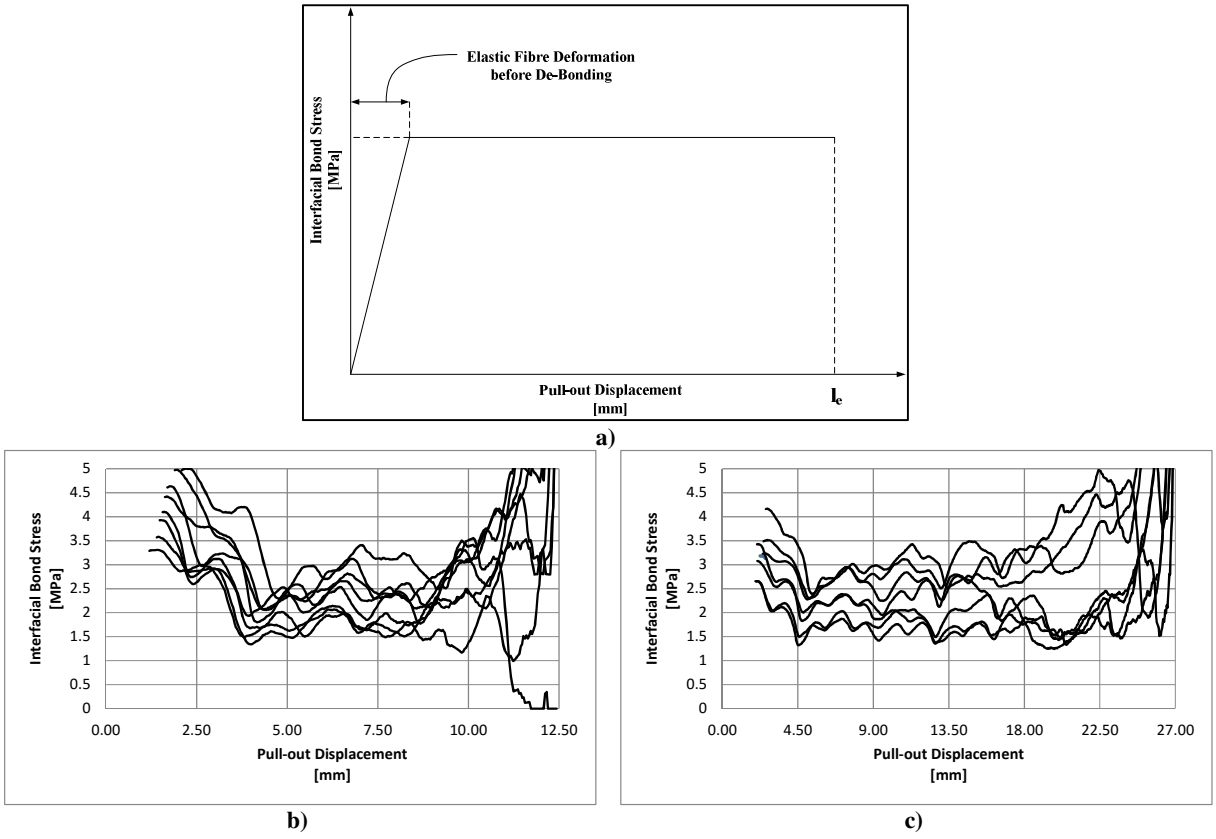

Figure 5.42: Interfacial bond development: ideal bond (a) true bond behaviour of virgin E2 for L12.5 (b) and LH (c)

The primary pitfall of Equation (5.2) is its dependency on the measure of pull-out length. This is visually depicted in Figure 5.42a and Figure 5.42b in the vicinity complete fibre pull-out, as unrealistic high interfacial bond stresses occur in this region. This is caused as the pull-out displacement l_i approaches l_e causing a division by a value nearing zero. It is furthermore important to note, that fibre rupture will require Equation (5.2) to be adjusted as follows:

$$\tau_i = \frac{F_i}{\pi d_{eq}(l_r - l_i)} \tag{5.4}$$

with l_r the pull-out length prior to rupture, replacing the initial embedment length l_e as used in Equation (5.2). It is thus evident that an average interfacial bond model requires complex adjustments to the existing approach. Furthermore, the exact position of fibre rupture is required in order to use Equation (5.4) successfully.

Figure 5.43 depicts the average interfacial bond stress of the various fibres between de-bonding and 50 % pull-out in order to prevent the unrealistic high bond present close to complete pull-out. It is stressed, that bond stresses of fibres experiencing rupture were set to zero as the exact position of rupture during the pull-out response could not be identified.

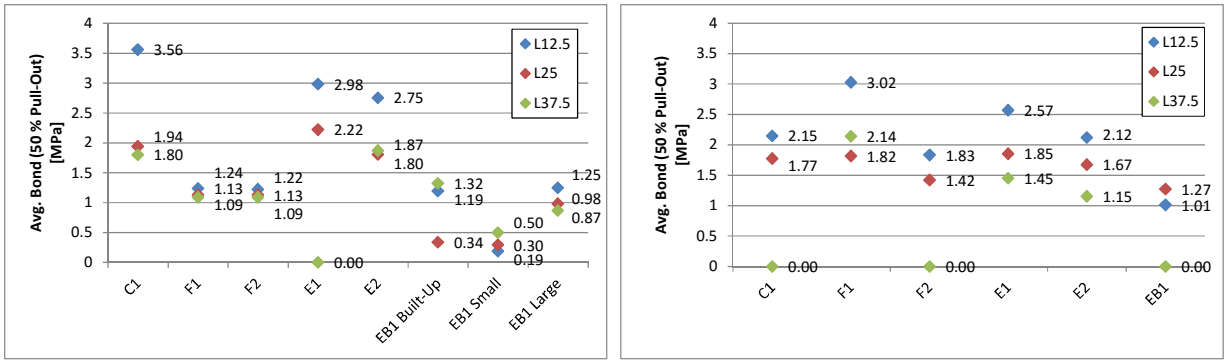

Figure 5.43: Average interfacial bond of virgin (a) and premixed (b) fibres

It is evident, that the region over which the averaged interfacial bond stresses occur is narrower than the region exhibited by the elastic bond determined according to the uniform bond model as depicted in Figure 5.41. Nevertheless, the average bond model also indicates higher bond stresses for lower levels of embedment in contrast to longer embedment lengths, similar to the uniform bond model. This can be ascribed to the inclusion of the high initial mechanical interlock in the averaged bond values over the post-peak region. The primary reason for this is attributed to the range over which the high initial mechanical interlock is present in the post-peak region shortly after de-bonding. The high initial mechanical interlock is thus more prominent for shorter embedment length, as shown in Figure 5.42b, in contrast to longer embedment lengths, as depicted in Figure 5.42c. This phenomenon is further highlighted in Figure 5.44.

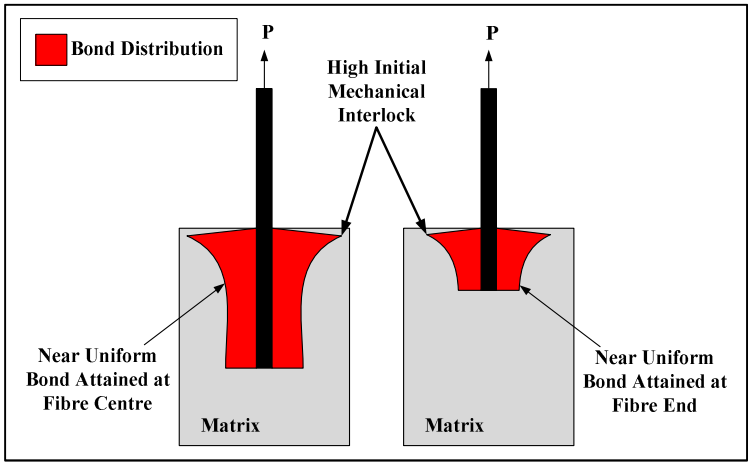

Figure 5.44: Interfacial bond stress development over the embedded fibre surface length

5.4.3 Energy dissipation

A useful performance measure for single fibres under SFPO is the ability of a fibre to dissipate energy. In contrast to the interfacial bond, determined according to the uniform bond model, thus quantifying the performance only at the peak-load instance during the pull-

out response, the energy dissipated provides information about the complete pull-out procedure. In addition, the energy calculation is not as susceptible to unrealistic high values near the fibre end and fibre rupture as the average bond model, which is assigned to the simple nature of calculating the dissipated energy (E_E) according to:

$$E_E = F \times \delta \tag{5.5}$$

with F and δ the force and pull-out displacement respectively. It is evident that upon fibre rupture, the pull-out load decreases to zero resulting in no further energy dissipation. However, due to the cumulative nature of the energy calculation, energy dissipated prior to rupture is easily quantified using Equation (5.5).

It is anticipated that fibres exhibiting higher pull-out forces also dissipate more energy. Another factor influencing energy dissipation is the embedment length, as longer fibre travel tends to absorb more energy. However, as aforementioned, upon rupture no further energy can be dissipated. Fibres typically exhibit constant energy dissipation as a result of rupture prior to de-bonding. This is typically observed for high embedment lengths of premixed F1, F2 and EB1 as well as virgin E1, as depicted in Section 5.1. In addition, built-up EB1 did not dissipate energy efficiently at an embedment L25, which is attributed to telescopic effects. Telescopic effects are experienced as some components contributing to the built-up system do not achieve sufficient bond properties with the surrounding matrix resulting in low energy dissipation.

Section 5.1 provided the energy dissipated by various fibres for different percentages of pull-out displacement. It is evident, that a steep overall slope of energy dissipated for different percentages of fibre pull-out represents a more efficient fibre-matrix interlock of the fibre geometry.

As the pull-out load is dependent on the cross-sectional area of macro synthetic fibres, energy dissipation of a single-fibre is not a suitable parameter for performance comparison. However, a comparable energy parameter is created by determining the single-fibre performance over a predefined area. Figure 5.45 depicts the single-fibre energy dissipation of single fibres over a surface area equal to 100 x 100 mm.

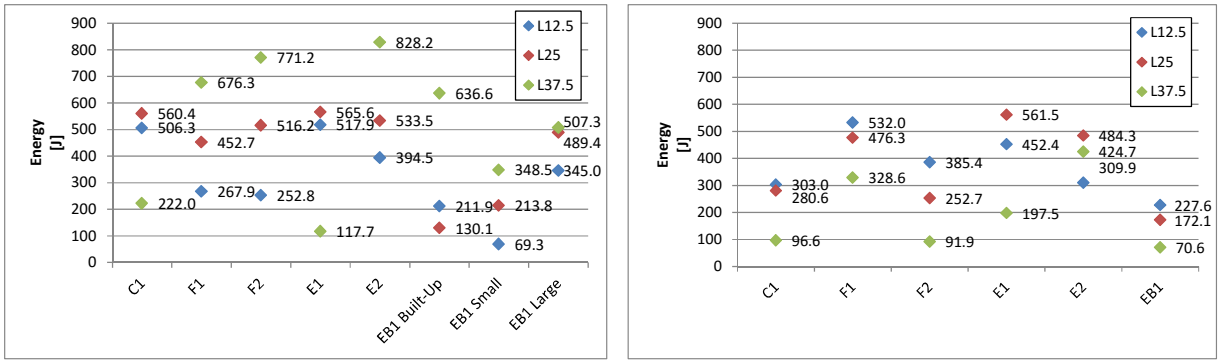

Figure 5.45: Virgin (a) and premixed (b) fibre energy dissipation over 100 x 100 mm

It is evident, that due to low rupture percentages of virgin fibres, pulled-out virgin fibres utilised the full embedment length to dissipate energy. This typically results in an increased energy dissipation for higher levels of embedment as visually depicted in Figure 5.45a. In contrast, premixed fibres exhibited high interfacial bond stresses, often characterised by fibre rupture. Such fibres only utilise the fibre length prior to rupture to dissipate energy, resulting in lower energy dissipation in contrast to shorter premixed embedment lengths undergoing pull-out as shown in Figure 5.45b.

5.4.4 Time dependent single-fibre pull-out

The response of single macro synthetic fibres subjected to sustained loads is believed to partially represent the behaviour responsible for time dependent cracked widening of cracked FRC elements.

It was established that fibre premixing has a significant influence on the time dependent behaviour, especially for flat polypropylene macro synthetic fibres. F1 exhibited CPO within an average of 180 minutes in the virgin state, while sustaining the applied loads for 1214 minutes when premixed. Additionally, considerably less instantaneous elongation was recorded for the premixed fibre state in contrast to virgin F1 fibres, being equal to 0.61 and 1.99 mm respectively. F2 experienced similar behaviour under TDPO with virgin fibres experiencing pull-out within an average of 89 minutes while premixed fibres withstood the applied loads for 2838 minutes. It is important to note that one premixed F2 did not undergo CPO. A different trend was however observed for the instantaneous elongation upon loading. Virgin F2 exhibited an immediate displacement of 0.43 mm in contrast to 0.45 mm of premixed fibres. Nonetheless, the difference can be regarded as insignificant.

The crimped fibre profile of C1 exhibited similar behaviour to flat fibres, as considerable higher performance was observed for premixed fibres in contrast to virgin fibres. While withstanding the applied load for 18 minutes on average in the virgin state, only one premixed specimen experienced CPO, recorded at 5227 minutes. The average instantaneous elongation experienced by virgin C1 was determined as 0.96 mm in contrast to 0.60 mm for the premixed fibre state, while the average TDPO (including CPO of 10 mm of one specimen) exhibited by premixed fibres was quantified as 8.41 mm.

More desirable behaviour was exhibited by the embossed macro synthetic fibres, E1 and E2. Upon completion of the investigation after six days, none of the tested specimens experienced CPO. Important TDPO experimental information of E1 and E2 is provided in Table 5.11.

Table 5.11: TDPO performance of E1 and E2

Fibre	Instantaneous elongation [mm]	Time dependent pull-out [mm]
Virgin E1	0.26	0.89
Premixed E1	0.39	1.20
Virgin E2	0.39	1.12
Premixed E2	0.37	1.12

It is evident that premixing has an insignificant influence on the TDPO performance of embossed macro synthetic fibres. In addition, the high modulus of elasticity of modified olefin fibres significantly reduces the instantaneous elongations in contrast to polypropylene fibres.

The built-up fibre EB1 generally exhibited favourable TDPO behaviour, as only small EB1 experienced CPO, recorded at an average of 5585 minutes. All other forms of EB1 investigated under TDPO sustained the loads for the duration of the test. Important test results are presented in Table 5.12.

Table 5.12: TDPO performance of EB1

Fibre	Instantaneous elongation [mm]	Time dependent pull-out [mm]
EB1 built-up	0.50	1.31
EB1 large	0.40	1.17
Premixed EB1	0.60	1.94

5.4.5 SEM imaging

The SEM images acquired of individual macro synthetic fibre surfaces highlight the extent of surface scrapings caused by SFPO experiments. Significant surface scraping represents a high interfacial bond with the surrounding paste, while little surface damage indicates poor bond characteristics. A scaling bar is provided in the bottom left corner, indicating a constant

magnification of 100 µm. It is important to note, that only the working distance, being the distance between the specimen and the microscope lens, was modified in order to acquire legible images.

Figure 5.34 provides images of macro synthetic fibres in the virgin fibre state. The images clearly depict the surface geometry provided to fibres to enhance fibre-matrix interlocking. In contrast, Figure 5.35 shows the surface roughening caused by the mixing process. Thus, comparing SEM images of macro synthetic fibres in both fibre states, premixed fibres are characterised by fine scrapings and significant surface roughening in contrast to virgin fibres.

It is evident, that SFPO has a significant influence on the appearance of virgin macro synthetic fibres as shown in Figure 5.36. This can be attributed to the embossed surface geometry as well as crimped fibre profiling, effectively anchoring the fibre into the matrix. More interestingly, the virgin flat fibres F1 and F2 experience slight to insignificant surface damage during SFPO as shown in Figure 5.36a, Figure 5.36b and Figure 5.36c respectively, characterised by poor bond behaviour of virgin flat fibres. Some lint is identifiable on the edge of F2, however the fibre surface remains largely intact and therefore not contributing significant interlock to the fibre-matrix interaction. It is thus important to note, that flat fibre geometries with longitudinal corrugations, inefficiently anchor virgin flat fibres into the concrete matrix.

Figure 5.37 provides the SEM images acquired of premixed macro synthetic fibres after SFPO. The surface damage of embossed and crimped fibre geometries seem insignificant to the damage examined for the virgin equivalent. This is also confirmed by SFPO experiments, not indicating a substantial increase in interfacial bond. Nevertheless, flat fibres express significantly more severe surface scrapings and lint in contrast to the virgin equivalent. It is thus recognised, that premixing considerably influences the bond characteristics of flat fibres. It is therefore clear, that the provided surface corrugations do not significantly affect the fibre-matrix interaction of flat fibres, which must rather be attributed to the surface roughening caused by premixing.

Figure 5.38 depicts the modes of failure as a result of fibre rupture caused by high bond characteristics of macro synthetic fibres. Generally, embossed fibres (E1 and E2) experience a failure mechanism represented by a shearing mode as shown in Figure 5.38d and Figure 5.38e. In contrast, the remaining fibres rather undergo sudden failure, represented by a clean break. The primary advantage of a shearing failure mode is the additional residual energy

absorption after fracture, as opposed to a clean break represented by abrupt rupture, characterised by no further energy dissipation.

It is apparent, that fibre embossing proves to be the most efficient fibre geometry for an enhanced fibre-matrix interlock. It seems convenient to provide an embossed fibre surface to macro synthetic fibres in general. It is however problematic to provide overly efficient geometries to low modulus of elasticity fibres, causing a possibility for high percentage fibre rupture, resulting in less energy dissipation. It is thus stressed, that the degree of interlocking must be a function of the fibre material in order to achieve adequate fibre performance.

5.5 Concluding Summary

Single-fibre pull-out experiments revealed that fibres subjected to in-service condition as a result of premixing have an increased pull-out resistance in contrast to virgin fibres. This is especially noted for virgin flat fibres, having no significant surface deformations resulting in a low fibre-matrix interlock. Rather the surface roughening caused by premixing is responsible for an enhanced interlock, which can be regarded as the primary mechanism responsible for the strong bond exhibited by flat fibres.

It is furthermore shown that shorter embedment lengths achieve higher bond characteristics compared to longer embedment lengths. This is primarily observed for premixed fibres as well as non-flat virgin fibres. It is therefore suggested to use an average bond model instead of the uniform bond model, thus accounting for the whole fibre pull-out process.

Additionally, a significant increase in time dependent pull-out resistance is observed for premixed fibres. More specifically, polypropylene based macro fibres show a high increase in performance under time dependent pull-out in the premixed state in contrast to virgin fibres. Nevertheless, complete pull-out was encountered by all non-embossed fibres within a few days, indicating concerning behaviour. Embossed fibres generally showed the highest pull-out resistance against sustained loading conditions, sustaining the loads throughout the duration of the experiment.

SEM images revealed significant surface scrapings caused by the premixing process. Flat premixed fibres indicate considerable surface damage/scrapings after single-fibre pull-out in contrast to the virgin equivalent. In addition, SEM imaging indicated that macro synthetic fibres with a non-flat geometry do not significantly experience more severe surface scrapings after single-fibre pull-out as a result of fibre premixing in contrast to their virgin state. It is

thus confirmed, that the primary mechanism responsible for an enhanced interlock of non-flat fibres is the fibre geometry, in contrast to flat fibres, which is ascribed to the mixing process.

CHAPTER 6
Macro-Mechanical Results

This chapter reports on the macro-mechanical performance of fibre reinforced concrete (FRC) using macro synthetic fibres with different geometrical properties. The three-point bending (TPB) and round determinate panel (RDP) tests were adopted as the primary macro-mechanical performance indicators. Furthermore, the effect of fibre length as well as prolonged mixing on the macro-mechanical performance of macro synthetic FRC was investigated, using the experimental framework at hand.

In addition, workability tests were conducted in the fresh FRC state, in order to examine the influence of different volume fractions of macro synthetic fibres on the fresh FRC characteristics.

In essence, it is established whether a relation between single-fibre and macro-mechanical performance parameters exists.

6.1 Three-Point Bending Results

The FRC performance under TPB was determined in terms of residual flexural tensile strength (RFTS) at CMODs equal to 0.5, 1.5, 2.5 and 3.5 mm as specified by EN 14651 (2005).

6.1.1 Residual flexural tensile strength

Figure 6.1 shows the RFTS accomplished by the addition of macro synthetic fibres having various geometric properties. It is important to note, that the performance is based on a mixing time of five minutes.

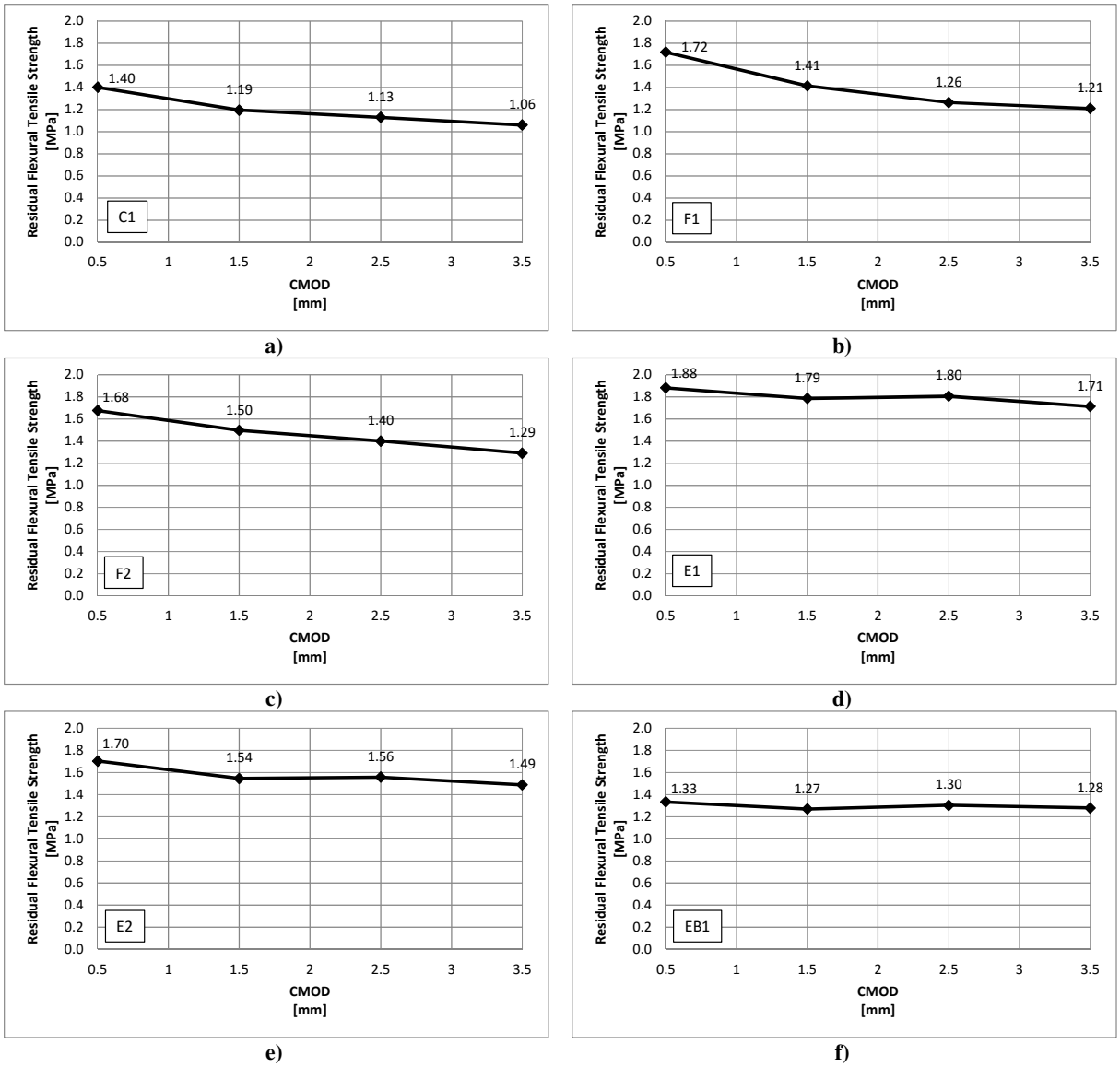

Figure 6.1: RFTS of C1 (a), F1 (b), F2 (c), E1 (d), E2 (e), EB1 (f)

It is evident that the residual flexural tensile strength decreases with an increase in crack opening. This is expected, as fibres undergo pull-out as well as rupture during crack widening, resulting in less fibres bridging the crack plane. Thus, the more uniform the RFTS with increasing CMOD, the more favourable the post-cracking performance of macro synthetic FRC.

6.1.2 The effect of fibre length on the RFTS

In order to investigate the effect of fibre length on the performance of macro synthetic FRC, additional fibre lengths to those presented in Table 3.1 were considered for C1 and F1. Figure 6.2 depicts the influence of 25 (FL25), 50 (FL50) and 75 mm (FL75) long fibres on the RFTS of FRC beams.

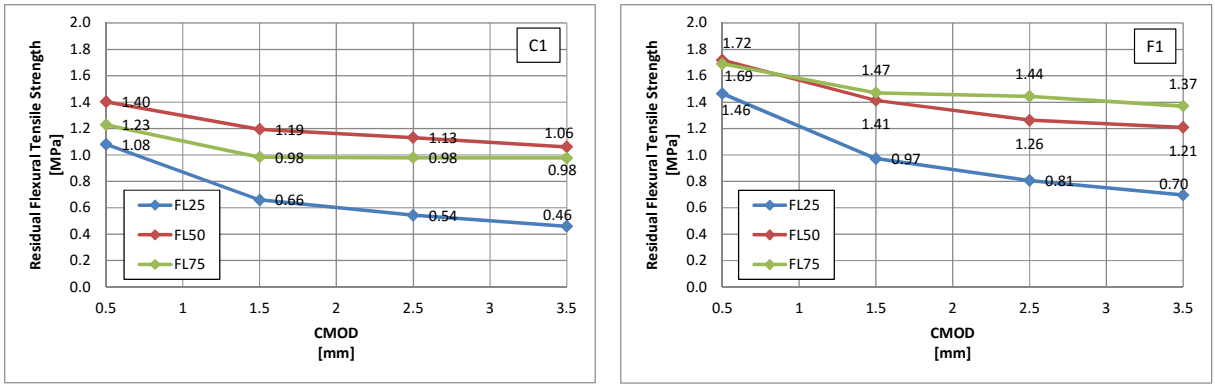

a) b)

Figure 6.2: RFTS for various lengths of C1 (a) and F1 (b) macro synthetic fibres

It is evident, that both fibres C1 and F1 provide the lowest RFTS for the shortest fibre length FL25. However, C1 is found to achieve the highest performance for a fibre length FL50, while the trend of RFTS of F1 is rising with increasing fibre length.

6.1.3 The effect of mixing time on the RFTS

As a result of the visual appearance of macro synthetic fibres subjected to premixing as well as the increased bond stress of premixed fibres on the single-fibre level, additional mixing times were adopted in order to investigate the effect of prolonged mixing. The methodology adopted to prepare beam specimens does not differ from the procedure described in Section 4.3.1, with the exception of a variation in mixing time after the addition of macro synthetic fibres to the fresh concrete. The additional considered mixing times amount to twenty and forty minutes. The effect of four fibre geometries corresponding to C1, F1, E1 and EB1 were considered for prolonged mixing. The RFTS at the specified CMODs corresponding to 5 (MT5), 20 (MT20) and 40 minutes (MT40) of mixing are illustrated in Figure 6.3.

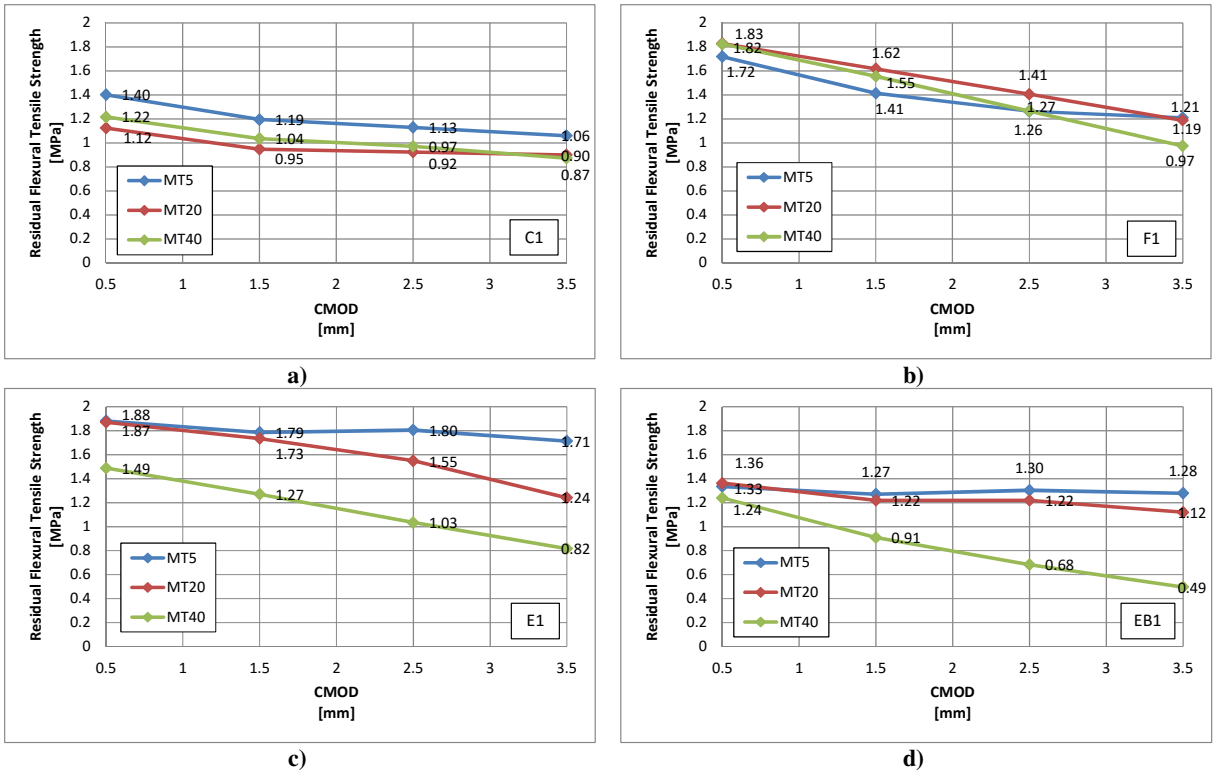

Figure 6.3: RFTS of C1 (a), F1 (b), E1 (c), and EB1 (d) subjected to prolonged mixing

It seems that the polypropylene fibres C1 and F1 are the least affected by prolonged mixing, as the RFTS varies over a small region. E1 and EB1 are however found to experience a substantial decrease in performance for an increase in mixing time. This is especially prominent for larger CMODs.

6.2 Round Determinate Panel Test

The primary parameter provided by RDP tests is the toughness of FRC panels, subjected to a centrally applied load. The toughness is a measure of energy dissipated, determined at different levels of central deflection, equal to 5, 10, 20 and 40 mm in accordance with ASTM C1550-12 (2012). Correspondingly, the results presented for the energy dissipation of RDPs are adjusted for the average thickness measurements (provided in Appendix C) according to Equation (2.14).

6.2.1 Toughness

Figure 6.4 shows the development of toughness of round macro synthetic FRC panels with increasing central deflection.

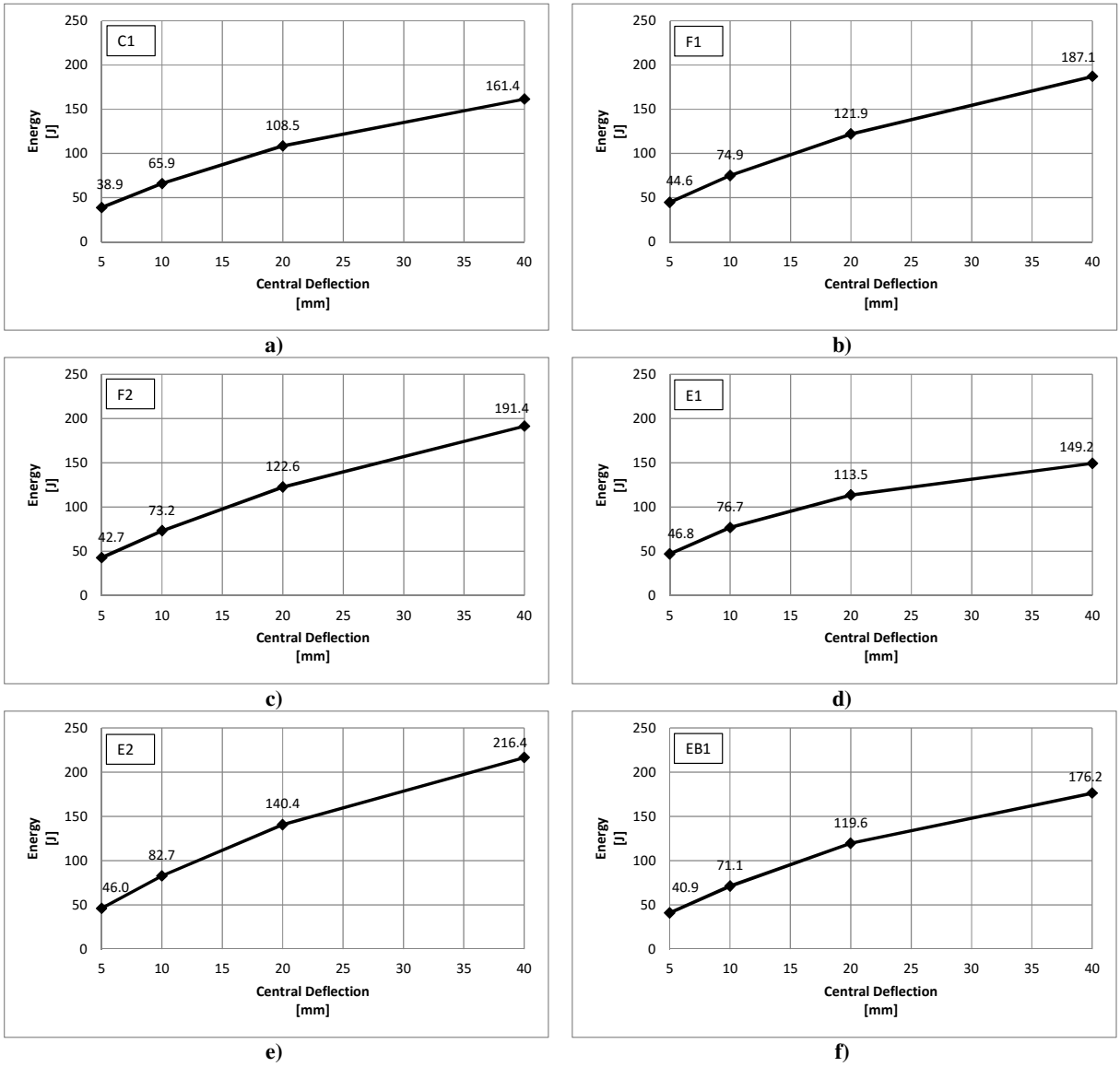

Figure 6.4: Toughness of C1 (a), F1 (b), F2 (c), E1 (d), E2 (e), EB1 (f) round FRC panels

It is evident, that the measured toughness is typically characterised by a decrease in slope for an increase in central deflection. This is ascribed to fibre pull-out as well as fibre rupture, reducing the ability of individual fibres to dissipate energy.

6.2.2 The effect of fibre length on toughness

Figure 6.5 shows the developed influence of fibre length of C1 and F1 on energy dissipation of macro synthetic FRC panels.

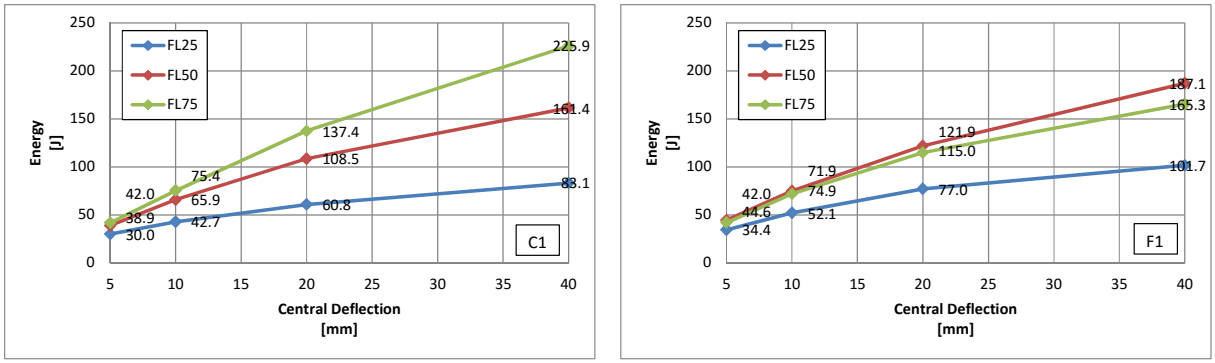

Figure 6.5: Toughness of various lengths of C1 (a) and F1 (b) macro synthetic fibres

It is apparent, that the fibre length differently affects the performance of crimped and flat fibres. Similar to the results obtained for TPB, FRC panels reinforced with shorter fibre lengths are characterised by low energy dissipation. While an increase in toughness is observed with increasing length of C1, the highest performance of F1 is achieved by the intermediate length FL50.

6.2.3 The effect of mixing time on toughness

Figure 6.6 depicts the effect of mixing time on the RDP toughness. The toughness at various levels of deformation corresponds to 5 (MT5), 20 (MT20) and 40 minutes (MT40) of mixing.

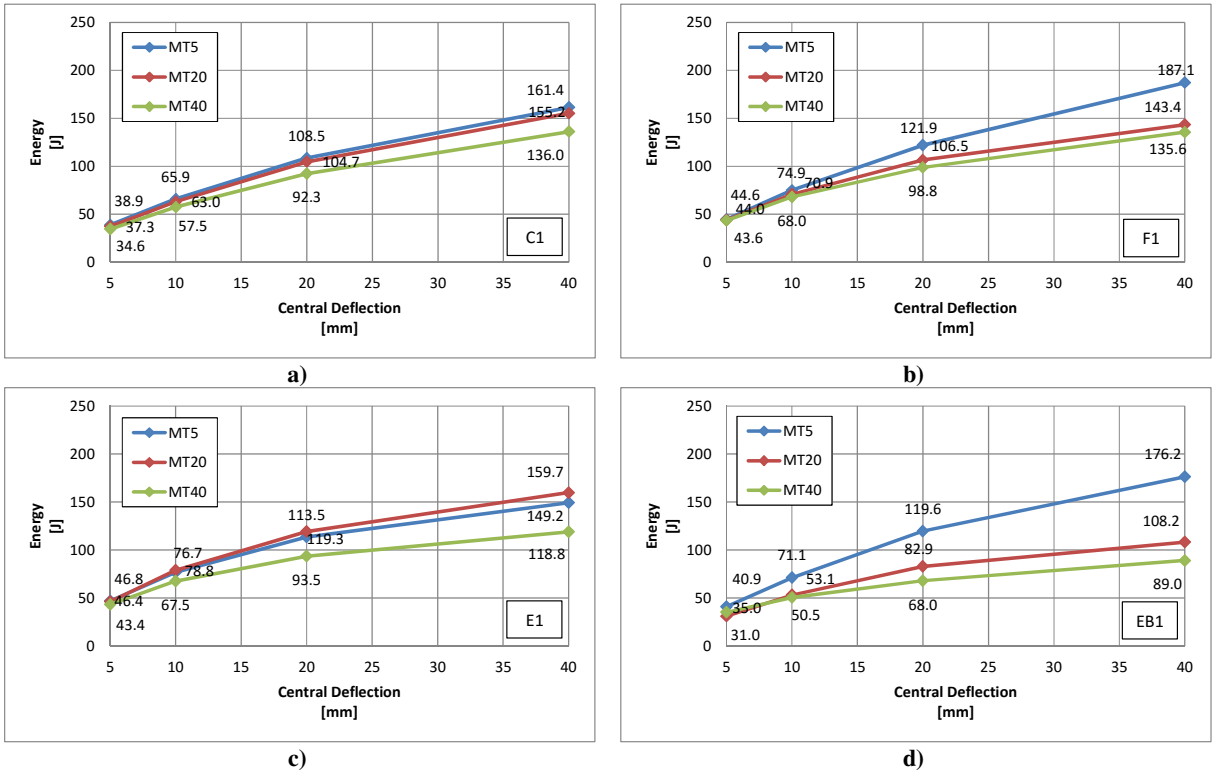

Figure 6.6: Toughness of C1 (a), F1 (b), E1 (c), and EB1 (d) subjected to prolonged mixing

It is evident, that prolonged mixing times negatively affect the performance under RDP conditions. Macro synthetic FRC panels typically exhibit a downward trend in energy dissipation with an increase in mixing time. EB1 seems most affected by prolonged mixing, due to the larger region over which the decrease in toughness occurs.

6.3 Discussion

6.3.1 Three-point flexural test results

The TPB test results are further discussed with reference to the RFTS as well as the mean axial tensile strength used in the ultimate moment capacity of FRC slabs, as discussed in Section 2.3.1.5.

Additionally, the results obtained for additional fibre lengths and prolonged mixing on the performance of macro synthetic FRC are further addressed.

6.3.1.1 Residual flexural tensile strength

The RFTS provides comparable results of the post-cracking performance using elastic bending theory. It is generally accepted, that higher RFTS during crack opening yield a more desirable performance. It is thus essential for FRC to retain the RFTS during crack opening. The averaged RFTS at the considered CMODs are presented in Figure 6.7.

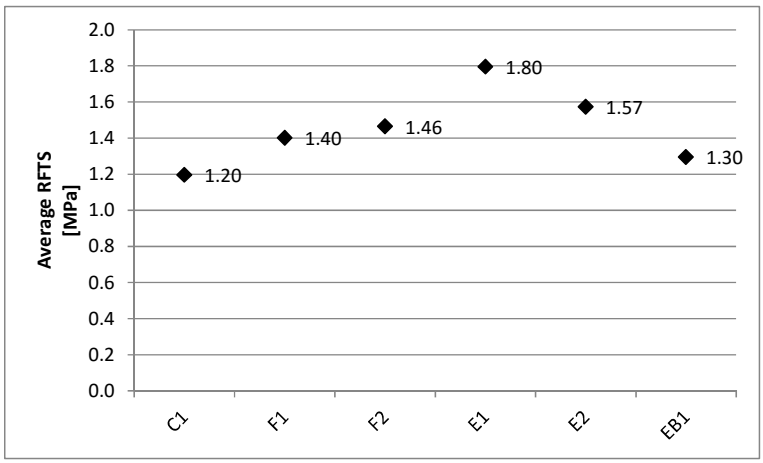

Figure 6.7: Average RFTS of macro synthetic FRC beams

It is evident, that the overall performance is dominated by the embossed fibre E1 and E2 followed by the performance of flat fibres. It is however stressed by Concrete Society (2013), that for macro synthetic FRC only the RFTS at a crack opening of 0.5 and 3.5 mm are of interest. RFTS at intermediate crack openings are typically utilised in the design approach for punching shear, not applicable to synthetic FRC.

The RFTS at CMOD of 0.5 and 3.5 mm of macro synthetic fibre reinforcement are illustrated in Figure 6.8a.

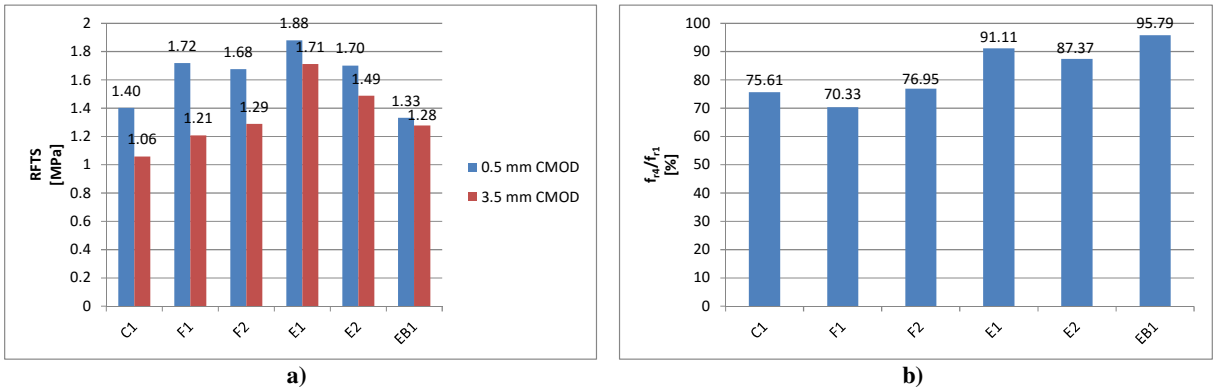

a) b)

Figure 6.8: RFTS at 0.5 mm and 3.5 mm CMOD (a) and ability to retain RFTS (b)

It is evident that embossed fibres show the highest resistance against a decrease in RFTS between a CMOD of 0.5 and 3.5 mm. This is furthermore depicted in Figure 6.8b, indicating high percentages of post-cracking performance preservation for embossed macro synthetic fibres. Polypropylene based fibres F1, F2 and C1 are more susceptible to the degree of deformation. It is evident that such fibres only retain 70 to 77 percent of their initial post-cracking performance. The high residual strength performance of embossed fibres is mainly attributed to the favourable bond characteristics as well as the higher modulus of elasticity of the fibre material.

6.3.1.2 Mean axial tensile strength

The ultimate moment capacity, governing the thickness design of ground supported FRC slabs is purely dependent on the combination of mean axial tensile strength ($0.29\sigma_{R4} + 0.16\sigma_{R1}$). It is thus evident, that ($0.29\sigma_{R4} + 0.16\sigma_{R1}$) is an important performance criterion for macro synthetic FRC. Figure 6.9 provides ($0.29\sigma_{R4} + 0.16\sigma_{R1}$) for the macro synthetic fibres investigated.

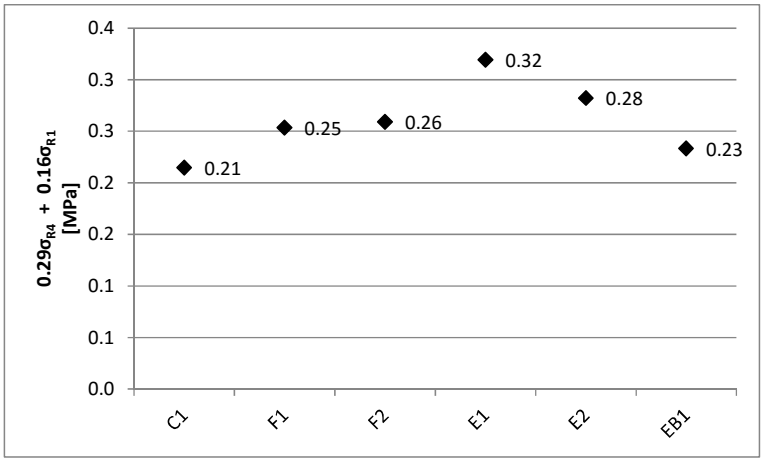

Figure 6.9: Combination of mean axial tensile strength ($0.29\sigma_{R4} + 0.16\sigma_{R1}$) of various macro synthetic fibres

It is evident that E1 and E2, as already established in Section 6.3.1.1, show the highest performance under TPB conditions. This can be ascribed to the efficient fibre geometry achieved by embossing as well as the high modulus of elasticity. In contrast, the two flat fibres F1 and F2 exhibit very similar behaviour under TPB, with F2 performing slightly better than F1. It is further stressed that flat fibres exhibit the highest performance of the investigated polypropylene fibres. When compared to crimped fibres, it is believed to be caused by the ability of flat fibres to dissipate more energy over a crack width of 3.5 mm, as a result of more advantageous pull-out- and straining behaviour.

Figure 6.10 depicts the $R_{e,3}$ value used in the thickness design of ground supported slabs by Concrete Society (2003), which has been superseded by the latest version of the TR 34 (Concrete Society, 2013), facilitating ($0.29\sigma_{R4} + 0.16\sigma_{R1}$). More interestingly, the shape outline exhibited by the $R_{e,3}$ values correspond to that of ($0.29\sigma_{R4} + 0.16\sigma_{R1}$). However, it is evident that the performance index of the two flat fibres swapped. It is stressed, that as the $R_{e,3}$ value is highly dependent on the flexural capacity of an un-cracked beam section, a larger flexural load results in a lower $R_{e,3}$ performance index, as indicated by Equation (2.6). This is confirmed by the average flexural load of F1 and F2 reinforced beam specimens, being 11.7 kN and 13.4 kN respectively. It is thus evident, that the $R_{e,3}$ value might provide misleading information regarding the post-cracking performance of macro synthetic FRC.

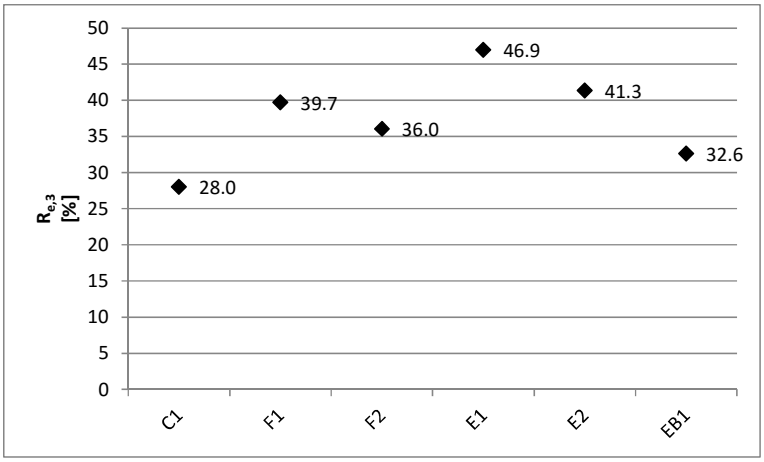

Figure 6.10: $R_{e,3}$ value of various macro synthetic fibres

6.3.1.3 The effect of fibre length on the TPB performance of macro synthetic FRC

It is important to note, that fibres were batched by weight, resulting in a constant fibre volume fraction. Therefore, longer fibres result in a smaller number of fibres and vice versa. Figure 6.11 depicts the TPB performance of various lengths of C1 and F1 on the TPB behaviour of macro synthetic FRC. It is evident, that the shortest fibre length FL25 experiences the lowest performance under TPB for both fibre types. As FL25 is considerably shorter than the critical fibre length of C1 and F1 as shown in Table 5.1 and Table 5.2 respectively, fibres rather pull-out in contrast to rupture. It is thus evident, that the energy dissipation of short fibres is limited to half the fibre length at maximum. Thus, due to the low energy dissipation, fibres exhibit poor post-cracking behaviour.

Furthermore, the highest TPB performance of the crimped fibre profile is observed for a fibre length FL50. It is evident that due to the high percentage of fibre ruptures experienced at an embedment of L37.5, the critical length of C1 was exceeded, resulting in less energy absorption.

In contrast to the crimped fibre, TPB performance of F1 increased with increasing fibre length as shown in Figure 6.11. It is thus believed, that longer F1 fibre lengths experience significant fibre straining in the absence of rupture at smaller crack openings, which is responsible for the advantageous fibre performance. Additionally, due to the nature of the small crack plane area exhibited by flexural beam tests, advantageous fibre distribution and orientation could have influenced the strong performance. This is confirmed by the high CoV, indicating the highest variability for F1 (FL75), for RFTS at CMOD of 0.5 and 1.5 mm, being 0.15 and 0.28 respectively.

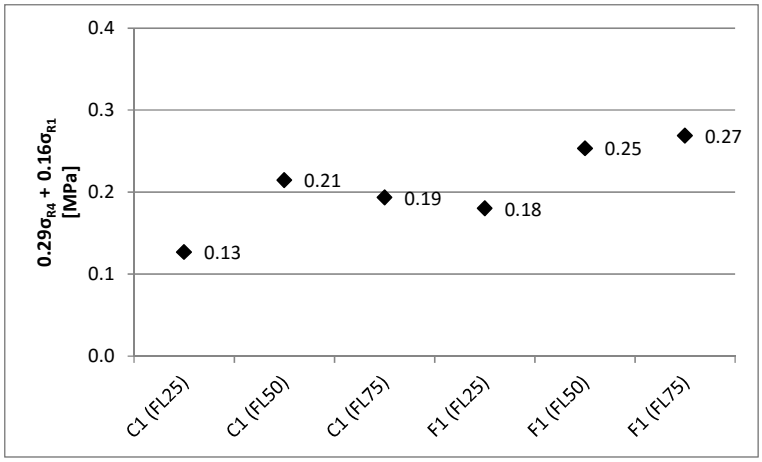

Figure 6.11: (0.29σR4 + 0.16σR1) for various lengths of C1 and F1

6.3.1.4 The effect of mixing time on the TPB performance macro synthetic FRC

It has been established that mixing time has a significant influence on the performance of FRC under TPB. It was observed that the RFTS typical follows a decreasing trend with an increase in mixing time. This phenomenon is visually depicted in Figure 6.12, with f_{R1}, f_{R2}, f_{R3} and f_{R4} equal to the RFTS at CMODs of 0.5, 1.5, 2.5 and 3.5 mm respectively. It is evident, that the performance of F1 is the most resilient against prolonged mixing, followed by C1, while the performance of E1 and EB1 is more vulnerable against extended mixing. This however appears only to affect the RFTS at larger CMODs, as fibres bridging the crack plane exhibit little straining and pull-out at smaller crack openings. It is believed that the decreasing performance at larger CMOD of embossed fibres can be attributed to two possibilities:

- Prolonged mixing partially destructs the embossed fibre surface responsible for an increased fibre-matrix interlock, thus experiencing a decrease in pull-out performance.
- Prolonged mixing influences the fibre performance similar to that of flat fibres, whereby the bond created between the fibre-matrix interface exceeds the fracture stress of the fibre, resulting in extensive fibre rupture.

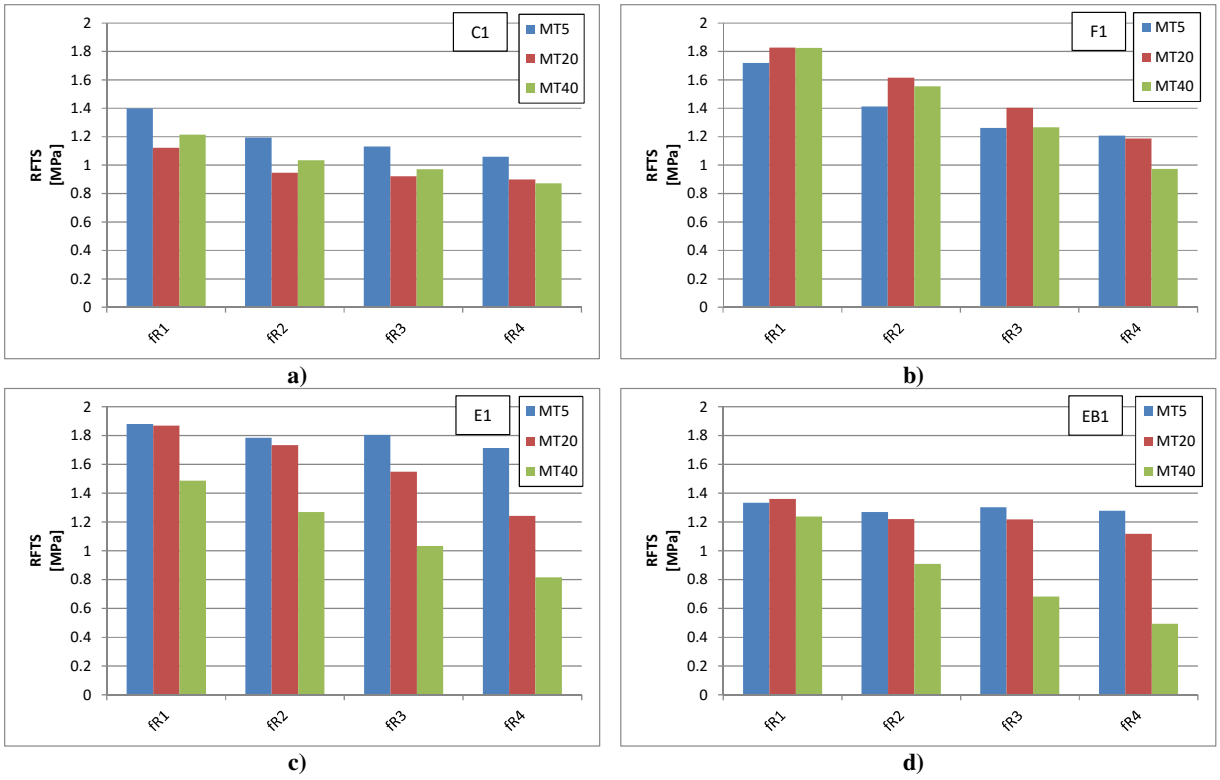

Figure 6.12: Effect of mixing on the RFTS of C1 (a), F1 (b), E1 (c) and EB1 (d)

6.3.2 Round determinate panel test results

The macro-mechanical results obtained by RDP test are further addressed in this section. Toughness is the primary performance parameter used for the discussion.

6.3.2.1 Toughness

The energy dissipation, also referred to as toughness of the macro synthetic FRC panels, is determined at central deflections of 5 (CD5), 10 (CD10), 20 (CD20) and 40 mm (CD40). The toughness of macro synthetic FRC round panels is depicted in Figure 6.13 for various levels of deformation.

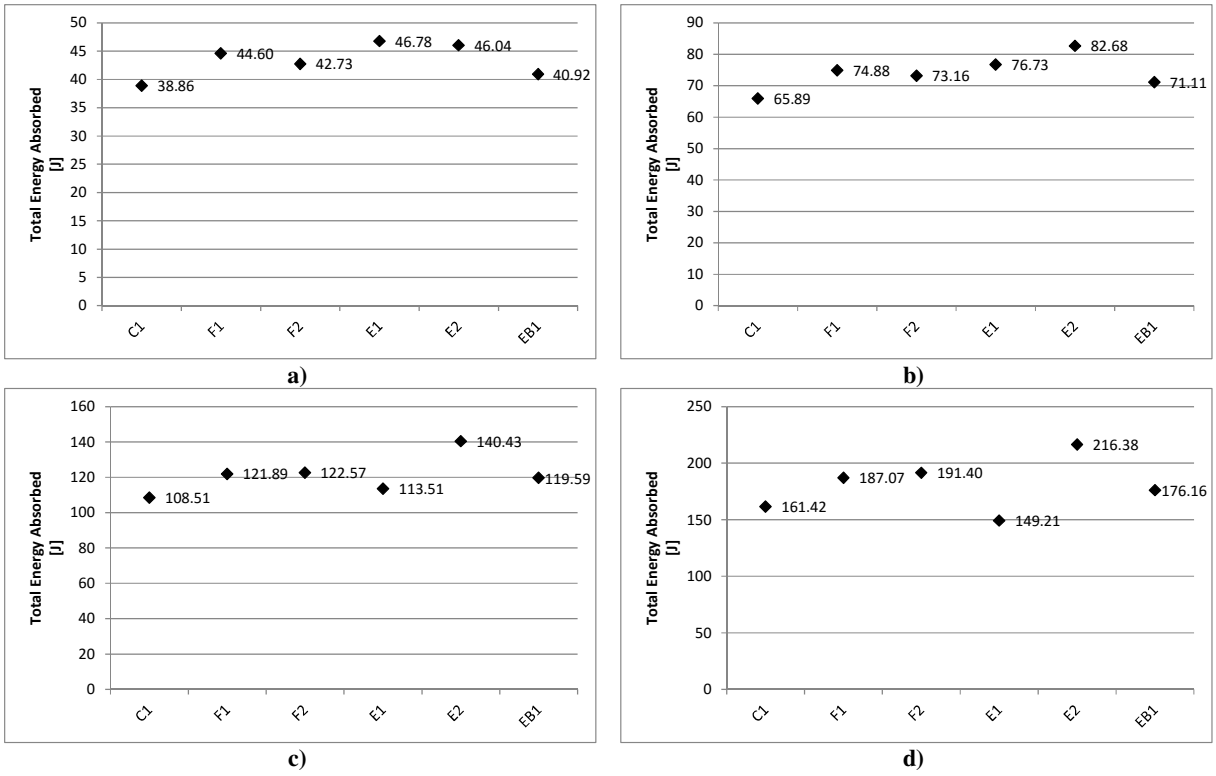

Figure 6.13: RDP toughness at central deflection of CD5 (a), CD10 (b), CD20 (c) and CD40 (d)

Due to the cumulative nature of energy, higher levels of central displacement result in an increase in energy dissipation. It is evident, that E1 is most influenced, as its performance decreases significantly relative to the remaining macro synthetic fibres.

It is important to note, that an increase in vertical displacement results in a larger crack opening. It is thus evident, that the macro synthetic fibre performance is largely dependent on the degree of deformation. The yield line approach can effortlessly be used to relate vertical deflection to crack opening using the schematisation shown in Figure 6.14. The relation between crack width (c) and central deflection is given by:

$$c = 2 \times \frac{\sqrt{3} \times \delta_B}{2r} \times t \qquad (6.1)$$

with δ_B, r and t the central displacement, radius and thickness of the panel respectively. It is however stressed, that the crack width is derived according to small crack rotations, i.e. small θ_c, as shown in Figure 6.14.

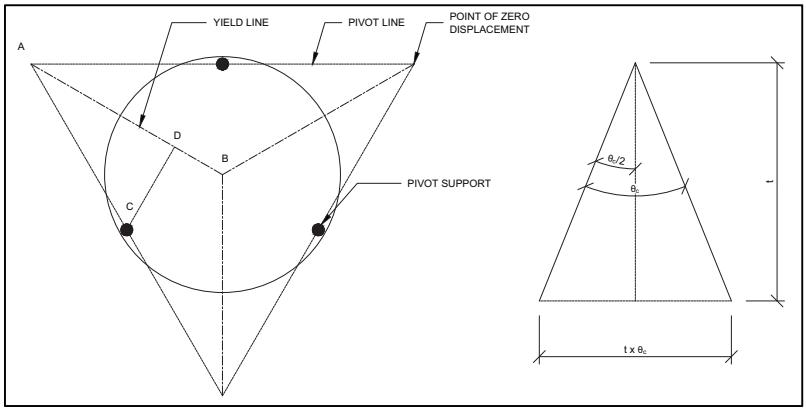

Figure 6.14: Schematisation of the yield line approach used for the determination of the crack width (Minelli & Plizzari, 2010)

At CD5 corresponding to 1.62 mm crack opening, the highest performance is observed for E1. This correlates with the results obtained under TPB for a similar crack width of 1.5 mm, as shown Figure 6.4. However, at CD10 (3.24 mm crack widening), the highest toughness is accomplished by E2. Beam tests however suggested, that at a similar crack width of 3.5 mm, E1 is governing the highest performance. It is thus clear, that some discrepancy exists between the two macro-mechanical approaches, which can be partially ascribed to a poor fibre distribution across the crack plane of beams as well as to the different nature in bending encountered by beam and panel specimens. While beam samples experience mono-axial bending about a single axis, RDP specimens undergo bi-axial bending.

6.3.2.2 The effect of fibre length on toughness of RDP

Figure 6.15 depicts the development of toughness for increasing fibre lengths of C1 and F1. It is evident that for the considered fibre lengths, the optimum fibre length is FL75 and FL50 for C1 and F1 respectively.

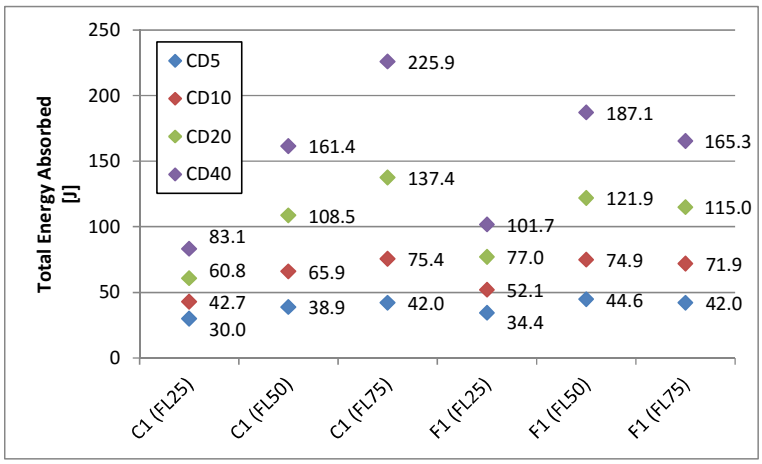

Figure 6.15: Toughness achieved by different lengths of the Geotex products

For both C1 and F1, the shortest fibres exhibited the poorest performance under RDP testing conditions. This can be attributed to the low anchorage length of the fibres being significantly less than the critical length. Hence, energy dissipation is limited to the little anchorage provided.

For F1, the highest toughness is observed for a fibre length FL50. This is ascribed to a high percentage of fibre rupture for fibre lengths exceeding FL50, as shown in Table 5.2. Although extensive straining is believed to dissipate significant energy upon cracking as for the TPB results discussed in Section 6.3.1.3, large crack openings, as in the case of RDP specimens, exceed the straining capacity of the fibres, causing fibre rupture.

In contrast, C1 attains a higher toughness with an increase in fibre length as depicted in Figure 6.15. Single-fibre results do not reflect this behaviour, as a result of significant fibre rupture leading to a decrease in energy dissipation. It is therefore evident, that a discrepancy exists between the two levels of investigation. This could be assigned to the bi-axial bending nature experienced by RDP specimens resulting in fibre snubbing as well as a possibility of favourable fibre distribution and orientation. Additionally, fibres closer to the tensile face experience high strains due to a non-uniform crack opening, while fibres closer to the compression face may strain without undergoing rupture. It must be further highlighted, that due to a beam-like failure mechanism, one RDP specimen reinforced with C1 (FL75) was discarded. Thus, the result presented corresponds to the minimum number of specimen required, creating room for misleading results. This is furthermore confirmed by the relatively high CoV, equal to 0.20.

6.3.2.3 The effect of mixing time on toughness of RDP

It is evident that prolonged mixing significantly influences toughness. Figure 6.16 highlights the typical decrease in energy dissipation as a result of extended mixing.

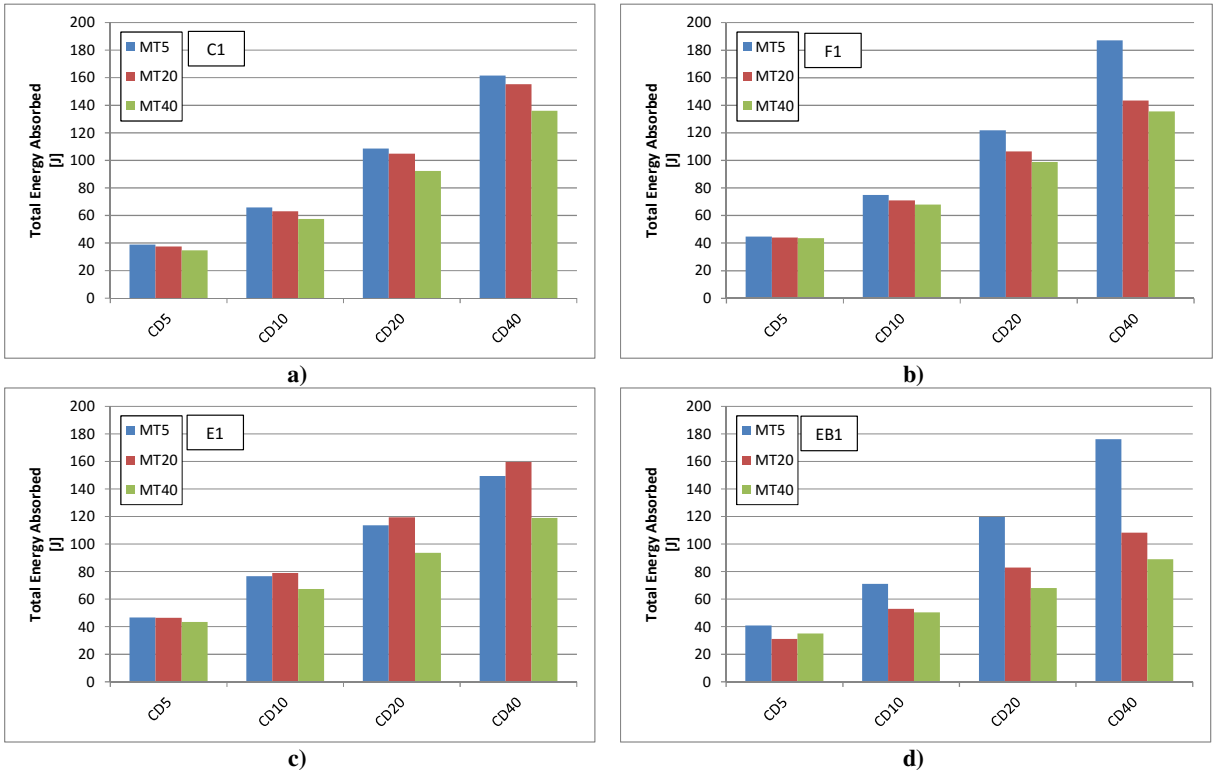

Figure 6.16: Effect of mixing on toughness of C1 (a), F1 (b), E1 (c) and EB1 (d)

The highest toughness characteristics are typically achieved at MT5, with a decreasing trend with an increase in mixing time. In addition, performance loss resulting from prolonged mixing increases with an increase in central deflection. This is especially applicable to F1, C1 and EB1. However, the flat fibre profile F1 seems most resilient against prolonged mixing compared to the remaining fibres. The embossed fibre E1 appears to follow a slightly different trend, as the highest performance is observed for the intermediate mixing time MT20. It is however stressed, that the CoV of the toughness corresponding to CD40, is significantly higher for MT20 in contrast to MT5 and MT40, being 0.18, 0.01 and 0.05 respectively. It is thus questionable, whether the results provided in Figure 6.16c represent the true behaviour.

6.4 Fresh FRC Characteristics

In addition to the aforementioned macro-mechanical tests, an investigation was performed on fresh macro synthetic FRC. The fresh FRC characteristics considered were those of fibre balling as well as the influence of various fibre volume fractions on the workability and the associated slump loss resulting from prolonged mixing.

6.4.1 Fibre balling

Fibre balling is the entanglement of individual macro synthetic fibres, causing the formation of fibre balls. It is believed that fibre balling is largely influenced by the fibre shape (length, profile, texture), stiffness, fibre and concrete volume as well as the type of mixer used.

The disadvantage associated with fibre balling is the formation of balls causing localised weak spots promoting proneness to cracking as well as a reduction in the anticipated volume fraction. Figure 6.17 shows a formed fibre ball, resulting from the mixing process using a 120 litre concrete pan mixer.

Figure 6.17: Identified fibre ball during mixing

6.4.2 Slump test

The slump test according to SANS 5862-1 (2006) is an indicative measure for the workability of concrete in its fresh state, being defined as the relative ease at which concrete can be placed, compacted and finished without separation or segregation of the individual materials (Addis, 2013).

6.4.3 Methodology

The mix design shown in Table 3.4 was prepared for a 10 litre FRC mix. Stones were washed prior to mixing, in order to eliminate any accumulation of fine/dust particles influencing fresh concrete characteristics. Before the addition of the dry material, the mixing pan was wetted in order to prevent water absorption and dried using industrial tissue paper. The concrete constituents were added afterwards in the order of sand, cement and stone. Dry mixing was limited to one minute before the addition of water, followed by an additional five minutes of mixing. Fibres were added afterwards by hand, using V_f of 0.33, 0.44 and 0.55 %

respectively. After the addition of macro synthetic fibres, the fresh FRC mixture was additionally mixed for five minutes before visual assessment of formed fibre balls.

It is important to note, that slump tests according to SANS 5862-1 (2006) were performed at regularly spaced intervals, with the first slump being performed directly before the addition of macro synthetic fibres followed by a second slump directly after five minutes of fresh FRC mixing. Thereafter slump tests were conducted at an interval of five minutes for an additional twenty minutes of mixing.

6.4.4 Results

6.4.4.1 Fibre balling

All macro synthetic fibres listed in Table 3.1 were visually assessed for fibre balling behaviour. No fibre balls were identified for the tested fibres using the methodology described in Section 6.4.3.

6.4.4.2 Slump loss

The slump loss result of the reference mix is shown in Figure 6.18.

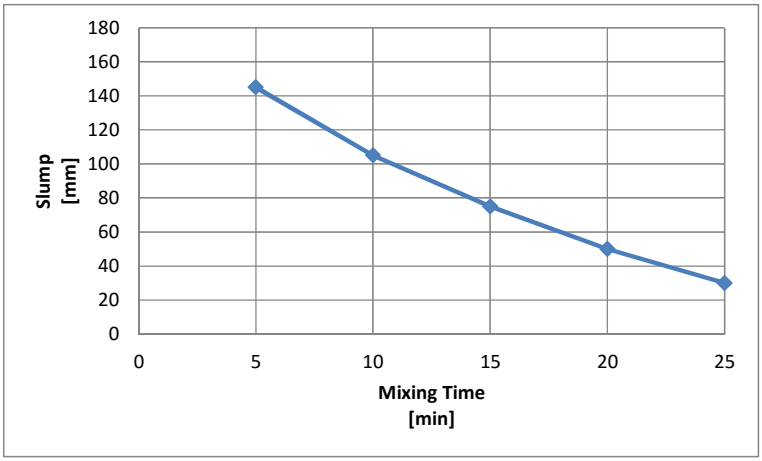

Figure 6.18: Slump loss of the reference concrete mix

The slump test results obtained for fresh FRC containing 3, 4 and 5 kg/m^3 macro synthetic fibres, are depicted in Figure 6.19. It is important to note, that the first slump result corresponds to a mixing time of five minutes prior to fibre addition.

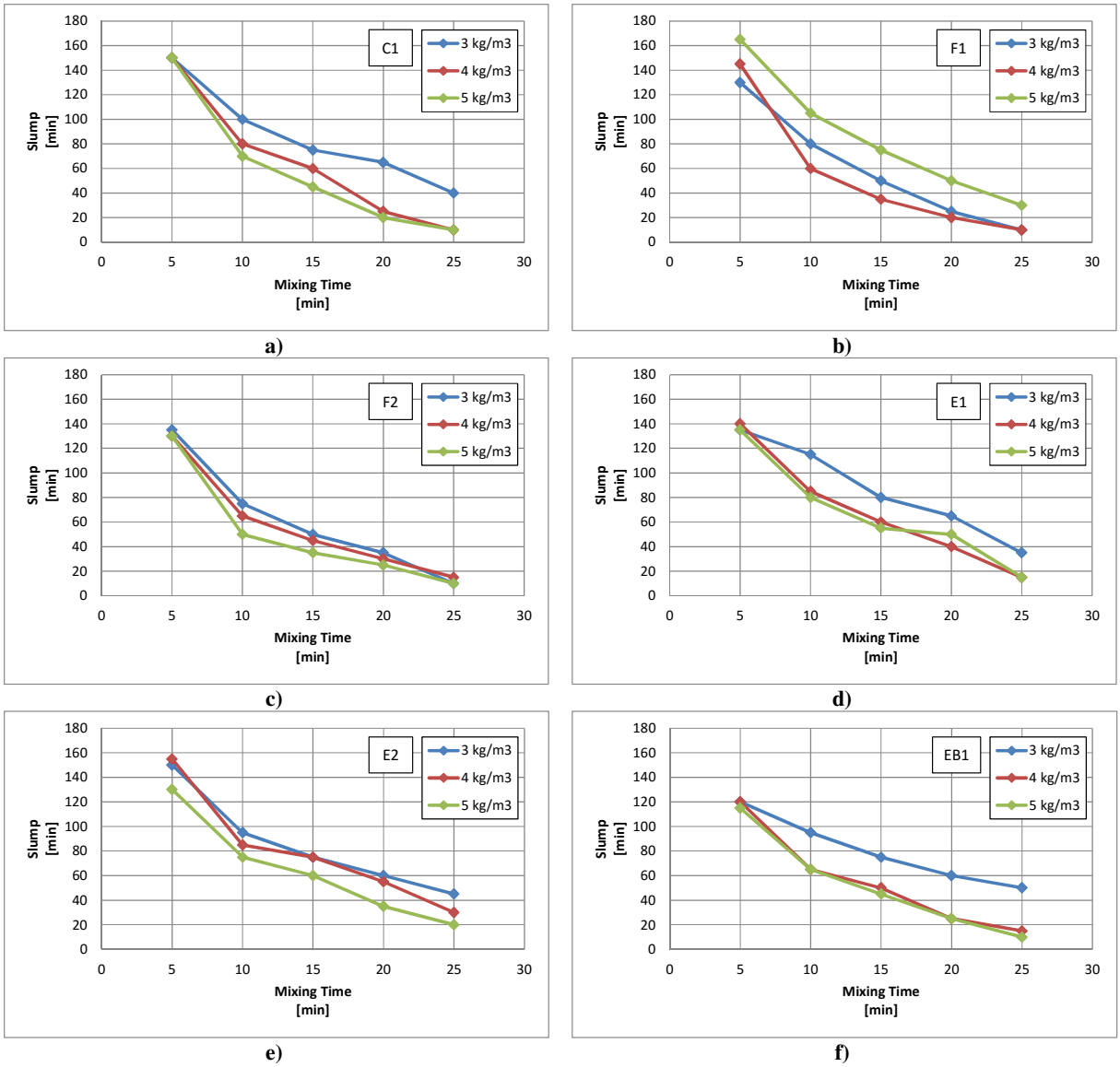

Figure 6.19: Slump loss of fresh macro synthetic FRC

6.4.5 Discussion

It has been established, that no fibre balling behaviour was observed for the investigated volume fractions of macro synthetic fibres using 10 litre FRC mixes. It is however stressed, that balling behaviour was observed for mixes prepared in a 120 litre concrete pan mixer. It is thus believed, that the volume as well as type of mixer influences balling behaviour and establishment.

Additionally, slump results revealed that the volume fraction of macro synthetic fibres significantly influences the workability of fresh FRC mixes. A decreasing trend in slump is observed for an increase in fibre volume fraction. This is attributed to additional material causing cohesion to the FRC mixture. It is however important to note, that slump results provided for F1, as shown in Figure 6.19b, do not follow the distinctive trend. It is evident,

that the initial slump without any addition of fibres resulted in a higher workability in contrast to the anticipated workability, being 165 mm instead of 145 mm. A possible reason can be allocated to insufficient drying of the mixing pan after wetting, resulting in a higher water content.

Furthermore, a significant decrease in slump is observed for prolonged mixing. This can be ascribed to the possible initiation of the hydration process of cement, the potential fibre damage caused by the mixing process, water evaporation as well as water absorption of the mixing pan.

6.5 Correlation

Due to the observation of discrepancies for the macro-mechanical investigation, the significance of the corresponding results can be questioned. Thus, macro-mechanical performance criteria obtained by TPB and RDP results are compared.

In addition, single-fibre pull-out (SFPO) results are related to the macro-mechanical results. Accordingly, SFPO and post-cracking macro-mechanical performance parameters are compared, in order to establish whether a link between the two investigational levels exists.

6.5.1 Macro-mechanical results

Figure 6.20 depicts the correlation between the $(0.29\sigma_{R4} + 0.16\sigma_{R1})$ and the $R_{e,3}$. Both performance parameters are typically used in the ultimate moment capacity of ground supported slabs, with the $R_{e,3}$ value being superseded by $(0.29\sigma_{R4} + 0.16\sigma_{R1})$.

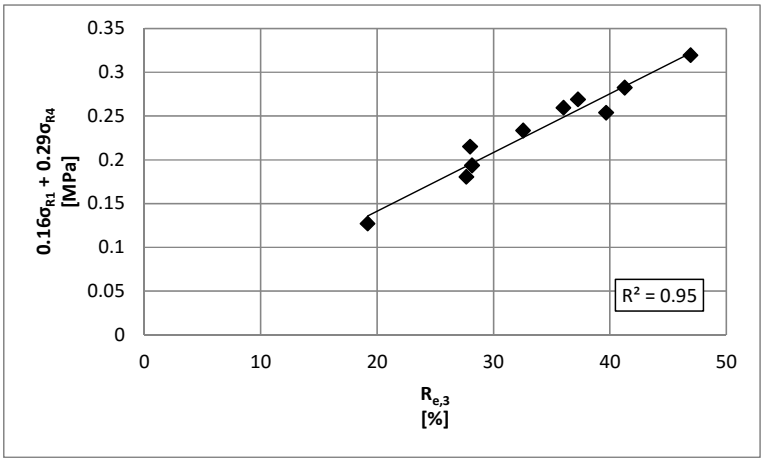

Figure 6.20: Correlation between $(0.16\sigma_{R1} + 0.29\sigma_{R4})$ and $R_{e,3}$

It is evident that a strong correlation, with an R^2 value of 0.95 between the $R_{e,3}$ value and $(0.29\sigma_{R4} + 0.16\sigma_{R1})$, exists. This is expected due to the similarity of the two approaches frequently adopted for the thickness design of ground supported slabs.

Bernard (2002) and Parmentier et al. (2008) showed that a relatively promising correlation between flexural beam and RDP tests exists, as shown in Figure 2.41. Figure 6.21 depicts the relation between TPB and RDP post-cracking performance parameters, chosen as ($0.29\sigma_{R4} + 0.16\sigma_{R1}$) and toughness respectively. It is important to note, that the RDP crack width corresponding to CD10 equates to 3.26 mm, while for CD40 the crack width amounts to 12.99 mm. In contrast, maximum crack widening during TPB equals 3.5 mm. It is thus evident, that a stronger correlation for similar crack widths (R^2 of 0.79) exists, in contrast to a RDP crack width corresponding to CD40 (R^2 of 0.37). It is presumed, that as a result of extensive crack widening, a substantial amount of fibres bridging the crack plane experience rupture or dissipate insignificant energy, resulting in overall reduced toughness. This is confirmed by a decrease in correlation for higher levels of deformation, indicating that fibre performance is significantly influenced by the degree of crack opening.

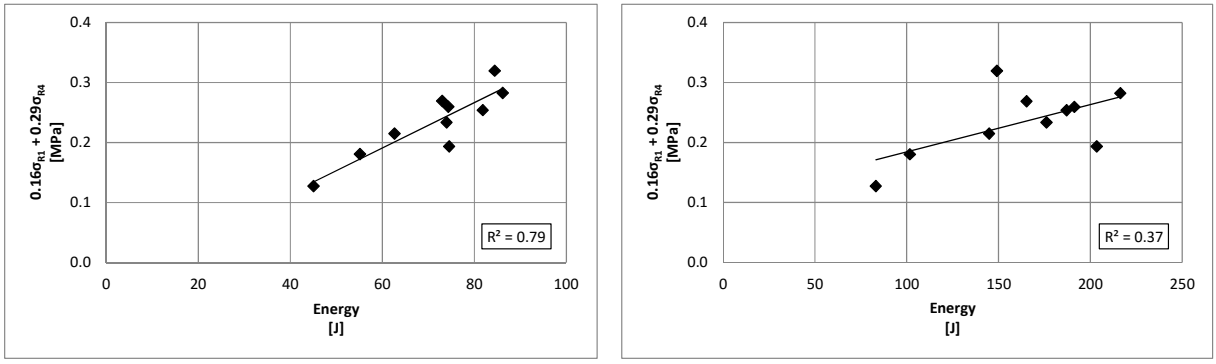

a) b)

Figure 6.21: ($0.29\sigma_{R4} + 0.16\sigma_{R1}$) and toughness at CD10 (a) and CD40 (b)

6.5.2 Single-fibre and macro-mechanical results

This section reports on the correlation of single-fibre results to performance parameters obtained on a macro-mechanical level.

6.5.2.1 SFPO and TPB test

Figure 6.22 depicts the connection between TPB and SFPO experiments. SFPO performance is measured in terms of single-fibre energy dissipation over a surface area of 100 x 100 mm. In order to simulate the maximum crack width experienced by TPB beam specimens, the dissipated energy corresponds to a pull-out displacement equal to 3.5 mm. It is important to note, that the embedment length used to obtain the required energy dissipation, is equivalent to a half of the fibre length.

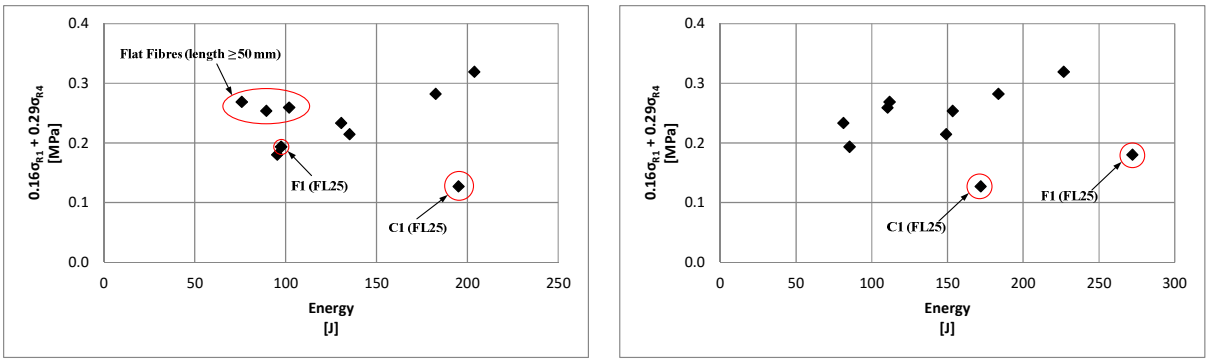

Figure 6.22: Relation between TPB and SFPO for virgin (a) and premixed (b) fibres

It is apparent, that especially virgin flat fibres do not follow the anticipated trend as depicted in Figure 6.22a. This is attributed to the low energy dissipation per surface area of flat fibres, as a result of the poor interfacial bond. In addition, premixed fibres of short length tend to deviate from the typical behaviour as shown in Figure 6.22b. It has been previously established, that short fibre lengths typically show the poorest macro-mechanical performance, while displaying enhanced energy dissipation per surface area. This is ascribed to the high initial mechanical interlock exhibited during de-bonding as described in Section 5.4.2. It is thus evident, that the performance of short fibres under SFPO overestimates the macro-mechanical performance.

6.5.2.2 SFPO and RDP test

The link between RDP and SFPO experiments is depicted in Figure 6.23. The energy determined under SFPO conditions is limited to a pull-out displacement of 12.99 mm for an embedment equal to a half of the corresponding fibre length. The SFPO energy is quantified as the energy dissipated over a surface area equal to 100 x 100 mm.

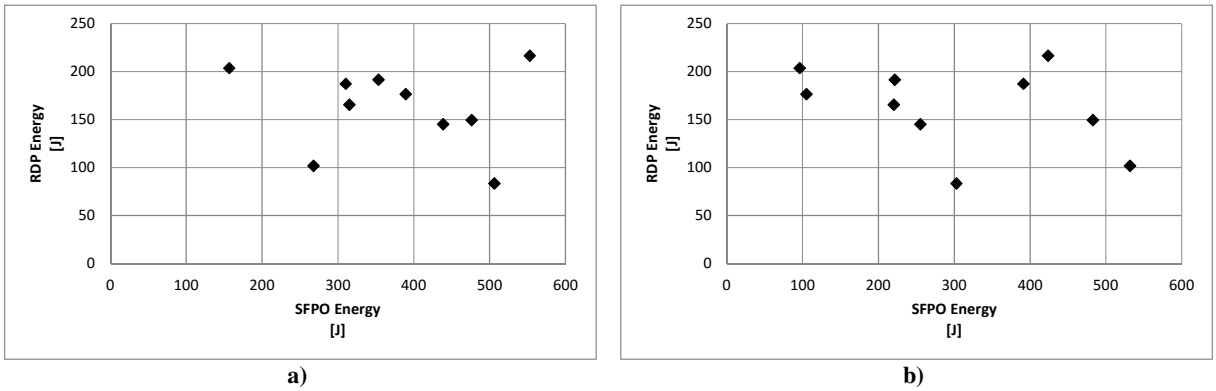

Figure 6.23: Relation between RDP and SFPO for virgin (a) and premixed (b) fibres

It is recognised, that a poor correlation between RDP and SFPO experiments for the simulation of a 12.99 mm crack width exists. It is presumed, that SFPO mechanisms do not

correlate to the fibre behaviour encountered during macro-mechanical RDP tests, primarily as a result of the extensive crack opening of RDP specimens. It is furthermore believed, that result deviation is additionally attributable to the bi-axial bending mechanism, possibly causing fibre snubbing, which is disregarded by the SFPO results.

6.5.3 Utility of results

It has been established, that correlation between SFPO and macro mechanical experiments for lower levels of deformation exists. Hence, a link is observed at smaller crack opening while a poor correlation is generally observed for larger crack openings. It is however important to note, that the two levels of investigation are characterised by very different mechanisms compared to that encountered during SFPO. SFPO experiments rather simulate a uniform crack opening similar to that encountered by uni-axial tensile tests, whereas macro-mechanical tests are characterised by a non-uniform crack opening. It appears that small non-uniform crack openings partially simulate uniform crack opening of macro synthetic FRC elements. This can be attributed to the mechanism-parallels in crack development upon cracking. For a small uniform crack opening, fibres bridging the crack plane are activated at approximately the same instance with little pull-out or fracture occurrences. Similar, little pull-out and fibre rupture is encountered during the initiation of a non-uniform crack opening, with fibres located close to the position of crack propagation being activated first. However, once significant crack widening is reached, exceeding the strain capacity of fibres, fibres bridging a uniform crack experience rupture or pull-out at approximately the same instance. In contrast, fibres bridging a non-uniform crack located at a position where crack opening exceeds the fibre strain capacity, experience rupture or pull-out first. This principle is visually explained in Figure 6.24.

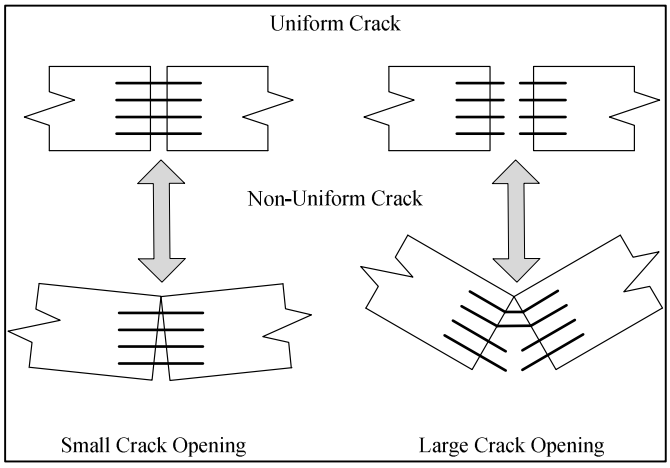

Figure 6.24: Uniform vs. non-uniform crack opening

6.6 Concluding Summary

Macro-mechanical experiments revealed that fibre geometry significantly influences the performance of macro synthetic fibre reinforced concrete (FRC). It was established, that embossed fibre geometries typically yield the highest performance criteria. This is especially noted for lower levels of deformation as encountered under three-point bending, with fibre E1 and E2 displaying more desirable performance parameters than alternative fibres. Flat fibres tested under three-point bending indicate slightly lower performance than the embossed equivalent. The crimped and built-up/embossed geometries exhibit the poorest performance under three-point bending.

Macro-mechanical experiments undergoing higher levels of deformation, as encountered by round determinate panel specimens, display similar results to those obtained under three-point bending. Performance parameters obtained by three-point bending and round determinate panel tests correspond, with the exception of E1. E1 exhibited the poorest performance in contrast to the remaining fibres.

The effect of fibre length proved to be crack width specific. The shortest fibre length investigated is found to exhibit the overall poorest macro-mechanical performance. While increasing three-point bending performance with increasing length is observed for flat fibres, crimped fibres revealed maximum performance for an intermediate fibre length. However, vice versa is observed for larger crack widths as encountered by round determinate panel tests. Thus a discrepancy exists between individual macro-mechanical tests, which is believed to be caused by the different bending mechanisms as well as maximum crack width exhibited.

Prolonged mixing indicated a significant influence on the post-cracking behaviour of macro synthetic FRC. Both round determinate panel and three-point bending experiments revealed a significant decrease in performance for fresh FRC subjected to extended mixing times. In addition, flat fibres show the highest resilience against prolonged mixing, while embossed built-up fibres exhibit a significant loss in performance.

Workability tests on fresh FRC revealed that concrete slump is severely influenced by the volume fraction of macro synthetic FRC. An increase in fibre volume typically decreased the workability of fresh FRC. In addition, fibre balling was investigated with the influence of various fibre contents. No balling behaviour was identified for the considered volume fraction.

Finally, the relation between various utilised experiments was investigated. Macro-mechanical post-cracking performance parameters indicate correlation for lower levels of deformation, whereas poorer correlation is observed for higher levels of deformation. Single-fibre performance typically increases with increasing macro-mechanical performance for smaller crack openings. This is especially noted for premixed fibres with the exception of short fibre lengths. Poor correlation is however observed for larger crack openings. This is attributed to the similar nature in mechanisms encountered by small uniform and non-uniform crack openings.

CHAPTER 7
Conclusion and Future Prospects

7.1 Conclusion

The primary aim of this research is to improve the general understanding of macro synthetic FRC in the cracked state using fibres with various geometrical properties. In particular, the investigational focus was based on the single-fibre and macro-mechanical performance of FRC. It was established that fibre geometry as well as fibre premixing significantly influences the single-fibre- and macro-mechanical performance of macro synthetic FRC.

The following significant conclusions can be drawn from the work presented in this research:

7.1.1 Single-fibre pull-out experiments

- Single-fibre pull-out (SFPO) experiments conducted on macro synthetic fibres embedded into concrete revealed that fibre geometry is an important component to consider for enhanced post-cracking FRC performance.
- It was found, that the mixing process of fresh FRC has a significant influence on fibre performance. This was especially noted for flat fibre geometries, exhibiting a significant increase in fibre-matrix bond characteristics.
- It was confirmed, that embossed fibre surface geometries provided the highest resistance against pull-out, followed by the performance of premixed flat fibres. This was verified with the aid of SEM imaging, revealing substantial surface damage analogous to a strong fibre-matrix interaction.
- SFPO experiments conducted on various embedment lengths displayed higher interfacial bond behaviour for shorter embedment lengths, ascribed to a high initial mechanical interlock. It was established, that the traditional model assuming a uniform distributed bond stress did not apply, and that an average bond model showcases more accurate single-fibre behaviour.

7.1.2 Time dependent pull-out experiments

- Concerning time dependent pull-out (TDPO) behaviour was observed for flat and crimped fibre geometries. Although premixing significantly increased the resistance of flat and crimped fibre profiles against sustained loading conditions, rapid pull-out was typically observed within a few days.
- Overall, virgin and premixed embossed fibres indicated significant resistance against TDPO, undergoing little instantaneous elongation and sustained loads for the duration of the experiment.

7.1.3 Macro-mechanical experiments

- Macro-mechanical performance tests confirmed the superior performance of embossed fibre surface geometries, followed by flat fibre shapes. It was however established, that the degree of crack opening significantly influences FRC behaviour. Thus, the application of FRC is essential in the choice of macro-mechanical performance test utilisation.
- It was established, that the factor of macro synthetic fibre length behaves differently under three-point bending (TPB) and round determinate panel (RDP) conditions. This was ascribed to the different bending mechanisms acting as well as the degree of crack opening.
- It was found that prolonged mixing times significantly influence the macro-mechanical performance of cracked macro synthetic FRC. Both TPB and RDP experiments suggest a mixing time of five minutes in order to achieve the highest post-cracking performance, indicating a reduction in performance with increasing mixing time.
- Macro-mechanical performance parameters displayed correlation for similar crack openings exhibited by TPB and RDP test specimens. Correspondingly, some relation was observed for SFPO and TPB performance parameters. Especially premixed fibres indicated the existence of a relationship, with the exception of short fibres. Poor correlation was observed for higher levels of deformation, as encountered by RDP specimens. This behaviour was allocated to the similarity in mechanisms of small uniform and non-uniform crack openings encountered by TPB specimens, while larger uniform and non-uniform crack openings are characterised by a different behaviour.

7.1.4 Fresh concrete characteristics

- No balling behaviour was identified for the fibre contents considered, which was attributed towards the volume of fresh FRC as well as the type of mixer used for the investigation.
- Different fibre volume fractions were found to severely influence the workability of fresh FRC. The typical trend indicated a decrease in slump with increasing fibre content.
- Prolonged mixing significantly influenced the slump loss, indicating a decrease in workability with increased mixing time.

7.2 Future Prospects

From the knowledge gained during this research, the following research aspects can be regarded as important and need further investigation:

- More research is required on a model simulating accurate fibre pull-out behaviour. Special emphasis must be attributed towards the high initial mechanical interlock and the post-peak behaviour of single macro synthetic fibres.
- Flat and embossed macro synthetic fibre profiles exhibited high single-fibre and macro-mechanical performance parameters. It is thus of interest whether a combination of different fibre profiles would increase the overall performance of FRC.
- Concerning behaviour was observed for uni-axial TDPO experiments conducted on single crimped- and flat polypropylene macro fibres. However, much remains unknown about the effect of snubbing on the time dependent performance of macro synthetic fibres.
- Single embossed macro synthetic fibres displayed significant resistance against TDPO. The measured pull-out displacement included fibre elongation as well as TDPO. X-ray computed tomography (CT) scanning would provide additional information about the individual mechanisms encountered during TDPO.
- The effect of fibre length indicated unexpected macro-mechanical behaviour. Thus additional research on the influence of fibre length and the corresponding mechanisms is required.

- It was established that fibre mixing has a significant influence on the performance as well as visual appearance of single macro synthetic fibres. Thus, more research is required on optimal mixing times for increased macro-mechanical FRC performance.
- Much remains unknown about the causes of fibre balling. Additional research is required on the phenomenon of fibre entanglement and its consequences on the performance of macro synthetic FRC.

7.3 Concluding Statement

The aim of this study was to improve the general understanding of cracked macro synthetic fibre reinforced concrete (FRC) using fibres with various geometrical properties. Significant insight was gained on the single-fibre and macro mechanical behaviour of FRC. However, much remains unknown about the mechanisms in the cracked FRC state, especially during extensive crack opening as well as the use of longer fibre lengths. Furthermore, concerning behaviour was observed on the single-fibre level under time dependent pull-out, thus creating enough room for additional research. Nevertheless, macro synthetic FRC is believed to possess the potential for delivering more economic concrete designs, aiming to replace conventional steel mesh in ground supported slabs.

References

ACI 211.1-91, 1999. *Standard Practice for Selecting Proportions for Normal, Heavyweight, and Mass Concrete*, Farmington Hills, Michigan: American Concrete Institute.

ACI 544.1R-96, 1996. Report on fibre reinforced concrete. *Farmington Hills, Michigan: American Concrete Institute*, p.58.

ACI Committee 544, 2002. State-of-the-Art Report on Fiber Reinforced Concrete Reported by ACI Committee 544. *ACI Structural Journal*, 96(Reapproved).

Addis, B., 2013. *Fundamentals of concrete* G. Owens, ed., Midrand, South Africa: Cement and Concrete Institute.

Addis, B. & Goodman, J., 2009. Concrete mix design. In *Fulton's Concrete Technology*. Midrand, South Africa: Cement and Concrete Institute, pp. 219–228.

Aitcin, P.C., 2000. Cements of yesterday and today, concrete of tomorrow. *Cement and Concrete Research*, 30, pp.1349–1359.

Alani, A.M. & Aboutalebi, M., 2013. Mechanical Properties of Fibre Reinforced Concrete - A Comparative Experimental Study. *International Journal of Civil, Environmental, Structural, Construction and Architectural Engineering*, (9), pp.318–323.

Alberti, M.G., Enfedaque, a. & Gálvez, J.C., 2014. On the mechanical properties and fracture behavior of polyolefin fiber-reinforced self-compacting concrete. *Construction and Building Materials*, 55, pp.274–288. Available at: http://linkinghub.elsevier.com/retrieve/pii/S0950061814000488 [Accessed March 9, 2014].

American Society for Testing and Materials, 2012. *Standard Test Method for Flexural Performance of Fiber-Reinforced Concrete (Using Beam With Third-Point Loading)*, West Conshohocken.

American Society for Testing and Materials, 2010. *Standard Test Method for Obtaining Average Residual-Strength of Fibre-Reinforced Concrete*, West Conshohocken.

Arkles, B., 2006. Hydrophobicity, hydrophilicity and silanes. *Paint & Coatings Industry Magazine*, (October). Available at: http://scholar.google.com/scholar?hl=en&btnG=Search&q=intitle:Hydrophobicity,+Hydrophilicity+and+silanes#0 [Accessed July 22, 2014].

ASTM C1550-12, 2012. Standard Test Method for Flexural Toughness of Fiber Reinforced Concrete (Using Centrally Loaded Round Panel). *ASTM International*.

Babafemi, A., 2015. *Tensile creep of cracked macro synthetic fibre reinforced concrete*. Stellenbosch University.

Babafemi, A. & Boshoff, W., 2014. Tensile creep of macro-synthetic fibre reinforced concrete (MSFRC) under uni-axial tensile loading. *Cement & concrete composites*, 55, pp.62–69. Available at: http://scholar.sun.ac.za/handle/10019.1/89619 [Accessed August 3, 2014].

Banthia, N. & Boyd, A., 2000. Sprayed fibre-reinforced polymers for repairs TT -. *Canadian Journal of Civil Engineering TA* -, 27, pp.907–915.

Bedi, R., Singh, S.P. & Chandra, R., 2014. Design Fatigue Lives of Polypropylene Fibre

Reinforced Polymer Concrete Composites. *Journal of Materials and Engineering Structures*, 1(2), pp.99–109. Available at: http://revue.ummto.dz/index.php/JMES/article/view/192.

Beglarigale, A. & Yazici, H., 2015. Pull-out behavior of steel fiber embedded in flowable RPC and ordinary mortar. *JCBM Construction and Building Materials*, 75, pp.255–265.

Bentur, A. & Mindess, S., 2006. *Fibre reinforced cementitious composites*, CRC Press.

Bernard, E.S., 2002. Correlations in the behaviour of fibre reinforced shotcrete beam and panel specimens. *Materials and Structures*, 35(3), pp.156–164. Available at: http://dx.doi.org/10.1007/BF02533584.

Bolat, H. et al., 2014. The effects of macro synthetic fiber reinforcement use on physical and mechanical properties of concrete. *Composites Part B: Engineering*, 61, pp.191–198. Available at: http://linkinghub.elsevier.com/retrieve/pii/S1359836814000535 [Accessed July 16, 2014].

Buratti, N., Mazzotti, C. & Savoia, M., 2011. Post-cracking behaviour of steel and macro-synthetic fibre-reinforced concretes. *Construction and Building Materials*, 25(5), pp.2713–2722. Available at: http://linkinghub.elsevier.com/retrieve/pii/S0950061810006999 [Accessed March 9, 2014].

Caggiano, A. et al., 2012. Fracture behaviour of concrete beams reinforced with mixed long/short steel fibre. *Construction and Building Materials*, 37, pp.832–840.

Chira, A. et al., 2016. Property improvements of alkali resistant glass fibres/epoxy composite with nanosilica for textile reinforced concrete applications TT -. *Materials & Design TA* -, 89, pp.146–155.

Coleman, H.W. & Steele, W.G., 2009. *Experimentation, Validation, and Uncertainty Analysis for Engineers*, Wiley. Available at: https://books.google.co.za/books?id=6VJ_7cCW3VkC.

Concrete Society, 2013. *Concrete industrial ground floors : A guide to design and construction*, Camberley, Surrey: Concrete Society.

Concrete Society, 2003. *Concrete industrial ground floors: A guide to design and construction*, London: Concrete Society.

Concrete Society, 2007. *Guidance on the use of macro-synthetic-fibre-reinforced concrete*, Camberley: Concrete Society.

Ding, Y. & Kusterle, W., 1999. Comparative study of steel fibre-reinforced concrete and steel mesh-reinforced concrete at early ages in panel tests. *Cement and Concrete Research*. Available at: http://www.sciencedirect.com/science/article/pii/S0008884699001775 [Accessed October 28, 2014].

Domone, P. & Illston, J., 2010. *Construction materials: their nature and behaviour - 4th edition* 4th ed., SPON Press. Available at: Stellenbosch University Engineering and Forestry Library [Accessed April 27, 2015].

EN 14651, 2005. *Test method for metallic fibred concrete - Measuring the flexural tensile strength (limit of proportionality (LOP), residual)*, BSI.

EN 14889-1, 2006. Fibres for Concrete: Part 1: 2006. Steel Fibres: Definitions, specifications

and conformity.

EN 14889-2, 2006. Fibres for Concrete: Part 2: 2006. Polymer Fibres: Definitions, specifications and conformity.

European Federation of National Associations of Specialist Contractors and Material Suppliers for the Construction Industry, 2011. *EFNARC Three Point Bending Test on Square Panel with Notch*,

European Federation of National Associations of Specialist Contractors and Material Suppliers for the Construction Industry, 1996. *European specification for sprayed concrete*,

Gossla, U. & Rieder, K.-A., 2009. Zeitabhängiges Verhalten von Makrokunststofffaserbeton und dessen Einfluss auf die Bemessung von Industriefußböden. *Beton- und Stahlbetonbau*, 104(2), pp.76–87. Available at: http://doi.wiley.com/10.1002/best.200900660 [Accessed March 9, 2014].

Hakamy, A., Shaikh, F.U.A. & Low, I.M., 2015. Effect of calcined nanoclay on microstructural and mechanical properties of chemically treated hemp fabric-reinforced cement nanocomposites TT -. *Construction and Building Materials TA* -, 95, pp.882–891.

Hannant, D.J., 1978. *Fibre cements and fibre concretes*, Chichester; New York: Wiley.

Hasan, M.J., Afroz, M. & Mahmud, H.M.I., 2011. An Experimental Investigation on Mechanical Behavior of Macro Synthetic Fiber Reinforced Concrete. *International Journal of Civil & Environmental Engineering*, 11(3), pp.18–23.

JAPAN SOCIETY OF CIVIL ENGINEERING, 1985. *Method of test for flexural strength and flexural toughness of SFRC*, JSCE-SF4.

Kaur, G., Singh, S.P. & Kaushik, S.K., 2012. Flexural Fatigue Strength of Steel Fibre Reinforced Concrete Containing Blends of Limestone Powder and Silica Fume. *International Journal of Emerging Technology and Advanced Engineering*, 2(6).

Kim, D.J. et al., 2011. Comparative flexural behavior of Hybrid Ultra High Performance Fiber Reinforced Concrete with different macro fibers. *Construction and Building Materials*, 25(11), pp.4144–4155. Available at: http://linkinghub.elsevier.com/retrieve/pii/S0950061811001917 [Accessed July 15, 2014].

Kovler, K., 1995. Interdependence of Creep and Shrinkage for Concrete under Tension TT -. *Journal of Materials in Civil Engineering*, 7, pp.96–101.

Li, V.C., Wang, Y. & Backer, S., 1990. Effect of inclining angle, bundling and surface treatment on synthetic fibre pull-out from a cement matrix. *Composites*, 21(2), pp.132–140.

MacDonald, F. et al., 2009. CASE HISTORIES USING SYNTHETIC FIBER REINFORCED CONCRETE. Available at: http://dc.engconfintl.org/shotcrete/5/ [Accessed July 23, 2014].

Marotzke, C. & Qiao, L., 1997. Interfacial crack propagation arising in single-fiber pull-out tests TT -. *Composites Science and Technology TA* -, 57(8), pp.887–897.

Martin, L. et al., 2011. An analysis of flexural strength and crack width for fiber-reinforced

shotcrete used in weak rock mines. *Trans Soc Min Metal Explor TP-09-062*.

Minelli, F. & Plizzari, G.A., 2010. *Fibre reinforced concrete characterization through round panel test- Part II: analytical and numerical study*, Korea Concrete Institute.

Mouton, C. & Boshoff, W., 2012. Initial study on the tensile creep of cracked steel fibre reinforced concrete. In J. A. O. Barros, ed. *8th RILEM International Symposium on Fibre Reinforced Concrete: challenges and opportunities (BEFIB 2012)*. RILEM Publications SARL, pp. 326–337.

Neville, A.M., 1996. *Properties of concrete TT* - 4th ed., New York : J. Wiley,.

Odendaal, C.M., 2015. *Establishment of performance-based specifications for the structural use of locally available macro-synthetic fibres*. Stellenbosch University.

Parmentier, B. et al., 2008. Dispersion of the mechanical properties of FRC investigated by different bending tests. In *Tailor Made Concrete Structures*. CRC Press, p. 123. Available at: http://dx.doi.org/10.1201/9781439828410.ch84.

Payrow, P. et al., 2011. Effect of surface treatment on the post-peak residual strength and toughness of polypropylene/polyethylene-blended fiber-reinforced concrete. *Journal of Composite Materials*, 45(20), pp.2047–2054.

Perrie, B., 2009. Fibre-reinforced concrete. In *Fulton's Concrete Technology*. Midrand, South Africa: Cement and Concrete Institute, pp. 329–336.

Prisco, M., Plizzari, G. & Vandewalle, L., 2009. Fibre reinforced concrete: new design perspectives. *Materials and Structures*, 42(9), pp.1261–1281. Available at: http://www.springerlink.com/index/10.1617/s11527-009-9529-4 [Accessed July 10, 2014].

Proctor, B.A., 1979. Fibre reinforcement of cement and concrete. *Fourth South African Building Research Congress*.

Purnell, P., 1998. *The durability of glass-fibre reinforced cements made with new cementitious matrices'*. Aston University, UK.

Purnell, P. & Beddows, J., 2005. Durability and simulated ageing of new matrix glass fibre reinforced concrete TT -. *Cement & concrete composites. TA* -, 27(9-10), pp.875–884.

Richardson, A., 2006. Compressive strength of concrete with polypropylene fibre addition. *Structural Survey*, 24(2), pp.138–153.

Richardson, A., Coventry, K. & Landless, S., 2010. Synthetic and steel fibres in concrete with regard to equal toughness. *Structural Survey*, (December), pp.128–140. Available at: http://www.emeraldinsight.com/journals.htm?articleid=1892016&show=abstract [Accessed August 3, 2014].

RILEM TC 162-TDF, 2003. Final recommendation of RILEM TC 162-TDF: Test and design methods for steel fibre reinforced concrete. *Materials and Structures*, 36(262), pp.560–567.

SANS 1083, 2006. *Aggregates from natural sources: aggregates for concrete*, Pretoria: South African Bureau of Standards.

SANS 50197-1, 2000. *Cement. Part 1: Composition, specification and conformity criteria for common cements*, Pretoria: South African Bureau of Standards.

SANS 5841, 2006. *Aggregate crushing value of coarse aggregates*, Pretoria: South African Bureau of Standards.

SANS 5844, 2006. *Particle and relative densities of aggregates*, Pretoria: South African Bureau of Standards.

SANS 5845, 2006. *Bulk densities and voids content of aggregates*, Pretoria: South African Bureau of Standards.

SANS 5860, 2006. *Concrete tests - dimensions, tolerances and use of cast test specimens*, Pretoria: South African Bureau of Standards.

SANS 5861-3, 2006. *Concrete tests - making and curing of test specimens*, Pretoria: South African Bureau of Standards.

SANS 5862-1, 2006. *Concrete testing: Consitency of freshly mixed concrete (slump test)*, Pretoria: South African Bureau of Standards.

SANS 5863, 2006. *Concrete tests - compressive strength of hardened concrete*, Pretoria: South African Bureau of Standards.

Silverstein, M.S. & Breuer, O., 1993. Wettability and flotation of etched ultra high molecular weight polyethylene fibres. *JPOL</cja:jid> Polymer*, 34(16), pp.3421–3427.

Soutsos, M.N., Le, T.T. & Lampropoulos, a. P., 2012. Flexural performance of fibre reinforced concrete made with steel and synthetic fibres. *Construction and Building Materials*, 36, pp.704–710. Available at: http://linkinghub.elsevier.com/retrieve/pii/S0950061812004345 [Accessed July 7, 2014].

Tayler, N., 2009. Evaluation of Proficiency Testing Results and the Elimination of Statistical Outliers. In South African National Accreditation System. Available at: http://www.nla.org.za/conferences/2009/2009_papers/Presentations/Tuesday, 15 September/T306 - Evaluation of PT results and the elimination of statistical outliers.pdf.

The Concrete Institute, 2013. Fiber Reinforced Concrete. Available at: http://www.theconcreteinstitute.org.za/wp-content/uploads/2013/10/Fibre-Reinforced.pdf.

Tissington, B., Pollard, G. & Ward, I., 1991. A study on the influence of fiber/resin adhesion on the mechanical behavior of ultra-high-modulus polyethylene fiber composites. *Mater Sci*, 26(82).

Toledo Filho, R.D. et al., 2009. Durability of compression molded sisal fiber reinforced mortar laminates TT -. *Construction and Building Materials TA* -, 23(6), pp.2409–2420.

Tolêdo Filho, R.D. et al., 2000. Durability of alkali-sensitive sisal and coconut fibres in cement mortar composites TT -. *Cement and Concrete Composites TA* -, 22(2), pp.127–143.

Walraven, J.C., 2009. High performance fibre reinforced concrete: progress in knowledge and design codes. *Materials and Structures*, 42(9), pp.1247–1260.

Wei, J. & Meyer, C., 2014. Improving degradation resistance of sisal fiber in concrete through fiber surface treatment TT -. *Applied Surface Science TA* -, 289, pp.511–523.

Wille, K. & Naaman, A.E., 2012. Pullout Behavior of High-Strength Steel Fibers Embedded

in Ultra-High-Performance Concrete. *ACI Materials Journal*, 109(4), pp.479–487. Available at: http://ez.sun.ac.za/login?url=http://search.proquest.com/docview/1027122696?accountid=14049.

Wimpenny, D. et al., The use of Steel and Synthetic Fibres in Concrete under Extreme Conditions. , 14889.

Won, J., Lim, D. & Park, C., 2006. Bond behaviour and flexural performance of structural synthetic fibre-reinforced concrete. *Magazine of Concrete Research*, (6), pp.401–410.

Appendix A : Single-Fibre Test Specimen Information

This appendix provides specimen information for the single-fibre investigation of this study.

A.1 Single-Fibre Pull-Out Compression Test Results

The compression test results obtained for single-fibre pull-out (SFPO) mix designs are listed in Table A.1 to Table A.6.

Table A.1: Compression tests results of C1 SFPO specimens

Mix: C1_virgin || Concrete || Slump: 160mm					
Cube	**Density [kg/m^3]**	**Strength [MPa]**	**Average [MPa]**	**Standard Deviation [MPa]**	**CoV**
1	2348	37.0	37.1	0.64	0.02
2	2365	36.4			
3	2339	38.0			
4	2350	37.1			
Paste					
Cube	**Density [kg/m^3]**	**Strength [MPa]**	**Average [MPa]**	**Standard Deviation [MPa]**	**CoV**
1	2156	37.3	37.0	1.74	0.05
2	2174	38.6			
3	2155	37.7			
4	2168	34.6			
Mix: C1_premixed || Concrete || Slump: 120mm					
Cube	**Density [kg/m^3]**	**Strength [MPa]**	**Average [MPa]**	**Standard Deviation [MPa]**	**CoV**
1	2370	38.2	39.5	1.37	0.04
2	2427	39.2			
3	2369	40.9			
4	-	-			
Paste					
Cube	**Density [kg/m^3]**	**Strength [MPa]**	**Average [MPa]**	**Standard Deviation [MPa]**	**CoV**
1	2211	39.4	42.3	2.65	0.06
2	2211	45.1			
3	2198	43.8			
4	2220	40.8			

Table A.2: Compression tests results of F1 SFPO specimens

Mix: F1_virgin ‖ Concrete ‖ Slump: 160mm					
Cube	**Density [kg/m^3]**	**Strength [MPa]**	**Average [MPa]**	**Standard Deviation [MPa]**	**CoV**
1	2419	33.2	35.3	1.47	0.04
2	2405	35.1			
3	2390	36.4			
4	2409	36.3			
Paste					
Cube	**Density [kg/m^3]**	**Strength [MPa]**	**Average [MPa]**	**Standard Deviation [MPa]**	**CoV**
1	2223	36.6	35.6	0.95	0.03
2	2219	36.3			
3	2217	34.7			
4	2219	35.0			
Mix: F1_premixed ‖ Concrete ‖ Slump: 135mm					
Cube	**Density [kg/m^3]**	**Strength [MPa]**	**Average [MPa]**	**Standard Deviation [MPa]**	**CoV**
1	2412	36.8	36.6	0.91	0.03
2	2403	37.3			
3	2404	35.2			
4	2408	37			
Paste					
Cube	**Density [kg/m^3]**	**Strength [MPa]**	**Average [MPa]**	**Standard Deviation [MPa]**	**CoV**
1	2198	37.1	35.3	2.73	0.08
2	2211	38.1			
3	2228	32.6			
4	2206	33.4			

Table A.3: Compression tests results of F2 SFPO specimens

Mix: F2_virgin ‖ Concrete ‖ Slump: 130mm					
Cube	**Density [kg/m^3]**	**Strength [MPa]**	**Average [MPa]**	**Standard Deviation [MPa]**	**CoV**
1	2396	35.8	35.9	1.57	0.04
2	2410	33.8			
3	2384	36.8			
4	2399	37.3			
Paste					
Cube	**Density [kg/m^3]**	**Strength [MPa]**	**Average [MPa]**	**Standard Deviation [MPa]**	**CoV**
1	2243	38.2	38.6	0.54	0.01
2	2198	39.1			
3	2236	38.1			
4	2189	39.0			
Mix: F2_premixed ‖ Concrete ‖ Slump: 160mm					
Cube	**Density [kg/m^3]**	**Strength [MPa]**	**Average [MPa]**	**Standard Deviation [MPa]**	**CoV**
1	2426	37.6	36.7	0.8	0.02
2	2416	35.8			
3	2390	36.4			
4	2391	37.0			
Paste					
Cube	**Density [kg/m^3]**	**Strength [MPa]**	**Average [MPa]**	**Standard Deviation [MPa]**	**CoV**
1	2219	38.2	37.9	0.58	0.02
2	2209	37.0			
3	2221	38.2			
4	2197	38.1			

Table A.4: Compression tests results of E1 SFPO specimens

Mix: E1_virgin ‖ Concrete ‖ Slump: 180mm					
Cube	**Density [kg/m^3]**	**Strength [MPa]**	**Average [MPa]**	**Standard Deviation [MPa]**	**CoV**
1	2339	33.2	33.5	0.62	0.02
2	2348	34.2			
3	2328	32.8			
4	2332	33.9			
Paste					
Cube	**Density [kg/m^3]**	**Strength [MPa]**	**Average [MPa]**	**Standard Deviation [MPa]**	**CoV**
1	2111	34.1	34.7	1.36	0.04
2	2116	36.8			
3	2131	34.1			
4	2129	33.9			
Mix: E1_premixed ‖ Concrete ‖ Slump: 130mm					
Cube	**Density [kg/m^3]**	**Strength [MPa]**	**Average [MPa]**	**Standard Deviation [MPa]**	**CoV**
1	2429	39.1	39.5	0.48	0.01
2	2384	39.3			
3	2425	39.4			
4	2394	40.2			
Paste					
Cube	**Density [kg/m^3]**	**Strength [MPa]**	**Average [MPa]**	**Standard Deviation [MPa]**	**CoV**
1	2227	40.4	40.9	0.83	0.02
2	2220	40.0			
3	2196	41.8			
4	2214	41.4			

Table A.5: Compression tests results of E2 SFPO specimens

Mix: E2_virgin ‖ Concrete ‖ Slump: 140mm					
Cube	**Density [kg/m^3]**	**Strength [MPa]**	**Average [MPa]**	**Standard Deviation [MPa]**	**CoV**
1	2373	36.7	35.1	2.77	0.08
2	2331	31.9			
3	2352	36.8			
4	-	-			
Paste					
Cube	**Density [kg/m^3]**	**Strength [MPa]**	**Average [MPa]**	**Standard Deviation [MPa]**	**CoV**
1	2170	39.6	38.2	1.75	0.05
2	2130	37.1			
3	2173	36.4			
4	2116	39.8			
Mix: E2_premixed ‖ Concrete ‖ Slump: 135mm					
Cube	**Density [kg/m^3]**	**Strength [MPa]**	**Average [MPa]**	**Standard Deviation [MPa]**	**CoV**
1	2387	39.4	38.8	0.47	0.01
2	2396	38.3			
3	2430	38.8			
4	2416	38.5			
Paste					
Cube	**Density [kg/m^3]**	**Strength [MPa]**	**Average [MPa]**	**Standard Deviation [MPa]**	**CoV**
1	2202	39.4	39.4	0.79	0.02
2	2206	40.5			
3	2198	38.8			
4	2198	38.8			

Table A.6: Compression tests results of EB1 SFPO specimens

Mix: EB1_virgin ‖ Concrete ‖ Slump: 140mm					
Cube	**Density [kg/m^3]**	**Strength [MPa]**	**Average [MPa]**	**Standard Deviation [MPa]**	**CoV**
1	2373	36.7	35.1	2.77	0.08
2	2331	31.9			
3	2352	36.8			
4	-	-			
Paste					
Cube	**Density [kg/m^3]**	**Strength [MPa]**	**Average [MPa]**	**Standard Deviation [MPa]**	**CoV**
1	2170	39.6	38.2	1.75	0.05
2	2132	37.1			
3	2173	36.4			
4	2116	39.8			
Mix: EB1_premixed ‖ Concrete ‖ Slump: 125mm					
Cube	**Density [kg/m^3]**	**Strength [MPa]**	**Average [MPa]**	**Standard Deviation [MPa]**	**CoV**
1	2412	36.5	36.9	1.59	0.04
2	2419	34.9			
3	2398	37.2			
4	2399	38.8			
Paste					
Cube	**Density [kg/m^3]**	**Strength [MPa]**	**Average [MPa]**	**Standard Deviation [MPa]**	**CoV**
1	2239	39.7	40.3	1.95	0.05
2	2212	38.0			
3	2215	41.1			
4	2203	42.5			
Mix: EB1_large ‖ Concrete ‖ Slump: 160mm					
Cube	**Density [kg/m^3]**	**Strength [MPa]**	**Average [MPa]**	**Standard Deviation [MPa]**	**CoV**
1	2313	36.0	34.2	2.07	0.06
2	2295	31.2			
3	2337	34.7			
4	2332	34.9			
Paste					
Cube	**Density [kg/m^3]**	**Strength [MPa]**	**Average [MPa]**	**Standard Deviation [MPa]**	**CoV**
1	2104	33.9	33.2	1.57	0.05
2	2103	32.7			
3	2129	31.3			
4	2144	35.0			
Mix: EB1_small ‖ Concrete ‖ Slump: 90mm					
Cube	**Density [kg/m^3]**	**Strength [MPa]**	**Average [MPa]**	**Standard Deviation [MPa]**	**CoV**
1	2385	37.1	38.5	1.42	0.04
2	2337	37.5			
3	2360	39.9			
4	2384	39.5			
Paste					
Cube	**Density [kg/m^3]**	**Strength [MPa]**	**Average [MPa]**	**Standard Deviation [MPa]**	**CoV**
1	2163	42.0	39.4	1.84	0.05
2	2183	37.8			
3	2184	39.0			
4	2172	38.9			

A.2 Single-fibre pull-out results

The SFPO experimental results are summarised in Table A.7 to Table A.12.

Table A.7: SFPO test results obtained for C1

Embedment length [mm]	F_{max} [N]	CoV	Interfacial bond [MPa]	50% Pull-out averaged bond [MPa]	Total energy [J]	No. of fractures	No. of useful results
Virgin							
12.5	92.63	0.24	3.17	3.56	0.55	0	8
25.0	130.60	0.10	2.23	1.94	1.22	2	8
37.5	151.06	0.05	1.72	1.8	0.72	7	7
Premixed							
12.5	73.77	0.21	2.52	2.15	0.33	1	12
25.0	139.71	0.10	2.39	1.77	0.61	9	11
37.5	133.41	0.14	1.52	-	0.32	12	12

Table A.8: SFPO test results obtained for F1

Embedment length [mm]	F_{max} [N]	CoV	Interfacial bond [MPa]	50% Pull-out averaged bond [MPa]	Total energy [J]	No. of fractures	No. of useful results
Virgin							
12.5	26.61	0.10	1.14	1.24	0.20	0	7
25.0	49.88	0.09	1.00	1.13	0.72	0	8
37.5	69.41	0.06	0.93	1.09	1.62	0	7
Premixed							
12.5	99.33	0.20	3.97	3.02	0.42	3	12
25.0	108.48	0.09	2.17	1.82	0.76	7	10
37.5	117.64	0.11	1.57	2.14	0.78	11	11

Table A.9: SFPO test results obtained for F2

Embedment length [mm]	F_{max} [N]	CoV	Interfacial bond [MPa]	50% Pull-out averaged bond [MPa]	Total energy [J]	No. of fractures	No. of useful results
Virgin							
12.5	23.95	0.18	1.06	1.22	0.18	0	8
25.0	41.24	0.17	0.89	1.04	0.57	1	8
37.5	46.24	0.24	0.84	0.90	1.51	1	8
Premixed							
12.5	68.03	0.36	2.43	1.83	0.27	3	12
25.0	75.07	0.14	1.34	1.42	0.35	10	11
37.5	68.25	0.14	0.81	-	0.19	12	10

Table A.10: SFPO test results obtained for E1

Embedment length [mm]	F_{max} [N]	CoV	Interfacial bond [MPa]	50% Pull-out averaged bond [MPa]	Total energy [J]	No. of fractures	No. of useful results
Virgin							
12.5	112.61	0.17	4.02	2.98	0.52	0	8
24.0	177.63	0.08	3.30	2.57	1.05	4	7
25.0	178.10	0.04	3.18	2.22	1.13	4	6
37.5	197.21	0.11	2.34	-	0.35	8	8
Premixed							
12.5	124.76	0.14	4.45	2.57	0.45	0	12
24.0	194.77	0.05	3.62	2.37	1.05	5	12
25.0	196.42	0.08	3.50	1.85	1.12	5	12
37.5	199.51	0.08	2.37	1.45	0.59	11	10

Table A.11: SFPO test results obtained for E2

Embedment length [mm]	F_{max} [N]	CoV	Interfacial bond [MPa]	50% Pull-out averaged bond [MPa]	Total energy [J]	No. of fractures	No. of useful results
Virgin							
12.5	121.95	0.12	3.66	2.75	0.56	0	8
25.0	193.91	0.14	2.91	1.80	1.25	0	8
27.0	204.50	0.10	2.85	2.36	2.31	0	7
37.5	288.89	0.07	2.89	1.87	3.50	5	8
Premixed							
12.5	108.70	0.19	3.27	2.12	0.44	0	12
25.0	215.59	0.12	3.24	1.67	1.37	0	11
27.0	222.09	0.14	3.09	2.02	1.64	2	12
37.5	225.88	0.19	2.26	1.15	1.80	3	12

Table A.12: SFPO test results obtained for EB1

Embedment length [mm]	F_{max} [N]	CoV	Interfacial bond [MPa]	50% Pull-out averaged bond [MPa]	Total energy [J]	No. of fractures	No. of useful results
Virgin							
12.5	55.58	0.11	2.08	1.19	0.19	0	7
25.0	56.95	0.30	1.02	0.34	0.19	0	8
29.0	110.03	0.07	1.69	1.26	1.13	0	8
37.5	149.29	0.11	1.86	1.32	1.74	1	7
Virgin_large							
12.5	31.12	0.39	1.58	1.25	0.17	0	8
25.0	54.19	0.07	1.38	0.98	0.48	0	7
29.0	67.69	0.04	1.49	1.56	0.68	1	8
37.5	72.73	0.06	1.23	0.87	0.63	4	4
Virgin_small							
12.5	6.57	0.24	0.51	0.19	0.01	0	6
25.0	17.29	0.26	0.67	0.30	0.09	0	8
29.0	27.08	0.06	0.90	0.62	0.25	0	7
37.5	30.13	0.16	0.77	0.5	0.22	3	8
Premixed							
12.5	30.78	0.18	2.02	1.01	0.07	6	12
25.0	39.66	0.20	1.30	1.27	0.10	11	12
29.0	35.39	0.13	1.00	0.69	0.08	11	12
37.5	35.22	0.14	0.77	-	0.06	12	12

A.3 Time Dependent Pull-Out Compression Test Results

The compression test results obtained for time dependent pull-out (TDPO) mix designs are listed in Table A.13 to Table A.18.

Table A.13: Compression tests results of C1 TDPO specimens

Mix: Geotex 500 range ‖ Concrete ‖ Slump: 140mm					
Cube	**Density [kg/m^3]**	**Strength [MPa]**	**Average [MPa]**	**Standard Deviation [MPa]**	**CoV**
1	2367	32.7	34.6	1.95	0.06
2	2409	36.2			
3	2399	33.1			
4	2380	36.3			
Paste					
Cube	**Density [kg/m^3]**	**Strength [MPa]**	**Average [MPa]**	**Standard Deviation [MPa]**	**CoV**
1	2196	37.3	38.9	1.29	0.03
2	2178	38.9			
3	2166	39.0			
4	2204	40.5			

Table A.14: Compression tests results of F1 TDPO specimens

Mix: F1_virgin ‖ Concrete ‖ Slump: 140mm					
Cube	**Density [kg/m^3]**	**Strength [MPa]**	**Average [MPa]**	**Standard Deviation [MPa]**	**CoV**
1	2423	32.1	33.8	1.23	0.04
2	2387	34.5			
3	2387	33.7			
4	2393	34.8			
Paste					
Cube	**Density [kg/m^3]**	**Strength [MPa]**	**Average [MPa]**	**Standard Deviation [MPa]**	**CoV**
1	2201	36.0	36.4	1.19	0.03
2	2188	36.9			
3	2185	35.0			
4	2190	37.8			
Mix: F1_premixed ‖ Concrete ‖ Slump: 130mm					
Cube	**Density [kg/m^3]**	**Strength [MPa]**	**Average [MPa]**	**Standard Deviation [MPa]**	**CoV**
	2368	35.9	35.5	1.33	0.04
	2382	36.5			
	2354	36.1			
	2362	33.5			
Paste					
Cube	**Density [kg/m^3]**	**Strength [MPa]**	**Average [MPa]**	**Standard Deviation [MPa]**	**CoV**
	2150	37.2	35.6	2.92	0.08
	2170	37.3			
	2176	31.2			
	2180	36.5			

Table A.15: Compression tests results of F2 TDPO specimens

Mix: F2 ǁ Concrete ǁ Slump: 130mm					
Cube	**Density [kg/m^3]**	**Strength [MPa]**	**Average [MPa]**	**Standard Deviation [MPa]**	**CoV**
1	2349	32.4	33.7	0.99	0.03
2	2365	33.6			
3	2374	34.2			
4	2377	34.7			
Paste					
Cube	**Density [kg/m^3]**	**Strength [MPa]**	**Average [MPa]**	**Standard Deviation [MPa]**	**CoV**
1	2189	31.2	33.4	1.56	0.05
2	2215	36.3			
3	2193	37.2			
4	2195	33.9			

Table A.16: Compression tests results of E1 TDPO specimens

Mix: E1ǀ Concrete ǁ Slump: 135mm					
Cube	**Density [kg/m^3]**	**Strength [MPa]**	**Average [MPa]**	**Standard Deviation [MPa]**	**CoV**
1	2377	35.3	34.2	1.54	0.05
2	2382	35.6			
3	2394	32.6			
4	2391	33.0			
Paste					
Cube	**Density [kg/m^3]**	**Strength [MPa]**	**Average [MPa]**	**Standard Deviation [MPa]**	**CoV**
1	2202	35.8	35.30	0.62	0.02
2	2200	35.8			
3	2207	34.5			
4	2200	35.1			

Table A.17: Compression tests results of E2 TDPO specimens

Mix: E2_virgin ǁ Concrete ǁ Slump: 115mm					
Cube	**Density [kg/m^3]**	**Strength [MPa]**	**Average [MPa]**	**Standard Deviation [MPa]**	**CoV**
1	2401	36.9	36.8	2.21	0.06
2	2403	39.1			
3	2388	37.4			
4	2389	33.8			
Paste					
Cube	**Density [kg/m^3]**	**Strength [MPa]**	**Average [MPa]**	**Standard Deviation [MPa]**	**CoV**
1	2211	40.7	37.5	3.25	0.09
2	2209	37.6			
3	2216	34.2			
4	-	-			
Mix: E2_premixed ǁ Concrete ǁ Slump: 130mm					
Cube	**Density [kg/m^3]**	**Strength [MPa]**	**Average [MPa]**	**Standard Deviation [MPa]**	**CoV**
1	2368	35.9	35.5	1.33	0.04
2	2382	36.5			
3	2354	36.1			
4	2362	33.5			
Paste					
Cube	**Density [kg/m^3]**	**Strength [MPa]**	**Average [MPa]**	**Standard Deviation [MPa]**	**CoV**
1	2150	37.2	35.6	2.92	0.08
2	2170	37.3			
3	2176	31.2			
4	2180	36.5			

Table A.18: Compression tests results of EB1 TDPO specimens

Mix: EB1_virgin + large || Concrete || Slump: 140mm					
Cube	**Density [kg/m^3]**	**Strength [MPa]**	**Average [MPa]**	**Standard Deviation [MPa]**	**CoV**
1	2395	38.8	37.3	1.25	0.03
2	2363	36.3			
3	2374	37.9			
4	2366	36.2			
Paste					
Cube	**Density [kg/m^3]**	**Strength [MPa]**	**Average [MPa]**	**Standard Deviation [MPa]**	**CoV**
1	2181	36.3	37.3	1.82	0.05
2	2191	38.2			
3	2180	35.3			
4	2200	39.3			
Mix: EB1_premixed + small || Concrete || Slump: 110mm					
Cube	**Density [kg/m^3]**	**Strength [MPa]**	**Average [MPa]**	**Standard Deviation [MPa]**	**CoV**
1	2400	34.1	38.4	3.1	0.08
2	2400	41.3			
3	2410	39.6			
4	2400	38.5			
Paste					
Cube	**Density [kg/m^3]**	**Strength [MPa]**	**Average [MPa]**	**Standard Deviation [MPa]**	**CoV**
1	2190	38.3	38.1	0.78	0.02
2	2180	39.1			
3	2180	37.5			
4	2190	37.4			

Appendix B : Three-Point Bending Test Specimen Information

This appendix provides information on test specimens used for the investigation on the macro-mechanical level based on three-point bending (TPB) specimens.

B.1 Normal Mixing Times

Table B.1 to Table B.10 provide beam test results, compression strength as well as workability properties of the mix design.

Table B.1: TPB test results of C1 (FL25)

Beam	F_L [kN]	[MPa]					Sand batch	f_{cu} [MPa]	Slump / *Slump without fibres*
		$f_{fct,l}$	f_{R1}	f_{R2}	f_{R3}	f_{R4}			
1	12.76	4.08	0.78	0.45	0.36	0.33	1	37.8	80 / *110*
2	13.55	4.34	1.09	0.71	0.61	0.54			
3	13.66	4.37	1.32	0.80	0.67	0.59			
4	12.71	4.07	1.15	0.74	0.60	0.46			
5	12.75	4.08	1.19	0.73	0.61	0.50			
6	12.76	4.08	0.95	0.53	0.40	0.34			
Mean	**13.03**	**4.17**	**1.08**	**0.66**	**0.54**	**0.46**			
St. Dev.	**0.45**	**0.14**	**0.19**	**0.14**	**0.13**	**0.11**			
CoV	**0.03**	**0.03**	**0.18**	**0.21**	**0.23**	**0.23**			

Table B.2: TPB test results of C1 (FL50)

Beam	F_L [kN]	[MPa]					Sand batch	f_{cu} [MPa]	Slump / *Slump without fibres*
		$f_{fct,l}$	f_{R1}	f_{R2}	f_{R3}	f_{R4}			
1	14.39	4.60	1.40	1.28	1.14	1.04	1	37.7	85 / *110*
2	14.19	4.54	1.56	1.12	1.06	0.96			
3	13.76	4.40	1.30	1.03	0.99	1.04			
4	13.36	4.28	1.48	1.42	1.36	1.31			
5	15.40	4.93	1.03	0.85	0.79	0.75			
6	13.85	4.43	1.64	1.46	1.43	1.25			
Mean	**14.16**	**4.53**	**1.40**	**1.19**	**1.13**	**1.06**			
St. Dev.	**0.71**	**0.23**	**0.22**	**0.23**	**0.24**	**0.20**			
CoV	**0.05**	**0.05**	**0.16**	**0.20**	**0.21**	**0.19**			

Table B.3: TPB test results of C1 (FL75)

Beam	F_L [kN]	[MPa]					Sand batch	f_{cu} [MPa]	Slump / *Slump without fibres*
		$f_{fct,l}$	f_{R1}	f_{R2}	f_{R3}	f_{R4}			
1	12.46	3.99	1.21	1.05	1.05	1.00	1	35.6	90 / *125*
2	12.48	3.99	1.35	1.05	1.06	1.10			
3	12.86	4.12	1.47	1.27	1.30	1.26			
4	12.14	3.88	0.92	0.71	0.69	0.69			
5	12.71	4.07	1.18	0.90	0.86	0.89			
6	12.52	4.01	1.23	0.92	0.91	0.92			
Mean	**12.53**	**4.01**	**1.23**	**0.98**	**0.98**	**0.98**			
St. Dev.	**0.25**	**0.08**	**0.19**	**0.19**	**0.21**	**0.19**			
CoV	**0.02**	**0.02**	**0.15**	**0.19**	**0.21**	**0.20**			

Table B.4: TPB test results of F1 (FL25)

Beam	F_L [kN]	[MPa]					Sand batch	f_{cu} [MPa]	Slump / *Slump without fibres*
		$f_{fct,l}$	f_{R1}	f_{R2}	f_{R3}	f_{R4}			
1	13.55	4.34	1.57	1.05	0.88	0.76	1	37.2	55 / *100*
2	12.50	4.00	1.34	0.94	0.78	0.67			
3	11.91	3.81	1.39	0.79	0.64	0.56			
4	12.83	4.11	1.61	0.91	0.78	0.68			
5	11.01	3.52	1.41	1.00	0.84	0.71			
6	13.16	4.21	1.47	1.14	0.92	0.79			
Mean	**12.49**	**4.00**	**1.46**	**0.97**	**0.81**	**0.70**			
St. Dev.	**0.92**	**0.29**	**0.11**	**0.12**	**0.10**	**0.08**			
CoV	**0.07**	**0.07**	**0.07**	**0.12**	**0.12**	**0.12**			

Table B.5: TPB test results of F1 (FL50)

Beam	F_L [kN]	[MPa]					Sand batch	f_{cu} [MPa]	Slump / *Slump without fibres*
		$f_{fct,l}$	f_{R1}	f_{R2}	f_{R3}	f_{R4}			
1	11.21	3.59	1.42	1.24	1.19	1.13	1	40.2	65 / *110*
2	11.19	3.58	1.83	1.60	1.45	1.37			
3	11.07	3.54	1.67	1.26	1.15	1.11			
4	13.73	4.39	1.98	1.53	1.49	1.44			
5	12.75	4.08	1.84	1.55	1.20	1.14			
6	10.11	3.24	1.57	1.31	1.10	1.07			
Mean	**11.68**	**3.74**	**1.72**	**1.41**	**1.26**	**1.21**			
St. Dev.	**1.32**	**0.42**	**0.21**	**0.16**	**0.16**	**0.15**			
CoV	**0.11**	**0.11**	**0.12**	**0.11**	**0.13**	**0.13**			

Table B.6: TPB test results of F1 (FL75)

Beam	F_L [kN]	[MPa]					Sand batch	f_{cu} [MPa]	Slump / *Slump without fibres*
		$f_{fct,l}$	f_{R1}	f_{R2}	f_{R3}	f_{R4}			
1	10.81	3.46	1.49	1.26	1.22	1.20	1	37.2	50 / *110*
2	15.30	4.90	2.07	1.83	1.79	1.67			
3	15.83	5.07	2.10	2.07	2.11	1.99			
4	13.47	4.31	1.40	1.25	1.17	1.06			
5	12.29	3.93	1.62	1.35	1.33	1.24			
6	12.20	3.90	1.46	1.07	1.05	1.06			
Mean	**13.32**	**4.26**	**1.69**	**1.47**	**1.44**	**1.37**			
St. Dev.	**1.94**	**0.62**	**0.31**	**0.39**	**0.41**	**0.38**			
CoV	**0.15**	**0.15**	**0.19**	**0.26**	**0.29**	**0.28**			

Table B.7: TPB test results of F2

Beam	F_L [kN]	[MPa]					Sand batch	f_{cu} [MPa]	Slump / *Slump without fibres*
		$f_{fct,l}$	f_{R1}	f_{R2}	f_{R3}	f_{R4}			
1	13.05	4.18	2.05	2.07	2.14	2.08	4	34.3	90 / *160*
2	12.45	3.98	1.33	1.35	1.43	1.47			
3	13.79	4.41	1.08	1.01	1.05	0.99			
4	13.14	4.20	1.02	0.82	0.86	0.87			
5	14.05	4.50	1.17	1.12	1.08	1.02			
6	13.88	4.44	1.36	1.25	1.26	1.22			
Mean	**13.39**	**4.29**	**1.33**	**1.27**	**1.30**	**1.28**			
St. Dev.	**0.62**	**0.20**	**0.37**	**0.44**	**0.45**	**0.45**			
CoV	**0.05**	**0.05**	**0.28**	**0.34**	**0.35**	**0.35**			

Table B.8: TPB test results of E1

Beam	F_L [kN]	[MPa]					Sand batch	f_{cu} [MPa]	Slump / *Slump without fibres*
		$f_{fct,l}$	f_{R1}	f_{R2}	f_{R3}	f_{R4}			
1	12.80	4.10	2.08	1.96	2.07	1.99	2	36.4	85 / *125*
2	13.83	4.43	2.07	1.99	1.95	1.80			
3	11.74	3.76	2.16	2.07	2.07	1.94			
4	12.19	3.90	1.54	1.59	1.69	1.65			
5	11.64	3.72	1.48	1.19	1.15	1.13			
6	12.84	4.11	1.94	1.93	1.90	1.78			
Mean	**12.51**	**4.00**	**1.88**	**1.79**	**1.80**	**1.71**			
St. Dev.	**0.82**	**0.26**	**0.29**	**0.34**	**0.35**	**0.31**			
CoV	**0.07**	**0.07**	**0.16**	**0.19**	**0.19**	**0.18**			

Table B.9: TPB test results of E2

Beam	F_L [kN]	[MPa]					Sand batch	f_{cu} [MPa]	Slump / *Slump without fibres*
		$f_{fct,l}$	f_{R1}	f_{R2}	f_{R3}	f_{R4}			
1	12.42	3.97	2.05	1.98	1.99	2.01	2	37.8	80 / *120*
2	10.99	3.52	1.23	1.10	1.11	1.07			
3	12.95	4.14	1.61	1.51	1.46	1.34			
4	13.63	4.36	1.66	1.51	1.59	1.58			
5	12.16	3.89	1.52	1.28	1.23	1.16			
6	13.01	4.16	2.15	1.89	1.96	1.75			
Mean	**12.53**	**4.01**	**1.70**	**1.54**	**1.56**	**1.49**			
St. Dev.	**0.91**	**0.29**	**0.34**	**0.34**	**0.37**	**0.36**			
CoV	**0.07**	**0.07**	**0.20**	**0.22**	**0.24**	**0.24**			

Table B.10: TPB test results of EB1

Beam	F_L [kN]	[MPa]					Sand batch	f_{cu} [MPa]	Slump / *Slump without fibres*
		$f_{fct,l}$	f_{R1}	f_{R2}	f_{R3}	f_{R4}			
1	13.05	4.18	2.05	2.07	2.14	2.08	2	34.3	90 / *160*
2	12.45	3.98	1.33	1.35	1.43	1.47			
3	13.79	4.41	1.08	1.01	1.05	0.99			
4	13.14	4.20	1.02	0.82	0.86	0.87			
5	14.05	4.50	1.17	1.12	1.08	1.02			
6	13.88	4.44	1.36	1.25	1.26	1.22			
Mean	**13.39**	**4.29**	**1.33**	**1.27**	**1.30**	**1.28**			
St. Dev.	**0.62**	**0.20**	**0.37**	**0.44**	**0.45**	**0.45**			
CoV	**0.05**	**0.05**	**0.28**	**0.34**	**0.35**	**0.35**			

B.2 Extended Mixing Times

The results obtained by TPB experiments, as well as the corresponding workability and compressive strength of the mix design for extended mixing, are presented in this section. Table B.11 to Table B.14 and Table B.15 to Table B.18 provide specimen information for twenty minute mixing and forty minute mixing time respectively.

Table B.11: TPB test results of C1 (MT20)

Beam	F_L [kN]	[MPa]					Sand batch	f_{cu} [MPa]	Slump / *Slump without fibres*
		$f_{fct,l}$	f_{R1}	f_{R2}	f_{R3}	f_{R4}			
1	12.26	3.92	1.00	0.83	0.81	0.78	4	36.6	75 / *125*
2	12.90	4.13	1.02	0.95	0.94	0.93			
3	12.62	4.04	1.26	1.21	1.21	1.15			
4	12.24	3.92	1.29	1.09	1.12	1.15			
5	13.41	4.29	1.16	0.84	0.74	0.69			
6	13.06	4.18	1.01	0.77	0.73	0.69			
Mean	**12.75**	**4.08**	**1.12**	**0.95**	**0.92**	**0.90**			
St. Dev.	**0.46**	**0.15**	**0.13**	**0.17**	**0.20**	**0.21**			
CoV	**0.04**	**0.04**	**0.12**	**0.18**	**0.22**	**0.24**			

Table B.12: TPB test results of F1 (MT20)

Beam	F_L [kN]	[MPa]					Sand batch	f_{cu} [MPa]	Slump / *Slump without fibres*
		$f_{fct,l}$	f_{R1}	f_{R2}	f_{R3}	f_{R4}			
1	14.82	4.74	1.69	1.45	1.23	1.03	4	38.6	75 / *105*
2	14.07	4.50	1.83	1.63	1.38	1.09			
3	13.32	4.26	1.77	1.64	1.47	1.28			
4	13.74	4.40	2.18	1.86	1.63	1.42			
5	13.81	4.42	1.83	1.68	1.36	1.17			
6	13.06	4.18	1.67	1.45	1.36	1.14			
Mean	**13.80**	**4.42**	**1.83**	**1.62**	**1.41**	**1.19**			
St. Dev.	**0.62**	**0.20**	**0.19**	**0.16**	**0.14**	**0.14**			
CoV	**0.04**	**0.04**	**0.10**	**0.10**	**0.10**	**0.12**			

Table B.13: TPB test results of E1 (MT20)

Beam	F_L [kN]	[MPa]					Sand batch	f_{cu} [MPa]	Slump / *Slump without fibres*
		$f_{fct,l}$	f_{R1}	f_{R2}	f_{R3}	f_{R4}			
1	12.79	4.09	1.80	1.84	1.77	1.31	4	37.6	80 / *135*
2	14.38	4.60	1.59	1.44	1.40	1.18			
3	13.82	4.42	2.09	2.08	1.89	1.49			
4	12.19	3.90	1.82	1.52	1.28	1.04			
5	14.07	4.50	2.33	2.17	1.86	1.51			
6	12.00	3.84	1.59	1.37	1.10	0.92			
Mean	**13.21**	**4.23**	**1.87**	**1.73**	**1.55**	**1.24**			
St. Dev.	**1.02**	**0.32**	**0.29**	**0.34**	**0.34**	**0.24**			
CoV	**0.08**	**0.08**	**0.16**	**0.20**	**0.22**	**0.19**			

Table B.14: TPB test results of EB1 (MT20)

Beam	F_L [kN]	[MPa]					Sand batch	f_{cu} [MPa]	Slump / *Slump without fibres*
		$f_{fct,l}$	f_{R1}	f_{R2}	f_{R3}	f_{R4}			
1	13.69	4.38	1.30	1.15	1.10	0.98	4	37.6	80 / *135*
2	13.86	4.43	1.74	1.52	1.55	1.43			
3	11.59	3.71	1.12	1.06	1.10	1.02			
4	12.35	3.95	1.29	1.17	1.16	1.03			
5	13.62	4.36	1.31	1.15	1.19	1.14			
6	12.65	4.05	1.41	1.27	1.22	1.10			
Mean	**12.96**	**4.15**	**1.36**	**1.22**	**1.22**	**1.12**			
St. Dev.	**0.91**	**0.29**	**0.21**	**0.16**	**0.17**	**0.16**			
CoV	**0.07**	**0.07**	**0.15**	**0.13**	**0.14**	**0.15**			

Table B.15: TPB test results of C1 (MT40)

Beam	F_L [kN]	[MPa]					Sand batch	f_{cu} [MPa]	Slump / *Slump without fibres*
		$f_{fct,l}$	f_{R1}	f_{R2}	f_{R3}	f_{R4}			
1	12.47	3.99	1.05	1.02	0.95	0.86	3	38.1	40 / *140*
2	11.27	3.61	1.19	0.95	0.88	0.73			
3	11.65	3.73	1.21	1.04	1.03	1.02			
4	12.63	4.04	1.41	1.22	1.14	1.06			
5	13.53	4.33	1.18	0.98	0.95	0.88			
6	11.55	3.69	1.25	1.02	0.89	0.67			
Mean	**12.18**	**3.90**	**1.22**	**1.04**	**0.97**	**0.87**			
St. Dev.	**0.85**	**0.27**	**0.12**	**0.09**	**0.10**	**0.15**			
CoV	**0.07**	**0.07**	**0.09**	**0.09**	**0.10**	**0.18**			

Table B.16: TPB test results of F1 (MT40)

Beam	F_L [kN]	[MPa]					Sand batch	f_{cu} [MPa]	Slump / *Slump without fibres*
		$f_{fct,l}$	f_{R1}	f_{R2}	f_{R3}	f_{R4}			
1	13.17	4.21	1.93	1.70	1.33	0.98	3	38.6	35 / *140*
2	12.30	3.94	1.31	1.11	0.93	0.75			
3	12.02	3.85	1.56	1.22	0.93	0.70			
4	12.42	3.97	1.57	1.17	0.90	0.75			
5	11.65	3.73	2.26	2.00	1.65	1.17			
6	13.83	4.43	2.31	2.14	1.85	1.50			
Mean	**12.57**	**4.02**	**1.82**	**1.55**	**1.27**	**0.97**			
St. Dev.	**0.80**	**0.26**	**0.41**	**0.45**	**0.41**	**0.31**			
CoV	**0.06**	**0.06**	**0.22**	**0.29**	**0.33**	**0.32**			

Table B.17: TPB test results of E1 (MT40)

Beam	F_L [kN]	[MPa]					Sand batch	f_{cu} [MPa]	Slump / *Slump without fibres*
		$f_{fct,l}$	f_{R1}	f_{R2}	f_{R3}	f_{R4}			
1	14.14	4.53	1.61	1.25	1.20	1.05	3	36.7	20 / *130*
2	14.25	4.56	1.71	1.42	1.01	0.72			
3	12.28	3.93	1.61	1.51	1.46	1.34			
4	12.35	3.95	1.14	0.94	0.69	0.50			
5	13.99	4.48	1.48	1.20	0.81	0.58			
6	13.12	4.20	1.38	1.30	1.02	0.70			
Mean	**13.36**	**4.27**	**1.49**	**1.27**	**1.03**	**0.82**			
St. Dev.	**0.90**	**0.29**	**0.21**	**0.20**	**0.28**	**0.32**			
CoV	**0.07**	**0.07**	**0.14**	**0.16**	**0.27**	**0.39**			

Table B.18: TPB test results of EB1 (MT40)

Beam	F_L [kN]	[MPa]					Sand batch	f_{cu} [MPa]	Slump / *Slump without fibres*
		$f_{fct,l}$	f_{R1}	f_{R2}	f_{R3}	f_{R4}			
1	12.49	4.00	1.47	0.96	0.76	0.57	3	34.6	20 / *115*
2	13.60	4.35	1.15	0.83	0.60	0.40			
3	12.32	3.94	1.02	0.77	0.62	0.49			
4	11.08	3.55	1.32	0.95	0.69	0.49			
5	12.68	4.06	1.31	1.03	0.77	0.58			
6	11.07	3.54	1.16	0.92	0.67	0.43			
Mean	**12.21**	**3.91**	**1.24**	**0.91**	**0.68**	**0.49**			
St. Dev.	**0.98**	**0.31**	**0.16**	**0.09**	**0.07**	**0.07**			
CoV	**0.08**	**0.08**	**0.13**	**0.10**	**0.10**	**0.15**			

Appendix C : Round Determinate Panel Test Specimen Information

This appendix contains information regarding round determinate panel (RDP) specimens, including flexural loads, energy dissipation, mix design compressive strength and RDP specimen thicknesses.

C.1 Normal Mixing Times

The RDP specimen information for mixes subjected to five minutes of mixing is presented in Table C.1 to Table C.10.

Table C.1: RDP test results of C1 (FL25)

	Specimen			CoV	Sand batch	f_{cu} [MPa]	Slump / *Slump without fibres*
	Panel 1	**Panel 2**	**Panel 3**				
Peak flexural load [kN]	23.8	25.6	26.1	0.05	1	36.5	90 / *125*
Corrected Load [kN]	23.0	24.3	23.9	0.03			
Total energy [J]	85.7	100.1	74.3	0.15			
Corrected energy [J]	83.4	96.4	69.7	0.16			
Average specimen thickness [mm]	76.4	76.9	78.3				
Standard deviation [mm]	1.43	1.10	1.16				
Minimum thickness [mm]	75	75	76				
Maximum thickness [mm]	79	79	80				
Valid / successful	X	X	X				

Table C.2: RDP test results of C1 (FL50)

	Specimen			CoV	Sand batch	f_{cu} [MPa]	Slump / *Slump without fibres*
	Panel 1	Panel 2	Panel 3				
Peak flexural load [kN]	22.3	25.7	23.6	0.05	1	35.7	85 / *140*
Corrected Load [kN]	22.0	23.5	23.4	0.02			
Total Energy [J]	113.0	172.8	161.9	0.07			
Corrected Energy [J]	111.9	161.6	161.2	0.09			
Average specimen thickness [mm]	75.5	78.4	75.2				
Standard deviation [mm]	1.27	2.37	1.03				
Minimum thickness [mm]	74	75	74				
Maximum thickness [mm]	78	82	77				
Valid / successful		X	X				

Table C.3: RDP test results of C1 (FL75)

	Specimen			CoV	Sand batch	f_{cu} [MPa]	Slump / *Slump without fibres*
	Panel 1	Panel 2	Panel 3				
Peak flexural load [kN]	26.0	25.8	26.0	0.00	1	40.0	85 / *110*
Corrected Load [kN]	23.5	24.3	24.6	0.02			
Total Energy [J]	228.6	251.3	165.2	0.21			
Corrected Energy [J]	211.8	240.11	158.81	0.20			
Average specimen thickness [mm]	78.9	77.3	77				
Standard deviation [mm]	1.20	1.25	1.83				
Minimum thickness [mm]	78	75	74				
Maximum thickness [mm]	82	79	79				
Valid / successful	X	X					

Table C.4: RDP test results of F1 (FL25)

	Specimen			CoV	Sand batch	f_{cu} [MPa]	Slump / *Slump without fibres*
	Panel 1	Panel 2	Panel 3				
Peak flexural load [kN]	24.2	22.9	26.7	0.08	1	33.6	85 / *110*
Corrected Load [kN]	23.7	21.7	24.0	0.05			
Total Energy [J]	114.8	95.0	109.5	0.10			
Corrected Energy [J]	113.2	91.1	100.9	0.11			
Average specimen thickness [mm]	75.7	77.1	79.2				
Standard deviation [mm]	1.95	1.37	1.48				
Minimum thickness [mm]	71	75	77				
Maximum thickness [mm]	78	79	81				
Valid / successful	X	X	X				

Table C.5: RDP test results of F1 (FL50)

	Specimen			CoV	Sand batch	f_{cu} [MPa]	Slump / *Slump without fibres*
	Panel 1	Panel 2	Panel 3				
Peak flexural load [kN]	25.8	23.1	30.0	0.13	1	37.8	65 / *130*
Corrected Load [kN]	24.2	23.2	24.7	0.03			
Total Energy [J]	174.8	180.9	247.0	0.20			
Corrected Energy [J]	166.3	181.3	213.6	0.13			
Average specimen thickness [mm]	77.5	74.9	82.6				
Standard deviation [mm]	1.43	1.79	2.72				
Minimum thickness [mm]	76	73	77				
Maximum thickness [mm]	80	78	86				
Valid / successful	X	X	X				

Table C.6: RDP test results of F1 (FL75)

	Specimen			CoV	Sand batch	f_{cu} [MPa]	Slump / *Slump without fibres*
	Panel 1	Panel 2	Panel 3				
Peak flexural load [kN]	24.8	26.2	22.6	0.07	1	38.1	50 / *110*
Corrected Load [kN]	23.4	24.3	24.7	0.03			
Total Energy [J]	183.4	155.0	162.9	0.09			
Corrected Energy [J]	175.6	146.4	173.9	0.10			
Average specimen thickness [mm]	77.2	77.9	71.8				
Standard deviation [mm]	2.30	1.29	1.62				
Minimum thickness [mm]	75	75	70				
Maximum thickness [mm]	81	79	74				
Valid / successful	X	X	X				

Table C.7: RDP test results of F2

	Specimen			CoV	Sand batch	f_{cu} [MPa]	Slump / *Slump without fibres*
	Panel 1	Panel 2	Panel 3				
Peak flexural load [kN]	13.4	26.1	24.5	0.32	4	36.2	90 / *120*
Corrected Load [kN]	13.9	23.9	24.5	0.29			
Total Energy [J]	213.7	209.8	158.6	0.16			
Corrected Energy [J]	219.4	196.3	158.6	0.16			
Average specimen thickness [mm]	73.7	78.4	75				
Standard deviation [mm]	0.82	0.97	1.49				
Minimum thickness [mm]	73	77	73				
Maximum thickness [mm]	75	80	78				
Valid / successful	X	X	X				

Table C.8: RDP test results of E1

	Specimen			CoV	Sand batch	f_{cu} [MPa]	Slump / *Slump without fibres*
	Panel 1	Panel 2	Panel 3				
Peak flexural load [kN]	26.7	24.8	25.7	0.04	2	35.8	75 / *115*
Corrected Load [kN]	23.8	22.1	23.8	0.04			
Total Energy [J]	161.3	163.0	159.2	0.01			
Corrected Energy [J]	148.0	149.3	150.4	0.01			
Average specimen thickness [mm]	79.4	79.5	77.9				
Standard deviation [mm]	2.88	1.08	2.08				
Minimum thickness [mm]	74	78	75				
Maximum thickness [mm]	84	81	81				
Valid / successful	X	X	X				

Table C.9: RDP test results of E2

	Specimen			CoV	Sand batch	f_{cu} [MPa]	Slump / *Slump without fibres*
	Panel 1	Panel 2	Panel 3				
Peak flexural load [kN]	24.1	23.9	24.9	0.02	2	39.4	75 / *110*
Corrected Load [kN]	23.8	21.9	24.0	0.05			
Total Energy [J]	245.0	218.9	207.1	0.09			
Corrected Energy [J]	242.6	205.2	201.4	0.11			
Average specimen thickness [mm]	75.5	78.3	76.4				
Standard deviation [mm]	1.58	1.16	1.26				
Minimum thickness [mm]	74	76	75				
Maximum thickness [mm]	78	80	78				
Valid / successful	X	X	X				

Table C.10: RDP test results of EB1

	Specimen			CoV	Sand batch	f_{cu} [MPa]	Slump / *Slump without fibres*
	Panel 1	**Panel 2**	**Panel 3**				
Peak flexural load [kN]	22.9	26.3	23.2	0.08	2	33.5	90 / *160*
Corrected Load [kN]	22.5	25.2	21.7	0.08			
Total Energy [J]	179.0	169.7	196.8	0.08			
Corrected Energy [J]	176.9	164.4	187.3	0.07			
Average specimen thickness [mm]	75.6	76.6	77.5				
Standard deviation [mm]	1.26	1.35	1.58				
Minimum thickness [mm]	73	75	75				
Maximum thickness [mm]	77	79	79				
Valid / successful	X	X	X				

C.2 Extended Mixing Times

The RDP panel test results, including specimen information and mix design compressive strength, are summarised in Table C.11 to Table C.14 and Table C.15 to Table C.18 for twenty minutes and forty minutes mixing times respectively.

Table C.11: RDP test results of C1 (MT20)

	Specimen			CoV	Sand batch	f_{cu} [MPa]	Slump / *Slump without fibres*
	Panel 1	**Panel 2**	**Panel 3**				
Peak flexural load [kN]	21.3	24.9	24.5	0.01	4	35.7	85 / *125*
Corrected Load [kN]	22.5	24.3	22.1	0.07			
Total Energy [J]	128.4	172.9	152.0	0.09			
Corrected Energy [J]	134.0	169.9	140.5	0.13			
Average specimen thickness [mm]	72.9	75.9	79				
Standard deviation [mm]	0.74	0.74	1.15				
Minimum thickness [mm]	72	75	77				
Maximum thickness [mm]	74	77	81				
Valid / successful		X	X				

Table C.12: RDP test results of F1 (MT20)

	Specimen			CoV	Sand batch	f_{cu} [MPa]	Slump / *Slump without fibres*
	Panel 1	Panel 2	Panel 3				
Peak flexural load [kN]	25.3	24.2	6.73	0.03	4	37.7	90 / *130*
Corrected Load [kN]	23.7	24.5	6.8	0.02			
Total Energy [J]	146.3	146.4	103.7	0.00			
Corrected Energy [J]	139.2	147.6	103.9	0.04			
Average specimen thickness [mm]	77.5	74.6	74.9				
Standard deviation [mm]	1.90	0.97	2.23				
Minimum thickness [mm]	73	73	70				
Maximum thickness [mm]	80	76	78				
Valid / successful	X	X					

Table C.13: RDP test results of E1 (MT20)

	Specimen			CoV	Sand batch	f_{cu} [MPa]	Slump / *Slump without fibres*
	Panel 1	Panel 2	Panel 3				
Peak flexural load [kN]	22.6	24.7	25.9	0.07	4	39.2	90 / *145*
Corrected Load [kN]	23.4	24.0	23.2	0.02			
Total Energy [J]	134.6	195.7	162.4	0.19			
Corrected Energy [J]	138.2	191.5	149.6	0.18			
Average specimen thickness [mm]	73.7	76.1	79.2				
Standard deviation [mm]	0.95	0.88	0.92				
Minimum thickness [mm]	72	75	78				
Maximum thickness [mm]	75	77	80				
Valid / successful	X	X	X				

Table C.14: RDP test results of EB1 (MT20)

	Specimen			CoV	Sand batch	f_{cu} [MPa]	Slump / *Slump without fibres*
	Panel 1	Panel 2	Panel 3				
Peak flexural load [kN]	22.8	23.3	23.8	0.02	4	38.4	60 / *125*
Corrected Load [kN]	22.4	23.5	22.6	0.03			
Total Energy [J]	114.6	119.8	94.7	0.12			
Corrected Energy [J]	113.0	120.3	91.2	0.14			
Average specimen thickness [mm]	75.7	74.8	76.9				
Standard deviation [mm]	1.70	1.03	1.29				
Minimum thickness [mm]	74	74	75				
Maximum thickness [mm]	79	77	79				
Valid / successful	X	X	X				

Table C.15: RDP test results of C1 (MT40)

	Specimen			CoV	Sand batch	f_{cu} [MPa]	Slump / *Slump without fibres*
	Panel 1	Panel 2	Panel 3				
Peak flexural load [kN]	25.3	22.7	22.8	0.06	3	38.0	40 / *120*
Corrected Load [kN]	24.7	22.3	21.7	0.07			
Total Energy [J]	140.6	138.0	139.0	0.01			
Corrected Energy [J]	138.0	136.3	133.6	0.02			
Average specimen thickness [mm]	77	75.9	75.6				
Standard deviation [mm]	0.82	1.66	1.26				
Minimum thickness [mm]	76	73	73				
Maximum thickness [mm]	78	79	78				
Valid / successful	X	X	X				

Table C.16: RDP test results of F1 (MT40)

	Specimen			CoV	Sand batch	f_{cu} [MPa]	Slump / *Slump without fibres*
	Panel 1	Panel 2	Panel 3				
Peak flexural load [kN]	17.7	22.9	26.5	0.20	3	37.8	35 / *140*
Corrected Load [kN]	16.0	24.8	25.9	0.24			
Total Energy [J]	170.0	114.2	123.0	0.21			
Corrected Energy [J]	157.5	121.5	127.7	0.14			
Average specimen thickness [mm]	78.9	72	75.9				
Standard deviation [mm]	0.88	0.94	1.10				
Minimum thickness [mm]	77	70	74				
Maximum thickness [mm]	80	73	77				
Valid / successful	X	X	X				

Table C.17: RDP test results of E1 (MT40)

	Specimen			CoV	Sand batch	f_{cu} [MPa]	Slump / *Slump without fibres*
	Panel 1	Panel 2	Panel 3				
Peak flexural load [kN]	25.7	22.1	25.5	0.08	3	39.0	20 / *140*
Corrected Load [kN]	24.0	22.2	23.5	0.04			
Total Energy [J]	131.0	119.2	119.6	0.05			
Corrected Energy [J]	124.5	119.7	112.3	0.05			
Average specimen thickness [mm]	77.6	74.8	78.2				
Standard deviation [mm]	1.58	2.44	2.53				
Minimum thickness [mm]	75	72	73				
Maximum thickness [mm]	80	79	81				
Valid / successful	X	X	X				

Table C.18: RDP test results of EB1 (MT40)

	Specimen			CoV	Sand batch	f_{cu} [MPa]	Slump / *Slump without fibres*
	Panel 1	Panel 2	Panel 3				
Peak flexural load [kN]	26.9	23.2	25.1	0.05	3	35.2	20 / *120*
Corrected Load [kN]	25.7	23.4	24.0	0.05			
Total Energy [J]	100.5	67.4	83.7	0.13			
Corrected Energy [J]	97.2	67.8	80.9	0.13			
Average specimen thickness [mm]	76.7	74.7	76.7				
Standard deviation [mm]	2.58	1.77	2.06				
Minimum thickness [mm]	74	72	74				
Maximum thickness [mm]	81	78	80				
Valid / successful	X		X				